

e-ISSN : 2320-0847
p-ISSN : 2320-0936



American Journal of Engineering Research (AJER)

Volume 4 Issue 4– April 2015

www.ajer.org

ajer.research@gmail.com

Editorial Board

American Journal of Engineering Research (AJER)

Dr. Moinuddin Sarker,

Qualification :PhD, MCIC, FICER,
MInstP, MRSC (P), VP of R & D
Affiliation : Head of Science / Technology
Team, Corporate Officer (CO)
Natural State Research, Inc.
37 Brown House Road (2nd Floor)
Stamford, CT-06902, USA.

Dr. June II A. Kiblasan

Qualification : Phd
Specialization: Management, applied
sciences
Country: PHILIPPINES

**Dr. Jonathan Okeke
Chimakonam**

Qualification: PHD
Affiliation: University of Calabar
Specialization: Logic, Philosophy of
Maths and African Science,
Country: Nigeria

Dr. Narendra Kumar Sharma

Qualification: PHD
Affiliation: Defence Institute of Physiology
and Allied Science, DRDO
Specialization: Proteomics, Molecular
biology, hypoxia
Country: India

Dr. ABDUL KAREEM

Qualification: MBBS, DMRD, FCIP, FAGE
Affiliation: UNIVERSITI SAINS Malaysia
Country: Malaysia

Prof. Dr. Shafique Ahmed Arain

Qualification: Postdoc fellow, Phd
Affiliation: Shah Abdul Latif University
Khairpur (Mirs),
Specialization: Polymer science
Country: Pakistan

Dr. sukhmander singh

Qualification: Phd
Affiliation: Indian Institute Of
Technology, Delhi
Specialization : PLASMA PHYSICS
Country: India

Dr. Alcides Chaux

Qualification: MD
Affiliation: Norte University, Paraguay,
South America
Specialization: Genitourinary Tumors
Country: Paraguay, South America

Dr. Nwachukwu Eugene Nnamdi

Qualification: Phd
Affiliation: Michael Okpara University of
Agriculture, Umudike, Nigeria
Specialization: Animal Genetics and
Breeding
Country: Nigeria

Dr. Md. Nazrul Islam Mondal

Qualification: Phd
Affiliation: Rajshahi University,
Bangladesh
Specialization: Health and Epidemiology
Country: Bangladesh

CONTENTS

Volume-4 Issue-4

S.No.	Manuscript Title	Page No.
01.	Evaluation for suitable propagation model to mobile Communications in South-South Nigeria urban-terrain P. Akinyemi S.O. Azi J.S. Ojo C.I. Abiodun	01-05
02.	Framework for Evaluation and Improvement of Work over Rigs in Oilfields Haitham Mansour Prof. Mohammad Munir Ahmad	06-13
03.	Compositional analysis of lignocellulosic materials: Evaluation of an economically viable method suitable for woody and non-woody biomass Augustine O. Ayeni Opeyemi A. Adeeyo Oyinlola M. Oresgun Temitayo E. Oladimeji	14-19
04.	Bayesian Belief Network Method for Predicting Asphaltene Precipitation in Light Oil Reservoirs Jeffrey O. Oseh (M.Sc.) Olugbenga A. Falode (Ph.D)	20-26
05.	Effects of variety and moisture content on some physical properties of okra pod Adejumo A.O.D Ajav E. A Igbeka J.C	27-33
06.	TAMIL PUTHANDU!... M.Arulmani V.R.Hema Latha	34-39
07.	The pre- stress concrete structure, Found to-be More Effective Then THE Reinforced concrete structure & System developed for mechanism OF, Anchoring devices in pre and post Tensioned concrete structural elements. Pradeep Nath Mathur Prof (Dr.) A. K. Sinha Prof. (Dr.) P.B.L.Chaurasia	40-49
08.	Urban Air Pollution and Its Effect on Forced Expiratory Volume of Lungs Dr. Gautam Kumar Lalwani Dr. Gopal Purohit Dr. Suresh Kumar Singh	50-54
09.	Coal Beneficiation Technology for Coking & Non-Coking Coal Meant For Steel and Thermal Power Plants Manoj Kumar Sharma Gohil Priyank Nikita Sharma	55-63
10.	Deployment of Palmic Concrete Pavement Blocks in Light and Heavy Traffic Situations. Eric Ababio Ohemeng Anita Asamoah-Duodu Kofi Owusu Adjei	64-73
11.	Evaluation and analysis of the role of citizen participation in urban development (Case study: the city of Nikshahar) Javad Raisi Gholam Reza Miri Mahsume Hafez Rezazade	74-78

12.	Design and Construction of a Spring Stiffness Testing Machine Olugboji Oluwafemi Ayodeji Matthew Sunday Abolarin Jiya Jonathan Yisa Alaya Garba Muftau Ajani Clement Kehinde	79-84
13.	Influence of Pva, Pvp on Crystal and Optical Properties of Europium Doped Strontium Aluminate Nanoparticles Abutu.A. Nathan AuduD. Onoja AlexanderN. Amah	85-91
14.	TAMIL NEW YEAR COOL DRINK?... ("PANAKARAM") M.Arulmani V.R.Hema Latha	92-101
15.	ARENKA NAYAKI IS MOTHER OF RAMA?... ("SRIRANGAM") M.Arulmani V.R.Hema Latha	102-107
16.	Weight Reduction of 12"-150 Class Plug valve Casting Body by Finite Element Analysis and Experimental Method Prof. Laukik B. Raut Pradnyawant .K.Parase	108-116
17.	A Visual Attention Based Improved Seam Carving For Content Aware Image Rescaling Aparna P Prabu.T	117-123
18.	Evaluation of 3D segmentation methods based on a criterion of homogeneity El Mostafa Rajaallah Basma Sirbal Mohcine Bouksim El Hassan Essoufi Taoufiq Gadi	124-131
19.	Problem of calculating time delay between pulse arrivals Olugboji Oluwafemi Ayodeji. Jiya Jonathan Yisa. Ajani Clement Kehinde	132-142
20.	Non-Auditory Health Hazard Vulnerability to Noise Pollution: Assessing Public Awareness Gap Tanjir Ahmed Taimur Rahman	143-147
21.	An Internet Based Anonymous Electronic Cash System Israt Jahan Mohammad Zahidur Rahman K M Akkas Ali Israt Jerin	148-152
22.	Mammogram Image Segmentation Quality Enhancement Using Clustering Techniques Mrs. Sandhya G Dr. D Vasumathi Dr. G T Raju	153-158

Evaluation for suitable propagation model to mobile Communications in South-South Nigeria urban-terrain

P. Akinyemi¹, S.O. Azi¹, J.S. Ojo², C.I. Abiodun¹

¹Department of Physics, University of Benin, Benin City, Edo State.

²Departments of Physics, Federal University of Technology Akure, Ondo State.

ABSTRACT: One of the underlying difficulties with the application of a predicting path loss models for any environment is that no two areas are identical in the composition of the building and terrain. Many research activities, such as simulation and system design, need a model of the channel under study. This research attempts to investigate the most effective propagation model in South-South part of Nigeria. Two Global Systems for Mobile Communications (GSM) base stations operating at 900MHz and 1800MHz bands were used for the experiment in a typical urban area. The field measurement results were compared with S U I model, Ericsson model, Friis model and Walficsh-Bertoni model for urban area. The results obtained indicate the least variation with Walficsh-Bertoni model for urban area.

KEY WORDS: predicting path loss model, GSM, Field measurements, Walficsh-Bertoni.

I. INTRODUCTION

In wireless communication, signal is transmitted by the transmitting antenna and received by receiving antenna any distortion in signal strength at receiver is known as path loss or Radio wave propagation Model or Radio Frequency Propagation Model. The propagation model is generally of three types. Empirical (statistical) model, Physical (deterministic) model and stochastic model. Empirical models are usually a set of equation derived from extensive field measurements. These models are simple and efficient to use. They are accurate for environments with the same characteristic as those where the measurements were made. One of the main draw backs of empirical model is that they cannot be used for different environment without modification. The deterministic model makes use of laws governing electromagnetic wave propagation to determine received signal power at a particular location. Stochastic model, on the other hand, model the environment as a series of random variable. Stochastic models are the least accurate but require the least information about the environment and use much less processing power to generate predictions. Each individual telecommunication link has to encounter different terrain, path, observation, atmospheric condition and other phenomena; it is intractable to formulate the exact loss for all environments. As a result, different models exist for different conditions. Correct prediction of path loss is a pivotal step of GSM network to estimate external interference level and cell radius accurately in network planning, particularly for conducting feasibility studies and during initial deployment studies to achieve perfect network planning.

II. LITERATURE REVIEW

Path loss is the reduction in power of an electromagnetic wave. Among numerous propagation models, the following are the most significant empirical models providing the foundation of mobile communication services.

1. FREE SPACE PROPAGATION MODEL

In radio wave propagation models, the free space model Predicts that received power decays as a function of T-R separation distance. The path loss for free space model when antenna gains are included is given by

$$PL \text{ (dB)} = - G_t - G_r + 32.44 + 20 \log (d) + 20 \log (f) \quad (1)$$

Where

G_t is the transmitted antenna gain in dB
 G_r is the received antenna gain in dB,
 d is the T – R separation distance in kilometers and
 f is the frequency (MHz)

2. The hata okumura model

The Hata-okumura model is an empirical formula for graphical path loss data provided by Yoshihisa Okumura, and is valid from 150 to 1500 MHz. The Hata model is a set of equations based on measurements and extrapolations from curves derived by Okumura. However, the model neglects terrain profile between transmitter and receiver, i.e. hills or other obstacles between transmitter and receiver are not considered. This is because both Hata and Okumura made the assumption that transmitter would normally be located on hills. The path loss in dB for the urban environment is given by

$$PL \text{ (dB)} = A + B \text{ Log } (d) \quad (2)$$

d is distance in kilometer

A represents a fixed loss that depends on frequency of the signal these parameters are given by the empirical formula.

$$A = 69.55 + 26.16 \log (f) - 13.82 \log (h_b) - a (h_m)$$

$$B = 44.9 - 6.55 \log (h_b)$$

Where

f is frequency measured in MHz

h_b is height of the base station antenna in meters

h_m is mobile antenna height in meters and

$a(h_m)$ is connection factors in dB

For effective mobile antenna height $a(h_m)$ is given by

$$a(h_m) = [1.1 \log (f) - 0.7] h_m - [1.56 \log (f) - 0.8]$$

3. COST – 231 Hata Model

To extend Hata – Okumura – model for personal communication system (PCS) application operating at 1800 to 2000 MHz, the European Co-operative for scientific and Technical Research (COST) came up with COST-231 model. This model is derived from Hata model

$$P_L \text{ (dB)} = 46.33 + 33.9 \log (f) - 18.82 \log (h_b) - a(h_m) + [44.9 - 6.55 \log (h_b)] \log (d) \quad (3)$$

Where, $a(h_m) = [1.1 \log (f) - 0.7] h_m - [1.56 \log (f) - 0.8]$

4. ECC – 33 Model

The ECC 33 path loss model, which is developed by Electronics Communication Committee (ECC), is extrapolated from the original measurements by Okumura and modified its assumptions so that it more closely represents a fixed wireless access (FWA) system.

The path loss model is defined as,

$$P_L \text{ (dB)} = A_{fs} + A_{bm} - G_t - G_r \quad (4)$$

Where,

A_{fs} is free space attenuation,

A_{bm} is basic median path loss,

G_t is BS height gain factor and

G_r is received antenna height gain factor

5 Walficsh-Bertoni model

Considered the impact of the rooftops and building height by using diffraction to predict average signal strength at street level

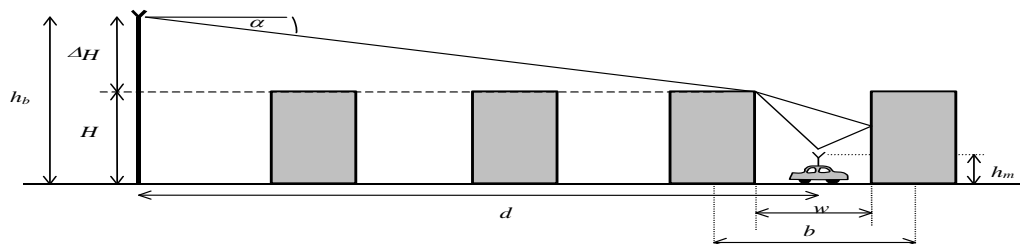


Fig.1: Propagation over rows of buildings from an elevated fixed antenna to a mobile at street level.

Path Gain

$$PG = (PG_0)(PG_1)(PG_2) \tag{5}$$

Free Space path gain

$$PG_0 = \left(\frac{\lambda}{4\pi R}\right)^2 \tag{6}$$

Reduction in the field at the roof top just before the mobile due to propagation past previous rows of buildings given by a factor Q

$$PG_1 = PL_{\text{rooftops}} = P(g)^2 = \left\{0.1 \frac{[\sin \delta \sqrt{d/\lambda}]^{0.9}}{0.03}\right\}^2 \tag{7}$$

$$\sin \delta = \frac{h_T - H_B}{R}$$

$$PG_1 = PL_{\text{rooftops}} = 0.01 \left(\frac{h_T - H_B}{0.03R}\right)^{1.8} \left(\frac{d}{\lambda}\right)^{0.9}$$

Diffraction of the roof top field down to the mobile (add ray power to get the small area average)

$$PG_2 = \left[\frac{1}{2\pi k \rho_1} \left(\frac{1}{|\theta_1|} - \frac{1}{2\pi - |\theta_1|}\right)^2 + \frac{|\Gamma|^2}{2\pi k \rho_2} \left(\frac{1}{|\theta_2|} - \frac{1}{2\pi - |\theta_2|}\right)^2 \right]$$

(8)

$$pG_2 = \left(\frac{\lambda}{4\pi R}\right)^2 (Q^2) \left(\frac{\lambda \rho}{2\pi^2 (H_B - h_m)^2}\right) = \left(\frac{\lambda}{4\pi R}\right)^2 \left(0.01 \left(\frac{h_{BS} - H_B}{0.03R}\right)^{1.8} \left(\frac{d}{\lambda}\right)^{0.9}\right) \left(\frac{\lambda \rho}{2\pi^2 (H_B - h_m)^2}\right) \tag{9}$$

$$= \frac{5.51}{32\pi^4} \left(\frac{(h_{BS} - H_B)^{1.8} \rho d^{0.9}}{(H_B - h_m)^2}\right) \frac{\lambda^{2.1}}{R^{3.8}}$$

For \mathcal{F}_M in MHz and \mathcal{R}_k in km

$$PL_T = 89.5 - 9 \log d - 10 \log \left(\frac{\rho}{(H_B - h_m)^2}\right) - 18 \log (h_{BS} - H_B) + 21 \log \mathcal{F}_M + 38 \log \mathcal{R}_k \tag{10}$$

III. MEASUREMENT PROCEDURE

A site verification exercise was done using testing tool (Ericsson k800i mobile station), calls were initiated at each test point until it established and the signal strength information sent over the air interface between the base station and the mobile station were read. For every site, received signal strength was measured at a reference distance of 200m from the base station and a subsequent interval of 200m up to 2000m in two GSM base stations in urban area of Benin, Edo State and Asaba, Delta State. The obtained values from field measurements are then compared with those calculated using the existing models. The essence of this is to investigate the degree of consistence of these existing models with field measurements.



Fig. 2: Image of the site used



Fig. 3: Log file showing the Rx-level distribution

Parameters	Values for Operator A	Values for Operator B
Base station transmitter power	40dBm	40 dBm
Base station antenna height	40m	42m
Mobile antenna height	1.2m	1.5m
Transmitter antenna gain	17.5 dBm	17.5 dBm
Frequency	900MHz	1800MHz
Feeder loss	2.52	2.58Db
Duplexer loss	4.5Db	4.75Db

Table 1: Simulation Parameter

Distances (Km)	Free Space model (dBm)	S U I model (dBm)	Cost 231 model (dBm)	Walfisch -Bertoni model (dBm)	Ericsson model (dBm)	Test Site (dBm)
0.2	77.56	85.74	104	96.90	116.57	98.38
0.4	83.57	99.63	114.36	108.35	125.70	108.29
0.6	87.1	107.75	120.42	115.04	131.05	114.86
0.8	89.6	113.52	124.72	119.79	134.84	120.22
1.0	91.53	117.99	128.05	123.48	137.80	123.79
1.2	93.12	121.65	130.78	126.49	140.19	126.95
1.4	94.5	124.74	133.08	129.05	142.22	128.97
1.6	95.62	127.41	135.68	131.26	143.98	133.90
1.8	96.64	127.41	136.84	133.21	145.54	136.73
2.0	97.56	131.88	138.41	135.00	146.93	139.30

Table 2: Path Loss Distribution Table for Operator A

Distances (Km)	Free Space model (dBm)	S U I model (dBm)	Cost 231 model (dBm)	Walfisch -Bertoni model (dBm)	Ericsson model (dBm)	Test Site (dBm)
0.2	83.58	92.42	113.27	102.37	120.66	104.94
0.4	89.60	106.23	123.58	113.82	129.80	114.30
0.6	93.12	114.30	129.62	120.51	135.14	120.83
0.8	95.62	120.03	133.90	125.26	138.94	126.01
1.0	97.56	124.47	137.22	128.95	141.88	129.80
1.2	99.14	128.10	139.93	131.96	144.28	134.56
1.4	100.48	131.17	142.23	134.51	146.31	137.13
1.6	101.64	133.83	144.22	136.73	148.08	142.32
1.8	102.66	136.18	146.00	138.68	149.63	147.46
2.0	103.58	138.27	147.54	140.43	151.02	150.24

Table 3: Path Loss Distribution Table for Operator B

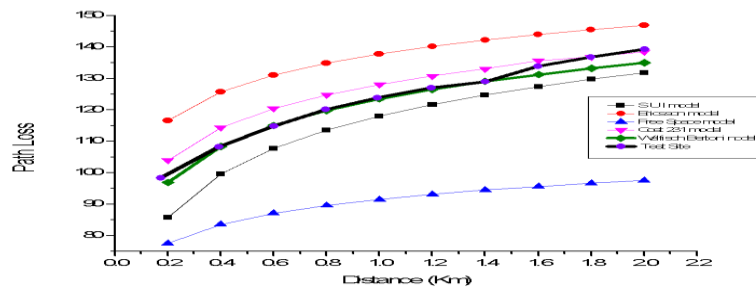


Fig. 4: Path loss Vs Distance Graph for Operator A

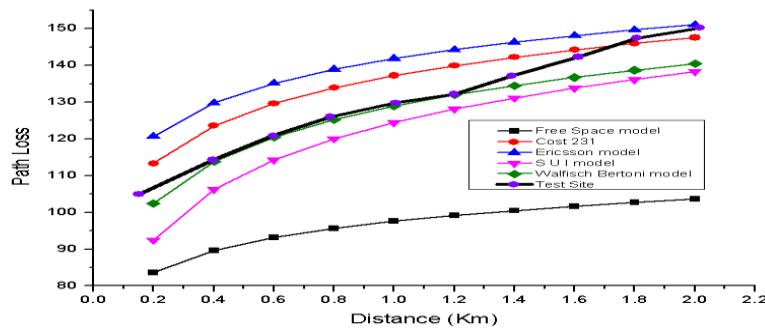


Fig. 5: Path loss Vs Distance Graph for Operator B

IV. CONCLUSION

In this paper, the measured path loss in two cells operating at 900MHz and 1800MHz are compared with theoretical path loss models: Hata, S U I, Ericsson, Cost 231, Free Space and walfish- Bertoni. The path loss distribution graph in Figure 1 and Figure 2 show the relationship that exists among the various propagation in terms of path loss. It can be seen that there are variations between field measurement results and the existing models. An exception is that of Walficsh-Bertoni model in which only a slight variation exists for distance up to 1.4km and 1.2km in operator A and B respectively. For other path loss model examined, there is an appreciable deviation from the measured results. This research thus shows that the Walficsh-Bertoni model for radio wave propagation is very effective for radio wave propagation path loss prediction in two states in South-South part of Nigeria.

REFERENCES

- [1] Erceg, V. and Greenstein, L. J., (1999). An Empirically based path loss model for wireless channels in urban environments. IEEE Journal on Selected Areas of Communications, Vol. 17, pp 1205-1211.
- [2] Parsons, J. D. (2000). The Mobile Radio Channel, Wiley and Sons, New York.
- [3] Rahman, T.A and Ser, G.B; (2000). Propagation measurement in IMT-2000 Band in Malaysia, IEEE Vehicular Technology, Vol. 1, pp 77-81
- [4] Raivio, K., and Laiho, J., (2001). Neural analysis of mobile radio access network. In proceeding of the International Conference on Data Mining (ICDM). PP 457-464
- [5] Saunders, S. R and Belloul, B., (2002). Making Wireless Networks Deliver, Ingenia of the royal Academy of Engineering, Vol. 12 pp. 36-40.
- [6] G. Mao, B. D. O. Anderson and B. Fidan, (2007) " Path Loss Exponent Estimation For Wireless Sensor Network Localization." Computer Network. Vol.51. Iss. 10, pp. 2467-2483.
- [7] T.S. Rappaport, (2003) "Wireless Communication", Pearson Education.
- [8] Emagbete, J.O and Edeko, F.O., (2009). Measurement Validation of the Hata-Like Models for Radio propagation path loss in Rural Environment at 1.8GHz. Journal of Mobile Communication 3(2), 17-21.
- [9] ITU-R Rec.P.526-11, (2009). Propagation by Diffraction. ITU.
- [10] Shoewu, O. and Adedipe, A., (2010). Investigation of Radio Waves Propagation Models in Nigeria Rural and Sub- Urban areas. American Journal of Scientific AND Industrial Research 1(2) pp. 227-322.

Framework for Evaluation and Improvement of Work over Rigs in Oilfields

Haitham Mansour¹, Prof. Mohammad Munir Ahmad²

¹(School of Science and Engineering/ Teesside University, UK & Omar Al-Mukhtar University, Faculty of Engineering Tobruk, Libya)

²(School of Science and Engineering/ Teesside University, UK)

ABSTRACT : The aim of the work is to develop a framework evaluation for operational performance of the work over rigs in oilfields. This framework is used as a basis to analyse and enhance the performance of the work over rig including the improvement in rig efficiencies and reduction in operational costs. The framework is built on the collection and analysis of the overall equipment efficiency (OEE) established from the data gathered by the work over and production engineers on the work over rig. It can be usefully adopted in certain circumstances to calculate the efficiency of work over rigs. The results of measure OEE are effective when used to improve the work over rig and ESP efficiencies. To illustrate some of our work we present and discuss results from one of many case studies, which demonstrate the value of maintenance strategies such as framework. The framework and OEE measure are shown to be effective when used to improve rig efficiency and reduce downtime cost. Finally, the work suggests a way that can help both work over rigs and ESP users to cooperate with an aim to help oil wells to produce more with efficient equipment at any oilfield

KEYWORDS - Overall Equipment Efficiency (OEE), Workover, efficiency

I. INTRODUCTION

The oil and gas industry spends millions of dollars each year collecting vast amounts of drilling data, yet has not made effective use of this data to improve drilling performance. With rig costs estimated to consume 37% or USD 92.5 billion of that spending, every effort to reduce drilling time has a direct impact on our bottom line. Estimates of non-productive time (NPT) ran from 15–40% or USD 14–37 billion, depending on well type, maintenance and operator [1].

Workover supports oilfields to return oil wells to production by delivering operating equipment reliability and operating equipment risk reduction. The oil wells are dependent of maintenance services such as cleaning, reinstatement and stimulation. These services can be performed by a limited number of workover rigs. Usually, wells need maintenance services and a preparation of the workover rigs must be defined. This preparation must consider some factors such as the well production, the type of service to be performed and time windows for the well maintenance [2].

There is a production loss associated to wells waiting for maintenance services, so it is important to attend them as soon as possible. Thus, the workover rig scheduling problem consists of finding the best schedule for the limited number of workover rigs, minimising the production loss associated with the wells waiting for maintenance service [3].

The workover rigs must service oil wells requesting maintenance as soon as possible. When a well requires maintenance, its production is reduced or stopped for safety reasons and some workover rig must service it within a given deadline. It is therefore important to service the wells in a timely fashion in order to minimise the production loss. The total cost includes the rig expenses (transport, assembly and operation), which are functions of time and distances, plus the losses of revenue in the wells waiting for the rig, which are dependent on time [4].

The purpose of the study is to investigate the current problems and practice in the workover activities in the Oilfield. This study evaluates the steps needed to implement Total Productive Maintenance (TPM), based on how it is defined by Nakajima (1988) and H. Mansour & M. Munir (2013) [3].

In this work the Practical Framework is mainly built on a quantitative measure of performance based on data collection and subsequent analysis of overall equipment effectiveness (OEE) originally introduced by Nakajima (1988). The Framework method, when implemented in the company, resulted in the operators recognising the benefits that OEE carries in tracking and reducing hidden losses to improve their workover rig's efficiency. In addition, in this research, we show how a simplified version of this OEE measure can be usefully adopted in certain circumstances to calculate the efficiency of workover rigs. Both Framework and the OEE measure are shown to be effective when used to improve equipment efficiency [6].

1.1 Workover Processes

Workover program is an orderly step-by-step procedure to be followed in conducting the workover operation. This procedure of the workover include the main stage of workover processes, the first step in the process is to move the rig to the location of the oil well where many procedures must be followed in order to return the oil well to normal production see fig 1. The procedures such as the rig up (R/U), rig down (R/D) and ESP installation, Run in Hole (RIH) and pull out of hole (POH) of the equipment such as ESP. The program must provide operating personnel with all information necessary to achieve the required objectives safely at the minimum cost and with the minimum expenditure of resources [7 and 8].

Oil well inspection and workover consists of measuring actual processes from start to finish the workover job. To keep oil wells ruing, they require maintenance and repair, from time to time, due to normal wear and tear, age and the effects of the environment to which the equipment is exposed. Workover operations include any number of activities performed on a well, after initial completion, including recompletion and remedial repair work to achieve the required objective safely, at the minimum cost, with minimum expenditure of resources [10].

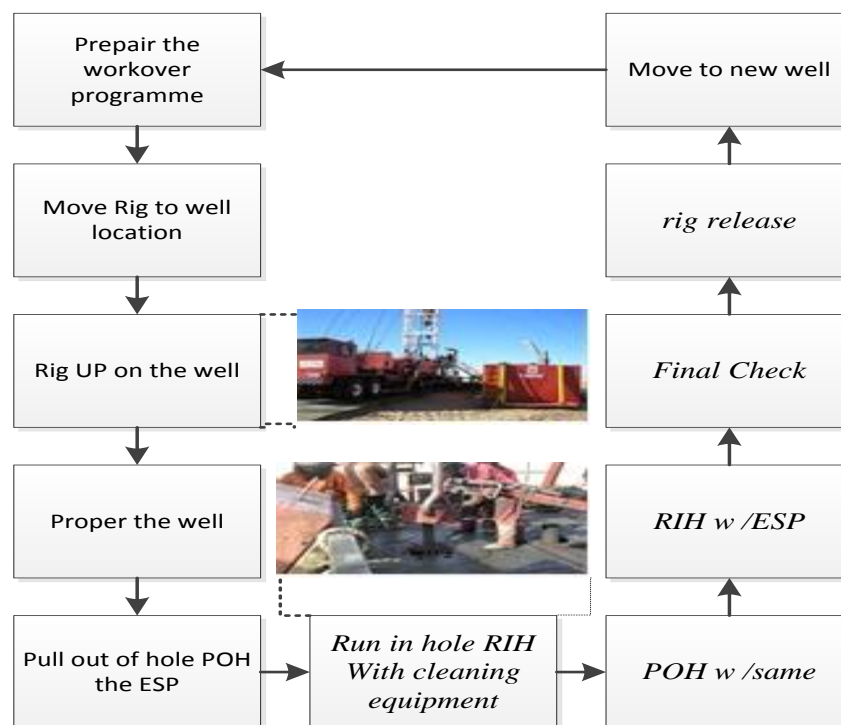


Figure 1: The Main Stage of Workover Processes (Mansour 2012)

II. PURPOSE OF OEE IN OIL INDUSTRY

In the oil industry, every well in the oilfield is a product line to produce the oil; it has many processes to keep the oil well in production [6]. The oil well is as a small manufacturing plant and each plant needs different equipment as the conditions for each plant are unique [1 and 7]. In the field of application of OEE in oil and gas industries, the researcher compares the overall equipment effectiveness in workover rigs with World Class Manufacturing [4 and 6].

2.1 Overall Equipment Effectiveness (OEE) For Workover

Equipment effectiveness includes equipment availability, performance efficiency and rate of quality of output. Operational performance data collection of the three OEE variables, availability, performance and quality [13and 3]

$$OEE = \text{availability} \times \text{performance} \times \text{quality}$$

The first element of the OEE calculation is process availability: It is the ratio of the workover time to the planned workover time [3].

$$\text{Availability \%} = \frac{\text{workover operating time}}{\text{planned workover time}}$$

$$\text{Planned workover time} = \text{TWT} - \text{breaks}$$

$$\text{Workover operating time} = \text{planned workover time} - \text{downtime}$$

The second element is “performance rate”. This element measures the ratio of the best time achieved to the actual time. That has been calculated in the method of evaluation of the workover [3].

$$\text{Performance \%} = \frac{\text{BTWT}}{\text{TWT}}$$

Where :

BTWT(hours) = total best (historical) time achieved by workover rig = moving + Rig Up
+ pulling ESP + RIH with equipment + POH with equipment + RIH with ESP + Final check + Rig release

TWT(hours) = total workover time (actual time) = moving + Rig Up + pulling ESP + RIH with equipment
+ POH with equipment + RIH with ESP + Final check + Rig release

The third element of the OEE calculation is the “quality rate”, and is used to indicate the proportion of defective time for good workover to the total workover time [3].

$$\text{Quality \%} = \frac{\text{time for good workover}}{\text{time for total workover}}$$

III. RIG EFFICIENCIES

The rig efficiencies of four rigs in different oilfields in Libya (Sarir, Nafoora and Messla oilfields) have evaluated to identify the gap for improvements. The below table 1 shows many examples of results obtained with evaluation method of the workover rig efficiency. It shows the average efficiency of the rigs and also the efficiency of the rigs.

Table 1: workover rig efficiencies

Rig No.	Oilfield name	Average rig efficiency %	Highest efficiency achieved by rig %	lowest efficiency achieved by rig %	Gap identified for improvement%
Rig 10	Sarir	70	93	48	45
Rig 23	Sarir	68	83	52	31
Rig 32	Nafoora	67	84	51	33
Rig 21	Messla	66	85	54	31

The variation in efficiencies identifies the potential for improvement. For example, the highest efficiency is 93% for rig number 10 in Sarir oilfield, and the lowest efficiency is 48% for rig 10 at the same oilfield. Therefore it is possible that in practice all the rigs could perform at 93% efficiency given the right procedures adopted with very little variation. Therefore, a workover rig in this case study should be most efficient if it is running at the highest efficiency achieved.

Each year, non-productive time during drilling operations costs the oil and gas industry billions of dollars; this equates to a loss of approximately one-third of oil and Gas Company's average annual drilling budget. The downtime Cost can give a good display to see the impact of the rig efficiency [9]. It can be seen in the figure 6 the improvement in each rig can be performed and the improvement of the efficiency of the rigs can be maintained. Each rig has target obtained hours in each steps of the workover operation.

The improvement in workover procedures greatly could reduce the downtime caused by incorrect operating procedures while a good workover program reduces downtime caused by worse workover procedures could be achieved [9].

Table 2: Summary statistics for Rigs downtime (DT).

	Rig10	Rig23	Rig32	Rig21
Av. Rig Efficiency %	70%	68%	67%	66%
Av. TWT	70.9	70.8	69.4	70.7
Av. DT hrs	13.1	22.8	14.54	20.5
Av DT cost £	19,926	33,816	20,863	33,514
DT cost %	20%	34%	20%	30%

The variation in downtime (DT) and its impact on different workover rigs (table 2) reflects the condition of the rig equipment, the quality of the rig equipment, the quality of workover programme and the company's operating policies, the location of the well, and the nature of the work.

The utilisation of the resources is the main factor that affects both the performance and profit of a company, this means decreasing the downtime hours and keeping operation running without any failures. The facility in this research will be workover Rig in the Libya area focusing on the performance improvement.

Is it possible for workover to implement TPM in the way it has been mentioned. In order to address this question the solution could lie in a simple and practical maintenance framework for these companies to follow, and allow them to improve their situations, taking into consideration their time, abilities and resources. The framework could be presented as a solution for workover rigs efficiency problem.

IV. PROPOSED FRAMEWORK

The framework's steps as shown in table 3 are strongly based on the twelve steps of Nakajima's development program with different degree of sophistication [13 and 6]. Framework, as a method concentrates on the elements that are practical and suitable for maintenance development program, which are training, autonomous maintenance, and periodic maintenance [6].

In this work, the framework can be defined as a procedure that provides a practical workover maintenance system for workover rig and production engineers in the oilfield. This procedure involves operators, Electrical Submersible Pump (ESP) technicians in the workover jobs acting as a team to monitor the workover procedures including ESP processes (installation and uninstallation) and reduce the production losses in the oil wells by return the oil well to production at right time. In the first section, framework is defined and its linkage to Nakajima's twelve steps of TPM illustrated. Then each framework step is defined in detail and the way it could be used and implemented.

Table 3: Brief description of framework steps.

Framework Steps	Description
One	Determine the gap between target and actual OEE in the workover activities.
Two	Introduction of framework to staff by the management
Three	Improve relationship between operators and maintenance people
Four	Launch education and training to improve worker's skills
Five	Monitor process performance, set/raise target level
Six	Implement autonomous maintenance
Seven	Implement periodic maintenance

The oil production company's workforce can implement framework steps without the need for external advisers. These steps, as shown in table 3 above are flexible and can be tailored by engineers and the management to the individual oil company's capabilities, where each company could develop its plans differently because of different needs and challenges they are faced with, depending on the different artificial methods applied in the oilfield, production equipment conditions, and type of rigs.

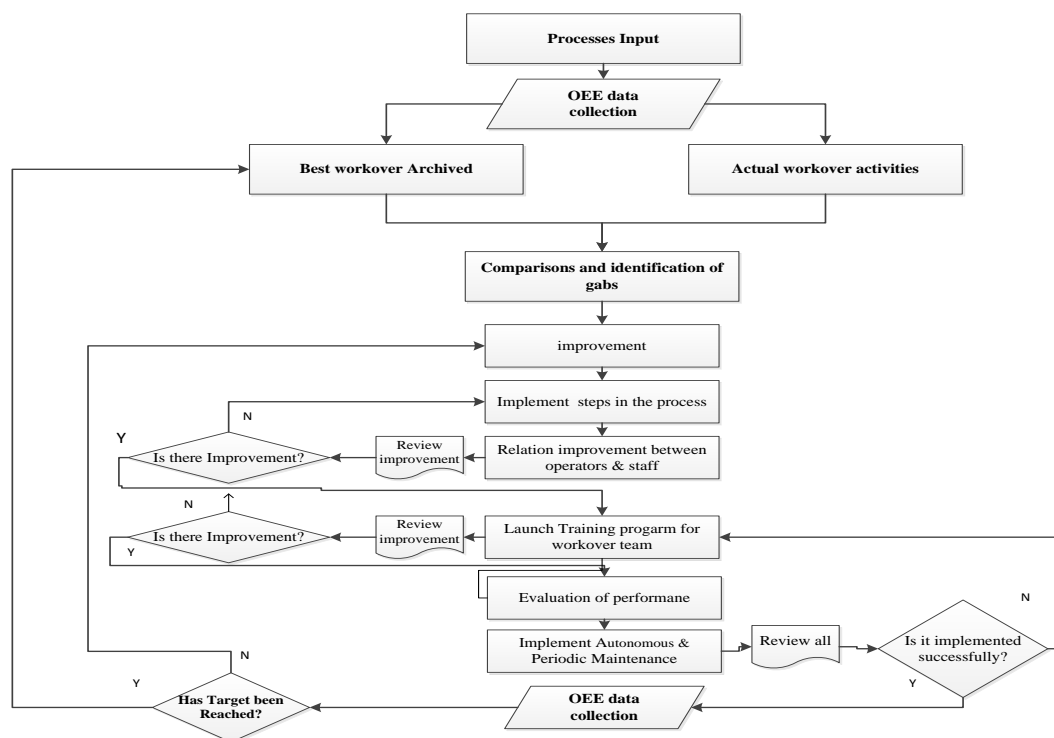


Figure 2: Framework for Evaluation and Improvement of Workover Rigs in Oilfields [6].

The fundamental measure of the method is the overall equipment effectiveness (OEE) value, which as described by Nakajima (1989), should be the driving force and provides direction for improvement-based activities within manufacturing organizations. The framework proposed in Fig. 2 supports workover rigs and production engineering department in oil companies in four ways; first, the framework is simple and easy to follow as it only has three stages and seven steps. Second, framework does not require a significant financial commitment; steps could be implemented by the production engineers at oilfields (there is no need for a consultant to explain and help implement the method) and training is carried out by the crew (operators) and workover engineers at the rig and this reduces the additional financial pressure. The maintenance technicians will train the workover operators on autonomous maintenance and will be responsible for planning their own periodic maintenance program. This is because maintenance technicians are the best people that have the maintenance skills to train workover operators, and also have the knowledge and experience to plan their periodic maintenance program [6].

Third, improvements could be achieved shortly after implementation. Fourth, the framework does not involve specialist TPM teams and committees; instead there is only a single team to which everyone in the company will be attached. The benefit that companies will gain by applying framework is through the reduction of lost time, wasted effort and incurred cost. [6]

V. CASE STUDY - WORKOVER RIG NUMBER (10)

In this case study a workover rig number 10 in Sarir oilfield has been chosen to implementing the framework, the introduction and preparation stages took seven working days, and the research was agreed to be applied on only two workover rigs. The ideal cycle time is a standard known value for the machine. The workover manager and the maintenance and ESP technicians were responsible for investigating any problems on the workover rig that caused the decline in OEE.

The implementation of framework on one workover rig took only a short time to be accomplished in this case study. The total time of the introduction and preparation stages was only seven working days. Each oil well has taken an average of 6 to 8 days from start to return the well to production. On the other hand, the implementation of AM helped in reducing breakdowns on the rig by controlling and eliminating contamination on the rig machines and in the surrounding area.

The purpose of this case study was to show that the Production Engineering Department (PED) management at oilfields can improve the workover rig's efficiency and quality which allows engineers to return the oil well to production in the correct time to minimise costs and maximise production.

Table 4: OEE for Rig data

Rig No	Well No.	DT (hrs)	BTW T In work (hrs)	Total operating Hours	Availability	Performance	Quality	OEE	Average OEE
Rig 10	well 1	13.2	44.5	75.5	88%	59%	53%	28%	27%
	well 2	22.8		85	87%	52%	46%	21%	
	well 3	14.4		70	79%	64%	53%	27%	
	well 4	22.5		54	65%	82%	62%	33%	

The practical method for evaluating the operational performance of workover activities in Sarir oilfield is varies greatly. The rig 10 efficiencies remain relatively constant when they are operated in the different locations. The table 4 shows the combined effect of rig efficiency and the efficiency to perform all other workover operations as the effective daily workover cost, which is a practical measure of the overall workover performance. Each rig has target obtained hours in each steps of the workover operation. The table 4 below shows many examples of results of current OEE obtained. The data obtained from the workover rig in Table 4 above showed that Average OEE was only 27%. After OEE was analysed we were able to show the PED the causes of loss on the equipment. When the causes were located and identified, it was explained to the PED management how the workover crew and ESP technicians could eliminate the causes of these problems with the help of framework. We explained to the PED management that when AM is implemented on the rig equipment it could help reduce and eliminate the causes of ESP failure.

4.1 Framework Application

The steps, as shown in table 3 in previous section (IV) are flexible and can be tailored by PED engineers and the PED management to the individual oilfield’s capabilities, where each oilfield could develop its plans differently because of different needs and challenges they are faced with, depending on the different artificial methods applied in the oilfield, production equipment conditions, and type of rigs. The fundamental measure of the method is the OEE value, which as described by H. Mansour and M. Munir (2013), should be the driving force and provides direction for improvement-based activities within workover rig activities [3].

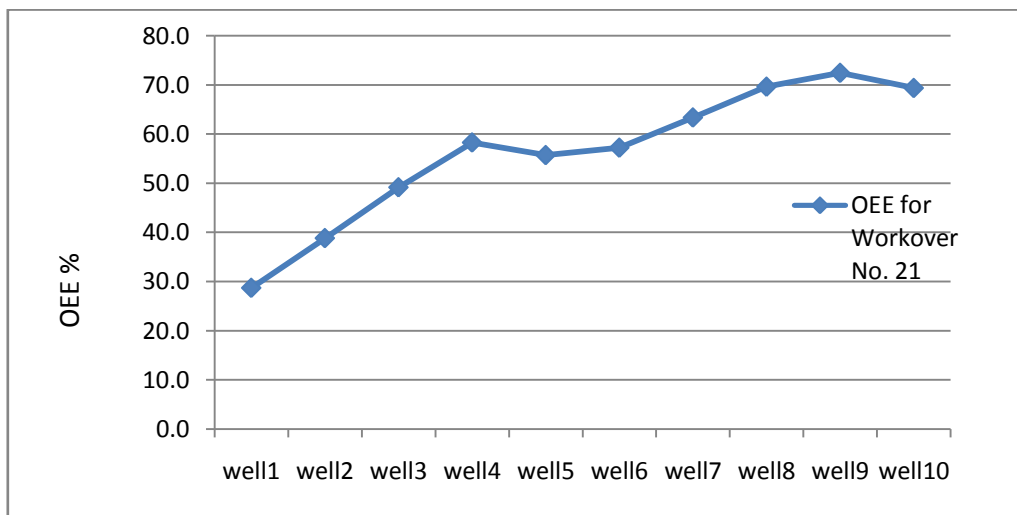


Figure 3: OEE for Rig 21

We explained to the PED that periodic maintenance would help reduce major and minor breakdowns on the machine thereby improving the condition of the machine. In addition, we explained how OEE could help the PED to track any causes of reduction in the workover rig’s efficiency.

The results of OEE has been improved, the OEE for the first rig selected has increased from approximately 29 % to 72 %. This is the result of improvement in: availability, performance efficiency and rate of quality as in Fig 3.

The framework introduced in this research contributes mainly in terms of the following features. First, the framework identifies factors that cause downtime. Second, the framework emphasizes the importance of focusing on crew-level factors. Third, the framework shows how the ramifications of downtime can occur by generating a feedback structure through managerial action and decisions. Finally, the framework provides a framework for tracing the causes of downtime and its impact on project performance.

Table 4 summarises overall evaluation results the DT cost impacts on the workover in each workover job from well number 1 up to well number 10 against the OEE results during the study period. The framework presented in this paper could assist managers in minimising the impact of downtime by providing insight into equipment management [6].

Table 4: Summarizes of overall evaluation results

Well No.	Previous OEE %	Current OEE %	Downtime/ hr	Downtime cost £
Well 1	28.7	28.7	20	33,514
Well 2	28.7	38.8	18	29,986
Well 3	38.8	49.2	14	23,215
Well 4	49.2	58.3	10	16,500
Well 5	58.3	55.7	8	13,405
Well 6	55.7	57.2	6	10,000
Well 7	57.2	63.4	5	8,400
Well 8	63.4	69.6	3	5,001
Well 9	69.6	72.4	3	5,024
Well 10	72.4	69.4	2	3,300

The implementation of framework on one workover rig took only a short time to be accomplished in this case study. The total time of the introduction and preparation stages was around 4 months. Each oil well has taken an average of 6 to 8 days from start to return the well to production. On the other hand, the implementation of AM helped in reducing breakdowns on the rig by controlling and eliminating contamination on the rig machines and in the surrounding area.

The workover process improvement opportunities continue to be identified based on OEE results and new variations of these measures can be implemented for other oilfields using the same artificial lift method [2 and 4]. Workover supports oilfields to return oil wells to production by delivering operating equipment reliability and operating equipment risk reduction. Good and bad workover procedures affect both the cost and time of operations [2 and 4].

VI. CONCLUSION AND FUTURE WORK

The result of the study was impressive, in that framework helped improve the overall equipment effectiveness of a chosen machine in the workover rigs, from 29% to approximately 72%. This was the result of a cooperative effort of the operator and the maintenance staff. The period of improvement was short, being only eight months. Due to this success, the management decided to commit to further implementation of framework on other workover rigs.

The results of the example show that the proposed method of OEE is very effective for doing improvements to increase the effectiveness of the workover procedures within specific time period by identifying the problem exactly. However, the importance of practical workover performance measure which can aid in rig procedures negotiation and rig selection. Improvements tools such as TPM can be applied to enhance the performance of workover activities. Further, the metric OEE for workover activities can be used as a benchmark at various levels to achieve world-class standard in other sectors such as manufacturing sector.

Extension to this work is to initiate further studies on the effectiveness of framework, based on the extension of cost analysis on different rig drilling and workover companies on both onshore & offshore operations with different cultural backgrounds. This would enable a comparison of the applicability of the method to different company's results with the research finding.

REFERENCE

- [1] Staveley, Catheryn, and Paul A. Thow. "Increasing Drilling Efficiencies Through Improved Collaboration and Analysis of Real-Time and Historical Drilling Data." *SPE Intelligent Energy Conference and Exhibition*. Society of Petroleum Engineers, 2010.
- [2] Ribeiro, Glaydston Mattos, Geraldo Regis Mauri, and Luiz Antonio Nogueira Lorena. "A simple and robust Simulated Annealing algorithm for scheduling workover rigs on onshore oil fields." *Computers & Industrial Engineering* 60.4 (2011): 519-526.
- [3] H. Mansour, M.Ahmad, , N. Dhafir and H. Ahmed: "Evaluation of operational performance of workover rigs activities in oilfields", *International Journal of Productivity and Performance Management* , Vol.62, No.2, pp. 204-218, 2013.
- [4] M. Masahiro, Y. Yutaka and K. Osamu, "ESP Performance in Mubarraz Field", *International Petroleum Exhibition and Conference*, SPE 87257, UAE. 2000.
- [5] M. Ahmad, & R. Benson, *Benchmarking in the Process Industries*, IChemE. 1999.
- [6] H. Mansour, M. Ahmad & F. Ahtita, "Practical Evaluation Workover Framework (PEWF) for Evaluation and Process Improvement of Workover Rigs", *Proceedings of 24th International Conference on Flexible Automation and Intelligent Manufacturing*, pp. 118-126, San Antonio, Texas, USA, 2014.
- [7] H. Mansour, M. Ahmad & H. Ahmed, "A practical method for evaluating operational performance of workover activities in Sarir oilfield", *Proceedings of 20th International Conference on Flexible Automation and Intelligent Manufacturing*, pp. 799-807, Helsinki, Finland, 2012.
- [8] H. Mansour, M. Ahmad & H. Ahmed, "Potential using of OEE in evaluating the operational performance of workover activities", *Proceedings of 23th International Conference on Flexible Automation and Intelligent Manufacturin.*, pp. 877-886, Porto, Portugal, 2013.
- [9] H. Mansour, M. Ahmad & G. Abdulrahman, "Downtime model development for evaluating operational performance of workover activities in AGOCO", *Proceedings of 23th International Conference on Flexible Automation and Intelligent Manufacturing*, pp. 865-876, Porto, Portugal, 2013.
- [10] H. Mansour, M. Ahmad & N. Dhafir. "An investigation into benchmarking of workover activities of rigs in the oilfields", *Proceedings of 20th International Conference on Flexible Automation and Intelligent Manufacturing*, pp. 775-781, Helsinki, Finland, 2012.
- [11] S. Zandieh, S.Tabatabaei, M. Ghandehary: "Evaluation of Overall Equipment Effectiveness in a Continuous Process Production System of Condensate Stabilization Plant in Assalooyeh", *interdisciplinary journal of contemporary research in business*, Vol.3, No.10, pp. 590 - 598, 2012.
- [12] L. Pintelon., S.K. Pinjala and A. Vereecke: "Evaluating the effectiveness of maintenance strategies", *Journal of Quality in Maintenance Engineering*, Vol.12, No.1, pp. 7 - 20, 2011.
- [13] S. Nakajima, *ntroduction to TPM: total productive maintenance*, 1988.

Compositional analysis of lignocellulosic materials: Evaluation of an economically viable method suitable for woody and non-woody biomass

Augustine O. Ayeni,^{1*} Opeyemi A. Adeeyo¹, Oyinlola M. Oresgun¹, Temitayo E. Oladimeji¹

¹Department of Chemical Engineering, Covenant University, Ota, Nigeria

ABSTRACT: The determination of the composition of lignocellulosic substrate is a crucial step in order to determine the overall efficiency of the processes designed to convert lignocelluloses to ethanol. Standard methods as gravimetric, chromatography, and spectroscopic are routinely explored in the scientific literature. This paper details our investigations in the application of economically viable gravimetric methods particularly suitable for developing countries. The methods were proven to be reproducible and representative for the analysis of biomass as sugarcane bagasse, siam weed, shea tree sawdust.

Keywords: Gravimetry, lignocelluloses, biomass, extraction, analysis

I. INTRODUCTION

The overall efficiency of processes designed to convert lignocellulosic biomass to ethanol lies on determining the compositions of such material. Lignocelluloses mainly consist of cellulose, hemicelluloses, and lignin which are bonded together by covalent bonding, various intermolecular bridges, and van der Waals' forces forming a complex structure, making it resistant to enzymatic hydrolysis and insoluble in water [1]. Lignocelluloses continue to be investigated as a source of fermentable sugars for biofuel (ethanol) production because of their high availability [2]. Lignocellulosic biomass includes all plants and plant derived materials, including agricultural crops and trees, wood and wood residues, municipal residues, and other residue materials [3]. The Cellulose (40–55% of total feedstock dry matter) is a glucose polymer linked by β -1,4 glycosidic bonds with the degree of polymerization from 10,000 in native wood to 1,000 in bleached kraft pulps. The basic building block of this linear polymer is cellobiose, a glucose-glucose dimer. Cellulose has a strong tendency to form intra- and inter-molecular hydrogen bonds by the hydroxyl groups on the linear cellulose chains, which stiffen the straight chain and promote aggregation into a crystalline structure and give cellulose a multitude of partially crystalline fiber structures and morphologies. Hydrolysis of cellulose results in individual glucose monomer. This process is also known as saccharification. Its density and complexity resist hydrolysis without preliminary chemical or mechanical degradation or swelling. In nature, cellulose is usually associated with other polysaccharides such as hemicellulose (xylan)/or lignin. It is the skeletal basis of plant cell walls [4]. It contains both crystalline (70%) and non-crystalline or amorphous (30%) structure. Hemicellulose (24–40% of total feedstock dry matter) is a short, highly branched polymer of five carbon (C_5) and six carbon (C_6) sugars. Specifically hemicellulose contain xylose (xylose has acidic group glucuronic acid which makes it more resistant to enzymatic hydrolysis) and arabinose (C_5) and galactose, glucose, and mannose (C_6). It is more readily hydrolyzed compared to cellulose because of the branched amorphous structure. A major product of hemicelluloses hydrolysis is the C_5 sugar. The monosaccharides released upon hemicellulose hydrolysis include a large fraction of pentoses [5]. Lignin is a highly cross-linked phenyl propylene polymer and the largest non-carbohydrate fraction of lignocellulose. It's the third major component of lignocellulosic biomass. In wood biomass it makes up 25–36% depending on the type of wood. It plays an important role in cell wall structure as a permanent bonding agent among plant cells. Unlike cellulose, lignin cannot be depolymerised to its original monomers. Lignin and hemicellulose form a sheath that surrounds the cellulosic portion of the biomass. Lignin protects lignocellulose against insect attack. This complexity has made it as resistant to detailed chemical

characterization as it is to microbial degradation, which greatly impedes the understanding of its effects. Cellulose, hemicelluloses, lignin and the other components are ordered in varying composition in the different parts of the fibre wall depending on the species of biomass. Extractives include non-structural components that are non-chemically bound components of biomass such as sucrose, nitrate/nitrite, protein, ash, chlorophyll, waxes. The extractives are removed because they potentially interfere with downstream analysis of biomass sample. Gravimetric analysis describes a set of methods for the quantitative determination of a sample or material based on the mass of a solid. Mostly, collected dried solids are weighed with an analytical balance. When carefully followed especially during weighing, gravimetric method can provide precise analysis. It provides very little room for instrumental error. It does not require expensive equipment. Determination of the composition of lignocellulosic substrates using gravimetric analysis exists in scientific literature. These included the monoethanolamine method [6], the trifluoroacetic acid method [7], concentrated sulphuric acid method [8]. Acid and neutral detergent method [9]. These methods are directly applicable to specific lignocelluloses, and the sources of the materials [2]. Therefore, the present study aims at a simple, economically viable, and readily available procedures devoid of very sophisticated equipment for lignocellulosics compositional analysis. Estimations of extractives, cellulose, hemicellulose, lignin, and ash can potentially be performed by gravimetric determination.

The study detailed our investigations using gravimetric method for the compositional analysis of lignocellulosic biomass with evaluations on sugar cane bagasse, siam weed, and shea tree sawdust [3,10-12].

II. MATERIALS AND METHODS

Chemicals, reagents, and raw biomass materials: All chemicals and reagents used in this study were of analytical grade and commercially available. Raw biomass materials were sugar cane bagasse, siam weed, and shea tree sawdust.

Preparations of raw biomass: Sugar cane (*Saccharum officinarum*) was purchased from an open market in late November, 2012 from Zaria Town (11°04'N 7°24'E), Kaduna State, Northern Nigeria. The juice was extracted from the sugar cane stalks (local name as Ireke) at a local mill in Ota (6°40'N 3°14'E), Ogun state, Nigeria. The biomass without the juice was air-dried in an open space (average temperature of 35±2 °C) for three days (8 h per day). The stem of the siam weed (*Chromolaena odorata*, local name as ewe Akintola or ewe Awolowo) was harvested from a nearby fallow land (bush) in Ota, Ogun State, South West, Nigeria [12]. After it was harvested, it was sun dried for days. The sample size was reduced to about 2 cm in length for effective milling. Size reduction was carried out on both sugarcane bagasse and siam weed by knifing and milling. The Shea tree (local name as Igi Ori), *Vitellaria paradoxa*, was harvested from the forest around Idanre (6°51'N 5°06'E), south west, Nigeria in early April 2010. The logs were reduced to different sizes at the central processing unit of the local sawmill (Ilepa, Ifo, Nigeria; 6°49'N 3°12'E) [10]. The residues after this milling were used for the compositional analysis. A portion of the materials was screened into different sizes using a sieve shaker. While the remaining portion was labeled as unscreened. Fig. 1 shows the biomass materials before and after size reduction.

Compositional analysis of the raw lignocellulosic materials: Each of the biomass materials was subjected to compositional analysis using the gravimetric method. Materials used in this study were all unscreened. The schematic representation of the step-by-step compositional analysis is as shown in Fig. 2.

Extractives: 2.5 g of dried raw biomass was loaded into the cellulose thimble. With the Soxhlet extractor set up, 150 mL of acetone was used as solvent for extraction. Residence times for the boiling and rising stages was carefully adjusted to 70 °C and 25 min respectively on the heating mantle for a 4 h run period. After extraction, the sample was air dried at room temperature for few minutes. Constant weight of the extracted material was achieved in a convection oven at 105 °C. The %(w/w) of the extractives content was evaluated as the difference in weight between the raw extractive-laden biomass and extractive-free biomass [13-15].

Hemicellulose: 1 g of extracted dried biomass was transferred into a 250 mL Erlenmeyer flask. 150 mL of 500 mol/m³ NaOH was added. The mixture was boiled for 3.5 h with distilled water. It was filtered after cooling through vacuum filtration and washed until neutral pH. The residue was dried to a constant weight at 105 °C in a convection oven. The difference between the sample weight before and after this treatment is the hemicellulose content (% w/w) of dry biomass [10, 13-15].

Lignin: 0.3 g of dried extracted raw biomass was weighed in glass test tubes and 3 mL of 72% H_2SO_4 was added. The sample was kept at room temperature for 2 h with carefully shaking at 30 min intervals to allow for complete hydrolysis. After the initial hydrolysis, 84 mL of distilled water was added. The second step of hydrolysis was made to occur in an autoclave for 1 h at 121 °C. The slurry was then cooled at room temperature. Hydrolyzates were filtered through vacuum using a filtering crucible. The acid insoluble lignin was determined by drying the residues at 105 °C and accounting for ash by incinerating the hydrolyzed samples at 575 °C in a muffle furnace. The acid soluble lignin fraction was determined by measuring the absorbance of the acid hydrolyzed samples at 320 nm. The lignin content was calculated as the summation of acid insoluble lignin and acid soluble lignin [16].

Cellulose: The cellulose content (%w/w) was calculated by difference, assuming that extractives, hemicellulose, lignin, ash, and cellulose are the only components of the entire biomass [13-15].

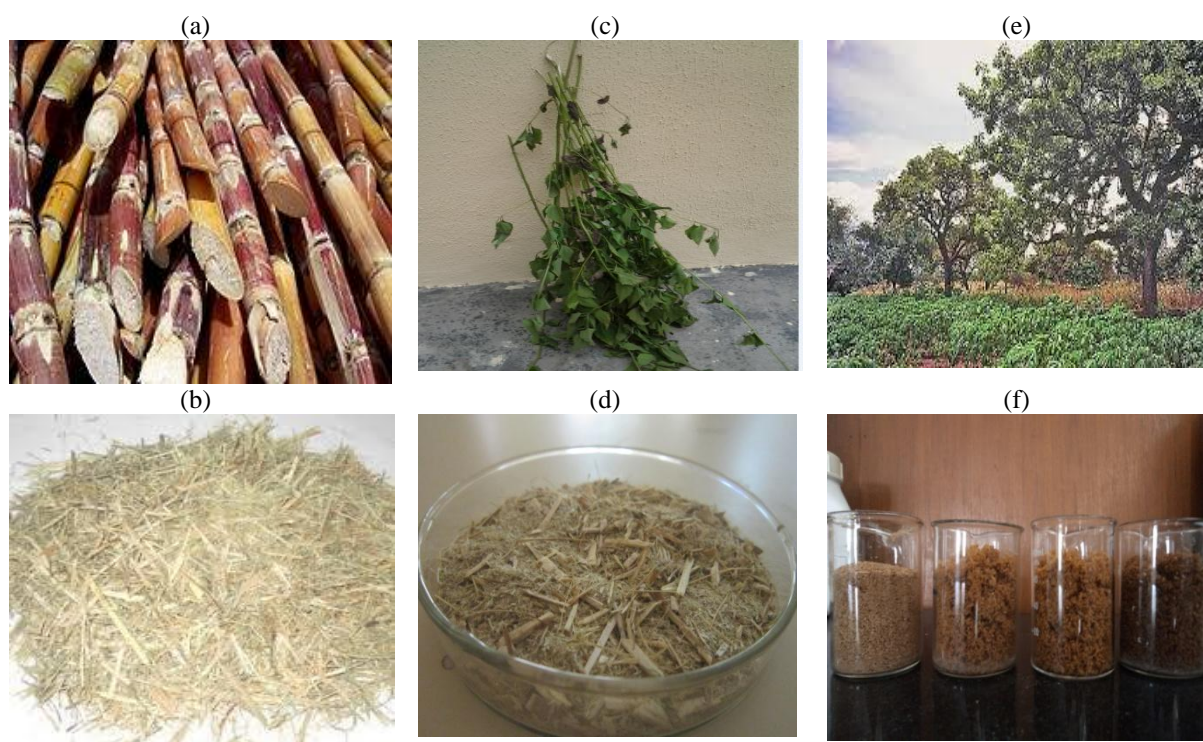


Fig. 1: Raw biomass before and after size reductions. Sugar cane (a); unscreened sugar cane bagasse (b). Siam weed including the leaves (c); unscreened sample of siam weed (d). Shea tree (e); screened shea tree sawdust (f).

III. RESULTS AND DISCUSSION

The basic compositions of the three lignocellulosic materials is as shown in Table 1. Each experiment was replicated twice; reported results indicate the average values of the replicated experiments. Studies have been reported for other varieties of sugarcane bagasse (Table 2)[18-22], and shea tree sawdust [10]. To the best of the authors knowledge, there is no comprehensive information for Nigeria sugarcane bagasse and siam weed varieties.

Results in this study are comparable to those available in the literature (Table 2). Biomass compositions vary according to whether woody or non-woody, geographical locations of materials, methods (procedures) developed for analysis, biomass variety, differences in solvents and the part of plants used in the compositional analysis. Shea tree composition falls within most reported values for woody biomass [23]. For example, Pettersen [24] reported lignin content for Douglar fir to be 32%(w/w) and for red pine lignin as 29%(w/w), total carbohydrate as 63%(w/w). Douglar fir total carbohydrate content was about 67%(w/w) [24]. Sugar cane bagasse total carbohydrate content was about 69%(w/w) which is comparable to most other reported values in the

literature (Table 2). Siam weed, an herbaceous plant, has a total carbohydrate content of about 70%(w/w) which is comparable to most herbaceous biomass values such as corn stover 61.7%(w/w), wheat straw 58%(w/w)[23].

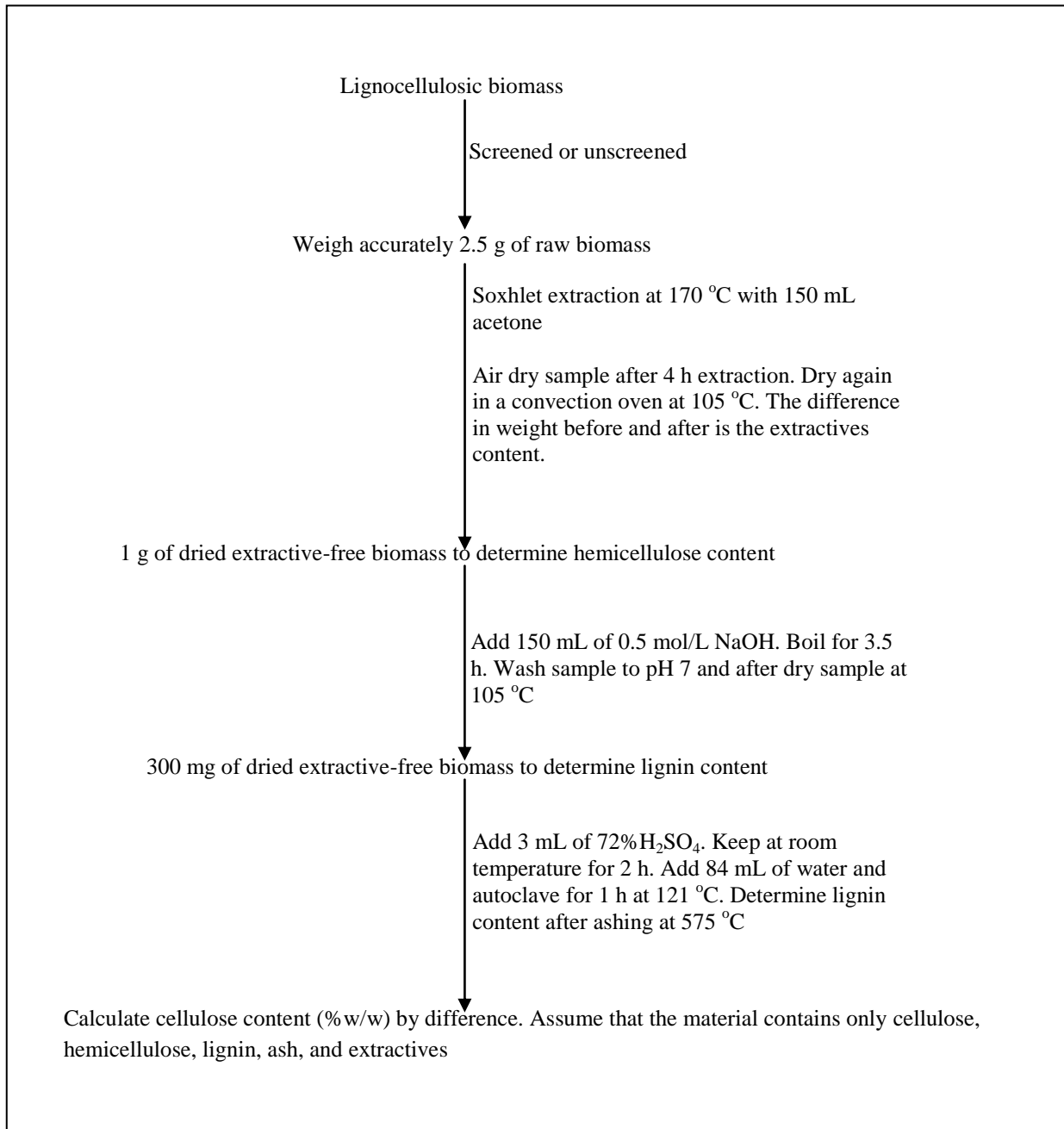


Fig. 2: Schematic representation of the compositional analysis of the lignocellulosic materials

Table 1: Compositional analysis of raw lignocelluloses of sugarcane bagasse, siam weed, and shea tree sawdust (%w/w)

	Sugarcane bagasse ^[18-22]	Siam weed ^[12]	Shea tree sawdust ^[10]
Extractives	2.14±0.6	4.8±0.9	1.9±1.7
Cellulose	35.28±1.2	40.2±2.3	45.9±9.2
Hemicellulose	33.28±0.8	29.9±0.7	20.3±11.5
Lignin	25.20±1.1	23.2±5.3	29.9±13.2
Ash	4.1±0.3	0.9±3.1	2.04±3.1

Table 2: Reported compositions (% dry weight) of sugarcane bagasse

Cellulose	Hemicellulose	Lignin	Ash	Extractives	References
37	28	21	-	-	[18]
39	26.2	24	-	-	[19]
26-47	19-33	14-23	1-5	-	[20]
43	31	11	6	9	[21]
49	16	27	8 ^a	-	[22]

^aaddition of ash, extractives and proteins

IV. CONCLUSIONS

This study has highlighted a very simple procedure for compositional analysis of both woody and non-woody lignocellulosic biomass. Comparable results were obtained for the tested raw materials and those reported by scientific literature. The procedures proved to be economically viable for developing countries since sophisticated equipment, expensive and scarce chemicals are not required (chemicals for the entire compositional analysis are common and readily available on the shelf). By extension, the method can be utilized in most established economies of the world because of the reliability and cost-effectiveness of the whole process.

REFERENCES

- [1] A. C. O'Sullivan, Cellulose: the structure slowly unravels, *Cellulose* 4(3), 1997, 73-207.
- [2] T. Foyle., L. Jennings and P. Mulcahy, Compositional analysis of lignocellulosic materials: Evaluation of methods used for sugar analysis of waste paper and straw, *Bioresource Technology*, 98, 2007, 3026-3036.
- [3] A. O. Ayeni., S. Banerjee, J. A. Omoleye, F. K. Hymore., B. S. Giri, S. C. Deskmukh, R. A. Pandey and S. N. Mudliar, Optimization of pretreatment conditions using full factorial design and enzymatic convertibility of shea tree sawdust, *Biomass and Bioenergy*. 48, 2013, 130-138.
- [4] P. Ademark, A. Varga, J. Medve, V. Harjunpaa, T. Drakenberg, F. Tjerneld and H. Stalbrand, Softwood hemicellulose-degrading enzymes from *Aspergillus niger*: purification and properties of a beta-mannanase, *Journal of Biotechnology* 63, 1998, 199-210.
- [5] R. R. Mod, R. L. Ory, N. M. Morris and F. L. Normand, Chemical properties and interactions of rice hemicellulose with trace minerals *in vitro*, *Journal Agriculture and Food Chemistry*, 29, 1981, 449-454.
- [6] L. Nelson and J. A. Leming, Evaluation of monoethanolamine method of cellulose determination for agricultural residues, *Tappi Journal*. 40 (10), 1957, 846-850.
- [7] D. Fengel and G. Wegener, Hydrolysis of polysaccharides with trifluoroacetic acid and its application to rapid wood analysis. In: Brown, R.D., Jurasek, L. (Eds.), *Hydrolysis of Cellulose: Mechanisms of Enzymatic and Acid Catalysis Advances in Chemistry Series No. 181. American Chemical Society*, 1979, pp. 145-158.
- [8] K. Grohmann, M. Himmel, C. Rivard, M. Tucker, J. Baker, R. Torget and M. Graboski, Chemical-mechanical methods for the enhanced utilisation of straw, *Biotechnology and Bioengineering Symposium*, 14, 1984, 137-157.
- [9] P. J. Van Soest, Use of detergents in the analysis of fibrous feeds. II: A rapid method for the determination of fibre and lignin, *Journal of Association Agricultural Chemistry*, 46, 1963, 829-835.
- [10] A. O. Ayeni, F. K. Hymore, S. N. Mudliar, S. C. Deskmukh, D. B. Satpute, J. A. Omoleye and R. A. Pandey, Hydrogen peroxide and lime based oxidative pretreatment of wood waste to enhance enzymatic hydrolysis for a biorefinery: process parameters optimization using response surface methodology, *Fuel*, 106, 2013, 187-194.
- [11] A. O. Ayeni, J. A. Omoleye, S. Mudliar, F. K. Hymore and R. A. Pandey, Utilization of lignocellulosic waste for ethanol production: Enzymatic digestibility and fermentation of pretreated shea tree sawdust, *Korean Journal of Chemical Engineering*, 31(7), 2014, 1180-1186.
- [12] A. O. Ayeni, A. Ayoola and A. Adetayo, Optimization of enzymatic digestibility of sodium hydroxide- hydrogen peroxide oxidative pretreated siam weed for reducing sugar production, *American Journal of Engineering Research*, 3(9), 2014b, 119-126.
- [13] C. D. Blasi, G. Signorelli, C. Di Russo, G. Rea, Product distribution from pyrolysis of wood and agricultural residues, *Industrial Engineering Chemistry Research*, 38(6), 1999, 2216-2224.
- [14] S. Li, S. Xu, S. Liu, C. Yang and Q Lu, Fast pyrolysis of biomass in free-fall reactor for hydrogen-rich gas, *Fuel Process Technology*, 85(8-10), 2004, 1201-1211.

- [15] L. Lin, R. Yan, Y. Liu and W. Jiang, In-depth investigation of enzymatic hydrolysis of biomass wastes based on three major components: cellulose, hemicellulose, and lignin, *Bioresource Technology*, 101(21), 2010, 8217-8223.
- [16] A. Sluiter, B. Hames, R. Ruiz, C. Scarlata, J. Sluiter and D. Templeton et al., Determination of structural carbohydrates and lignin in biomass: laboratory analytical procedure (LAP). Golden, CO: National Renewable Energy Laboratory; April 2008. NREL Report No.: TP-510-42618. Contract No.: DE-AC36-99-G010337. Sponsored by the U.S. Department of Energy.
- [17] S. N. Walford, Sugarcane bagasse: How easy is it to measure its constituents, *Proceeding of South African Sugar Technology Association*, 81, 2008, 266-273.
- [18] E. P. S. Bon, Ethanol production via enzymatic hydrolysis of sugarcane bagasse and straw. Paper presented at the Food and Agricultural Organisation Symposium: The role of agricultural biotechnologies for production of bio-energy in developing countries 2007, www.fao.org/biotech/presentation/bon.pdf.
- [19] R. Aguilar, J. A. Ramirez, G. Garrote and M. Vazquez, Kinetic study of the acid hydrolysis of sugarcane bagasse, *Journal of Food Engineering* 55, 2002, 309-318.
- [20] Paturau, J.M. (1989) By-products of cane sugar industry. Third edition. Elsevier, Amsterdam, Netherlands.
- [21] C. Martin, H. B. Klinker, A. B. Thomsen, Wet oxidation as a pretreatment method for enhancing the enzymatic convertibility of sugarcane bagasse, *Enzyme Microbiology and Technology*, 40, 2007, 426-432.
- [22] L. Mesa, E. Gonzalez, C. Cara, E. Ruiz, E. Castro and S. I. Mussatto, An approach to optimization of enzymatic hydrolysis from sugarcane bagasse based on organosolv pretreatment, *Journal of Chemical Technology Biotechnology*, 85, 2010, 1092-1098.
- [23] A. O. Ayeni, Short-term lime pretreatment and enzymatic conversion of shea tree sawdust into ethanol, Ph.D Thesis 2013, Covenant University, Ota, Nigeria.
- [24] R. C. Pettersen, The chemical composition of wood. In R.M. Rowell (ed). The chemistry of solid wood, American Chemical Society, 1984, Washington, USA, pp 57-126.

Bayesian Belief Network Method for Predicting Asphaltene Precipitation in Light Oil Reservoirs

*¹Jeffrey O. Oseh (M.Sc.) and ²Olugbenga A. Falode (Ph.D)

^{*1}C & PE, COE, Afe Babalola University, Ado-Ekiti, Nigeria.

²PE, FOT, University of Ibadan, Ibadan, Nigeria.

ABSTRACT: - Asphaltene precipitation is caused by a number of factors including changes in pressure, temperature, and composition. The two most prevalent causes of asphaltene precipitation in light oil reservoirs are decreasing pressure and mixing oil with injected solvent in improved oil recovery processes. This study focused on predicting the amount of asphaltene precipitation with increasing Gas-Oil Ratio in a light oil reservoir using Bayesian Belief Network Method. These Artificial Intelligence-Bayesian Belief Network Method employed were validated and tested by unseen data to determine their accuracy and trend stability and were also compared with the findings obtained from Scaling equations. The obtained Bayesian Belief Network results indicated that the method showed an improved performance of predicting the amount of asphaltene precipitated in light oil reservoirs thus reducing the number of experiments required.

Keywords: (Asphaltene Precipitation, Bayesian Belief Network, High Gas-Oil Ratio, Light Oil Reservoirs, Scaling Equation).

I. INTRODUCTION

Asphaltene precipitation and deposition in petroleum reservoirs fluids during production has proved to be a difficult problem to define and study as it can cause plugging of reservoir formation, wellbore, tubing and production facilities. Field conditions conducive to asphaltene precipitation include primary depletion, acid stimulation, gas-lift operations and miscible flooding, just to mention a few. Asphaltene precipitation during primary depletion of highly undersaturated reservoirs due to changes in pressure, temperature and compositions or during application of any of the improved oil recovery processes was described by many authors [Kokal and Sayegh, 1995; Michell and Speight, 1973; Leontaritis and Mansoori, 1989; Mofidi and Edalat, 2006 and Rassamdana, 2006].

Asphaltenes comprises the heaviest and the most polar fraction of crude oil [Kokal and Sayegh, 1995; Michell and Speight, 1973]. Asphaltenes exist in the form of colloidal dispersions and are stabilized in solutions by resins and aromatics that act as peptizing agents. Asphaltene precipitation and deposition may occur deep inside the reservoir, near the wellbore and/or in processing facilities [Leontaritis and Mansoori, 198]. Asphaltene precipitation is a function of pressure, temperature and live crude oil composition. Asphaltene have a tendency to precipitate as the pressure is reduced, especially near the bubble point (however, precipitation can occur even at higher pressures than the bubble point, depending on the crude). Another important reason for precipitation is the stripping of crude oil by gas. When gas is added to the crude (as may be happening during the production from the gas-cap wells) the composition of the crude changes and may lead to precipitation. This is the same mechanism during de-asphalting of crude in a refinery where propane and butane are used for stripping the asphaltenes. The precipitated asphaltenes then deposit near, or in the wellbore. This may lead to increase in formation damage (skin), and subsequently more precipitation.

1.1. Aims of the study: The aims of this study are to investigate the effects of increasing gas-oil ratio on the stability of asphaltene in light oil reservoirs and to select the best Bayesian Belief Network predictor for asphaltene precipitation.

1.2. Objective of the study: A numerical model “(Bayesian Belief Network Model) for predicting the amount of asphaltene precipitated in light oil reservoirs was developed instead of using approximate and complex analytical equation. Factors affecting asphaltene precipitation in light oil reservoirs like temperature, pressure, crude oil composition, gas gravity, oil gravity, $^{\circ}$ API, and dilution ratio which are believed to have effects on asphaltene stability are included in the model to determine their effects on asphaltene precipitation.

II. SCALING EQUATION AND BAYESIAN BELIEF NETWORK METHOD

2.1. Scaling Equation: The use of aggregation/gelation phenomena in the scaling model first presented by [Rassamdana *et al.*, 1989] led to model independency on asphaltene properties. They claimed that asphaltene precipitation is similar to aggregation/gelation phenomena and thus used the scaling/fractal theory to describe asphaltene precipitation. The scaling model is a simple model that requires the dilution ratio, m , and molecular weight of injected fluid (called diluents), to predict the amount of asphaltene precipitation, [Hirschberg *et al.*, 1984; Hu *et al.*, 2000; Hu and Guo, 2001]. These variables were combined into two dimensionless variables and, defined as follows:

$$X = \frac{Rm}{Mw^z} \quad (2.1)$$

and

$$Y = \frac{wt\%}{Rm^{z'}} \quad (2.2)$$

Where with numerical value of -2 is recommended as a constant exponent that is independent of the type of crude oil and the precipitating agent and is considered as an adjustable parameter with the numerical value in the range of 0.25-0.6 depending upon the type of crude oil and precipitant.²⁴ the scaling equation has been represented in terms of and by polynomial function.

$$Y = A_1X + A_2X + A_3X^2 + A_4X^3 \quad (2.3)$$

The coefficients A_{1-4} should be determined through data fixing using experimental data. The development of scaling model by (Rassamdana *et al.*, 1989; Hirschberg *et al.*, 1984; Hu, *et al.*, 2000) was based on data from Iranian southwest oil reservoirs. Later on, (Hu *et al.*, 2004) applied a tuned scaling model to predict asphaltene precipitation for two kinds of heavy oils from Canada and U.S.A.

The effects of the temperature, molecular weight of -alkane precipitants, and dilution ratio on asphaltene precipitation in a Chinese crude oil have been studied experimentally by [Meshad *et al.*, 2008]. Hu *et al.*, (2004) have also studied asphaltene precipitation because of CO₂ injection [Floridi, 2004] they proposed a generalized corresponding state principle (CSP) for the prediction of asphaltene precipitation. The CSP theory complemented the scaling equation for asphaltene precipitation under the influence of -alkane precipitant. In their study, their parameters and exponents of a corresponding state equation was capable of describing the asphaltene precipitation behaviour in the studied high-pressure CO₂ injected crude oil systems. They indicated that the generalized corresponding state theory was suitable for prediction of asphaltene precipitation from petroleum fluids as a result of the addition of miscible solvents at various temperatures and pressures. Thermodynamically, asphaltene precipitation is not dependent of the reservoir pressure. However, the effect of pressure is not included in the scaling model developed by [Rassamdana *et al.*, 1996].

[Pearl *et al.*, 2000; Meshad *et al.*, 2008] included the effect of pressure on the nucleation onset and the amount of asphaltene precipitation in the scaling model. In the new scaling model, the relation between the dilution ratio and the molecular weight of diluents and the amount of asphaltene precipitation has been presented in two variables and as follows:

$$x = \frac{Rm}{Mw^z} \quad (2.4)$$

And

$$y = \frac{wt\%}{Rm^{z'}} \quad (2.5)$$

To include the effect of reservoir pressure and asphaltene precipitation in the new scaling model, the variables and, defined as follows:

$$X = \frac{x}{\rho c_1} \quad (2.6)$$

And

$$Y = \frac{y}{x c_2} \quad (2.7)$$

In the new scaling equation, similar to the original scaling equation has been expressed in terms of by a polynomial function of eq. 3. Thus, the new scaling equation includes seven adjustable parameters of A_{1-4} , c_1 , c_2 , and Z . These parameters should be estimated using experimental data. Scaling models to a less degree than thermodynamic models require parameter tuning to predict asphaltene precipitation for different oil and reservoir conditions assuming that necessary laboratory data are available. Therefore, the need for parameter tuning for each specific oil and reservoir condition is the limitation of scaling models.

To remove such limitation, this study presents a comprehensive model that investigates the effect of increasing gas-oil ratio on the stability of asphaltene in light oil reservoirs and to define and select the best BBN predictor that predicts the asphaltene precipitation in a gas-cap well instead of approximate and complex analytical equation under the prevailing conditions of temperature, pressure, oil composition, gas gravity, oil gravity, 0 API, and dilution ratio which are believed to have effects on asphaltene stability. The presented model is based on an artificial intelligence (AI) method that is still in the primary stages of development and presents promising results that still require extensive study to be matured. A BBN is applied particularly when the fundamentals of the model structure, cause-effect relation between variables, are faced with problems of conceptual uncertainty (*Langseth, 2008; Pourret, 2008; Norsys, 1996*). The preference of BBN among AI methods was due to the facts that: (1) Asphaltene precipitation is causative in nature, (2) BBN is capable of extracting an interrelation between causes and effects quantitatively, (3) BBN algorithms can learn from experiments, and are also fault tolerant in the sense that they can handle inaccurate and incomplete data, (4) fast response, simplicity and capacity to learn are the advantages of BBN compared to classical (conventional) methods, and (5) there is no limitation in the flow of information in a BBN model from causes to effects and vice versa. The latter fact allows one to predict the dilution ratio at nucleation onset for a given pressure and diluents and trivial asphaltene weight percent. Moreover, the BBN model training using a complete databank covering oil conditions of interest removes the limitation associated with the scaling model. Because the required data for training does not include asphaltene properties, one does not face difficulties associated with thermodynamic models in applying a trained BBN model. A very brief introduction to fundamentals of BBN is included as a background, and then the BBN model was developed to predict the asphaltene precipitation in a light oil reservoir. A comparison was made between the BBN model predictions and the scaling predictions.

2.2. Bayesian Belief Network (BBN) Method: A BBN is a graphical probabilistic model to represent and study an uncertain domain. A BBN can also be used to deal with the systems that are of a cause-nature. However, a BBN is a mathematical Structure that uses conditional independences for the speed of inference, instead of real model of causalities. Historically speaking, a suggested link between causality and conditional independence indeed goes back to Reichenbach,¹⁸ representing conditional independences, which can be obtained as consequences of the causal relationships, provides a natural and consistent way to express what is known about the different phenomena. Probabilistic relationships, such as conditional independences, can be used to investigate the causal structure dealing with uncontrolled observations [*Pourret, 2008*].

A BBN consists of a set of nodes and directed edges between nodes. Nodes represent uncertain events or variables [*Pourret, 2008*]. Nodes can be either continuous or discrete random format. The states bin ranges of a discretized node are exclusive. The directed edges are the links between a pair of nodes, and their direction represent causal influence of one node (parent node) on the other one (child node). In the context of BBN, each node is associated with a probability distribution. Nodes without parents are called root nodes and have an associated prior probability (PP) distribution. For child nodes, the probability distribution takes the form of conditional probability (CP) that represents the correlation between a parent and a child node. The edges of a bin represent the statement that each variable is conditionally independent of its non-descendent in the graph given its parent in the same graph [*Norsys, 1996*]. A BBN requires four basic elements to represent knowledge of the process under consideration: set of nodes, directed edges, conditional probability distribution, and the prior probability distribution. New information for a variable, called evidence, can be used to instantiate the node representing the variable by setting the probability of one of the states of that node to 100 (on a percentage basis). The number of nodes receiving evidence can be different from one to many at different times depending upon the information availability. Introducing evidence to a model allows for the updating probability distribution of uninstantiated nodes that can be used to calculate numerical values for such nodes as predictions. The mathematical procedure to update probability distribution is called "inference", and 'Bayes' rule is the basis for carrying out the inference in a BBN. When there is a shortage of information, the evidence of the probabilistic BBN model help us update our knowledge of the process, even in the case of inaccurate

data. This is an advantage of BBN over other modeling methods that do not deliver any result when a set of input is not complete.

III. RESEARCH METHODOLOGY

3.1. Data Acquisition Analyses: The 250 data sets used in this work were collected from the static asphaltene precipitation tests conducted on the North Arab-D reservoir of Ghawar field in Saudi Arabia containing undersaturated light oil¹. Data are further extrapolated from the existing ones in order to have a more extensive database for the network. Of the 250 data points, 175 (70%) of the data points were used to train the network, 10 (4%) of the data sets were used to cross-validate the relationships established during training process and the remaining 65 (26%) data points were used to test the network and to evaluate their accuracy through statistical analysis.

3.2. Simulating API Gravity and Gas Specific Gravity of the Mixture

The data given does not reflect the gravity of the resulting mixture which is also believed to have a serious influence on whether a particular fluid will experience asphaltene precipitation or not and these was simulated using the Glaso's (1980) correlation for estimating the gas solubility as a function of the API gravity, pressure, temperature, and gas specific gravity.

$$R_s = \gamma_g \left[\left(\frac{API^{0.989}}{(T-460)^{0.172}} \right) (Pb^*) \right]^{1.2255} \quad (3.1)$$

Where $P_b^* = 10^x$ is a correlating number with the parameter x defined thus as:

$$x = 2.8869 - [14.1811 - 3.3073 \log(P)]0.5 \quad (3.2)$$

3.3. Statistical analyses used for model performance and validation.

The statistical inferences below were used to evaluate the model performance and validation:

$$MSE = \frac{1}{N} \sum_{i=1}^n (ei)^2 = \frac{1}{N} \sum (Ti - Outi)^2 \quad (3.3)$$

$$RMSE = \sqrt{\frac{1}{M} \sum_{i=1}^m (Ti - Outi)^2} \quad (3.4)$$

$$R^2 = 1 - \frac{(Ti - Outi)^2}{\sum_{i=1}^m Ti^2} \quad (3.5)$$

$$\sigma = \sum_{i=1}^n |(Yi^{exp} - Yi^{model}) / Yi^{exp}| \quad (3.6)$$

$$\sigma_{ave} = \sum_{i=1}^n (|(Yi^{exp} - Yi^{model}) / Yi^{exp}|) / n \quad (3.7)$$

$$Ei = \frac{Outi - Ti}{Ti} \times 100 \quad (3.8)$$

$$\%MAE = \frac{1}{N} \sum_{i=1}^n |Ei| \quad (3.9)$$

$$R = \sqrt{1 - \frac{\sum_{i=1}^n (Ye - Ym)}{\sum_{i=1}^n (Ye - Y')}} \quad (3.10)$$

$$\text{Where } Y' = \frac{1}{n} \sum_{i=1}^n Ye \quad (3.11)$$

IV. ANALYSES OF RESULTS AND INTERPRETATION

Ghawar Field Record: The Arab-D reservoir of Ghawar field is situated in the North East province in the Kayaker desert in the North West of Saudi Arabia.

Crude Oil and Gas Properties of Ghawar Field: The crude oil was sampled using a conventional bottomhole sampler. The crude oil fluid composition is shown in **Table A1** and **A2**. It has a bubble point pressure of ~1900psia at a reservoir temperature of 215°F and a GOR of 580scf/stb. The crude oil properties do not vary significantly across the area of interest. The dead crude has an asphaltene content of ~3.0 wt. %.

The composition of the injected gas (that was injected in the 1960s and 1970s) is presented in **Table A1**. This was the associated gas from the crude after processing at the gas oil separating plant (GOSP). The gas used in the experiment was prepared from the high pressure production trap (HPPT) gas after flashing it at 1,300 psia and 75°F. The model was validated using the input parameters in **Table A1** and **A2** from Ghawar field, one of the major fields in Saudi Arabia.

4.1. Results

Table A: Fluid Properties of North Ghawar-Arab D Reservoir in Saudi Arabia, Kokal et al. (1995).

Table A1: Crude Oil and Gas Properties

Component	Mole %			
	Molecular Weight	Reservoir Fluid	Injected Gas (Actual)	Injected Gas (Experiment)
N ₂	28.01	0.14	0.41	0.34
CO ₂	44.01	5.89	12.30	12.62
H ₂ S	34.08	1.82	1.91	2.49
C ₁	16.04	24.01	56.00	56.00
C ₂	30.07	9.79	17.45	16.23
C ₃	44.10	7.49	8.20	8.39
C ₄	58.12	4.92	2.64	2.86
C ₅	72.15	3.95	0.84	0.83
C ₆	86.18	3.14	0.25	0.25
C ₇₊	100.20	38.85	0.00	0.01
C ₇₊ MW	100.20	240		
C ₇₊ SG		0.8652		
BPP (psia)		~1900@220°F		

Table A2: Bulk Deposit Test

GOR (scf/stb)	550	597	643	736	125	195
Oil charged (cc)	60	60	60	60	60	60
Gas charged (cc)	0	2	4	8	30	60
Pressure (psia)	30	30	300	300	300	300
Temp.	21	21	215	215	215	215
Amount Precipitated (mg)	17.	33	58	62	81.1	132
Precipitated asphaltene (ppm)	43	73	13	13	182	29

Table 4.1: Statistics of the R-values on network performance for the training, testing, and the entire data sets.

EM Learning Algorithm	Mean	Max. Absolute Error	Min. Absolute Error	Standard deviation (σ_{ave})	Ave. Standard deviation (σ)	Correlation coefficient R
Training data sets	0.50056448	0.7823412	0.47112483	0.348197	0.002106	0.99889887
Testing data sets	0.00461453	0.0049139	3.8788E-07	0.1678	0.001864	0.99428189
Entire data sets	0.00465241	0.0075961	5.7153E-07	0.76423	0.0027981	0.99907533

Table 4.1a: Validating the trained data sets.

Best Network	Training Data Sets		Validating Data Sets	
	Training	Cross-Validation	Training	Cross-Validation
Runs #			2	2
Period	100	100	99	100
Min. MSE	0.000195835	0.000448607	0.000122137	0.000211566
Max. MSE	0.000195835	0.000448607	0.000505758	0.000211565

Table 4.1b: Validating the trained data sets

All Runs #	Training Minimum	Cross-Validation Minimum
Minimum MSE	7.1183E-06	5.20314E-06
Average Minimum MSE	0.000201394	0.000340931
Average Maximum MSE	0.000329268	0.000380287

Table 4.1c: Validating the trained data sets

All Runs #	Min	Cross Validation	Cross Validation
Average Min. MSE	0.000201394	0.000340931	6.89124E-05
Average Max. MSE	0.000329268	0.000380287	0.000152968

Table 4.2: Best Network Performance.

Network Performance	Correlation coefficient (R-value)					
	MSE	MAE	MAE (Max.)	MAE	(σ)	R
Training data sets	7.1183E-06	0.00069148	0.00930148	4.01298E-06	0.2579	0.99849887
Testing data sets	1.1214E-06	0.00055299	0.00491395	3.8788E-06	0.1678	0.99398189

Table 4.3: Relative absolute deviation (σ) and average relative absolute deviation (σ_{ave}) for simulated data.

Scaling Methods	Rassamdana et al. (1996)	Yu-Feng et.al. (2000)	Ashoori et.al. (2003)	BBN Model (This study)		
				Training data sets	Testing data sets	Entire data sets
(σ)	1.071688	4.9586	68.8602	0.1678	0.248194	0.76423
(σ_{ave})	0.003897	0.018031	0.2504	0.001864	0.0013062	0.00279818

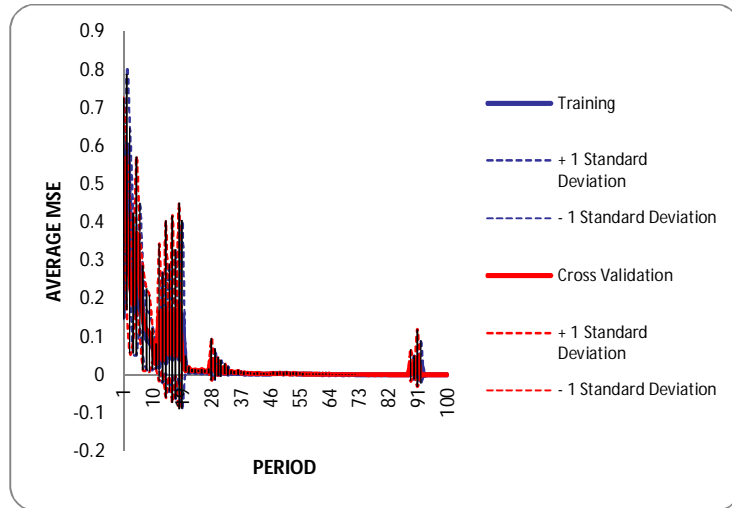


Figure 4.1: Average MSE with standard deviations boundaries for 3 Runs

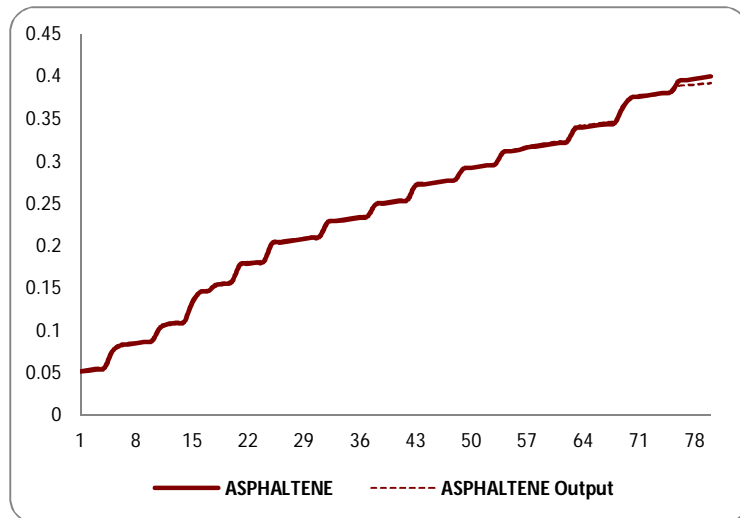


Figure 4.2: Bayesian Belief Network testing the desired output and actual network output

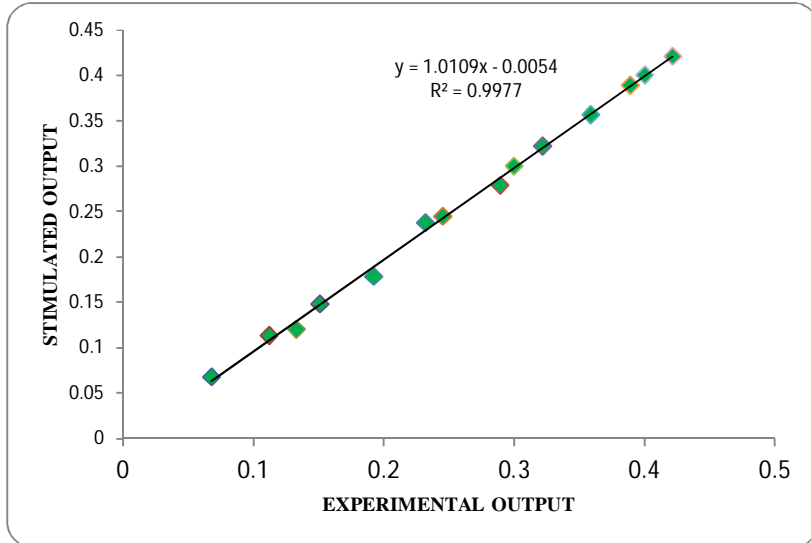


Figure 4.3 Comparison of experimental data with stimulated values that used to train the network.

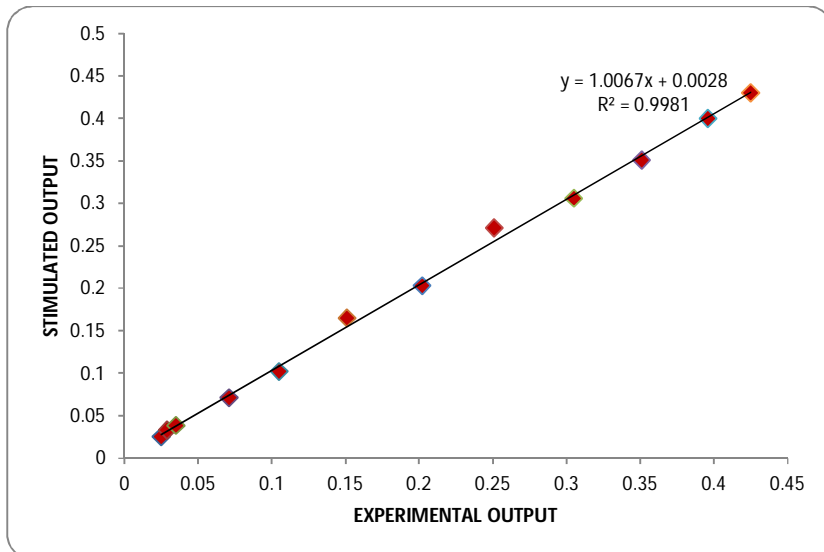


Figure 4.4 Comparison of experimental data with stimulated values of the entire data used in the network

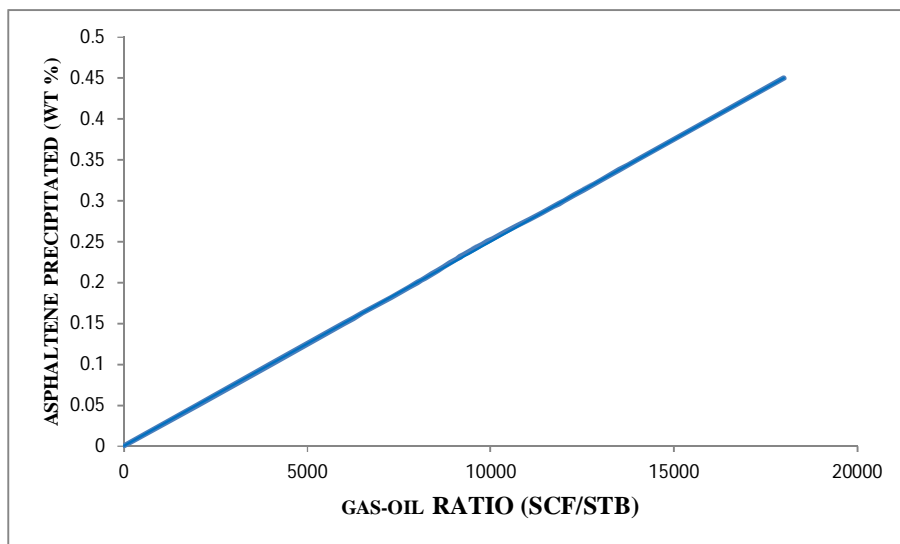


Figure 4.5: Asphaltene precipitated as a function of Gas-Oil Ratio (GOR)

4.2. Interpretation of Results

Table 4.1 shows the results of the optimization of the networks. The network of correlation coefficient, R , of 0.9985 trained with the EM learning algorithm gave the best performance and was shown in Fig. 4.3.

Table 4.3 illustrates the accuracy of each method to predict the amount of asphaltene precipitation by comparison the relative absolute deviation (and average relative absolute deviation $_{ave}$) are defined as shown in equation (3.6) and (3.7) respectively. As it is apparent, the deviation is the less for BBN model, while it is much higher for scaling equations as shown in Table 4.3. This analyses shows that the BBN model is more accurate than the other methods to simulate the asphaltene precipitation.

Fig. 4.1, and Fig. 4.2 shows the training processes, its validations and the testing process on the used data points, respectively. The correlation coefficient R -values between the predicted and the actual values of the measured asphaltene weight percent are shown in Fig. 4.3 and 4.4. This shows that the BBN predicted asphaltene precipitation values are very close to the actual values of all data sets. Fig. 4.5 has shown that asphaltene precipitation is a function of gas injection and increases with increasing gas-oil ratio. However, the amount of asphaltene precipitated is relatively small. There is evidence that some of the asphaltene dissolve as the pressure is reduced below the bubble point. These effects have resulted in preventing severe asphaltene build ups in the well. In Table 4.3 shown, the BBN model showed dominance over scaling equations when their absolute deviations and relative absolute deviations are compared.

V. CONCLUSION AND RECOMMENDATIONS

5.1. Conclusion

In this study, A Bayesian Belief Network (BBN) model was developed to predict and simulate the amount of asphaltene precipitation in a high-gas oil ratio well as a function of dilution ratio, temperature, oil volume, gas volume, gas-oil ratio, gas gravity, stock tank oil gravity, and pressure. The results of this study clearly indicate that asphaltene precipitation is a function of gas injection and increases with increasing gas-oil ratio. The results from BBN model were compared with predicted values using some scaling equations. The performance of the BBN model was measured using correlation coefficients (R), Mean Squared Error (MSE), and absolute error. The reported results confirmed that BBN approach used for asphaltene precipitation prediction have good statistical performance values of correlation coefficient with Minimum Absolute Mean Squared Error and Mean Squared Error values.

5.2. Recommendations

The main recommendations of this study are:

- Produce the oil wells at as low a GOR as possible. This will reduce the amount of asphaltene precipitation and subsequent deposition.
- Constant monitoring of asphaltene build-up in the wellbores should be maintained

- Constant monitoring of the cleanout procedures to improve processes for future cleanouts should be sustained.
- Solvent should be injected into the oil reservoir to prevent plugging.
- Examine the use of asphaltene dispersants in severe deposition cases.
- Examine the suspended asphaltenes in the crude and increase demulsifier dosage to prevent the asphaltene turning to emulsion and causing production problems.

NOMENCLATURES

Symbols

Rm	Dilution ratio
Mw	Molecular weight of the diluents
P	Pressure
T	Temperature
V _o	Oil volume
V _g	Gas volume
Y _g	Gas gravity
Y _o	Stock tank oil gravity
°API	American Petroleum Institute
GOR	Gas-Oil Ratio
Wi	Weight percent of asphaltene precipitation
Z	Adjustable parameter constant
Z'	Constant exponent
C ₁ , C ₂	Constants
n	Constant
A _i	Scaling equation coefficients of equation (2.3)
X	Function defined by equation (2.1)
Y	Function defined by equation (2.2)
x	Function defined by equation (2.4)
y	Function defined by equation (2.5)
BBN	Bayesian Belief Network
R _s	Dissolved gas specific gravity of the mixture
BPP	Bubble point pressure
MSE	Mean Squared Error defined by equation (3.3)
MAE	Mean Absolute Error
MAE (Max.)	Maximum Absolute Error of the Mean
RMSE	Root Mean Squared Error defined by equation (3.4)
E _i	Absolute Error function defined by equation (3.8)
%MAE	Percent mean error defined by equation (3.9)
R	Correlation coefficient defined by equation (3.10)
Greeks	
σ	Absolute Deviation defined by equation (3.6)
σ _{Ave}	Average Deviation defined by equation (3.7)

REFERENCES

- [1]. Floridi, L. (2004). The Blackwell guide to the philosophy of computing and information; Blackwell publishing Ltd.: Oxford, U.K.; ISBN: 0-631-22919-1.
- [2]. Hirschberg, A.; De Jong, L.N.J.; Schipper, B.A.; and Meijer, J.G. (1984), Influence of temperature and pressure on asphaltene flocculation. SPE Journal 24, 283-293.
- [3]. Hu, Y.F.; Chen, G.J.; Yang, J.T.; and Guo, T.M. (2000), A study on the application of scaling equation for asphaltene precipitation. Fluid phase equilibrium 171, 181-195.
- [4]. Hu, Y.F.; Guo, T.M. (2001), Effect of temperature and molecular weight of precipitants on asphaltene precipitation. Fluid phase equilibrium 192, 13-25.
- [5]. Hu, Y.F.; Li, S.; Liu, N.; Chu, Y.P.; Park, S.J.; Mansoori, G.A.; and Guo, T.M. (2004), Measurement and corresponding state modeling of asphaltene precipitation in Jilin reservoir oils. Journal of petroleum science engineering 41, 169-182.

- [6]. Kokal, S.L. and Sayegh, S.G. (1995) "Asphaltenes: The cholesterol of petroleum", SPE 29787 paper presented at the 6th Middle East Oil Show, Bahrain.
- [7]. Langseth, H. (2008); Bayesian networks in reality: The good, the bad, and the ugly. In advances in mathematical modeling for reliability; Bedford, T., Quigley, J., Walls, L., Alkali, B., Daneshkhah, A., Hardman, G., Eds.; IOS Press: Amsterdam, the Netherlands, ISBN: 1-586-03865-6.
- [8]. Leontaritis, K.J. and Mansoori, G.A. (1989) "Asphaltene deposition: A comprehensive description of problems manifestations and modeling approaches", SPE paper 18892 presented at the SPE production operations symposium held in Oklahoma City, OK, March 13-14.
- [9]. Meshad, A.K.; Mofidi, A.M.; Shariatpanahi, F.; and Edalat, M. (2008), Development of scaling equation with function of pressure to determine onset of asphaltene precipitation. *J. Jpn. Pet. Inst.* 51, 102-106.
- [10]. Michell, D.L and Speight, J.G. (1973). "The solubility of asphaltenes in hydrocarbons solvents", *Fuel*, vol. 53, pp. 149-152
- [11]. Mofidi, M. and Edalat, M. A (2006), simplified thermodynamic modeling for predicting asphaltene precipitation. *Fuel* 85, 2616-2621.
- [12]. Norsys. (1996). Netica application for belief networks and influence diagrams: User's guide, versions 1.05 for windows; Norsys software corporation: Vancouver, British Columbia, Canada.
- [13]. Pearl, J. (2000); Causality-models, reasoning, and inference; Cambridge University Press: Cambridge, U.K., ISBN: 0-521-77362-8.
- [14]. Pourret, O. (2008); Introduction to Bayesian Networks. In Bayesian Networks: A practical guide to applications; Pourret, O., Naim, P., Marcot, B., Eds.; John Wiley and Sons, Ltd.: Chichester, U.K., ISBN: 0-470-06030-1.
- [15]. Rassamdana, H. (1996): Asphalt flocculation and deposition: II "Formation and growth of fractal aggregates", *AIChE Journal*, 42, 3318-3332.
- [16]. Rassamdana, H.; Dabir, B.; Nematy, M.; Farhani, M.; and Sahimi, M. (1996) Asphalt flocculation and deposition: I. The onset of precipitation. *AIChE Journal* 42, 10-22.
- [17]. Rassamdana, H.; Farhani, M.; Dabir, B.; Mozaffarian, M.; and Sahimi, M. (1999) Asphalt flocculation and deposition. V. Phase behaviour in miscible and immiscible injections. *Energy Fuels*, 13 (1), 176-187.

Effects of variety and moisture content on some physical properties of okra pod

Adejumo A.O.D¹, Ajav E. A² and Igbeka J.C²

¹Agricultural Engineering Department, Federal College of Agriculture, Ibadan.

²Agricultural and Environmental Engineering Department, University of Ibadan, Ibadan.

ABSTRACT: Some physical properties of four varieties of okra pods NHAe47-4, LD88, V-35 and 'Elesoagbonrin' were determined at moisture content levels of 7, 14, 21 and 28 percent (wet basis) which are useful in the design of its processing, handling and storage equipment. The properties determined and mean values were length(107.97mm), diameter(35.17mm), mass(13.27g), true density(0.26g/cm³), bulk density (0.18g/cm³), porosity(58.06%), projected area(723.23mm²), surface area(2627.55mm²) and shape (conic/ribbed). The axial dimensions, individual pod mass, true and bulk densities increased as moisture content increases between 7 and 28% w.b. for the four varieties. The effect of moisture content was highly significant on the properties ($p = 0.05$).

KEYWORDS: Okra, Pod, Physical Properties

I. INTRODUCTION

World production statistics for fruit and vegetable shows okra (*abelmosus esculentus* (L) moench) as the fourth main vegetable produced by India whom is ranked second in the world vegetable producer (Eipeson and bhowmik [1]). Okra can be found in almost every market in Africa. In Nigeria, okra is ranked second best vegetable in order of importance, in Ghana, it is the fourth most popular vegetable, in Cameroon, it is the second most important vegetable in the market after tomatoes, in Sudan, it is the third most popular vegetable (Ogungbaigbe [2] and Schippers [3]).

Mohsenin [4], stated that Agricultural produce are subjected to various physical treatments involving mechanical, thermal, electrical, optical and sonic techniques and devices from the field to the consumer; therefore, it is essential to understand the physical laws governing the response of the crop so that machine, processes and handling operation can be designed for maximum efficiency and highest quality of the end product. The criterions used for describing shape and size includes charted standards, roundness, sphericity, measurement of axial dimensions, resemblance to geometric bodies and average projected area. He stated that sphericity of most agriculture produce is within the range of 0.32 to 1.00.

Visvanathan et. al. [5], determined the effect of moisture content (7.6-21 % w.b) on physical properties of Neem (*Azadirachta* India) nut. The diametral axis, porosity, bulk density and particle density decreased linearly but mass of 1000 nuts increased with increased moisture content. Waziri and Mittal [6], commended that Agricultural material pose special problems in determining their physical properties because of their diversity in shape, size, moisture content and maturity levels. Dutta et. al. [7], determined the dependence of physical properties of Gram on moisture content and obtained average 1000-grain weight of 0.173 kg, a mean surface area of 133.4 mm² and sphericity of 74 % at 10.9 % m.c db, bulk density and kernel density decreases in moisture range 9.64-31.0 % db.

Oje [8], carried out studies on locust bean pods and seeds physical properties relevant to dehulling and obtained the pods major diameter ranging from 76 to 277 mm and 8-12 m for the seeds. Adejumo et. al. [9, 10] studied the effects of moisture content and variety on frictional, aerodynamic, and selected mechanical properties of okra pod and observed that frictional and aerodynamic properties increased with increase in moisture content and varied among the varieties. Impact and compressive force, energy and young modulus decreased with increase in moisture content and also varied among the varieties. All the parameters were significant at 5% level.

II. MATERIALS AND METHODS

The initial moisture content of the four varieties of Okra NHAe47-4 and LD88 obtained from National Horticultural Research Institute, Idi-Shin, Ibadan; V-35 obtained from Institute of Agricultural Research and Training, Moor Plantation, Ibadan; and 'Elesoagborin' (Yoruba) were determined by the oven method ASAE Standards [11]. Methods developed by Visvanathan et al. [5] were used for sample preparation to obtain desired moisture content.

2.1 Linear Dimensions

Shape and size are inseparable physical properties and are both generally necessary if an object is to be satisfactorily described.

Thirty dry okra pods were randomly selected from each variety as samples. Plate 1 shows the dry okra pod samples. Two linear dimensions of each pod namely length and diameter were measured with a Vernier Caliper, reading to 0.01 cm. The shapes of pods were compared with the charted standards Moshnenin [12].

Okra pod surface area was determined by using a method adopted by Oje and Ugbor [13]. The pod surface was carefully coated in a light sensitive flexible paper. The surface edges on the paper were then pencil-traced on graph paper and the surface measured by counting the squares within the traced marks.



Plate 1. Okra Pod Samples

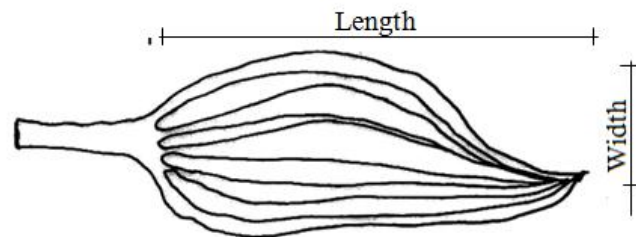


Fig. 1: Linear Dimensions of Okra pod

2.1 Gravimetric dimensions

The bulk density of dry okra pod at different moisture content was determined by filling a container (open top rectangular box of 200 x 100 x 100 mm) of known self-weight to the brim with dry okra pod and weighed to determine the net weight of the pod. Uniform density was achieved by tapping the container 10 times in the same manner in all measurements, the bulk density was calculated as:

$$\rho_b = \frac{w_s}{w_o} \quad (1)$$

Where ρ_b is bulk density (g/cm³), w_s is weight of sample (g) and w_o is volume occupied (cm³)

The true or particle density of dry okra pod was determined by the water displacement method. Dry okra pod absorbs water easily, thus each pod was carefully wrap in a thin, light, sensitive flexible nylon paper and carefully immersed to disallow air spaces (Oje and Ugbor [13]).

$$\rho_t = \frac{w_s}{w_d} \quad (2)$$

Where ρ_t is bulk density (g/cm³), w_s is weight of sample (g) and w_d is volume of water displaced (cm³)

Porosity of dry okra pods were determined theoretically from bulk and true densities of pods using the relationship presented by Jain and Bal[14] as follows;

$$P_p = \frac{\rho_b}{1 - \rho_t} \quad (3)$$

Where ρ_b is bulk density (g/cm³), ρ_t is particle density (g/cm³) and P_t is porosity (%).

2.3 Statistical experimental design and analysis

A – 2 x 4 factorial in completely Randomized Design, (CRD) experimental design was used with a total of 960 observations (4 variety x 4 moisture content levels x 30 samples) each for major diameters, length, bulk and true densities, porosity, surface area for pod respectively.

III. RESULTS AND DISCUSSION

Results obtained from the study are presented in Tables 1 to 7 and in Figures 2 to 6. The effect of moisture content (mc) on the pod length and diameter for the four varieties were as shown in Tables 1 to 4. It was observed that the pod length and diameter increased with increase in moisture content. There is significant difference in the mean of pod length from 7 to 28 % moisture content at 5% significant level. Pod length of variety NHAe47-4 increased from 104.01 to 105.35 mm, V-35 from 89.59 mm to 89.64 mm, LD88 from 89.27 to 90.28 mm and 'Elesoagbonrin' from 127.59 to 129.63 mm while the diameter increased from 46.17 to 48.54 mm, 27.37 to 37.33 mm, 32.01 to 34.28 mm and 27.37 to 28.48 mm for the varieties respectively. The grand mean pod length was 103.18 mm while that of the diameter was 36.20 mm. The relationships among the dimensions and moisture content were logarithmic with R^2 0.52 – 0.99 as presented in Figures 2 and 3.

The results as presented in Tables 2 and 3 showed that as dry okra pod absorbs water, it increases radial rather than axial due to the swollen effect which is radial. 'Elesoagbonrin' gave the highest pod length (128.67 mm) and LD88 gave the least (89.78 mm). NHAe47-4 gave the highest diameter (47.23 mm) and 'Elesoagbonrin' the least (27.96 mm).

The results are similar to those reported for okra by Adejumo [9] but not in accordance with that of Visvanathan[5] for Neem (*Azadirachta* India) nut. The shape of okra pod is regarded as conic /ribbed as compared with the charted standards (Mohsenin [12]). It tapers towards the apex and the cross section is more or less angular. The overall mean length and diameter are 107.97mm and 35.17mm respectively.

Processing, handling and storage were affected by size and shape of okra pod. The size of the pod determined the size and orientation of the hopper seat, which directs the product into the threshing chamber and the adjustment of the concave clearance. If the inlet and the concave clearance are small, the pods get choked in the hopper and the seed could be crushed on the cylinder.

The information on the interaction between okra varieties and moisture content (Table 4) is necessary in knowing whether a concave clearance and a screen specified for one variety at a given moisture content can be used for another at the same or different moisture content, thus reducing the number of threshing drums and screens in processing the four varieties in the moisture content range of 7 to 28 %.

The true (particle) density of okra pod generally increased with increase in moisture content. NHAe47-4 decreased from 0.21 g/cm³ at 7 % to 0.19 g/cm³ at 14 % then increased to 0.21 at 28 % moisture content, V-35 increased from 0.21 g/cm³ to 0.33 g/cm³; LD88 decreased from 0.27 g/cm³ at 7% to 0.25 g/cm³ at 14 % then increased to 0.3 g/cm³ at 28 % moisture content and 'Elesoagbonrin' increased from 0.29 to 0.3 g/cm³.

TABLE 1: OVERALL AVERAGE OF SOME PHYSICAL PROPERTIES OF OKRA POD

	length (mm)	Diameter (mm)	Mass (g)	True Density (g/cm ³)	Bulk Density (g/cm ³)	Porosity (%)
Means	107.97	35.17	13.27	0.26	0.14	58.06
Std. dev.	17.65	7.97	4.07	0.12	0.02	27.66
Minimum	78	24.5	3.13	0.08	0.10	17.16
Maximum	136	54	25.43	0.27	0.19	91.97

95% confidence interval

TABLE 2: MOISTURE CONTENT EFFECT ON SOME PHYSICAL PROPERTIES OF OKRA POD

Moisture Content	Length (mm)	Diameter (mm)	Mass (g)	True Density (g/cm ³)	Bulk Density (g/cm ³)	Porosity (%)
7%	112.45 ^A	33.35 ^B	12.08 ^c	0.24 ^B	0.13 ^C	59.20 ^A
14%	112.96 ^A	33.69 ^B	12.78 ^{bc}	0.24 ^B	0.13 ^C	58.83 ^A
21%	103.27 ^B	36.46 ^A	13.66 ^{ab}	0.25 ^{AB}	0.14 ^B	58.21 ^A
28%	103.20 ^B	37.16 ^A	14.56 ^a	0.29 ^A	0.15 ^A	55.92 ^A
LSD	4.44	2.04	1.02	0.02	0.004	0.07

TABLE 3: VARIETY EFFECT ON SOME PHYSICAL PROPERTIES OF OKRA PODS

Variety	Length (mm)	Diameter r (mm)	Mass (g)	True Density (g/cm ³)	Bulk Density (g/cm ³)	Porosity (%)
NHAE 474	104.67 _B	47.23 ^A	19.10 ^A	0.20 ^C	0.12 ^{B A}	40.51C
V-35	98.10 ^C	32.31 ^B	11.16 ^C	0.25 ^B	0.16 ^A	74.32A
LD 88	89.78 ^D	33.16 ^B	10.50 ^D	0.28 ^{AB}	0.15 ^B	72.39AB
'Elesoagbonrin'	128.69 _A	27.96 ^D	12.32 ^B	0.30 ^A	0.14 ^C	69.95B
LSD	2.50	0.73	0.51	0.014	0.002	3.00

TABLE 4: ANALYSIS OF VARIANCE FOR SOME PHYSICAL PROPERTIES OF OKRA POD.

Source of Variance	df	Length (mm)	Diameter (mm)	Mass (g)	True Density (g/cm ³)	Bulk Density (g/cm ³)	Porosity (%)
M.c	3	11.71***	6.91***	8.56***	2.88*	51.69***	0.82 NS
Variety	3	318.67***	1019.45** *	471.55** *	15.11***	646.5***	711.41***
Mc x Variety	15	393.82***	409.01***	114.16** *	4.55***	383.34***	149.65***
Error	442						
Total	474						

* = significantly different at 5%, ** = significantly different at 1%, *** = significantly different at 0.1%, ns = not significantly different

TABLE 5: POD PROJECTED AND SURFACE AREAS

Item	Means	Std Error	Lower Bound	Upper bound
Pod Project Area(mm ²)				
Nhae47-4	1033.10 ^a	23.31	985.83	1080.37
V-35	622.80 ^{bc}	23.31	595.53	670.07
Ld88	556.70 ^c	23.31	509.43	630.97
'Elesoagbonrin'	680.30 ^b	23.31	633.03	727.57
Overall Average	723.23	11.65	699.59	746.86
Pod Surface Area(mm ²)				
Nhae47-4	3615.70 ^a	85.54	3442.22	3789.18
V-35	2269.60 ^c	85.54	2096.12	2443.08
Ld88	2032.20 ^c	85.54	1858.72	2265.68
'Elesoagbonrin'	2592.70	85.54	2419.22	2766.18
Overall Average	2627.55	42.77	2540.81	2714.29

10% Moisture Content. 95% Confidence Interval.

TABLE 6: ANALYSIS OF VARIANCE FOR POD PROJECT AND SURFACE AREAS

Source of Variance	Df	Pod Projected Area (mm ²)	Pod Surface Area (mm ²)
Variety	3	83.252*	66.520*
Error	36		
Total	39		

* = Significantly different at 5%

TABLE 7: SEED/CHAFF RATIO

Rep	1	2	3	Average
NHAe47-4	1.33	1.33	1.33	1.33
V-35	1.31	0.99	1.58	1.29
LD88	2.00	1.71	2.53	2.08
'Elesoagbonrin'	1.29	1.21	1.35	1.31
Average				1.50

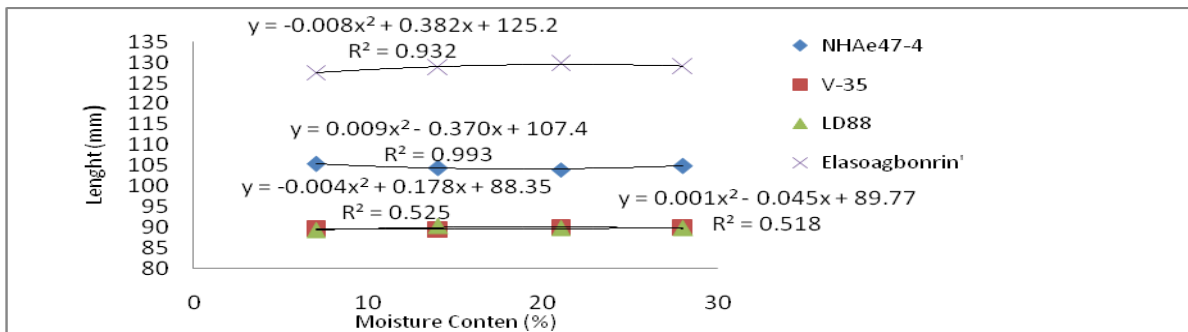


Fig.2: Effect of Moisture Content on Okra Pod Length

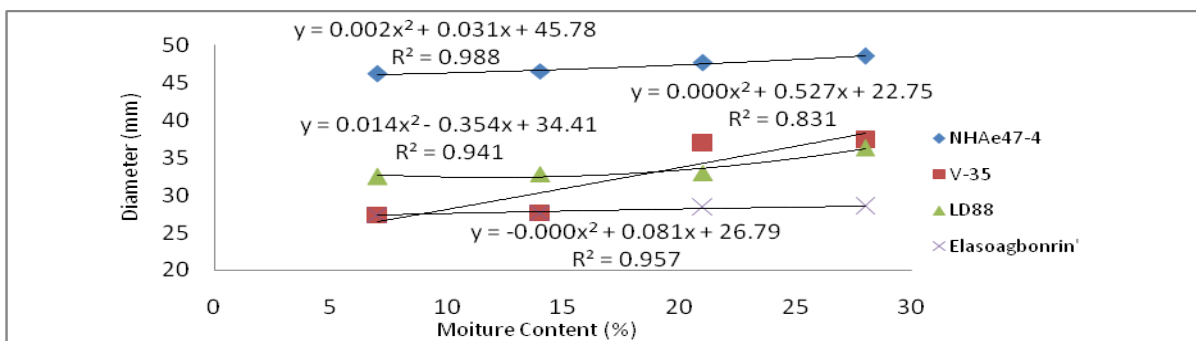


Fig.3: Effect of Moisture Content on Okra Pod Diameter

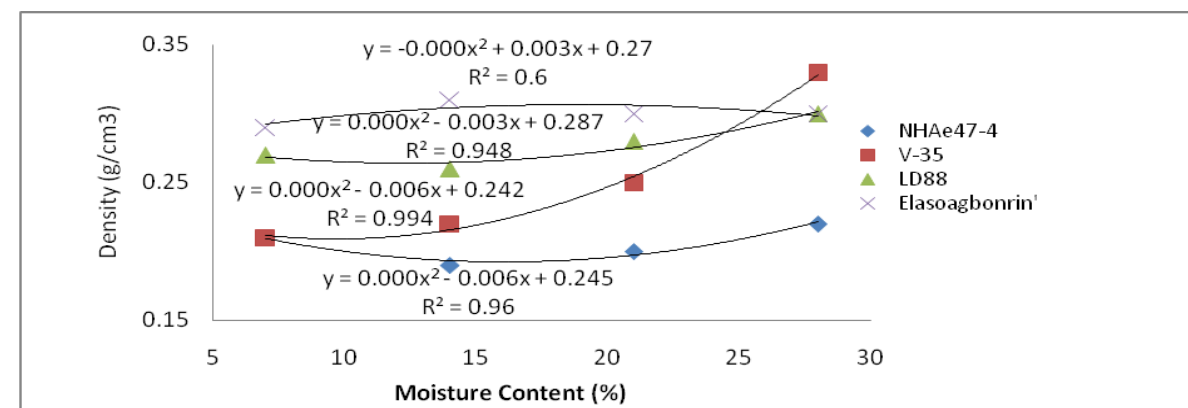


Fig.4: Effect of Moisture Content on True Density of Okra Pod

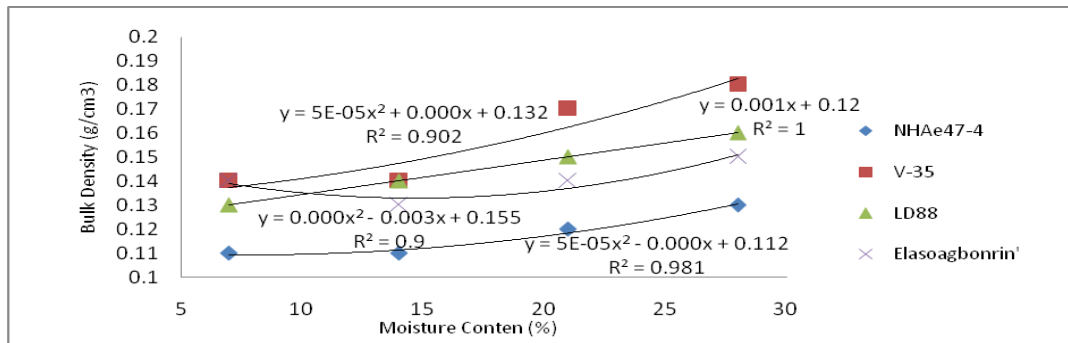


Fig.5: Effect of Moisture Content on Bulk Density of Okra Pod

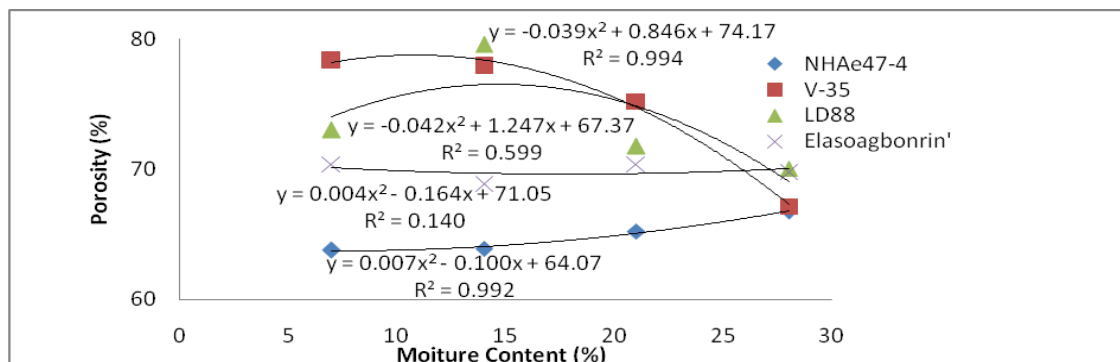


Fig.6: Effect of Moisture Content on Porosity of Okra Pod

Bulk densities of pods increased with increase in moisture content. NHAe47-4 pod density increased from 0.11 to 0.13 g/cm³, V-35 pod increased from 0.14 to 0.18 g/cm³, LD88 pod increased 0.12 to 0.16 g/cm³ and 'Elesoagbonrin' pod increased from 0.14 to 0.15 g/cm³ at 7 to 28 % moisture content respectively. All relationships among the dimensions are logimic as expressed in Figure 4 and 5. There is no difference between means of pod true density at 7 to 21 % moisture content (Tables 2 and 3).

The true density of okra pod generally increases with increase in moisture content in accordance with results obtained for frictional and aerodynamic properties Adejumo [9], but not in agreement with those of Visvanathan et. al. [5] and Dutta [7] for Neem (*Azadirachta India*) nut and gram respectively. The results suggest that the pod increase in weight does not commensurate with volume increase as the moisture content increases. This is due to the fibrous nature of the pod, which absorbs the moisture with little swell in size. Pod true density is in the range of 0.25 to 0.26 g/cm³ for the moisture content range of 7 to 28 % (w.b). Increase in pod bulk densities with moisture content suggests that increase in the mass of pod outweigh the volume. Thus, the increase in bulk volume of pod is negligible.

The analysis of variance (Table 4) shows that there is a significant difference in moisture content effect on the pod true and bulk densities at 5 % level. Likewise the varieties effect on pod true and bulk densities are significantly different at 5 % level. The interaction between variety and moisture content are also significant except for the pod true density. The true and bulk densities of pod are in the range 0.14 - 0.26 g/cm³.

In agricultural produce processing, the true and bulk densities are of important practical application. The knowledge of density is useful in the design of silos and storage bins, processing and handling machines, maturity and quality evaluation of products, which are essential in grain marketing. Others include determination of Reynolds number, thermal properties in heat transfer problems, chemical composition, separation of products by flotation etc.

The effects of moisture content on okra pod porosities are as shown in Figure 6. The porosity of NHAe47-4 pod decreased from 47.8 % at 7 % moisture content to 36.1 % at 14 % and increase to 36.6 % at 28 % moisture content. The porosity of V-35 pod increased from 29.5 % at 7 % moisture content to 36.6 % at 14 % moisture content, and decreased to 26.4 % at 28 % moisture content. LD88 pod decreased from 48.7 % at 7 % moisture content to 43 % at 14 % moisture content and increased to 46.3 % at 28 % moisture content. 'Elesoagbonrin' pod increased from 51 % at 7 % moisture content to 54.9 % at 14 % and decreased to 51.3 % at 28 % moisture content. There are no significant difference (5 % level) between means of pod porosity at 7 to 28 % moisture content (Tables 2, 3 and 4).

The variation in the porosity of okra pod is in two groups. NHAe47-4 and LD88 decreased to a minimum in the range 14 - 21 % moisture content and increased thereafter, while V-35 and 'Elesoagbonrin' increased to maximum in the same moisture content range and decrease thereafter as moisture content increased from 7 to 28 % (w.b). Analysis of variance shows that the effects of moisture contents on porosity of okra pod are not significant unlike variety and their interactions at 5 % level.

The utilization of okra pod porosity can be seen in the area of drying (heat and air flow), storage and aeration, bagging and marketing of seed and design of processing and plant machinery.

The results of okra pod projected and surface areas at 10 % moisture content and mass of pod (7 to 28 % moisture content) are presented in Table 5. Analysis of variance is presented in Table 6.

The projected area of Okra pod varied with the variety with grand mean of 723.23 mm². Pod projected area are: 1033.10 mm², 622.80 mm², 556.70 mm² and 680.30 mm²; and pod surface area are 3615.70 mm², 2269.60 mm², 2032.20 mm² and 2592.70 mm² for the four varieties respectively (NHAE47-4, V-35, LD88 and 'Elesoagbonrin'). There is no difference between means of V-35 and LD88 pod surface area with a grand mean of 2627.55 mm² for the four studied varieties. Okra seed/chaff ratio ranges from 0.99 to 2.53 with mean of 1.50 (Table 7).

The mass of pod increases with increase in moisture content. This is because the absorbed water increases the self-weight of the pod. Tables 1 to 4 show that there is no significant difference between means of V-35 and LD88 mass of pod. The mass of pod is significant at 5 % on moisture content levels and among the varieties. The mean value of mass of pod was 19.10 g for NHAE47-4, 11.16 g for V-35, 10.50 g for LD88 and 12.32 g for 'Elesoagbonrin'. The grand mean value was 13.30 g at moisture content of 7 to 28 %.

The analysis of variance shows that the means of the pod projected and surface area are significantly different among the variety at 5 % level. NHAE47-4 gave the highest projected area and LD88 the least projected area, NHAE47-4 gave the largest surface area, followed by 'Elesoagbonrin' then V-35 which is not significantly different from LD88. Variation in the parameters are due to diversity of agricultural material properties in agreement with Waziri and Mittal [6], who state that agricultural materials pose special problems in determining their physical properties.

The projected and surface areas are usefully in obtaining the drag force, design of storage bin, processing and handling equipment of Okra pod.

IV. CONCLUSION

From the results obtained in this study, the following conclusions were drawn;

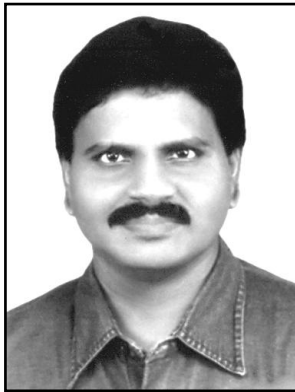
- i The linear dimensions of pod, equivalent diameter, true and bulk density of pod increases with increase in moisture content.
- ii The four Okra varieties (NHAE47-4, V-35, LD88 and 'Elesoagbonrin') pods were different with respect to linear dimensions, equivalent diameter, number of seed per pod, pod projected area, pod surface area, true and bulk densities and porosity.
- iii The mean Okra pod length and diameter were 107.97 mm and 35.17 mm regarded as conic/ribbed during the analysis of rate processes.
- iv The true densities of Okra pod were higher than the bulk densities with ranges 0.25 – 0.27 g/cm³ (true) and 0.10 – 0.19 g/cm³ (bulk).
- v The mean Okra pod projected area was 723.23 mm² and pod surface area was 2627.55 mm². These parameters varied significantly with the varieties.

REFERENCES

- [1]. W.E.Elipeson, and S.R.bhowmik, "Indian fruit and Vegetable processing Industry-potential and challenges". Journal of fruits, vegetables and Nuts, vol.40 No.5.Pp 7 – 12, 1992.
- [2]. L. O.Ogungbaigbe, "Economic potentials and limitations of frontline vegetables in selected states in Nigeria". Proceeding of Horticultural Society of Nigeria. Pp 220 – 231, 2001.
- [3]. R.R.Schippers, "African Indigenous vegetables". An Overview of the cultivated species Chatham, UK: Natural Resources Institute/ACP-EU Technical Centre for Agricultural and Rural Cooperation. Pp 1 - 7, 103 – 118, 2000.
- [4]. N.N. Mohsenin, "Physical characteristics and Mechanical properties" Revised Edition. Gordon and Breach Science Publishers. New York. Pp 94 - 96, 798 – 804, 1986.
- [5]. R.Visvanathan, P. T. Palanisany, L.Gothandapani, and V. V.Sreenarayanon, "Physical Properties of Neem Nut". Journal of Agricultural Engineering Research vol. 63, Pp. 19 – 26, 1996.
- [6]. A. N.Waziri, and J. P.Mittal, "Design – Related physical Properties of Selected Agricultural Products". Journal of Agricultural Mechanization in Asia, Africa and Latin America. Vol.14, No. 1. Pp 59 – 62. 1983.
- [7]. S. K.Dutta, U. K.Nema, and R. K.Bhardwaj, "Physical Properties of Gram". Journal of Agricultural Engineering Research. Vol. 39. Pp. 259 – 268, 1988.
- [8]. K. Oje, "Locust Bean Pods and Seeds: Some Physical Properties of Relevance to Dehulling and Seed Processing". Journal of Food Science and Technology. Mysore Vol.30 No.4.Pp. 253- 255. 1993.
- [9]. A.O. Adejumo, E. A. Ajav, J. C. Igbeka, T. A. Ilori, "Effects of Moisture Content and Variety on Frictional and aerodynamic Properties of Okra(Abelmosus Esculentus (L) Monech)". Proceeding of Nigerian Institution of Agricultural Engineers. Pp. 249-255, 2009.
- [10]. A.O. Adejumo, E. A. Ajav, J. C. Igbeka and T. A Ilori. "Effects of Moisture Content and Variety on Selected Mechanical Properties of Okra(Abelmosus Esculentus (L) Monech)". Proceeding of Nigerian Institution of Agricultural Engineers. Vol. 32, Pp. 470-478, 2011.
- [11]. ASAE STANDARDS." Standards Engineering Practices" 40th Edition. Adopted by: American Society of Agricultural Engineers.USA. Pp.449, 450 and 457, 1993.
- [12]. N. N. Moshnenin, "Physical Properties of Plant and Animals materials". Gordon and Breach Science Publishers, New York. Pp. V – vi. 1980.
- [13]. K. Oje, and E. K. Ugbor, "Some physical Properties of Oil bean seed". Journal of Agricultural Engineering Research. Vol.50. Pp. 305 – 313. 1991.
- [14]. R. K. Jain, and S. Bal. "Properties of Pearl Millet". Journal of Agricultural Engineering Research. Vol. 66. Pp. 85 – 91, 1997.

TAMIL PUTHANDU!...

(Scientific Research Article)



M. Arulmani, B.E.
(Engineer)



V.R. Hema Latha, M.A., M.Sc.,
M.Phil. (Biologist)

Heart felt advance **PUTHANDU WISHES** is conveyed to all the citizens of India and all people of global nations. "**PUTHANDU**" shall mean "**STEP INTO NEW AGE**" called by Proto Indos of Ancient India. In **Indo Culture** many parts of India Puthandu being observed during the month between **MARCH-APRIL**. In **THAILAND**, "**Thai New Year**" being observed on "**APRIL 13**". In South India Puthandu being observed on "**APRIL 14**".

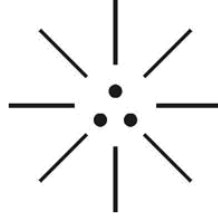
This scientific research focus that "**PUTHANDU**" (Tamil New Year) shall mean the day when **HUMAN ANCESTORS** Considered descended from **MARS PLANET** to **EARTH PLANET** around 3,00,000 years ago during "**Dark Age**" of Universe **HUMAN ANCESTORS** shall also be called as "**MAKKAL MUTHALVAR**". Makkal Muthalvar shall be considered as godly person (Devas Angel race) Considered born during the month "**February - March**" and lived in **MARS PLANET** in the early universe. During **expanding Universe** the godly Populations Considered descended to **EARTH PLANET** (Kachcha Theevu) during "**MARCH - APRIL**" and began "**NEW LIFE**". The philosophy of origin of human ancestors shall be represented as below.

(i)



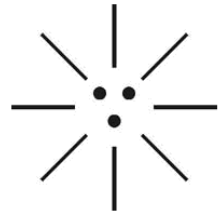
அகிலன்
(Supreme Artist)

(ii)



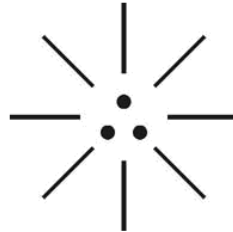
தமிழ்
(Immortal Music)

(iii)



மாயன்
(Mortal Earthly Soul)

Further the "TAMIL" shall be Considered as the "LAW OF GLOBAL MUSIC "(Sangeetham) responsible for existence of entire global Matters of the Universe.



அம்மா
(Law of Music)

- i) Right dot in "LA" (Like "PITCH")
- ii) Left dot is "LALA" (Like "MELODY")
- iii) Center dot is "LALALA" (Like "RHYTHM")

Don't we know the full text of "INDIAN NATIONAL ANTHEM" (or) "SRILANKAN NATIONAL ANTHEM" (or) "PAKISTAN NATIONAL ANTHEM" ... "NO WORRY" ... The whole national Anthem of entire world shall be sung by **three-in-one** Musical note elements as below

"LA... LALA... LALALA..."

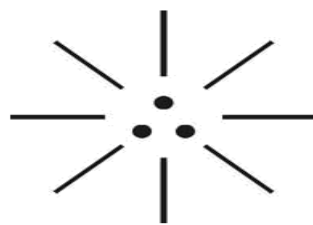
JANA... GANA... MANA... (LA... LALA... LALALA...)
JAYAHE... JAYAHE... (LALALA... LALALA...)

INDIAN NATIONAL ANTHEM



**" Jana Gana Mana Adhinayaka Jaya He
Bharat Bhagya Vidhata
Punjab Sindh Gujarat Maratha
Dravida Utkala Banga
Vindhya Himachal Yamuna Ganga
Uchhala Jaladhi Taranga
Tubh Shubha Name Jage
Tubh Shubha Ashisha Mange
Gahe Tubh Jaya Gata
Jan Gan Mangaldayak Jay He
Bharat Bhagya Vidhata
Jaye He ! Jaye He ! Jaye He !
Jaye,Jaye,Jaye,Jaye He "**

Further "TAMIL" shall be considered as the law of "GLOBAL LOVE". Mother kisses son lovingly!... Father kisses daughter lovingly!... Husband kisses wife lovingly!!!... What does mean kiss?...



**முத்தம்
(Law of Love)**

- i) Right dot is "TONGUE" (Like MOON)
- ii) Left dot is "LIPS" (Like EARTH)
- iii) Center dot is "HEART" (Like SUN)

Further "TAMIL" shall be considered as Law of "GLOBAL PEACE".



TAMIL ALIAS?...

அம்மாவம்... நய்யை...

அப்பாவம்... நய்யை...

ஆதியம்... நய்யை...

அந்தமும்... நய்யை...

தையம்... நய்யை...

சித்திரையம்... நய்யை...

- Author

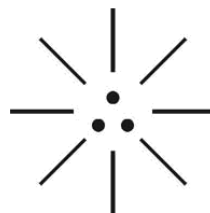
The philosophy of "ALIASING" adopted in Digital signal processing technology like Temporal aliasing (Digital Audio), Spatial aliasing (Digital image) might be derived from the fundamental Musical law of "AMMA".



Left: An aliased image of the letter A in Times New Roman. Right: An anti-aliased image. (See also: Font rasterization)

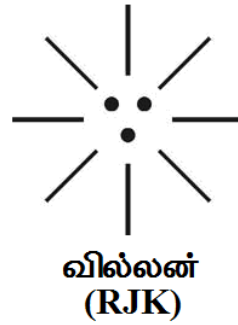
A recent Trial case study on "YUTHAMA VILLAN" shall be Considered as evidence on focusing **Ancient Tamil culture**. The **KBR** (K. Balachander), **RJK** (Rajkamal), **TGM** (Thiru Gnana Sampandam) shall be Considered as **Three-in-one** element of "GLOBAL CINEMA". TGM shall be considered as "NSK-2015". (Humanist Humour)

(i)



உத்தமன்
(KBR)

(ii)



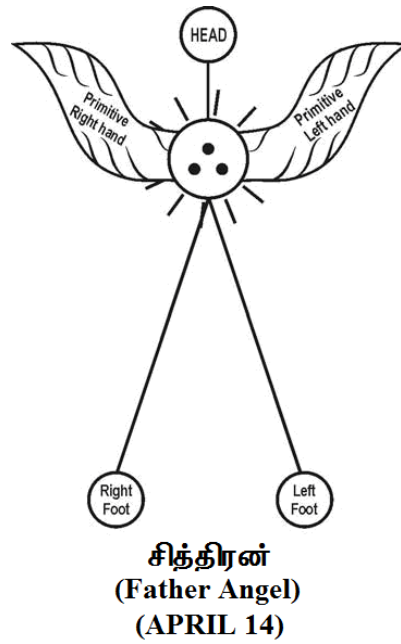
"KBR" is Like "BRAHMAN" (Yuthaman)

"RJK" is Like "MAYAN" (Villan)

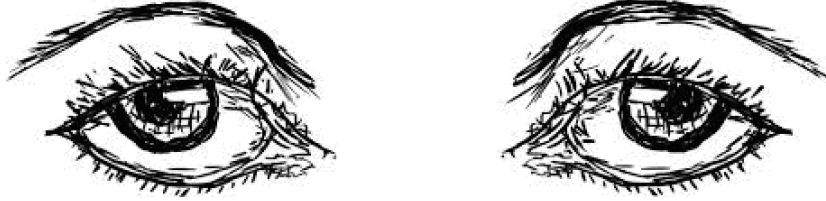
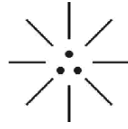
"TGM" is Like "REEL" (Humour Link)

The Philosophy of human ancestors shall be viewed as described below.

(i)



(ii)



சித்திரா
(Mother Angel)
(APRIL 14)

Namaste to "MAKKAL MUTHALVAR" in the "new age"!... Makkal Muthalvar shall also be considered as Three-in-one Divine Medicine "THIRIKADUKAM" (Sukku, Milagu, Thippili).

- Beloved Global children.

The pre- stress concrete structure, Found to-be More Effective Then THE Reinforced concrete structure & System developed for mechanism OF, Anchoring devices in pre and post Tensioned concrete structural elements.

Pradeep Nath Mathur¹, Prof (Dr.) A. K. Sinha², Prof. (Dr.) P.B.L.Chaurasia³

¹Ph.D. Research Scholar, Gyan Vihar University, Jaipur (Rajasthan) INDIA.

² Director, Centre of Excellence in Climate Change & water, Suresh Gyan Vihar University, Jaipur (Rajasthan) INDIA & H.O.D. Civil Engg. Suresh Gyan Vihar University, Jaipur (Rajasthan) INDIA.

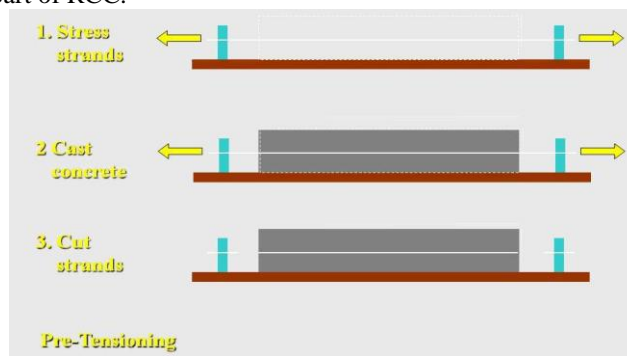
³ Vice- Chancellor, ICFAI University, Jaipur (Rajasthan) INDIA

Dean (School of Engineering & Technology) Suresh Gyan Vihar University, Jaipur (Rajasthan) INDIA & Director, Centre of Excellence Energy Research & Utilization, Suresh Gyan Vihar University, Jaipur (Rajasthan) INDIA.

ABSTRACT: - The pre-stressing concrete Used for casting of section is quite different from reinforced cements concrete (RCC.) in concrete Technology. The pre- stressing system used is of two kind, pre- tensioning & posttensioning methods. The prestressing by pre & post tensioning device mechanism, developed for Anchoring system in concrete structural element is adopted for structures. In modern type of Pre stressing electricity with Low voltage and high current is used in anchoring for a concrete member & sulphur Coating as applied on steel bars working, as duct material before the casting of concrete member. While supplying electricity in the structure sulphur get melted up because heat generated in the steel structure & allow them for pre stressing. No provision of any duct is required .The High strength steel alloy structure could be anchored by tightening nuts at both the ends. The Pre-stressing in concrete structure is found more effective then RCC technology. To-day prestressing is preferred for large structures like bridges etc. ,it is required to adopted for all small concrete structure sections also. It is to-days demand to replace RCC completely by Pre-stress concrete, because of RCC have large section with less strength as compare to pre-stress concrete. In RCC System it is rein-forced first and then loaded after casting, when ever in the Pre stressing system, where reinforcement which may called 'tendons' are as one kind used for stressing in the concrete itself . They are stressed first then casted & force is applied. It is required that, effective & less cost (Economic) anchoring devices must be available for the prestressing techniques; It is because of its initial investment is high and less pre-stress work is restricted also, must be possible to make adoption easily. It is found possible to make concrete having light weight & high strength in all structures. High strength alloy steel & Rich strength concrete may be used along with large prestressing force application along with avoiding grouting in to post-tensioned duct.

I. INTRODUCTION:-

It is known that, tensile stresses are completely resisted by steel bars of the section as concrete is weak in it and compressive stresses are resisted by concrete section itself which are induced in above neutral axis only. "This concept gave birth to pre-stressed concrete practically." In this context high Strength tensile steel & concrete are basic components considered an element of the structure also in practice steel is stressed first which induce tensile strength, & compressive stress in the concrete while whole concrete resists external forces when required to be bear by section. Theoretically precast is the design and developed the anchoring system for post-ensioning prestressing. Pre stressing in concrete technology is quite different form reinforced cement concrete (Rcc) in the sense that technologically both are divergent modes. Pre-stressing is the application of a predetermined force or moment to an element in the structures such that combined internal stresses resulting from applied force or moment and positive from external loads will be within specific limits and hence section is entirely compressive. Wires or strands or Tendons are stressed between anchorages. In fact structural behavior of RCC and Pre-stressed concrete is totally different. While steel is an integral part of RCC Section. Bond between steel and concrete plays an important part in RCC. And tension in steel develops when concrete begins to crack and during cracking strains of concrete are transferred to steel through bond. In Pre-stressing bond between steel and concrete does not exist, that is stress in steel does not depend on strain in concrete. A stress in steel varies with bending moment along the length of beam in RCC. Whereas there is, no variation stress in steel along the length of beam. In Pre-stress anchoring in section have less complex analysis. Crack control in RCC. Is a problem because of it is required that stresses in steel should be limited. In Pre-stressing with the inclusion of anchoring crack control is not difficult. There is no need to limit stress in steel. The phenomenon of steel acting as tension flange of a beam analogous to section is a part of RCC. Otherwise steel acting as tension flange of a beam analogous to section is a part of RCC.



Post-tensioning Pre-stress diagram

Difference between reinforced concrete and pre-stressed concrete:-

S.N	Reinforced cement concrete(RCC)	Pre-stress concrete
1	Steel can resist tension but concrete cannot resist.	Steel inducing pre-stress force. (If this can be by other means then steel is of no use.)
2	The concrete get cracked due to tension and strains are through steel bands.	Band between steel & concrete is not necessary. (As stress in steel does not depends on concrete strain and stresses in steel do not vary along the length.)
3	Banding moment change means change in resultant force.	Banding moment change means change in location of pre-stress line.
4	Stresses in steel must limit because, it controls cracking.	Stresses in steel must be unlimited to control cracking.
5	Required IS Code is IS:456-2000	Required IS Code is IS: 1343-2012
6	In RCC reinforcement is not stressed before casting	In pre-tensioning reinforcement is stressed before casting & in post-tensioning reinforcement is placed in duct after casting also stressed.
7	RCC member steel play passive role.	Active role of steel is played by in pre stressed concrete member.
8	In RCC stress in steel is variable with lever arm.	In Pre stress concrete the stresses in steel is constant.

9	In Pre stress concrete members, deflections are less.	In RCC deflections are more due to eccentric force induced couple.
10	RCC is less durable, as it is less dense.	Pre stress concrete is more durable.
11	RCC has fatigue resistance less.	Pre stress concrete fatigue resistance is more as compare to RCC.
12	RCC has initial cost less.	Pre stress concrete has initial cost more.
13	RCC has large section for given load.	Pre stress concrete has smaller section for given load.
14	RCC can take fewer loads for given section.	Pre stress concrete can take more loads for given section.
15	RCC Requires less strength concrete for casting for given load.	Pre stress concrete Requires high strength concrete for casting for given load.
16	RCC gives less space for the required section	Pre stress concrete gives more space for the required section.
17	RCC do not require special equipments for casting.	Pre stress concrete does require special equipments for casting.
18	In RCC the phenomenon of steel acting as tension analogous to section.	In Pre-stress anchoring in section have less complex analysis.
19	Bond between steel and concrete plays an important part in RCC. Crack control is difficult. Crack control in RCC. Is a problem. As tension in steel develops when concrete begins to crack and during cracking strains of concrete are transferred to steel through bond.	In Pre-stressing with the inclusion of anchoring crack control is not difficult.
20	Steel acting as tension flange of a beam analogous to section is a part of RCC. & stresses in steel should be limited.	There is no need to limit stress in steel

Advantage of pre-stress concrete over Rcc:-

- i) In pre-stressing system, complete section of a structural element is in use hence smaller section is required.
- ii) In pre-stressing concrete system section is smaller; hence the available space is more.
- iii) In pre-stressing concrete system section passes shear resistance increased.
- iv) Pre-stressing concrete system has more resistance to fatigue, impact and vibrations.
- v) Pre-stressing concrete system saves concrete from creaking, also once the pre-stress concrete structure is creaks; it behaves as a RCC Structure.
- vi) Pre-stressing concrete system can take more loads which come on it, for a small section of concrete.
- vii) pre-stressing concrete system protects concrete section from creaking, also once the pre-stress concrete structure creaks it behaves like a RCC Structure
- viii) Complete section is in use hence smaller section is needed.
- ix) Its shear resistance increased.
- x) It has more resistance to frutigue, impact and vibrations

The major disadvantages of simple RCC:

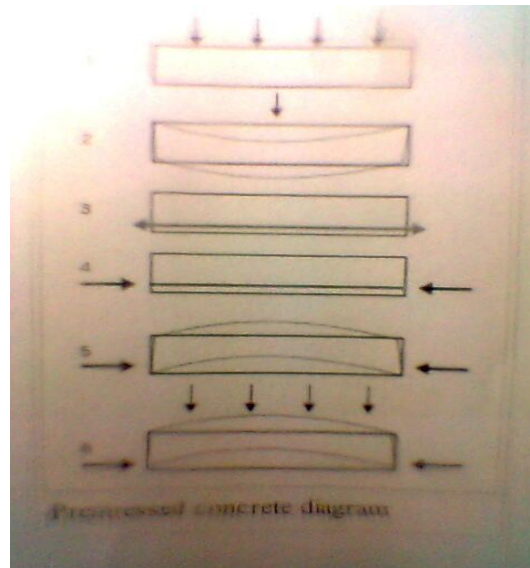
- i) RCC is weak in crack resistance at working load, causing corrosion in reinforcement and concrete.
- ii) In RCC it is impossible to use high tensile steel in practice as tensile reinforcement hence, loss of load carrying capacity of the member.
- iii) There is trouble of permanent negative strain as due to shrinkage and creep in concrete, it is seen that, permanent strain is greater than, initial strain in mild steel. Results In low pre-tension & the section sooner disappears also, member behave as simply reinforced.

Some Suggestions made by:

- i) C.R. Steiner (1908) of USA recommended the tightening of reinforcing rod after some shrinkage and creep of concrete had taken place.
- ii) According to ACI Committee "Pre-stressed concrete is the one in which there have been introduced internal stresses of such magnitude and distribution that the stresses resulting from giving external loadings are counteracted to a desired degree. P. Jackson (1886) of USA obtained patents for pre-tensioning steel tie rods in artificial stones and concrete arch to serve as floor slabs.
- iii) K. Doring (1888) of Germany suggested pre-tensioning of wires in reinforced concrete floor structures.
- iv) R. E. DILL (1925) of Nebraska used high strength steel bars.

Pre stressed concrete structures are classified as:

- i) Pre-tensioning: The steel Reinforcement is
- ii) Tensioned before placing of concrete.
- ii) Post-tensioning: The tendon is tensioned in duct, after concrete has hardened.

**Pre-stress concrete diagram****Tensioning Devices:**

The principal upon which devices works are as under-

- 1) Mechanical devices
- 2) Hydraulic devices
- 3) Electrical devices
- 4) Chemical device

Methods of pre-stressing:

- i) Freyssinet system.
- ii) Gifford-Udall system.
- iii) Magnel Blaton system.
- iv) Lee-McCall system.

Basic assumptions made:-

- i) Concrete is a homogenous material.
- ii) In working stress condition steel and concrete behave elastically, under suspended load condition without withstanding any small amount of creep.
- iii) The plane section is assumed remain plane before bending even after bending.

Type of losses in pre stress-**Pre-tensioning:**

- a) Elastic deformation, Shrinkage and Creep of concrete.
- b) Relaxation of stress in steel.

Post-tensioning:

- a) In concrete no loss due to elastic deformation takes place if wires are tensioned simultaneously.
- b) Relaxation of stress in steel.
- c) Shrinkage & Creep of concrete
- d) Anchorage slips in steel .
- e) Friction between steel & concrete.

REVIEW OF LITERATURE:-

The design and development of anchoring mechanisms are a function of pre-stressing perfection the compression and takes part in resisting moments. There is no corrosion of Steel and sections are much smaller. Self weight is reduced because anchors also do not add to self weight of structural elements, this saves cost of foundations which have to bear less loads.

According to **IS 1343 (1980)** anchoring devices may add to a smaller section of disadvantages along with high strength concrete and steel as well as skilled labor, yet there is an overall economy in using prestressed concrete because decrease in member sections results in decrease in Design loads, Economical structure and foundations. The only common items in RCC. And pre-stressing are materials – concrete and steel, but anchors need high strength tendons to establish compressive stresses in all sections.

FRP reinforcement can have advantage over steel in being lighter in weight, higher in tensile capacity, more resistance to corrosion and electromagnetically transparent. Several manufacturing methods are available for fabrication of FRP reinforcement for concrete. For rod and grid type reinforcement, pultrusion and braiding are the most commonly used manufacturing methods because of low cost, high quality and efficient fiber orientation. Flat or round FRP rods come in a variety of surface shapes, E.g. Dimpled, Indented or Coated with sand in order to provide better bonding with concrete.

Taerwe ET. al. (1992) has considered that concrete is conventionally reinforced with steel bars and tendons. It is well known that the deterioration of concrete structures can mostly be attributed to corrosion of the reinforcing steel. This results from exposure to environments high in moisture and chlorides. Chlorides come from sources such as sea water or de-icing salts used in the winter time on bridges and parking garages.

Coating the steel reinforcement with a layer of epoxy has been the most common method of several practices used for controlling corrosion some recent failures have left doubts about the dependability of epoxy coating protection. Galvanizing of steel reinforcement, another form of protective coating, is suspected of UN satisfactory protection in chloride contaminated concrete, of impairing steel to concrete bonding & of causing hydrogen embrittlement of pre-stressing tendons.

Nanny et.al. (1996) concluded that ultimate load capacity is generally controlled by the anchor rather than the tendon itself, suggesting that anchor efficiency can be improved. It is explained that the three classes of anchor systems (That is wedge, resin potted and spike) offer advantages and disadvantages. The degree of complicity in terms of installation procedure varies for wedge type anchors, dry lubrication and sand coating on the two faces of the wedges are helpful. Protection of the tendon can be attained with a sleeve. High temperature did not adversely affect the performance of the system tested. Wedge anchor systems are suitable for pre-tensioning application.

Spike anchors if used with dry fiber ropes may work relatively well. This system requires the longest setup time resulting from the combination of removal of the plastic sheath, combing and spreading of the individual fibers and proper placement of the spike with a uniform distribution of fibers all around it.

For wedge anchors, grit should be present on the wedge surface to ensure proper gripping of the tendons. When comparing carbon stress tendons with Arapree tendons both of which utilize plastic wedges, the carbon stress system with applied grit does not show the slippage of the untreated Arapree wedges.

For resin/Grout Potted anchors, failure may be due to pull-out of the tendon from the resin/Grout anchor without rupture of the tendon however parabolic system may show shifting and erecting of the resin plugs. The plotted anchors are by far the easiest to setup for testing when pre-installed. The practical drawbacks include pre-cutting the tendons to length and curing time for the resin/Grout.

Lin & Ned (2001) assert that in pre-tensioning, anchoring mechanism is not integral working part of structural element. However at the construction stage and/or manufacturing of pre-tensioning members, tendons are stretched by jacks and anchored at the ends. After concrete has set and hardened, the tendons are separated from anchors thereby imposing pre-stressing in the beam or structural elements. The system consists of two bulk heads anchored against the ends of a stressing bed. The tendons are pulled between the two bulk heads. A pre-stressing bed is used for casting usual units and possibly shorter units. It supports vertical reactions due to

which pre-stressing of bent cables can be done. Hoyer system shall be analyzed. The anchoring devices for holding pre-tensioning strands to the bulkheads remain on the wedge and friction principle. One common device consists of a split cone wedge, which is made from a tapered conical pin. The existing tapered conical pin is drilled axially and tapped & then cut in half longitudinally to form pair of wedges. The anchoring block has a conical hole in which tapered conical pin holes are strands. These grips can be used for single wires as well as for twisted wire strands. Alternately the pin is not drilled, but is cut in half longitudinally and the flat surface is machined and serrated. As a third option, quick release grips which are more complicated and costly, are used especially when wires are to be held in tension only for short periods. Another method, under study is to add mechanical end anchorages to the pre-tensioned wires. Dorland anchorage, consisting of clips, can be gripped to the tendons under high pressure and the edges of the clips can then be welded together at several points. In such mechanical anchorages, tendons of greater diameter can be permitted. In post-tensioning systems, mechanical pre-stressing, electrical pre-stressing by application of thermal energy and chemical post-stressing by using expanding cement shall be the part of research.

METHODOLOGY / LABORATORY WORK :- Some of the systems shall be studied, analyzed and verified in efficiency and strength so that minimum pre-stress losses occur. The first anchoring system FREYSSINET had quite useful advantages and yet needed improvement and / or additions and deletions. Other systems under study shall be Magnel Blaton, Gifford Udall (with two types of anchoring-plate anchorage and tube anchorage), PSC Mono wire system & Lee Mecall systems.

Electric pre-stressing shall be experimented in which bars shall be stretched by means of heating using electrical energy. It shall be considered as a transition from RCC. To pre-stressing. Chemically pre-stressing or self stressing shall be experimented in which self stressing cement shall be used that expands chemically after setting and during hardening.

Finally comprehension of theoretical nature of pre-stressing anchoring technology which is a significant part can be analyzed on rational basis and critical study of the existing devices modification there of as well as attempt towards development of better and efficient mechanisms will be a purposeful possibility. Role of welding shall be attempted and highlighted practically for strong grips.

Electrical pre-stressing:- This is modern type of pre-stressing. We use electricity for working of Anchoring device system. It is introduced by Biller & Carlson. For post-tensioning we use sulphur coating to cause duct material while casting with concrete. When electric current is passed

Through the tendons it gets heated up and sulphur coating is melted. The tendons end as threaded & nutted. By tightening those Anchoring of the section is achieved.

PRACTICAL APPROACH:

We consider for Fe-410 steel bar – 8mm ϕ

The properties come between cast iron and wrought iron. It is having property of getting hardened and tempered, also has 0.1%-1.1% of carbon & granular like structure.

Its sp. Gr.-7.85 & melting point between 1300⁰ to 1400⁰ C.

The ultimate compressive strength is 180-350 MPa. & ultimate tensile strength is 310-700 MPa.

It is found to be tough, malleable and ductile in nature.

The coating thickness of sulphur material forming a duct, on steel bar shall be considering - 0.5 mm. A mould is using to cast as a beam by concrete on coated steel bar. Mould is shown in figure below- dimensions 420x150x150 mm. cu. M15 Grade concrete having ratio 1:2:4 is prepared of required workability then it is poured to fill the mould to cast required beam. After 24 hours it is taken out from mould & cured for 7 days the casted beam required is two for our experiment of same dimensions. The prepared beam as figured below- Now the base plate on both ends of beam is placed. Electric current is passed so that coating is melted & at bars nuts are tightened at both sides so that required anchoring purpose is solved.



FIGURE:- Beam with sulphur coated steel bar

FIGURE: Transverse test on pre-stress beam



FIGURE : Transverse test on RCC beam

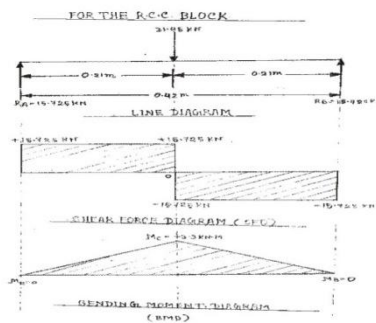


Figure- Universal Testing Machine with Plotter & Hydraulic Load Dial

Result –

The Peak load of Pre-stress beam = 32.50 KN.

The Peak load of RCC beam = 31.45 KN.



Beam with base plate and nut is shown in figure

Heat generated about 170⁰ C which causes sulphur to be melt & bars to elongate at this time we will tighten the nuts by using mechanical tools. Some losses will occur in

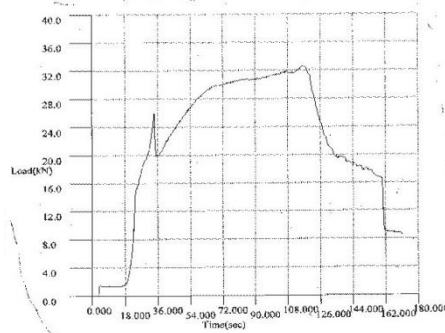
Beam after anchoring been done hence it needs 24 hours for further test . Now considering beam as simply supported & using UTM (Universal Testing Machine) as for calculation of bending moment.

This process is applied for both the conditions that are flat & transverse so that graphs may be made for both the conditions. Under UTM the distance between supports is fixed. Width, Thickness & Crosshead Travel is first found then Peak Load, Cross Head Travel at Peak & Transverse strength is found. *Plotter attached with UTM machine draw complete graph till start to specimen break*

Transverse Test Report is as under:

1)

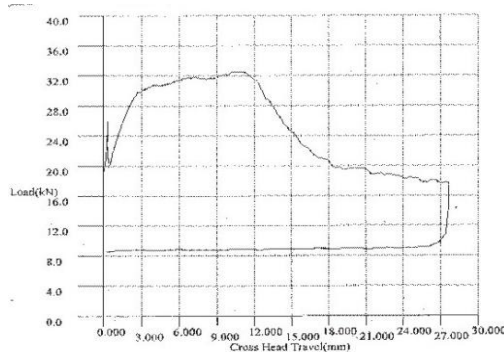
Machine Model : TUE-C-1000.
 Machine Serial No. : 2009/50
 File name : A4, CIVIL, UTM.
 Material Type : RCC Beam 1 (Pre-stress)
 Distance between
 Supports : 420.00 mm
 Width : 150.00 mm
 Thickness : 250.00 mm
 Max. Cross head
 Travel : 250.00 mm
 Peak Load : 32.50 KN.
 Cross head Travel
 At Peak : 11.20 mm
 Transverse strength : 06.07 N/mm²



Transverse Test Report is as under:

2)

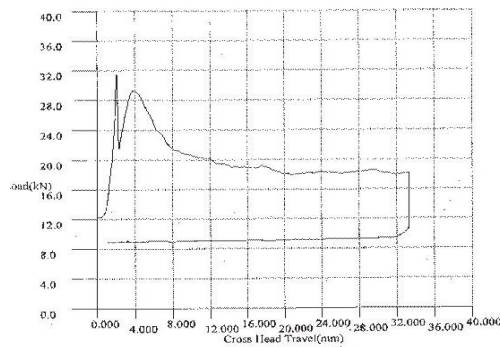
Machine Model : TUE-C-1000.
 Machine Serial No. : 2009/50
 File name : A4, CIVIL, UTM.
 Material Type : RCC Beam 2 (Pre-stress)
 Distance between
 Support : 420.00 mm
 Width : 150.00 mm
 Thickness : 250.00 mm
 Max. Cross head
 Travel : 250.00 mm
 Peak Load : 32.50 KN.
 Cross head Travel
 At Peak : 11.20 mm
 Transverse strength : 06.07 N/mm²



Transverse Test Report is as under:

3)

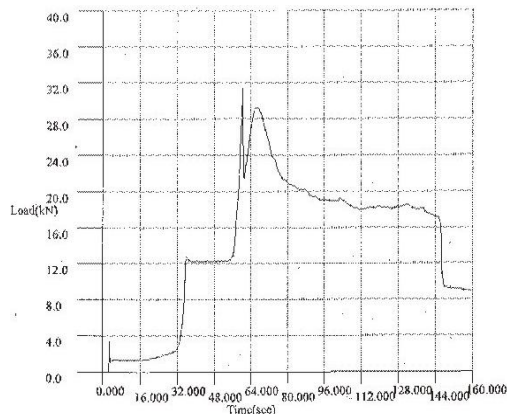
Machine Model : TUE-C-1000.
 Machine Serial No. : 2009/50
 File name : A4, CIVIL, UTM.
 Material Type : RCC Beam 3
 Distance between
 Support : 420.00 mm
 Width : 150.00 mm
 Thickness : 250.00 mm
 Max. Cross head
 Travel : 250.00 mm
 Peak Load : 31.45 KN.
 Cross head Travel
 At Peak : 2.20 mm
 Transverse strength : 05.87 N/mm²



Transverse Test Report is as under:

4) Machine Model : TUE-C-1000.
 Machine Serial No. : 2009/50
 File name : A4, CIVIL, UTM.
 Material Type : RCC Beam 4
 Distance between
 Support : 420.00 mm
 Width : 150.00 mm
 Thickness : 250.00 mm
 Max. Cross head
 Travel : 250.00 mm
 Peak Load : 31.45 KN.
 Cross head Travel
 At Peak : 2.20 mm

Transverse strength : 05.87 N/mm²



CONCLUSION:-

We found from study that pre stress concrete anchoring devices influencing tremendously to the civil engineering decisions. It involve various process of pre stressed concrete which help us very much in understanding the mechanism of the working system & various tools are available to performing for structures called anchoring devices, Further we knew that structures by pre stress are more reliable, strong & reduced in size as compared to RCC . Hence we can say that by using anchoring devices better concrete structures can be made. Also pre stress beam can take more loads that are taken by RCC beam. It is one of the simple methods for anchoring the beam at cheaper rate.

RECOMMENDATIONS:-

As we knew about the methods of pre stressing i.e. pre & post tensioning systems are better effective in their respective fields.

But the post-tensioning system has less loss then the other system of pre-tensioning in pre stressing. The reliability and accuracy of anchoring device meet the requirement of design & specifications.

CONCLUSION & RECOMMENDATIONS:-

We came to conclusion to adopt pre-stress concrete in practice by using this method for all kind of structural work to-day. As pre-stressed structures are found more economical may be at long run but with small section can take more loads in a structure. It has been found more strength & durability as compare to RCC structure. Rich concrete grade can be used with high strength alloy steel hence, density and load caring capacity may enlarge. Other benefits of pre-stressing property of light weight along with high strength may be adopted by including FRP to reduce cracks as resistance to cracks is obtained, also gives more space, impact, fatigue, vibration etc. The cracks in RCC. May be eliminated having large section but, load caring capacity is increased with less sized section in pre-stressing. As it can be made high strength and light weight sections with using pre-stressing in FRP (Fiber Reinforced Polymers) the crack is also controlled. In prestressing concrete about 10 to 20 percent losses may be due to, creep and shrinkage in concrete. As we know even greater numbers of expensive equipment are required in using this process, though it is found effective then unstressed RCC structures.

It is sincere recommendation for adopting pre-stressing in all possible concrete structures instead of RCC works.

REFERENCE:-

- [1]. Dolan, Charles W (1990), "Developments in Non metallic Pre-stressing Tendons" PCI – Journal Volume 35 No.5 pp80-88.
- [2]. Guyon, Y., Prestressed Concrete, C.R. Book Limited, London, Fourth Edition 1960.
- [3]. IJBSE. Preliminary Publications, Seminar on Problems of Prestressing, Madras, January 30 to February 2, 1970.
- [4]. IJBSE. Publications, Prestressed Concrete Works in India, 1973.
- [5]. IJBSE. Preliminary Publications, Seminar on Prestressed Concrete Structures, Bombay, January 18-21, 1975.
- [6]. IJBSE. Preliminary Publications, Seminar on Tall Structures and Use of Prestressed Concrete in Hydraulic Structures, Srinagar, May 24-26, 1984.
- [7]. PCI Design Handbook Precast Prestressed Concrete, Prestressed Concrete Institute, Chicago, Illinois, 1978.
- [8]. Symposium, T.Y. Lin Symposium on Prestressed Concrete, Special Commemorative Issue, Journal of the Prestressed Concrete Institute, Vol. 21 No. 5, September-October 1976.
- [9]. Cooley. E.H, Friction in post-tensioned prestressing systems, Research Report No. 1, Cement and Concrete Association (London) 1953.
- [10]. Goldowski, R. J. and Lorenzetti, J.J., An interaction method for prestress losses in a prestressed concrete structure, Journal of the Prestressed Concrete Institute, March-April 1972.
- [11]. Hernandez, H.D. and Gamble, Structural Research Series No.417, University of Illinois, Urbana. May 1975.
- [12]. PCI Report, Recommendations for estimating prestress loss, Report of PCI Committee on prestress loss, Journal of Prestressed Concrete Institute, Vol. 20, No. 4, July- August 1975. Pp. 43-75.

Urban Air Pollution and Its Effect on Forced Expiratory Volume of Lungs

Dr. Gautam Kumar Lalwani¹, Dr. Gopal Purohit²,
Dr. Suresh Kumar Singh^{3*}

¹Tech.A, Department of Chemical Engineering, Faculty of Engineering & Architecture, J.N.V. University Jodhpur (India)

²Sr. Professor, Department of Respiratory Diseases & Tuberculosis, Dr.S.N. Medical College Jodhpur (India)

³Associate Professor, Department of Civil Engineering & Architecture, Faculty of Engineering, J.N.V. University Jodhpur (India)

ABSTRACT: Air pollution in urban areas is due to different natural & man-made sources of pollution. Traffic is the main source of urban air pollution. Increasing vehicles are deteriorating the air quality of urban areas. The polluted air gets entry in the human body through inhalation. Various pollutants present in the ambient air damage the respiratory system and hence various pulmonary Function values are reduced. This reduction is evaluated in terms of Indexes. The objective of this study is to co-relate spirometric abnormalities with duration of exposure and Air Quality Index and to assess the reduction in lung capacity in terms of reduction of "Forced Expiratory Volume (FEV). The study was done at various locations of Jodhpur City, India. The study reveals that the 'Forced Expiratory Volume (FEV) of lungs decrease as the Exposure Duration and pollutants concentration increases. The estimated multiple regression equation for Reduction in Forced Expiratory Volume for 1second (FEV) (i.e. Index for FEV) is developed as

$$Y_E = 0.047X_1 + 0.002X_2 - 0.066$$

The calculated values of 'y_E' give direct indication of damage severity without any medical or Pulmonary Function Test. The values y_F will be in between 0 to 1. If the value is more, this means the extent of damage is high.

KEY WORDS: Lung capacity, Forced expiratory Volume for 1second (FEV)SO₂, NO₂, AQI, Multiple regression analysis, Pulmonary Function Test, ANOVA, Particulate Matter (PM)

I. INTRODUCTION:

Urban air quality has a major impact on the physical & mental health of urban residents worldwide. Various air pollutants get entry in the human body through respiratory system. They damage the respiratory system and interfere with the natural metabolic and other activities of human body. Due to damage of respiratory system various "Pulmonary Function Values" are reduced. The present study is conducted at Jodhpur City to assess the reduction of Forced expiratory Volume for 1second (FEV) of residents due to ambient urban air pollution.

Jodhpur is the second largest city of Rajasthan and is situated in the western part of Rajasthan (India). The increased Army/Air Force, Industrial, Trade & Commerce and Tourism activities have led to expansion and growth of the city and other related economic activities up to a great extent. Although there are more than 100 pollutants/contaminants, which are broadly classified into two categories Particulate Matter and Gases. Here we are concerned with few important pollutants like Respirable Suspended Particulate Matter (PM₁₀), SO₂, and NO₂ only as vehicle pollution is the major source of pollution and most of the time ambient atmospheric condition remains unstable with moderate wind speed. Many environmental cum medical studies have been carried out worldwide to establish a link between different type of pollutants, respiratory diseases and level of pollution that would significantly affect human health. The acute health effect of suspended particulate matter (SPM), even at short term low levels exposure; include increased daily mortality and hospital admission rates for exacerbation of respiratory disease [5]. Long term exposure to PM_{2.5} increases the risk of the non accidental mortality. Living

close to busy traffic appears to be associated with elevated risk [2]. The available human clinical results do not establish a mechanistic pathway leading to adverse health impacts for short term NO₂ exposure at present day ambient environment [3]. In all the analytical studies total mortality was directly associated with long term exposure to particulate matter [4]. Each day our lungs are directly exposed to more than 7000 liters of air, which contain varying amount of inorganic, organic particles and various types of gases. Hence it is required to assess the damage on the basis of air quality of the area. In this case study relationship between severity of the damage in terms of reduction in forced expiratory volume & exposure duration and concentration of pollutants (in terms of Air Quality Index) has been established.

II. METHODS AND METHODOLOGY OF CASE STUDY:

As per EPA guidelines concept of Air Quality Index (AQI) has been adopted. The AQI of different locations of Jodhpur has been determined to select the various spots for study. On these particular spots the most affected persons like traffic police, shopkeepers & their workers, watchman, hawkers etc. were selected for the study on the basis of their continuous exposure. The respiratory parameter considered in the study was Forced Expiratory Volume (FEV) and it was measured with the help of computerized Spirometer. Fine Particulate Sampler and High Volume Sampler were used in this study to measure the concentration of various pollutants considered in study. AQI was determined on the basis of concentration of pollutants.

2.1 Observations, Calculations and Analysis:

Concentrations of various pollutants (i.e. SO₂, NO₂ and PM₁₀) were measured at selected locations of Jodhpur. Following four sites were selected as shown in table-1, for the measurements of concentration of various pollutants and for measurement of Forced expiratory Volume of exposed population. Annual Mean values of pollutants measured at various sampling stations are given in table-1. From these concentrations of the pollutants, values of sub-indexes of respective pollutants were calculated to predict AQI. The formulae for sub-indexes calculation are depending on the range of concentration of respective pollutant and are given in table-2.

The highest value of sub-indexes for various pollutants for that sampling station is considered as AQI for that particular sampling station and is given in table-3.

Table 1: Annual Mean values of pollutants measured at various sampling stations

Sampling Stations No.	Location in Jodhpur	Parameters		
		SO ₂ (µgm/m ³)	NO ₂ (µgm/m ³)	PM ₁₀ (µgm/m ³)
1	Ratanada Bazar Circle	8.4	16.23	95.0
2	Akhliya Circle	11.87	18.16	115.0
3	Jalori Gate Circle	14.19	22.29	129.0
4	Nai Sarak – Sojati Gate Chauraha	21.19	24.66	143.0
Note- Periods of sand storms and rainy days were discarded.				

Table 2: Formulae used for sub-index calculation at different concentration of pollutant [1]

Pollutant	Concentration (X)	Formula
SO ₂	X < 40	Sub-Index = 2.386363 X
	X ≥ 40	Sub-Index = 1.6178737 (X-40) +100
NO ₂	X < 60	Sub-Index = 1.666666 X
	X ≥ 60	Sub-Index = 0.6220754 (X-60) +100
PM ₁₀	X ≤ 50	Sub-Index = X
	50 < X ≤ 150	Sub-Index = 0.500000 (X-50) + 50
	X > 150	Sub-Index = 0.936768 (X-150) +100
Note: 1. Average concentration based on 24 hours (In ppb) 2. The formula for AQI for SPM has been used for calculating AQI for RSPM i.e. PM ₁₀ . The readings for SO ₂ are calculated in µgm/ m ³ . In above formula concentration of the pollutant are in ppb but we measure in µgm/ m ³ so that we convert this using Ideal Gas Law for SO ₂ (1 µgm/m ³ = 0.381807252 ppb), for NO ₂ (1 µgm/m ³ = 0.534413876 ppb).		

Table 3: AQI value at different sampling station

Sampling Stations No.	Parameters and Sub-Index			AQI
	SO ₂ (µgm/m ³)	NO ₂ (µgm/m ³)	PM ₁₀ (µgm/m ³)	
1	7.66	14.46	72.5	72.5
2	10.82	16.17	82.5	82.5
3	12.93	19.86	89.5	89.5
4	19.31	21.96	96.5	96.5

After determination of AQI the exposed persons were selected for determining the reduction in FEV. The selection of persons was based on exposure duration (1 to 5 years of exposure, minimum exposure 8 hours or more each day). Persons having hereditary/ previous respiratory diseases, smoking habits, chewing of tobacco & alcoholic etc. were not taken for study. The control population was selected who were not exposed /little exposed to such environment but belongs to same socio- economic background for comparison purpose.

The actual value of FEV and predicted value of FEV was measured with the help of computerized spirometer for all the selected persons. Measured value is designated as FEV and predicted value is designated as FEV_p. The study subjects were divided in various categories depending upon their exposure duration

Index is developed to find out the extent of damage and percentage of volume reduction in fraction. This Index is designated as IFEV which is calculated with the help of following formulae:

$$\text{IFEV} = (\text{FEV}_p - \text{FEV}) / \text{FEV}_p \quad \text{---- (1)}$$

The Pulmonary function parameter FEV was measured for different persons for their different exposure duration at all sampling station. Numbers of observations for different exposure duration and for different AQI are given in Table-4 and Table-5. Mean values of IFEV (Index that represent reduction in Forced Expiratory Volume for 1.0 sec) was calculated for each case and is given in Table-4 and Table-5.

For the controlled population (population which was not exposed to urban pollution but belongs to same class of society) total 38 numbers of observations was taken and mean value of IFEV was calculated and its value was found 0.07

Table 4: Mean Values of IFEV for 1, 2, &3 years exposure

AQI	1 Yr. Exposure		2 Yr. Exposure		3 Yr. Exposure	
	No. of Obs.	Mean IFEV	No. of Obs.	Mean IFEV	No. of Obs.	Mean IFEV
72.5	27	0.1056	27	0.1181	28	0.1938
82.5	29	0.1095	29	0.1369	27	0.2320
89.5	27	0.1125	30	0.1453	28	0.2330
96.5	36	0.1435	34	0.1757	29	0.2340

Table 5: Mean Values of IFEV for 4 and 5 years exposure

AQI	4 Yr. Exposure		5 Yr. Exposure	
	No. of Obs.	Mean IFEV	No. of Obs.	Mean IFEV
72.5	26	0.2640	27	0.2710
82.5	28	0.2713	27	0.3090
89.5	35	0.2714	32	0.3180
96.5	28	0.2830	27	0.3289

Calculated and measured data shows the increasing trend for all the cases, which is not truly linear but most appropriate relation to represent this increasing trend is linear only. Regression analysis was done for IFEV and significance tests were applied to verify the consistency & significance of all the parameters of the multiple regression model. Various values of different parameters, coefficients and constants for developed model are given in table-6, table-7 and table-8.

Table- 6 Model summary

Model	R	R ²	Std. error of the Estimate
IFEV	0.943	0.889	0.02588

‘R’ is multiple co-relation coefficients. As the value of R is positive (from ANOVA Table) it is a positive co- relation. ‘R²’ is coefficient of determination whose value is 0.889. It indicates that two independent variables Exposure Duration (EXDUR) and Air quality index (AQI) jointly account for the variation in IFEV up to 88.9% and remaining 11.1% variation is due to other reasons.

Table -7 ANOVA (Dependent Variable: IFEV)

IFEV	Sum of squares	df	Mean square	F
Regression	0.092	2	0.046	76.64
Residual	0.011	17	0.0006	
Total	0.103	19		

H₀: β₁ = β₂ = 0 & H₁: not all β_k = 0 (For k= 1, 2)

Where, d.f. is ‘degree of freedom’, and F is ‘Ratio of Mean Squares’

ANOVA Table-7 gives the value of calculated value of F_{calculated}.(i.e. F=76.64) and critical value of F from standard tables (i.e. F_{k, n-k-1, α}=3.59).

Here, F_{calculated} > F_{k, n-k-1, α}, Hence, reject H₀ at α (= 0.05) level of significance, therefore significance of individual β’s be tested by ‘t - test’.

Table -8 Coefficients (Predictors: (Constant), AQI, EXDUR)

IFEV	Coefficients		t
	b	Std. Error	
Constant	-0.066	0.057	-1.155
EXDUR	0.047	0.004	11.439
AQI	0.002	0.001	2.417

Where, Std. Error is ‘Square root of ratio of Sum of Squares to Category of Samples’ and t is ‘ratio of Parameters difference (calculated value minus value from std. tables) to Standard error’.

H₀: β_j = 0 & H₁: β_j ≠ 0: (j = 1, 2)

The calculated values for ‘t - statistics’ for β₁ and β₂ are given in table-8.

t (for β₁) = 11.439

t (for β₂) = 2.417

The value of t_{n-k-1, α/2} = 2.11

Here t > t_{n-k-1, α/2}; therefore reject H₀.

Hence, β₁ ≠ 0 and β₂ ≠ 0

As the estimated b₀, b₁ and b₂ are

b₀ = (-) 0.066

b₁ = 0.047

b₂ = 0.002

Hence finally estimated multiple regression equation for IFEV that relate the extent of damage to the exposure duration and air quality index can be expressed as:

$$Y_E = 0.047X_1 + 0.002X_2 - 0.066$$

Where

Y_E = IFEV

X_1 = Exposure duration

X_2 = Air Quality Index

III. CONCLUSION:

The quality of ambient air in Jodhpur is worsening day by day due to increase of air pollutants concentration. Although the level AQI which is recorded as 'Moderate' (AQI < 100) but reduction in forced expiratory volume of lungs for exposure duration of 5 years is significant. Data indicated that as the Exposure Duration increases the percentage reduction in FEV of lungs increases. It also shows that the value of AQI index increases the reduction of forced Expiratory Volume of lungs increases. It is revealed from the study that exposure duration and deteriorated air quality both are responsible for reduction of FEV of lungs. The significant reduction in IFEV is due to air pollutants because the reduction is negligible in control population. It reflects that the 'Forced Expiratory Volume' of lungs decrease as the Exposure Duration increases as well as the pollutants concentration increases.

The estimated multiple regression equations directly gives relationship between decrease in FEV of lungs, exposure duration and air quality index.

$$Y_E = 0.047X_1 + 0.002X_2 - 0.066$$

. The values Y_E will be in between 0 to 1, if the value is more, this means the damage is high. Reduction in FEV indicates obstructive airways disease and diminished lung volume. It reveals that if residents are exposed to polluted ambient air, they may suffer from obstructive lung diseases which include; asthma, bronchitis and chronic obstructive pulmonary disease (COPD).

Hence from the developed equation, reduction in Forced Expiratory Volume of lungs can be calculated. The calculated values of ' Y_E ' give direct indication of damage extent and will also help in identifying the respiratory diseases without any medical or Pulmonary Function Test.

REFERENCES:

- [1]. Azman Z.A., Lay L.T., Fadzillah, O. & Haslina, M. (1994) 'A Proposed Air Quality Index for Malaysia', Serdang: University Pertanian, Malaysia
- [2]. Chen H, Goldberg MS, Villeneuve PJ "A systematic review of the relation between long term exposure to ambient air pollution and chronic diseases". Rev Environ Health, 2008 Oct-Dec;23(4)243-97.
- [3]. Hesterberg TW et al. "Critical review of human data on short term nitrogen dioxide exposure evidence for NO2 non-effect levels". Crit Rev Toxicol (2009);39(9);743-81.
- [4]. Pelucchi C et al. "Long term particulate matter exposure and mortality: a review of European epidemiological studies" BMC Public Health ,2009 Dec8;9:453.
- [5]. Schwela D. "Air pollution and health in urban areas". Rev Environ Health. 2000 Jan-Jun;15(1-2):13-42.
- [6]. User manual (1999), 'RMS Medspiror', Recorders & Medicare System, (European Respiratory Society, ERS-93) 181/5 Phase I, Industrial Area, Chandigarh(India)

Coal Beneficiation Technology for Coking & Non-Coking Coal Meant For Steel and Thermal Power Plants

¹, Manoj Kumar Sharma, ², Gohil Priyank, ³, Nikita Sharma

¹, M.Tech. Scholar, TIEIT Bhopal (M.P.) India

², M.Tech. Student, TIEIT, Bhopal (M.P.) India

³, B.Sc. (Hons), Student, Govt. P.G. College, BHEL, Bhopal (M.P.) India

Abstract: There are 21 coking coal washeries in production both in private and public sectors. Production of clean coal in these washeries during 1989-90 was 12 million tonne and it is expected to go up to 37 million, tonne during 2015-16. Planning Commission has taken the decision that non-coking coal meant for Thermal Power Plants situated far away from feeding coalfield, should be beneficiated. Coal Washing is a process of separation mainly based on difference in Specific Gravity of Coal and associated impurities like Shale, Sand & Stones etc so that we get relatively pure marketable coal without changing its physical properties. The Washed Coking Coal is meant for Steel Plants. The Washed Power Coal/Washed Non-Coking Coal/Middling is dispatched to various Power Houses. The Coal Washery Rejects are the major environmental hazard during the process of Coal Washing. Considering the fact of requirement of millions of tones clean coal for the end-users, mainly power houses, this problem will have to be solved effectively. The benefits of low ash coal burning in boilers are realized but reimbursement of extra cost of beneficiation for washed non-coking coal needs to be considered

Key Words: Coking Coal, Middlings, Rejects, Deshaling, Coal Washing, Steel Plant, Power Houses

I. INTRODUCTION

There are a number of washeries under construction now and these are expected to be completed by 2018. Present washeries face problems in optimum production more on quality aspects than on quantity and it appears that trend of using imported coking coal of low ash to blend with indigenous high ash coal for steel sector requirement, may continue for some time to come on considerations of optimized steel production. A coal preparation plant (CPP) is a facility, washes coal of soil and rock, crushes it into graded sized chunks (sorting), stockpiles grades preparing. A CPP may also be called a coal handling and preparation plant (CHPP), The more of this waste material that can be removed from coal, and lower its total ash content. The greater its market value and lower its transportation costs. Besides the above coking coal washeries, Bina deshaling and Piparwar beneficiation plants are in advance stages of construction in non-coking coal sector. Future prospects of washeries for non- coking coal beneficiation appear to be bright as, in view of sharp rise in demand for coal, there is increasing trend in mechanized mining of inferior seams resulting in deterioration in quality and consequent reluctance by consumers to accept the same.

Grading of Coal	
Table-1	
A. Coking Coal	
Grade	Parameter
Steel I	Ash > 15%
Steel II	Ash > 15% < 18 %
Washery I	Ash > 18% < 21 %
Washery II	Ash > 21% < 24 %
Washery III	Ash > 24% < 28 %
Washery IV	Ash > 28% < 35 %

B. SEMI COKING COAL

Grade	Parameter
Semi Coking I	Ash + moisture < 19 %
Semi Coking II	Ash + moisture > 19 % < 24 %

C. NON-COKING COAL

Grade	Gross Calorific Value bands for Non-Coking Coals (In Kilo Calories/Kilogram)
G1	Above 7000
G2	6701 to 7000
G3	6401 to 6700
G4	6101 to 6400
G5	5801 to 6100
G6	5501 to 5800
G7	5201 to 5500
G8	4901 to 5200
G9	4601 to 4900
G10	4301 to 4600
G11	4001 to 4300
G12	3701 to 4000
G13	3401 to 3700
G14	3101 to 3400
G15	2801 to 3100
G16	2501 to 2800
G17	2201 to 2500

D. HARD COKE

Grade	Ash %
Beehive Ordinary	> 31 % < 36 %
Beehive Premium	< 27 %
Beehive Superior	> 27 % < 31 %
By Product Ordinary	> 25 % < 30 %
By Product Premium	< 25 %

SUITABILITY OF COAL**E. HARD COKE**

Industry	Type of Coal Required
Steel making, sponge iron industry	Non-coking coal of high Initial Deformation Temperature (IDT) (>1200 degrees Celcius)
Steel making	Coking and semi-coking coal, direct feed and washed; blendable coal; low ash % Assam and Ranigunj coal
Steel castings	Non-coking coal
Special Smokeless Fuel (SSF)	Semi-coking coal of Coking Index 8 10
Power sector	Non-coking coal; middlings of coking coal washeries; washed coal of non-coking coal washeries
Old boilers	Superior grades of non-coking coal
Halwais, domestic use, hotels, etc.	Non-coking coal; CIL Coke / LTC Coke
Glass and potteries	Long Flame non-coking coal
Cokeries / coke oven plants	Coking and semi-coking coal
Cement sector	Non-coking coal; middlings of coking coal washeries
Cast iron castings	Hard coke
Briquette making / domestic fuel making	Semi-coking and non-coking coal; middling & rejects of washeries
Bricks	Non-coking coal; middlings of coking coal washeries

II. COAL INDIA LIMITED (CIL)

Coal India Limited is an Indian state-controlled coal mining company headquartered in Kolkata, West Bengal, India. It is the largest coal producer company in the world, and contributes around 81% of the coal production in India. Union Government of India owns 79.65% of the shares in CIL and controls the operations of CIL through Ministry of Coal. In April 2011, CIL was conferred the Maharatna status by the Union Government of India. On 31 March 2013, its market capitalization was INR 1.952 trillion (US \$35.9 billion) making it India's 5th most valuable company by market value.

CIL is the largest coal producing company in the world. It produced 462.422 MT (million tonne) coal during FY 2013–14. Coal India operates through 81 mining areas in eight states in India. It has 470 coal mines out of which 164 are open cast, 275 are underground and 31 are mixed mines. Production from open cast mines during 2012-13 was 91.65% of total production of 422-462 MT. Underground mines contributed to 8.35% of production. CIL further operates 17 coal washeries, out of which 12 are for coking coal and 5 are for non-coking coal.

Subsidiaries:

Coal India produces coal through seven of its wholly owned subsidiaries. It's another wholly owned subsidiary CMPDIL carries out the exploration activities for other subsidiaries. It provides technical and consulting services to it and to third party clients for coal exploration, mining, processing and related activities. CIL also has a wholly owned subsidiary in Mozambique, Coal India Africana Limitada.



Fig. 1 View of Bhojudih Coal Washery under (BCCL)

Employees:

Coal India had 457,926 employees as on 31 March 2013. Out of which 304,792 were workmen, 33,542 were supervisors and 19,592 were Executives. Coal India spent Rs.273.21 billion on Employee benefits which accounted for 52.47% of the total expenditure incurred during FY 2013–14.

The Details of Number of Employees, Revenue for FY 2012-13 and Production of Coal is Given in the Table-2

Subsidiary	Employees	Revenue INR billion (FY 2012-13)	Coking coal (MT)	Non-coking coal (MT)	Total Coal Production (MT)
Bharat Coking Coal Limited	61,698	89.37	26.970	4.243	31.213
Central Coalfields Limited	48,126	92.38	16.156	31.905	48.061
Central Mine, Planning & Design Institute Limited	3,142	6.05	-	-	-
Coal India Africana Limitada	-	-	-	-	-
Eastern Coalfields Limited	74,276	97.40	0.043	33.868	33.911
Mahanadi Coalfields Limited	22,065	120.93	-	107.894	107.894
Northern Coalfields Limited	16,073	99.86	-	70.021	70.021
South Eastern Coalfields Limited	73,718	176.48	0.157	118.062	118.219
Western Coalfields Limited	54,960	74.23	0.330	41.957	42.287
<i>Sub-total</i>	<i>354,058</i>	<i>756.72</i>	<i>43.656</i>	<i>407.950</i>	<i>451.606</i>
North Eastern Coalfields	2,376	-	-	0.605	0.605
Dankuni Coal Complex	551	-	-	-	-
CIL Headquarters	941	13.78	-	-	-
Total	357,926	770.49	43.656	408.555	452.211

Plants on different principles and in various sizes are conceived as follows for commercial exploitation:

Table .3 Various Sizes of Coal Treated

Technology	Size of Coal (mm)
Photometric Ore Sorter	125-50 50-20
In pit de-shales	1200-200 200-13/6
Electronically controlled moving pan jig	400-40 200-30
Dry Shale Extractor	200-100 100-50

Pilot plants for dewatering fines below 0.5mm obviating froth flotation are conceived as follows:

Table .4 Processes of Various Sizes of Coal Treated

Technology	Size of coal treated (mm)
AED/FC Dry Process	1-0.1
Column Flotation	0.5-0
Oil Agglomeration	0.5-0
Oleo Flotation	0.5-0
Slurry Jig	3-0.1
Spiral Concentrator	3-0.1

Coking coal

Also known as metallurgical coal is used to create coke, one of the key irreplaceable inputs for the production of steel. There are many varieties of coal in the world, ranging from brown coal or lignite to anthracite. The property that really sets coking coals apart from other coals is caking ability, which is the specific property required in order to make coke suitable for making steel. Coke quality is largely influenced by coal rank, composition, mineral content and the ability to soften when heated, become plastic, and re-solidify into a coherent mass. Bituminous class coals of high, medium, and low volatile rank that possess these properties are called “coking” coals. Coke is produced by heating coking coals in a coke oven in a reducing atmosphere. As the temperature of the coal increases, it becomes plastic, fusing together before re-solidifying into coke particles. This is known as the caking process. The quality of the resultant coke is determined by the qualities of the coking coals used, as well as the coke High quality coking coals are in great demand by steel producers, who need these coals to make high quality coke to maximize the productivity of their blast furnace operations.

Non-Coking Coal

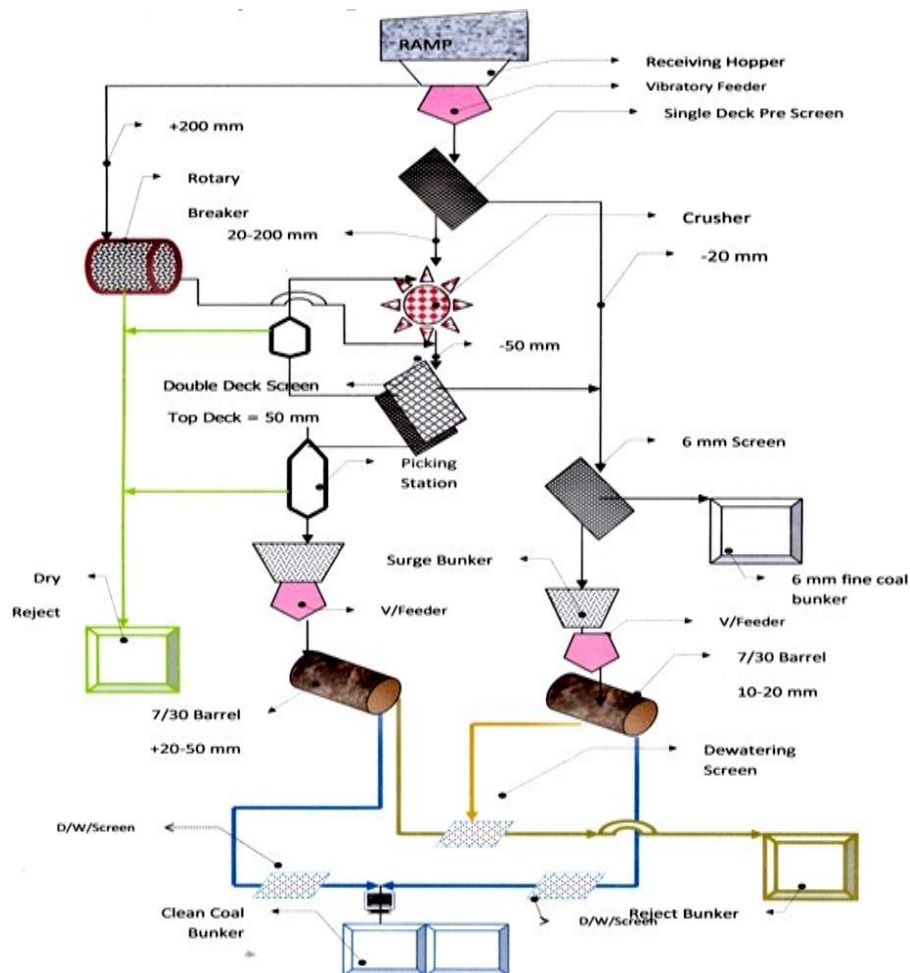
Used for cement, fertilizer, glass, ceramic, paper, chemical and brick manufacturing, and for other heating purposes. These are such type of coal which doesn't have properties like Coking Coal.

III. COAL WASHERIES UNDER OPERATION IN INDIA

Table .5 Coal Washeries under operation in India

Sl. No.	Type of Type of Coal	Sector	No.	Capacity (Mty)
1	Coking	Coal India	11	19.68
		Other PSUs	3	4.85
		Private	4	6.42
		Sub -Total	18	30.95
2	Non -coking	Coal India	7	20.20
		Private	21	50.15
		Sub -Total	28	70.35
		Total	46	101.30

Fig.2 Flow Diagram for Coal Beneficiation Plant



Effect of High Ash

- Staging and fouling of water walls
- Reduced flame stability
- Reduced availability of coal mills
- Increased requirement for land for dumping
- Higher emissions
- High boiler erosion
- Damage to and high erosion of pulverizers
- Damage of conveyor belts, coal crusher
- Blockage of chutes and feeders

III. COAL WASHING TECHNOLOGY OPTIONS

Clean coal technology being practiced in coal washeries in India, as pre-combustion clean coal technology, mainly focus on cleaning of coal by removing ash from coal. Earlier only coking coal was being washed because steel making needs coking coal of ash of 17 to 18%. The raw coal ash in Indian coking coal varies from 25 to 30%. Now-a-days, Ministry of Environment & Forests has put restriction on the use of high ash coal in power sectors, which necessitated priority to wash non-coking coal also. The choice of process equipment involved in coal washing depends on factors such as the type of coal being treated; the market requirement and the economics. Continuous research and development efforts, including trial and adoption of latest equipment/ technology are being done Coal Washing Technologies under trial in India.

Washability:

The washability characteristics of a coal reserve are provided by obtaining liberation data on the raw coal sample. Liberation refers to the amount of physical breakage required to separate material of different material densities. Low density material is clean coal whereas high density material is reject (rock). The intermediate density material is called middling. Liberation data is commonly obtained by float and sink analysis. The procedures for this analysis are detailed in Australian Standard AS 4156.1-1994 “Coal preparation - Higher rank coal - Float and sink testing”.

IV. METHODOLOGY**Coal Sampling:**

Sampling of coal is an important part of the process control in the CPP. A grab sample is a one-off sample of the coal at a point in the process stream, and tends not to be very representative. A routine sample is taken at a set frequency, either over a period of time or per shipment. Coal sampling consists of several types of sampling devices.

**Fig 3 Coal stacker****Fig. 4 Coal Stockpile****Fig.5 Coal Reclaimer****Fig.6 Coal Handling Plant**

Crusher:

Crushing reduces the overall top size of the ROM coal so that it can be more easily handled and processed within the CPP.

Thickeners:

Thickeners are used for dewatering slurries of either tailings or product. A thickener is a large circular tank that is used to settle out the solid material from the water in the feed slurry. The separated water is clarified and reused as process water in the CPP.

Thickeners are sized according to the volume of feed slurry to be processed. Typical size ranges are from 13 to 40m in diameter and 3-4m high. The floor of the thickener is conical, sloping gently down toward the centre. The feed is pumped into the feed well, at the centre of the thickener, near the top.

Gravity Separation:

Gravity separation methods make use of the different relative densities of different grades of coal, and the reject material.

Jigs:

Jigs are a gravity separation method for coarse coal. Different types of jigs:

Dense Medium Process:

Dense medium gravity separation methods use a material such as magnetite to form a medium denser than water to assist in separation.

Cyclones:

A cyclone is a conical vessel in which coal along with finely ground magnetite (media) is pumped tangentially to a tapered inlet and short cylindrical section followed by a conical section where the separation takes place. The higher specific gravity fractions being subject to greater centrifugal forces pull away from the central core and descend downwards towards the apex along the wall of cyclone body and pass out as rejects/middling. The lighter particles are caught in an upward stream and pass out as clean coal through the cyclone overflow outlet via the vortex finder.

Dense Medium Baths (DMB):

Different types of DMB:

- a) Wemco drums
- b) Tromp shallow bath
- c) Teska bath
- d) Leebar bath
- e) Drewboy bath
- f) Daniels bath
- g) Chance cone
- h) Barvoys bath

Fine Coal Method:

Fine coal is cleaned using froth flotation methods. Denver cells and Jameson Cells are two flotation methods used. Spirals perform a simple, low cost and reasonably efficient separation of finer sized material, based on particle density and size.

Dewatering Product Coal:

Water is removed from the product to reduce the mass, and runoff on the stockpile. Different methods of dewatering exist, including:

- ❖ Coarse coal centrifuges
- ❖ Screen bowl centrifuges
- ❖ Slurry screens
- ❖ Dewatering cyclones
- ❖ Horizontal belt filters

Dewatering Tailings (Reject):

Water is removed from tailings to recycle water. Filters, centrifuges and thickeners are used in this part of the process. The black water which is produced as a by-product is typically placed in a coal slurry impoundment.

Screening:

Screens in screening plant are used to group process particles into ranges by size. These size ranges are also called grades. Dewatering screens are used to remove water from the product. Screens can be static, or mechanically vibrated. Screen decks can be made from different materials such as high tensile steel, stainless steel, or polyethylene.

Control and Instrumentation:

Control and instrumentation is a very important part of a CPP. Measurement of flow, density, levels, ash and moisture are inputs to the control system. PLCs are used extensively in plant design. SCADA systems are typically used to control the process.

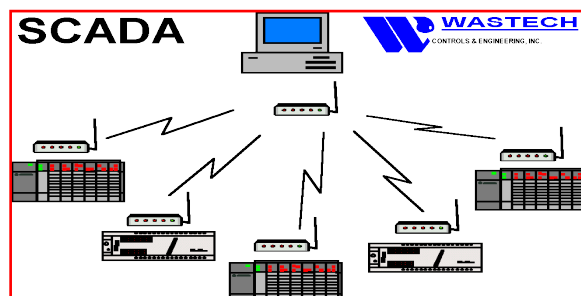


Fig.7 Scada System

V. OBJECTIVE OF STUDY

- ❖ Technical and Financial Feasibility of Producing Low Ash Coal for use in remote power station.
- ❖ Capturing heat content in washery rejects for generating Power using Fluidized Bed-Boiler based Power Plant at pit head.

VI. Data Obtained From Coal Washery Under BCCL, A Subsidiary of Coal India Limited

Table. 6 Washery and their Capacity

Washing Process:			
Washery	System of Washing		
Sudamdih	2 Stage HM Cyclone (37-0.5mm), Flotation (-0.5mm)		
Patherdih	Deshaling Jig(75-0mm), HM Bath(75-13mm),		
Moonidih	2 Stage HM Cyclone (30-0.5mm), W/O Cyclone(-0.5mm)		
Mohuda	HM Cyclone (25-0.5mm), Flotation (-0.5mm)		
Madhuban	Batac Jig (13-0.5mm), Flotation(-0.5mm)		
Dugda-II	HM Cyclone (13-0.5mm), Flotation (-0.5mm)		
Bhojudih	Deshaling Jig (75-0mm), HM Bath (75-25mm),		
	Batac Jig (25-0.5mm), Flotation (-0.5mm)		
	HM Cyclone (13-0.5mm)		
Details of Existing Washeries :			
S. No.	Name of Washery	Year of Commissioning	Operable Capacity
			MTY
A. Coking Coal			
1	Dugda-II	1968	2.00
2	Bhojudih	1962	1.70
3	Patherdih	1964	1.60
4	Sudamdih	1981	1.60
5	Moonidih	1983	1.60
6	Mohuda	1990	0.63
7	Madhuban	1998	2.50
TOTAL (Coking Coal)			11.63
B. Non-Coking Coal:			
	Dugda - I	1961/1998	1.00
TOTAL (Non-Coking Coal)			1.00

VIII. ENVIRONMENTAL AWARENESS

- ❖ Effluent treatment / Re-circulation arrangement
- ❖ Water Sprinkling in a radius of nearly 2 km of the Washery
- ❖ Tree Plantation around Washery premises and colonies done every year.
- ❖ Rain Water Harvesting.

IX OTHER KEY ACTIVITIES FOR EFFECTIVE POLLUTION CONTROL

- ❖ Systematic and scientific excavation of the slurry ponds to make the space available for settling of fines in the ponds / dyke area itself and recycle back the clear water through pumps for re-use in the plant as process water.
- ❖ The recycling pumps have been fully renovated and are operating under strict supervision to avoid any out flow of even clear water.
- ❖ Market has been found for sale of old stock of slurry of the Washery.

X. FUTURE SCOPE OF WORK

- ❖ Various recommendations made by earlier committees on washeries like strengthening of Coal Preparation Engineering Institute and cadre for operating personnel, start of a Central Training Institute.
- ❖ The production of better quality of coke from metallurgical coal either by using inferior quality coal with lower reactive content, or non-coking coal in blend. It should be decided after successful trial at the pilot plant stage.
- ❖ To build up strong indigenous base cost effectiveness, availability of spare parts and other considerations standardization of equipment is very desirable.
- ❖ Sufficient stress has to be given by the national laboratories and academic institutions in the country to interact with washeries and impart know-why.
- ❖ Regular interaction with consumers, particularly with steel plants and thermal power stations is essential.
- ❖ Necessary infrastructure by way of pilot plants should be built, to achieve the purposes.
- ❖ CPEI of CMPDI, conceived as Central Organization for coal washeries, should, initiate actions and monitor implementation of all issues connected with washeries with assistance, if necessary, from practicing professionals abroad, scientific and educational institutes in the country, washery administrators and equipment manufacturers.

XI. CONCLUSIONS

- ❖ Challenges in deterioration in quality of raw coal emphasis on increased mechanization/open cast mining.
- ❖ Coal preparation should be recognized as a technological necessity for the coal industry.
- ❖ coal washeries should be recognized as an industry with its own technology and skills entirely different from the mining industry
- ❖ Detailed geological investigations should be conducted. Linkages should be established for all the existing and future washeries, over a span of at least 15-20 years, so that effective operational planning in washeries is possible.

REFERENCES

- [1]. Stuart Nicole, The Principles of Coal Preparation, 1997,
- [2]. Coal Preparation Society of India
- [3]. Southern African Coal Processing Society
- [4]. Coal India Limited Annual Report Journals
- [5]. Wikipedia, the free encyclopedia.
- [6]. Coal India. 27 May 2013. Retrieved 17 October 2013.
- [7]. Economic Times. 17 October 2013. Retrieved 18 October 2013.
- [8]. Arch Coal, Inc. 19 March 2013. Retrieved 20 October 2013.
- [9]. Press Information Bureau, Government of India. 30 January 2015.
- [10]. Economic Times. 11 April 2011. Retrieved 19 October 2013.
- [11]. Coal India gets Maharatna status". Business Standard. 11 April 2011.
- [12]. NSE India. 31 March 2013. Retrieved 19 October 2013.
- [13]. The Hindu. 31 March 2013. Retrieved 19 October 2013.

Deployment of Palmic Concrete Pavement Blocks in Light and Heavy Traffic Situations

¹Eric Ababio Ohemeng , ²Anita Asamoah-Duodu , ³Kofi Owusu Adjei

^{1,2,3}(Kumasi Polytechnic, Department of Building Technology, Ghana).

Corresponding author's e-mail: ohemengababioeric@yahoo.com

Abstract: The main objective of this research was to investigate the viability of deploying palmic concrete pavement blocks (PCPBs) in light and heavy traffic situations. The term "palmic concrete" refers to any concrete containing palm kernel shell and ordinary aggregates. In this study cement, fine aggregate, coarse aggregate and palm kernel shell (PKS) were used. It was observed that density and strengths of the PCPBs decreased as the PKS content increased. Although, the strengths of the PCPBs lowered as the percentage of PKS increased, compressive strengths of 30.00 N/mm² to 48.70 N/mm² which are satisfactory for light traffic and heavy traffic situations could be achieved if 0% to 30% PKS contents are used. A model was also developed to predict the density of PCPBs through laboratory analysis. The model is only capable of predicting the density of palmic concrete products if the water cement ratio, the curing age, the aggregates cement ratio and the curing condition used are within the tested range.

Keywords: palmic concrete pavement blocks, water cement ratio, compressive strength, curing age.

I. INTRODUCTION

The controlling of agricultural by-products has become a momentous subject in the world due to the escalating rate at which such products are being generated. Several researchers have made a consequential attempt to deploy agro by-products (Nimityongskul and Daladar, 1995; Abdullah, 1996; Elinwa and Awari, 2001; Malhotra and Mehta, 2004; Olanipekun et al., 2006; Teo et. al, 2006a), which demonstrated the viability of utilizing gigantic amount of such materials in concrete products. Among the agro waste, palm kernel shell (PKS) is one of the most common environmental issues in the contemporary world. Palm kernel shell is produced during palm oil processing. It was estimated that over 4.56 million tonnes of PKS waste is produced annually (Teo et al., 2006b). A small fraction of these wastes are traditionally used as solid fuels for steam boilers to run turbines for the electricity production of a palm oil mill; and the best part of them ended up in landfills. The burning of these waste are associated with the emission of dark smoke and the carryover of partially carbonized fibrous particles due to incomplete combustion of the fuels (Sumiani, 2006). According to Ramli (2003), nearly 5 million hectares of palm oil trees are anticipated by the year 2020. In order to alleviate these difficulties, numerous researchers have made an indispensable endeavour to utilize PKS in concrete mixes. The density of PKS concrete is anticipated to be lowered than normal weight concrete by virtue of the low specific gravity of palm kernel shell. Research conducted by Okafor (1988), demonstrated that the density of PKS concrete was approximately 1758 kg/m³, representing about 73% of that of ordinary concrete. Similarly, Basri et al. (1999) reported that the density of PKS concrete was reduced by about 20% as compared to that of ordinary crushed stone concrete. Also, Mannan and Ganapathy (2004) and Alengaram et al. (2008) experienced a reduction in density of PKS concrete of approximately 22% and 24% respectively as compared to that of normal weight concrete.

Various researches pertaining to the strengths of PKS concrete have also been conducted by renowned researchers in the world. It has been observed that the incorporation of PKS aggregates in concrete mix reduces its strengths. Basri et al. (1999) mentioned that the compressive strength of PKS concrete was about 50% lower than that of normal concrete. Shafiqh et al. (2012) realized a slump in compressive strength of concrete when oil

palm shell was used. Experimental studies conducted by (Okafor, 1988; Okpala, 1990; Abdullah, 1996; Basri et al., 1999; Mannan and Ganapathy, 2001; Mannan & Ganapathy, 2002; Mannan and Ganapathy, 2004; Teo et al., 2006a; Teo et al., 2007; Alengaram et al., 2008; Alengaram et al., 2011; Osei & Jackson, 2012; Yusuf & Jimoh, 2013; Ikponmwoosa et al., 2014) clearly show that the inclusion of PKS in concrete reduces its mechanical properties. The literature review presented emphatically shows that studies relating to the use of PKS in concrete have been conducted. However, little attention has been given to the potential use of PKS as fine aggregate in concrete mixes, particularly for concrete pavement blocks (CPBs). Hence, the current research is aimed at investigating the feasibility of using PKS as partial replacement for fine aggregate in the production of CPBs. The use of PKS in CPBs will contribute to providing environmentally friendly solution for PKS disposal problem in the world.

II. EXPERIMENTAL STUDIES

2.1 Materials

Ordinary Portland cement (OPC), fine aggregate (sand), coarse aggregate (stones), ground palm kernel shell (GPKS) and water were the materials used to develop the palmic concrete pavement blocks (PCPBs). Samples of the cement, sand, stones, and GPKS used are shown in Figure 1.



Figure 1: Samples of the materials used to develop the PCPBs

2.1.1 Cement

Ordinary Portland cement (CEM I 42.5 N) produced by Ghana cement works (Ghacem) that conformed to EN 197-1 and labelled OPC was used. The mean particle size (μm) and specific gravity of the OPC were 4 and 3.14 respectively. Table 1 displays the chemical composition of the OPC.

Table 1: Chemical composition of ordinary Portland cement

Chemical composition	Content (%)
Silicon dioxide (SiO_2)	19.70
Aluminium oxide (Al_2O_3)	5.00
Ferric oxide (Fe_2O_3)	3.16
Calcium oxide (CaO)	63.03
Magnesium oxide (MgO)	1.75
Potassium oxide (K_2O)	0.16
Sodium oxide (Na_2O)	0.20
Sulphur oxide (SO_3)	2.80
Loss on ignition (LOI)	2.58

2.1.2 Fine aggregate, coarse aggregate, ground palm kernel shell and water

Natural river sand from Jacobu in the Ashanti Region of Ghana was used for the PCPBs. The sand was dried in an opened place to remove the moisture. The sand conformed to zone II as per IS: 383 – 1970. The GPKS used also conformed to zone II as per IS: 383 – 1970. The coarse aggregate used in this study were 10 mm nominal size, and were tested as per IS: 383 – 1970. Tables 2 and 3 show the physical properties and the sieve analysis of the sand, stones, and GPKS respectively. Potable water was used for the preparation and curing of the PCPBs.

Table 2: Physical properties of sand, stones and ground palm kernel shell

Material	Specific gravity	Compacted bulk density (kg/m^3)	Fineness modulus	Moisture content (%)
Sand	2.60	1695.00	2.53	2.04
Stones	2.63	1723.00	1.97	1.39
GPKS	1.21	864.5	2.52	-

Table 3: Sieve analysis of sand, stones and GPKS

IS sieve size (mm)	Weight retained			% retained			% passing		
	sand	stones	GPKS	sand	stones	GPKS	sand	stones	GPKS
12.50	0.0	0.00	0.0	0.00	0.00	0.00	100.00	100.00	100.00
10.00	0.0	105.98	0.0	0.00	8.58	0.00	100.00	91.42	100.00
4.75	0.0	990.20	0.0	0.00	80.16	0.00	100.00	11.26	100.00
2.36	25.6	137.89	38.40	4.35	11.16	4.35	95.65	0.10	95.65
1.18	127.0	-	190.80	21.56	-	21.60	74.09	-	74.05
0.60	164.5	-	246.82	27.94	-	27.93	46.15	-	46.12
0.30	135.4	-	203.56	23.00	-	23.03	23.15	-	23.09
0.15	89.2	-	135.00	15.15	-	15.28	8.00	-	7.81
pan	47.1	1.20	69.05	8.00	0.10	7.81			

2.1.3 Preparation of the ground palm kernel shell

Palm kernel shells were collected from palm oil factory in Jacobu, a town in Ashanti Region of Ghana. The shells were washed in potable water and dried in an open place to remove the moisture. With the aid of metallic mortar and pestle, the palm kernel shells were ground into smaller particles.

2.2 Methods

2.2.1 Proportion of the mix

The mix proportion was 1: 1.5: 3 (cement: fine aggregate: coarse aggregate). The percentage weight of the GPKS was 0%, 10%, 20%, 30%, 40%, 50%, and 60% by volume of sand. Different water cement ratios (0.30, 0.35, 0.40, and 0.45) were used for the experiment. The plain concrete was used as a control test and denoted as Ay, where y is the water cement (w/c) ratio. The rest of the batches with GPKS were denoted as Bx/y. Where B is the batch with certain percentage (%) of GPKS, x is the volume percentage of GPKS and y is the w/c ratio. Table 4 exhibits the mix proportion of the aggregates used for the PCPBs.

Table 4: Mix proportion

Batch	Constituents of PCPBs (weight in kg)				
	Water	Cement	Coarse aggregate	Sand	GPKS
A0.30	1.02	3.40	10.20	5.10	0.00
A0.35	1.19	3.40	10.20	5.10	0.00
A0.40	1.36	3.40	10.20	5.10	0.00
A0.45	1.53	3.40	10.20	5.10	0.00
B10/0.30	1.02	3.40	10.20	4.59	0.26
B10/0.35	1.19	3.40	10.20	4.59	0.26
B10/0.40	1.36	3.40	10.20	4.59	0.26
B10/0.45	1.53	3.40	10.20	4.59	0.26
B20/0.30	1.02	3.40	10.20	4.08	0.52
B20/0.35	1.19	3.40	10.20	4.08	0.52
B20/0.40	1.36	3.40	10.20	4.08	0.52
B20/0.45	1.53	3.40	10.20	4.08	0.52
B30/0.30	1.02	3.40	10.20	3.57	0.78
B30/0.35	1.19	3.40	10.20	3.57	0.78
B30/0.40	1.36	3.40	10.20	3.57	0.78
B30/0.45	1.53	3.40	10.20	3.57	0.78
B40/0.30	1.02	3.40	10.20	3.06	1.04
B40/0.35	1.19	3.40	10.20	3.06	1.04
B40/0.40	1.36	3.40	10.20	3.06	1.04
B40/0.45	1.53	3.40	10.20	3.06	1.04
B50/0.30	1.02	3.40	10.20	2.55	1.30
B50/0.35	1.19	3.40	10.20	2.55	1.30
B50/0.40	1.36	3.40	10.20	2.55	1.30
B50/0.45	1.53	3.40	10.20	2.55	1.30
B60/0.30	1.02	3.40	10.20	2.04	1.56
B60/0.35	1.19	3.40	10.20	2.04	1.56
B60/0.40	1.36	3.40	10.20	2.04	1.56
B60/0.45	1.53	3.40	10.20	2.04	1.56

*Note: Density of sand = 1695.0 Kg/m³ and density of GPKS = 864.5 Kg/m³. Therefore, weight of GPKS for an equivalent volume of sand (conversion factor) = 864.5/1695.0 = 0.51

2.2.2 Preparation and curing of PCPBs

Mixing of concrete and compaction of the blocks were done mechanically. Steel mould with internal dimensions of 200mm in length, 100mm in width and 60mm in depth was used to mould the PCPBs. The prepared PCPBs were packed on boards and covered with polythene sheets for 24 hours before curing started. The specimens were then placed in a curing tank for specific number of days (i.e. 7 days, 14 days and 28 days).

2.2.3 Testing of specimens

The density and compressive strength of the PCPBs were determined in accordance with BS 1881 – Part 114 (1983) and BS 6717 – Part 1 (1986) respectively. The water absorption was tested in conformity with ASTM C 642 (2006). To test the flexural strength, a centre line was marked at the top of the specimen perpendicular to its length. The PCPBs were tested under the centre line load while simply supported over supporting span of 150 mm. The flexural strength was then calculated from the formula; $\sigma = 3/2 (LF / BD^2)$, where σ is the flexural strength (N/mm²), L is the span length (mm), F is the maximum applied load (N), B is the average width of the specimen (mm), and D is the average thickness (mm). For the splitting tensile test, line loads were applied to the top and bottom of the PCPB using two steel bars. Plywood strips were inserted between the bars and the blocks to ensure even load distribution. Upon failure, the maximum applied load was recorded and the splitting tensile strength was calculated from the formula; $T = (0.868 \times K \times F) / (L \times D)$. Where T is the splitting tensile strength (N/mm²), F is the load at failure (N), L is the length of the failure plane (mm), D is the thickness of the specimen at the failure plane (mm), and K is the correction factor for the thickness, calculated from the equation, $K = 1.3 - 30 (0.18 - t/1000)^2$, t is the thickness of specimen.

III. RESULTS AND DISCUSSION

3.1 Effect of w/c ratio and palm kernel shell content on strengths of PCPBs

The results of the strengths of PCPBs for various w/c ratios and PKS contents are summarized in Table 5. It can be noticed that several strengths were obtained when different w/c ratios were used. Water cement ratio of 0.40 was found to be the optimum. By comparing the optimum w/c ratio to the other w/c ratios, the compressive strength was decreased by about 20%, 14% and 6% when w/c ratios of 0.30, 0.35 and 0.45 were applied irrespective of the percentage of PKS aggregate used. Study conducted by Okpala (1990) revealed that the quantity of water used for the preparation of PKS concrete has significant effect on its compressive strength. For PKS concrete mix of 1:1:2, w/c ratio of 0.5 was found to be the optimum. The compressive strength was reduced by about 10.8%, 25.7% and 32.9% when w/c ratios of 0.60, 0.70 and 0.80 were used respectively. In the same study, when a mix of 1:2:4 was used and the same range of w/c ratio was applied, the compressive strength was lowered by approximately 12.7%, 31.2% and 39.1% when w/c ratios of 0.60, 0.70 and 0.80 were applied respectively. In this study, the flexural strength was also affected when different w/c ratios were used. A slump of about 15%, 10% and 5% were observed when w/c ratios of 0.30, 0.35 and 0.45 were used. Okpala (1990) noticed the impact of w/c ratio on flexural strength of PKS concrete. For concrete mix of 1:1:2, w/c ratio of 0.5 was the optimal. The flexural strength was declined by about 10.0%, 18.1% and 24.2% when w/c ratios of 0.60, 0.70 and 0.80 were used respectively. In the current study, the splitting tensile strength experienced a reduction of approximately 19%, 13% and 7% when w/c ratios of 0.30, 0.35 and 0.45 were used notwithstanding the amount of PKS aggregate applied. Okafor (1988) showed that the splitting tensile strength of PKS concrete varied in the range of 2.0 N/mm² to 2.4 N/mm² with varying w/c ratio of 0.48 to 0.65. This indicates that the splitting tensile strength was reduced by about 17% when w/c ratio of 0.65 was used. In the present investigation, the differences in mechanical properties may be due to the different quantities of water used for the preparation of the PCPBs. Mixes produced from w/c ratios of 0.30 and 0.35 may be little dry causing insufficient compaction and hence leading to decrease in strengths. Mixes made from w/c ratio of 0.45 may be quite wet and this might have created voids in the concrete as the results of the evaporation of excess water from the PCPBs after hydration reaction.

It can also be observed that the strengths of the PCPBs reduced as the palm kernel shell content increased (Table 5). The decrease pattern of the strengths is similar for the four different w/c ratios. The compressive strength lowered from 39.26 N/mm² to 15.14 N/mm², 42.90 N/mm² to 16.58 N/mm², 48.70 N/mm² to 19.37 N/mm², and 45.83 N/mm² to 17.81 N/mm² at 0.30, 0.35, 0.40, and 0.45 w/c ratios respectively. The test results of Basri et al. (1999) showed that PKS concrete have lower compressive strength than ordinary concrete by 42% to 55% and 41% to 50% at 28 days and 56 days respectively depending on the curing environment. Mannan et al. (2002) reported that PKS concrete have approximately 52% lower compressive strength than crushed stone concrete. Similarly, Shafiqh et al. (2012) mentioned that on average, the compressive strength of PKS concrete in their study was about 21% lighter than normal weight concrete. The present investigation also shows that the incorporation of PKS as fine aggregate in concrete reduces its compressive strength as compared to the normal concrete. For this study, the splitting tensile strength was lessened from 4.09 N/mm² to 1.86 N/mm², 4.43 N/mm² to 2.11 N/mm², 5.10 N/mm² to 2.34 N/mm², and 4.76 N/mm² to 2.24 N/mm² at 0.30, 0.35,

0.40, and 0.45 w/c ratios in order. The measured 28-day splitting tensile strength is in the range of 1.86 N/mm² to 5.10 N/mm². Previous studies (Abdullah, 1996; Mannan and Ganapathy, 2002; Teo et al., 2006a; Alengaram et al., 2008; Shafigh et al., 2012) showed that the 28-day splitting tensile strength of PKS concrete in moist curing is in the range of 1.10 N/mm² to 3.54 N/mm². It can be observed that the splitting tensile strength obtained in this study is significantly higher than previous studies. Generally, the splitting tensile strength of normal weight concrete is 8% to 14% of compressive strength (Skosmatka et al., 2002). It can be concluded that the splitting tensile strength of the PCPBs tested in this study is within the range. In the current research, the flexural strength declined from 5.11 N/mm² to 2.65 N/mm², 5.43 N/mm² to 2.91 N/mm², 6.01 N/mm² to 3.13 N/mm², and 5.73 N/mm² to 3.05 N/mm² at 0.30, 0.35, 0.40, and 0.45 w/c ratios respectively. The 28-day flexural strength of the PCPBs in this study ranged from 2.65 N/mm² to 6.01 N/mm². Previous studies (Okpala, 1990; Mannan & Ganapathy, 2002; Teo et al., 2006a; Alengaram et al., 2008; Alengaram et al., 2011, Shafigh et al. 2012) revealed that PKS concrete have flexural strength in the range of 2.13 N/mm² to 6.99 N/mm². The 28-day flexural strength of the current study is on average 14% of the 28-day compressive strength. Research conducted by Shafigh et al. (2012) showed that flexural strength of PKS concrete with compressive strength of 34 N/mm² to 54 N/mm² is in the range of 4.42 N/mm² to 6.99 N/mm². They further stated that the flexural strength / compressive strength ratio was in the range of 12.9% to 14.8%, with an average of 13.7%. By comparing, it can be observed that this study has a similar average flexural / compressive strength ratio with that of (Shafigh et al. 2012). From the analysis, it is obvious that the inclusion of PKS in concrete mix as fine or coarse aggregate reduces its strengths. However, the rate of reduction is likely to be reduced if the PKS aggregate is used as partial replacement for the normal aggregate. The reason for the decline in strengths in the current research could be attributed to the smooth surface of the palm kernel shell aggregates which might have weakened the adhesion between the boundaries of the palm kernel particles and the cement paste.

Table 5: 28 day strengths tests results

Water cement ratio	PKS content (%)	Compressive strength (N/mm ²)	Splitting tensile strength (N/mm ²)	Flexural strength (N/mm ²)
0.30	0	39.26	4.09	5.11
	10	36.29	3.82	4.84
	20	32.07	3.41	4.43
	30	26.94	3.04	3.95
	40	23.19	2.71	3.60
	50	18.07	2.23	2.97
	60	15.14	1.86	2.65
0.35	0	42.90	4.43	5.43
	10	38.25	4.02	5.03
	20	34.41	3.58	4.59
	30	28.69	3.30	4.29
	40	24.83	2.75	3.62
	50	20.44	2.55	3.41
	60	16.58	2.11	2.91
0.40	0	48.70	5.10	6.01
	10	44.88	4.65	5.59
	20	41.02	3.97	5.12
	30	32.90	3.64	4.71
	40	27.99	3.07	4.02
	50	22.54	2.76	3.63
	60	19.37	2.34	3.13
0.45	0	45.83	4.76	5.73
	10	42.68	4.43	5.43
	20	39.92	3.70	4.99
	30	31.42	3.41	4.43
	40	26.05	2.87	3.76
	50	21.45	2.57	3.42
	60	17.81	2.24	3.05

3.2 Impact of curing age on strengths of PCPBs

The influence of curing age on strengths of PCPBs is exhibited in Figures 2, 3, and 4. Critical examination of Figure 2 shows that the compressive strength was increased by about 32% when the curing age moved from 7 days to 28 days irrespective of the PKS content used. Experimental study carried out by Olanipekun et al. (2006) clearly demonstrates the effect of curing age on PKS concrete. For concrete mix of 1:1:2, compressive strengths of 15 N/mm² to 24 N/mm² were obtained within curing age range of 7 days to 28 days. This suggests that at 25% PKS replacement, the compressive strength was increased by approximately

60% when the curing period moved from 7 days to 28 days. Yusuf and Jimoh (2013) also experienced similar trend in their research. For PKS concrete mix of 1:2:4, the compressive strength moved from 10.21 N/mm² to 15.8 N/mm², indicating an increase of about 55% when the curing age rose from 14 days to 56 days. Osei and Jackson (2012) also noticed the influence of curing period on PKS concrete. A compressive strength of 9.34 N/mm² to 15.00 N/mm², representing an upsurge of about 61% was observed. This indicates that at 50% replacement of the coarse aggregate by PKS, the compressive strength was increased by about 61% when the curing age moved from 7 days to 28 days. Similarly, Ikponmwosa et. al (2014) reported that at 20% substitution of coarse aggregate with PKS, the compressive strength was increased from 13.53 N/mm² to 19.77 N/mm² for a curing age range of 7 days to 56 days, representing an increase of approximately 46%.

Figure 3 displays the impact of curing period on splitting tensile strength of the developed PCPBs. Careful study of the figure shows that the splitting tensile strength was increased by approximately 33% when the curing age moved from 7 days to 28 days regardless of the PKS content applied. Yusuf and Jimoh (2013) also noticed a similar direction in their experimental study. For PKS concrete mix of 1:1:2, the splitting tensile strength increased from 0.23 N/mm² to 1.25 N/mm². This implies that the splitting tensile strength was increased by about 81.6% when the curing period moved from 3 days to 56 days.

The influence of curing age on flexural strength is shown in Figure 4. It is obvious that the flexural strength increases as the curing age increased. A rise of about 31% in flexural strength was noticed when the curing period moved from 7 days to 28 days. Ikponmwosa et. al (2014) noticed that at 30% replacement of coarse aggregate by PKS, the flexural strength was moved from 1.03 N/mm² to 1.51 N/mm² for a curing age range of 7 days to 28 days, representing an upsurge of about 47%. Also, Yusuf and Jimoh (2013) observed an increase in flexural strength of PKS concrete when the curing age increased. For PKS concrete mix of 1:2:4, the flexural strength was moved from 1.12 N/mm² to 1.78 N/mm², indicating an increase of approximately 59% when the curing period moved from 7 days to 28 days. The increase in strengths as a result of change in curing age may be due to the hydration reaction of the cement paste which increases the strengths of concrete as curing age increases.

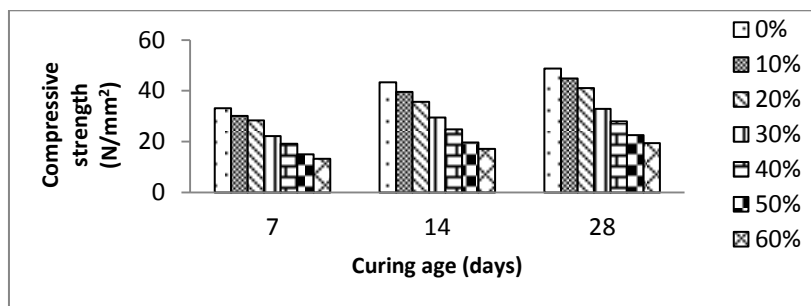


Figure 2: Compressive strength of different curing ages for w/c ratio of 0.40

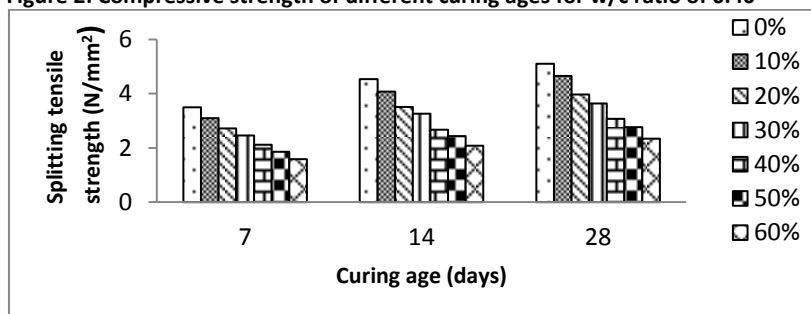


Figure 3: Splitting tensile strength of different curing ages for w/c ratio of 0.40

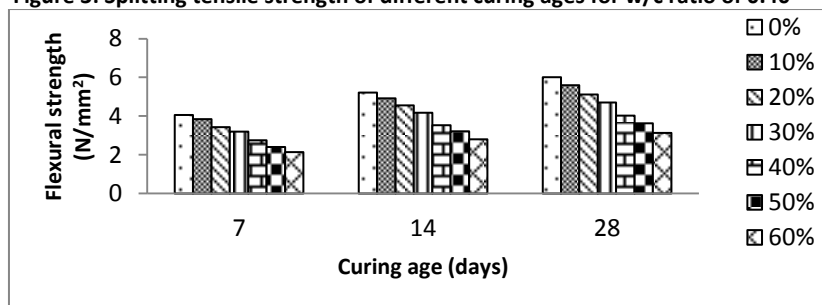


Figure 4: Flexural strength of different curing ages for w/c ratio of 0.40

3.3 Influence of palm kernel shell content on water absorption

The effect of palm kernel shell content on water absorption of the PCPBs is demonstrated in Table 6. It is noticeable that the water absorption increases as the percentage of the palm kernel aggregate rises. The water absorption moved from 1.46% to 1.77%, indicating a rise of about 21% when 60% of the sand was substituted with PKS aggregates. Olanipekun et al. (2006) noticed the effect of PKS on water absorption of concrete. They reported that the percentage water absorption increases with increase in the percentage replacement level of coarse aggregate with PKS. For mix ratio 1:1:2, the value range from 0.41% to 5.88% for PKS concrete (10% to 100% replacement levels). The water absorption of PKS concrete under air drying curing and full water curing were 11.23% and 10.64% respectively (Teo et al., 2007). And these values are higher than that of normal weight concrete (Newman & Choo, 2003). It can be noticed that the water absorption values found in this study are within that of normal weight concrete. The upsurge in water absorption may be attributed to the increase of voids in the PCPBs as a result of the poor bond between the palm kernel particles and the cement paste in the mix. It may also be due to the difference between the water absorption of fine aggregate and that of palm kernel shell. The relationship between palm kernel content and percentage increase in water absorption was found to be linear (Figure 5). The $R^2 = 0.9962$ indicates that 99.62% of the variation in water absorption can be explained by palm kernel shell content.

Table 6: Effect of PKS content on water absorption

Water cement ratio	PKS content (%)	Water absorption (%)	% rise in water absorption
0.40	0	1.46	0.00
	10	1.51	3.42
	20	1.56	6.85
	30	1.60	9.59
	40	1.65	13.01
	50	1.71	17.12
	60	1.77	21.23

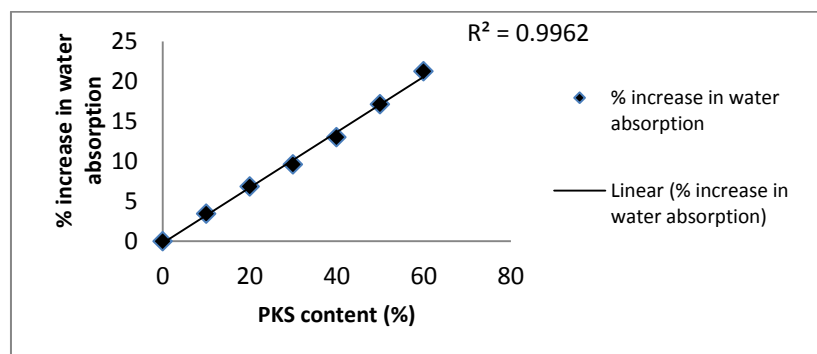


Figure 5: Relationship between PKS content and % increase in water absorption

3.4 Effect of PKS aggregates and w/c ratio on density of PCPBs

The density of the developed PCPBs obtained from the experiment is displayed in Table 7. It is observable that the rate of reduction in density increases as the PKS content increases. The density was lowered by about 11% when 60% of the fine aggregate was substituted with PKS irrespective of the w/c ratio used. Research conducted by Okafor (1988) showed that the density of PKS concrete was approximately 1758 kg/mm³, representing about 73% of that of normal concrete. Likewise, Basri et al. (1999) noticed that the density of PKS concrete was declined by approximately 20% as compared to that of ordinary crushed stone concrete. Alengaram et al. (2008) also experienced a reduction in density of PKS concrete by about 24% as compared to that of normal weight concrete. The slump in density may be due to the low specific gravity of palm kernel shell (1.21) as compare to that of sand (2.60). Partially replacing volume of the sand by PKS would certainly reduce the masses of the PCPBs.

The influence of w/c ratios on density of PKS concrete is demonstrated in Table 7. It can be noticed that different densities were obtained when different w/c ratios were applied. By comparing the optimal w/c ratio to the other w/c ratios, the density was decreased by approximately 12%, 7% and 2% when w/c ratios of 0.30, 0.35 and 0.45 were applied regardless of the percentage of PKS aggregate used. Okpala (1990) had similar experience when different w/c ratios were used in his study. A density range of 1630 kg/mm³ to 1780 kg/mm³ were obtained for 1:1:2 concrete mix. This shows that the density of the PKS concrete was lowered by about 8% when w/c ratio of 0.80 was used. For concrete mix of 1:2:4, the density was reduced from 1700 kg/mm³ to 1600

kg/mm³, representing approximately 6% reduction in density when w/c ratio of 0.80 was applied. For the current study, the differences in densities may be influenced by the different quantities of water used for the preparation of the PCPBs. Mixes produced from w/c ratios of 0.30 and 0.35 may be little dry causing insufficient compaction and hence leading to decrease in masses. Mixes made from w/c ratio 0.45 may be quite wet and this might have created voids in the concrete as the results of the evaporation of excess water from the PCPBs after hydration reaction and these voids are likely to affect the masses of the PCPBs.

Table 7: Experimental testing results of density

Water cement ratio	PKS content (%)	Density (kg/m ³)		
		7 days	14 days	28 days
0.30	0	2342.92	2348.27	2353.57
	10	2326.98	2333.01	2336.34
	20	2250.79	2257.83	2266.46
	30	2200.26	2203.49	2209.79
	40	2110.30	2116.31	2123.90
	50	2094.69	2099.16	2105.51
	60	2078.65	2082.13	2087.69
0.35	0	2478.41	2481.02	2488.17
	10	2411.17	2416.63	2426.11
	20	2368.09	2373.26	2377.01
	30	2319.17	2327.20	2334.32
	40	2287.56	2288.33	2298.78
	50	2242.17	2245.92	2251.42
	60	2200.91	2208.46	2216.41
0.40	0	2615.11	2622.81	2633.17
	10	2577.24	2584.17	2589.44
	20	2532.72	2537.65	2543.92
	30	2505.83	2514.07	2519.07
	40	2468.11	2474.82	2478.35
	50	2424.79	2431.05	2437.61
	60	2365.25	2371.45	2375.99
0.45	0	2568.37	2586.17	2594.17
	10	2532.53	2536.31	2544.75
	20	2495.54	2498.91	2502.46
	30	2456.37	2457.11	2462.35
	40	2413.11	2419.72	2425.72
	50	2358.42	2363.54	2369.17
	60	2310.79	2317.62	2324.08

3.5 Development of model for predicting the density of the developed PCPBs

The model was developed based on the experimental results presented in Table 7. Multiple regression analysis was used to develop the predictive equation with the help of Statistical Analysis System (SAS). Multiple regressions give the opportunity to establish the evidence that one or more independent variables cause another dependent variable to change (Blaikie, 2003). In so doing, the analysis establishes the relative magnitude of the contribution of each predictor variable. It also offers the opportunity to examine what proportion of the variance in the outcome variable is explained by each predictor variable and or / their combined effect (Brace et al., 2003). In this case the predictor variables (independent variables) were represented by water cement ratio, curing age and PKS content while the criterion variable (dependent variable) was density of PCPBs.

3.5.1 Predicting the density of the developed PCPBs

With the application of SAS, the necessary outputs required for predicting the density are shown in Tables 8, 9 and 10. Table 8 presents the model summary of the results for the regression analysis. The R-square ($R^2 = 0.857$) which is the coefficient of determination shows that there is strong correlation between the criterion variable (density) and the predictor variables (water cement ratio, curing age and PKS content). The table also demonstrates that the adjusted $R^2 = 0.852$. Using the analysis of variance (Table 9) and the adjusted R^2 , the following conventional statistical report was extracted (adjusted $R^2 = 0.852$, $F_{3, 80} = 160.117$, $P < 0.0001$). As $P < 0.0001$, it implies that the model is statistically significant. The parameter estimate column (Table 10), gives the coefficients of the predictor variables in the regression equation. Subsequently, the following equation for predicting the density was derived:

$$\text{Density of PCPBs} = 1814.539 + 1827.581 \text{ w/c ratio} + 0.560 \text{ curing age} - 4.464 \text{ PKS content} \quad (\text{Adjusted } R^2 = 0.852).$$

The 1814.539 is a constant value for predicting the density of the developed PCPBs. The 1827.581 means if water cement ratio is increased by one unit, density of the developed PCPBs will on average increase by 1827.581. The 0.560 indicates that if curing age is increased by one unit, density of the PCPBs will on average increase by 0.560. The - 4.464 suggests that if PKS content is increased by one unit, density of the developed PCPBs will on average decrease by 4.464. The adjusted $R^2 = 0.852$ indicates that 85.2% of the variation in density can be explained by water cement ratio, curing age and PKS content. The t-values and the respective P – values reported in Table 10 indicate the significant contribution of w/c ratio, curing age and PKS content in predicting the density of the PCPBs. The t-values measure how strongly each variable influence the prediction of the density. Table 10 also demonstrates that the contribution of water cement ratio and PKS content in determining the density of PCPBs is statistically significant ($P < 0.0001$) whilst that of the curing age is statistically insignificant ($P > 0.05$).

3.5.2 Test of Goodness of fit

The adjusted R^2 of 85.2% is very high and this suggests that the equation is relatively good. Analysis of variance (Table 9) also indicates that the regression equation is statistically significant ($P < 0.0001$). These parameters are indications of the goodness of fit of the equation.

Table 8: Model summary of the regression analysis

Root MSE	Dependent mean	Coefficient of variance	R-square	Adjusted R-square
56.77641	2352.51889	1.09778	0.857	0.852

Table 9: Analysis of variance table showing the significance of the regression model

Analysis of Variance					
Source	DF	Sum of squares	Mean square	F-value	Pr > F
Model	3	1548442.695	516147.565	160.117	<.0001
Error	80	257884.822	3223.560		
Corrected Total	83	1806327.517			

Table 10: Parameter estimates table showing the coefficients of the independent variables in the regression equation

Parameter Estimates					
Variable	DF	Parameter Estimates	Standard Error	t-value	Pr > t
Intercept	1	1814.539	44.564	40.718	<.0001
Water cement ratio	1	1827.581	110.816	16.492	<.0001
Curing age	1	0.560	0.710	0.790	<.432
PKS content	1	- 4.464	0.310	- 14.413	<.0001

IV. CONCLUSIONS

Based on the experimental results of this study, the following conclusions can be drawn.

- Both physical and mechanical properties of the concrete pavement blocks were affected when palm kernel shell was used as a partial replacement for sand. Decrease in density, compressive strength, splitting tensile strength and flexural strength was observed when part of the sand was substituted with PKS. But the water absorption of the PCPBs increased as the PKS content increased. Comparison between the current study and the previous studies shows that both physical and mechanical properties of PKS concrete reduced, whether the PKS aggregate is used as coarse or fine aggregate in the concrete mix. However, the rate of reduction is declined if the PKS aggregate is used as partial replacement in the mix.
- Although, the strength of PCPBs decreased as the PKS content increased, compressive strength of 30.00 N/mm² to 48.70 N/mm² which are satisfactory for light and heavy traffic situations could be achieved if 0% to 30% PKS contents are used.
- A model was developed to predict the density of the PCPBs. The effect of PKS content and w/c ratio on the prediction was statistically significant ($p < 0.0001$) whilst that of curing age was statistically insignificant ($p > 0.05$). The model is only capable of predicting the density of palmic concrete products if the w/c ratio, the curing age, the aggregate cement ratio and the curing condition used are within the tested ranged.
- The model shows that increase in w/c ratio results in increase in density. This does not mean that whenever w/c ratio is increased, density of PCPBs would be increased. This is happening as a result of the range of w/c ratios used. From the experiment, it was realized that after the optimum w/c ratio (0.40) was used, the density started declining when w/c ratio of 0.45 was employed. This presupposes

that if a different range of w/c ratios of say 0.40 to 0.75 is used, the effect of w/c ratio on the prediction of density may probably be the reverse. Hence, the model should not be applied outside the range of w/c ratios used in this study.

REFERENCES

- [1]. Abdullah, A.A.A. (1996). Palm oil shell aggregate for lightweight concrete. *Waste Material used Concr Manuf*, pp. 624 – 636.
- [2]. Alengaram, U.J., Jumaat, M.Z. and Mahmud, H. (2008). Ductility behaviour of reinforced palm kernel shell concrete beams. *Eur J Sci Res*, Vol. 23, pp. 406 - 420.
- [3]. Alengaram, U.J., Jumaat, M.Z., Mahmud, H. and Fayyadh, M.M. (2011). Shear behaviour of reinforced palm kernel concrete beams. *Const Build Mater*, Vol. 25, pp. 2918 – 2927.
- [4]. American Society for Testing and Materials (2006). Standard Test method for density, absorption, and voids in hardened concrete. *ASTM C642*, Philadelphia.
- [5]. Basri, H.B., Mannan, M.A. and Zain, M.F.M. (1999). Concrete using waste oil palm shells as aggregate. *Cem Con Res*, Vol. 29, pp. 619 - 622.
- [6]. Blaikie, N. (2003). Analyzing quantitative data. UK: SAGE publication.
- [7]. Brace, N., Kemp, R. and Snelgar, R. (2003). SPSS for psychologists. A guide to data analysis using SPSS for windows.
- [8]. British Standard Institution (1983). Method for determination of density of hardened concrete. BS 1881, Part 114, BSI London.
- [9]. British Standard Institution, (1986). Method for testing compressive strength of concrete. BS 6717, Part 1, BSI London.
- [10]. Elinwa, A.U. and Awari, A. (2001). Groundnut husk ash concrete. *Nigerian Journal of Engineering Management*, Vol. 2, pp. 8 - 15.
- [11]. Ikponmwo, E.E., Salau, M.A. and Olonode, K.A. (2014). Suitability of crushed palm kernel shell as coarse aggregate in structural concrete. *Current Advances in Civil Engineering*, Vol. 2, pp. 59 – 67.
- [12]. IS: 383-1970. Specifications for coarse and fine aggregates from natural sources for concrete. Bureau of Indian Standards, New Delhi, India.
- [13]. Malhotra, V.M. and Mehta, P.K. (2004). Pozzolanic and Cementitious Materials. *Taylor & Francis*, London.
- [14]. Mannan, M.A. and Ganapathy, C. (2001). Mix design for oil palm shell concrete. *Cem Con Res*, Vol. 31, pp. 1323 - 1325.
- [15]. Mannan, M.A. and Ganapathy, C. (2002). Engineering properties of concrete with oil palm shell as coarse aggregate. *Constr Build Mater*, Vol.16, pp. 29 – 34.
- [16]. Mannan, M.A., Basri, H.B., Zain, M.F.M. and Islam, M.N. (2002). Effect of curing conditions on the properties of OPS-concrete. *Build Environ*, Vol.37, pp. 1167 – 1171.
- [17]. Mannan, M.A. and Ganapathy, C. (2004). Concrete from an agricultural waste oil palm shell *Building and Environment*, Vol. 39, pp. 441 - 448.
- [18]. Newman, J. and Choo, B.S. (2003). Advanced concrete technology. Oxford: Jordan Hill.
- [19]. Nimityongskul, P. and Daladar, T.U. (1995). Use of coconut husk ash, corn cob ash and peanut shell ash as cement replacement. *Journal of Ferro cement*, Vol. 25, pp. 35 - 44.
- [20]. Okafor, F.O. (1988). Palm kernel shell as a lightweight aggregate for concrete. *Cem. Con. Res*, Vol. 18, pp. 901 - 910.
- [21]. Okpala, D.C. (1990). Palm kernel shell as a lightweight aggregate in concrete. *Building and Environment*, Vol. 25, pp. 291 - 296.
- [22]. Olanipekun, E.A., Olusola, K.O. and Ata, O. (2006). A comparative study of concrete properties using coconut shell and palm kernel shell as coarse aggregates. *Building and Environment*, Vol.41, pp. 297 - 301.
- [23]. Osei, D.Y. and Jackson, E.N. (2012). Experimental study on palm kernel shell as coarse aggregates in concrete. *International Journal of Scientific & Engineering Research*, Vol. 3, pp. 1 – 6.
- [24]. Ramli, A. (2003). Short-term and long-term projection of Malaysian palm oil production. *Oil Palm Industry Economic Journal*, Vol. 3, pp. 32 – 36.
- [25]. Shafiq, P., Jumaat, M.Z., Mahmud, H.B. and Hamid, N.A.A. (2012). Lightweight concrete made from crushed oil palm shell: Tensile strength and effect of initial curing on compressive strength. *Construction and Building Materials*, Vol. 27, pp. 252 - 258.
- [26]. Skosmatka, S.H., Kerkhoff, B. and Panarese, W.C. (2002). Design and control of concrete mixtures. 14th ed., USA, Portland Cem. Asso.
- [27]. Sumiani, Y. (2006). Renewable energy from palm oil – innovative on effective utilization of waste. *J Clean Prod*, Vol.14, pp. 87 – 93.
- [28]. Teo, D.C.L., Mannan, M.A. and Kurian, J.V. (2006a). Flexural behaviour of reinforced light weight concrete beams made with oil palm shell. *Journal of Advanced Concrete Technology*, Vol. 4, pp. 459 – 468.
- [29]. Teo, D.C.L., Mannan, M.A., Kurian, V.J. and Zakaria, I. (2006b). Flexural behaviour of reinforced lightweight OPS concrete beam. In: 9th International Conference on Concrete Engineering and Technology, Malaysia, pp. 244 - 252.
- [30]. Teo, D.C.L., Mannan, M.A., Kurian, V.J. and Ganapathy, C. (2007). Lightweight concrete made from oil palm shell: Structural bond and durability properties. *Building and Environment*, Vol. 42, pp. 2614 - 2621.
- [31]. Yusuf, I.T. and Jimoh, Y.A. (2013). The transfer models of compressive to tensile, flexural and elastic properties of palm kernel shell concrete. *International Journal of Engineering*, Vol. 2, pp. 195 – 200.

Evaluation and analysis of the role of citizen participation in urban development (Case study: the city of Nikshahar)

Javad Raisi¹, Gholam Reza Miri (Corresponding author)²,
Mahsume Hafez Rezazade³

¹MSc student in Department of Geography and Urban Planning, College of human science, Zahehan Branch, Islamic Azad University, Zahedan, Iran

^{2,3} Assistant professor in Department of Geography and Urban Planning, College of human science, Zahehan Branch, Islamic Azad University, Zahedan, Iran

Abstract: From the second half of the twentieth century, the concept of participation with a new attitude has become the key issue in the development programs, especially in urban development programs. It is necessary to know the influencing factors in this case to strengthen and expand public participation in planning. This study aims to clarify the extent of participation and its impact on the level of citizen participation. The research method of this study is survey method and the data has been obtained from the questionnaire. 317 persons were selected by using Cochran formula as a statistic community. Spearman correlation coefficient is used in order to analyze the data and test hypotheses. Research findings show that there is a meaningful correlation between the average of economic and social factors and the average of citizen participation of the city of Nikshahar and also between citizen participation and urban development and their satisfaction with life.

Keywords: participation, urban development, citizens, Nikshahr

I. INTRODUCTION

Although participation has been linked with human life in general but it has been emerged from politics after World War II in new sense. This type of participation was established in some industrialized countries in the realm of economic and industrial to associate people in ownership and strengthen the sustainable basis of the industry and economy. By developing the concept of participation and its penetration into all areas of life, today we speak of conditions that all people have realistic and informed interference in their self-determination. However, this development is still not seen practically. Among the factors that prevent the rapid spread of participation, the lack of a philosophy is obvious that attempts to provide competent participation, makes it easy to understand and makes an obligation toward it. Participation is a subjective phenomenon which cannot be effective and become a part of popular culture without an effective philosophy (Alavitabar, 2000, 60).

Citizen Participation in the management and administration of cities» is one of the backgrounds of participation. This participation is one of the necessities of urban life and it will be realized when the urbanites change to citizen from a person who merely live in a place called "city". Recognition, organizing and determining of the position of institutions and organizations in relation to the urban development, is one of the most important issues of urban management. Communication between the institutions and coordinating their activities in line with the objectives and policies of sustainable urban development are factors which is very important in urban management. These sets of characteristics are referred to as urban management structure (Javadi, 2003, 16-17).

Today, urban management is one of the parameters of urban development and the managers are more successful in managing of the affairs of the cities that benefit from the citizen participation in urban projects and cities will be more advanced and more developed when its citizens participate in the affairs of the city. In participatory urbanism, its own citizens determine the fate of the city and the residents of the city are the main determinants in all different areas of the city. The concept of participation can be tracked and found in the ancient Greek cities. In the postmodern age, citizen participation appears in the form of aggregation participation. Aggregation participation is a process which the citizens manage their affairs through it by using of channels such as institutions, organizations and groups and will show their roles. From the 1980s onward, it

has been given increasing attention to the participatory approach in development plans and urban development. So that it is the main component of urban development project in the comprehensive participation of civil society, constructive units (individuals and groups in the city) (Ziari and et al, 2009,679).

So it can be said that public participation in the decision-making process of city has been one of the main elements of the government. The increase of public participation in urban affairs can play an important role in urban balancing (Abbaszadeh, 2008, 44). If citizens look at the participation in the city affairs as the participation in their own destiny, they strengthen some of their character traits such as leadership, self-responsibility in the form of working groups and will prepare the background to change and develop the city. Finally, the participation was considered as an essential element in sustainable development and it is reminded as the missing link in the development process and experts believe that the participation will enhance the competence and integrity of individuals (Almond and et al, 1998: 42).

This study investigate the participation of citizens in urban affairs of Nikshahar at first and then it will identify possible causes of the lack of participation by citizens and finally it will present some appropriate patterns and strategies for greater and more effective public participation to provide successful implementation of urban projects and to achieve sustainable development.

History of the research : Khodavardian (2006) In a book entitled "an introduction to the ways of the attraction of public participation" that has been published by publications of the municipalities points to the concept of participation and its objectives and then describes the method of the villagers participation in the village administration and finally he propounded the factors influencing people's participation and its obstacles and has concluded that public participation is dependent to the establishment of participation and people relationships with governmental bodies and institutions and related organizations.

Ahmadi (2000) In his thesis entitled "public participation in the reconstruction of quake-hit cities" that it has been achieved in the College of Fine Arts of Tehran University has studied the role of public participation in the reconstruction of earthquake-stricken cities and the way of their participation and he has investigated the effects of public participation in accelerating of the implementation of these elements and concluded that the role of people in these projects are poor.

Kasalai (2000) In his Master Thesis entitled" the role of participative management in urban management of the new cities, new city of Pardis" that it was achieved in university of Shiraz, has concluded that the new structure of urban management in new cities are without the participation of the public and non-governmental organizations and bottom-up planning system cannot be seen in it.

Hossaini (2003) In his thesis entitled" Mechanisms of citizen participation in designing urban development plan and presenting appropriate model for the city of Kalardasht" that was achieved in university of Tarbiat Modares of Teharn, has studied methods and techniques for citizen participation in providing urban development plan and has codified a suitable model in urban planning.

Sandres (2003) in his article on citizen participation in urban affairs, concluded that urban participation of citizens can be known as the serious and active, conscious, intentional, efficient and organized participation of elements of civil society and economic, social and cultural activities of urban life to achieve collective goals. Obviously this process in addition to the achievement of collective goals it will increase the collective self-esteem, social interaction, experience and skills of the participants.

Research hypotheses

1. There is a meaningful correlation between economic, social factors and public participation in urban affairs.
2. It seems that there is a meaningful correlation between the level of citizen participation in urban development and life satisfaction

Theories

The importance and necessity of public participation in planning and urban development: And actively involvement in the management of the community is one of the most important factors for the growth and development of any society. Each step in the development must be accompanied by the people because the increase in the supply of labor is the main condition for fulfillment of the affairs that causes increase the efficiency in supplying of needs and causes the actual development. In recent decades, international attention has been focused on development problems while urban services and the ways of presenting it is one of the main matters that participation can be effective in it. The fulfillment of the goals of urban services is dependent on the citizens' participation in decisions and valuating the demand of the majority before the release of the plan and finally culture implementing should be done after the performance of the project In order to gain the support of the citizens for the project. Public participation has an important place in sustainability and institutionalization of any development plan because governments are not able to meet the people constant demand alone. General -

private partnerships is one of the best forms of such co-operation which is based on understanding of this point that the public and private sectors can benefit by sharing resources, knowledge and expertise to improve and provide basic services to all citizens.

It is widely acknowledged that the participation is a phase of development practically and knows development as equal to the participation hence; any development will not be realized unless people are encouraged to improve their standard of living. The experience of many developing countries, including our country shows that the focus planning and evaluating top-down approach has not had desirable results. Whatever the level of participation is more limited, the efficient implementation of the programs may be reduced and the cost of implementation and monitoring will increase and the vulnerability of plans and policies will rise (Rezvani, 2003:214).

People, resources and participation are the three main foundation of human sustainable development with the exception that the participation in comparison with the other two has an essential role other factors have the desired activity within the framework of it. Public participation is an urgent need in all phases of planning, implementation and evaluation. In another word the participation is a key factor in sustainable development because it is the means of reaching to and the goal of it and it is referred to as the missing link of the development process (Shoryabi, 2007:34).

Nowadays, the use of potentials and intellectual, physical, and financial capitals of public and private sector is one of the effective strategies in the management of the participation that its outcome will be the decrease of cost, the increase of income and improving of performance of urban management.

The geographical location of the studied area: The city of Nikshahr is located in Southeastern of Iran and in the south of city of Iranshahr, North of Chabehar, West of city of Sarbaz and it has an area of 23,930 square kilometers and a population of 188,713 people and it is located at longitude 58 ' 51° S to 61'15°S and latitude 25'45°N to 57'1° N. The city of Nikshahr is the third largest city in the province after the cities of Iranshahr and Zahadan. It is consisted of three towns and cities, 16 districts and 816 villages.



Figure 1: Map of the study area

II. DISCUSSION AND CONCLUSION

The first hypothesis

There is a meaningful correlation between economic, social factors and public participation in urban affairs: The Spearman correlation coefficient test is used for testing the first hypothesis. This test is able to show the relationship between economic, social factors and the level of citizen participation in the city of Nikshahr.

Table 1: Results of Spearman correlation test to measure the average of the citizen's economic and social factors and the average of the level of citizen participation in urban design

The level of participation	Socio- economic factors	Indices	
0/89	1/000	Correlation coefficient	Socio- economic factors
0.000	0.000	Significance level	
317	317	numbers	
1/000	0/89	Correlation coefficient	The level of participation
0.000	0.000	Significance level	
317	317	numbers	

Source: search results

According to the table above, the amount of significant level of 0.000 is less than 0/01 and On the other hand, the lower and upper grades of all indices are positive therefore, it can be said with 99% confidence that there is a significant correlation between the average of the citizen's economic and social factors and the average of the level of the citizen participation in the city of Nikshahr. As it can be seen that the obtained correlation coefficient is high so it indicates that the variables of economic and social factors have a large influence on citizen participation in urban design. Thus, by the increase of economic and social foundation of citizens, their participation will increase in urban affairs and by decrease of economic and social foundation of citizens their participation will decrease, so the first hypothesis will be proved.

The second hypothesis: It seems that there is a meaningful correlation between the level of citizen participation in urban development and life satisfaction. The Spearman correlation coefficient test is used for testing the second hypothesis. According to the Spearman correlation coefficient test, correlation coefficient, the level of significance and the number of person have been shown in following table.

Table 2: Results of Spearman correlation test to measure the economic and social average and the average of the citizen participation in urban design

The level of participation	Life satisfaction	Indices	
1/000	0/153	Correlation coefficient	Socio- economic factors
0.000	0.000	Significance level	
317	317	numbers	
0/153	1/000	Correlation coefficient	The level of participation
0.000	0.000	Significance level	
317	317	numbers	

Source: search results

According to the table above, the amount of significant level of 0.000 is less than 0/01 and On the other hand, the lower and upper grades of all indices are positive therefore, it can be said with 99% confidence that there is a significant correlation between the indices of life satisfaction and the level of citizens' participation of the city of Nikshahr. As it can be seen that the obtained correlation coefficient is high so it indicates that the variables of life satisfaction of the citizens have a large influence on citizen participation in urban design. Thus, by the increase of life satisfaction of citizens, their participation will increase in urban affairs and by decrease of life satisfaction of citizens their participation will decrease, so the second hypothesis will be proved.

III. CONCLUSION

Generally, it can be said that the need for citizen participation in urban affairs is felt because of economic crisis and instability, environmental crises and many other factors in this world. For this reason, the main goal of this research is the citizens' role of the city of Nikshahr in urban affairs that various theories have been used for explaining it and following results were obtained:

According to the obtained results, economic and social factors have a large influence on citizen participation in urban design. This means that by the increase of socio-economic foundation of the citizens, their participation will increase in urban affairs and by the decrease of socio-economic foundation of the citizens, their participation will decrease.

The results also showed that the more the citizens' participation, the more the citizens 'satisfaction from authorities and the city steps toward the development.

Suggestions

1. Hold regular meetings with the managers at the specified time.
2. Gaining the citizens trust through actualizing their ideas.
3. using of the potential of schools and universities for participation in cultural and social affairs.
4. Codifying of programs in urban neighborhoods in the city to increase and strengthen social capital among citizens.
5. Profit participation and provide the necessary tools for attracting public participation for profit affairs.
6. Listening to the feedback from citizens regarding urban projects.

REFERENCES

- [1]. Abbaszadeh, 2008, Factors affecting the participation of citizens in the affairs of the city, Isfahan University.
- [2]. Ahmadi.H, 1998, the emergence of the idea and developing of participation in Urban Planning, Journal of Humanities and Social Research Center, the second number.
- [3]. Alavitabar.A, 2000, the study of the pattern of citizen participation in managing urban affairs, The first edition, published by the municipalities organization in the country, Tehran.
- [4]. Hosseini.A, 2003, Mechanisms for citizen participation in urban development plan and provide appropriate models, the case of Golsar of Rasht, Thesis in Geography and Urban Planning, Tarbiat Modarres University, Tehran.
- [5]. Javadi.A, 2003, urban management in Iran: the ups and downs, Municipalities Magazine, No. 47, Tehran.
- [6]. kasalai.A, 2000, the role of participative management in urban management of the new cities, new city of Pardis, MS Thesis, University of Shiraz.
- [7]. Khodavardian.M, 2006, an introduction to the ways of the attraction of public participation, Publication of municipalities.
- [8]. Rezvani.M, 2003, evaluating the development of the country using taxonomic analysis, The Journal of Tehran University Faculty of Litratures and Sciences.
- [9]. Sanders, 2003, citizen participation in urban affairs
- [10]. Shoryabi.H, 2007, assessing of citizen participation models in urban development projects and provide optimum model, Urban Planning Master's thesis, University of Tarbiat Modarres
- [11]. Ziari and et al, 2009, Sustainable urban development, No. 22, published by the Journal of Geography.

Design and Construction of a Spring Stiffness Testing Machine

Olugboji Oluwafemi Ayodeji¹, Matthew Sunday Abolarin²,

Jiya Jonathan Yisa³, Alaya Garba Muftau⁴, Ajani Clement Kehinde⁵

(Mechanical Engineering Department, Federal University of Technology, Minna, Niger State, Nigeria)

ABSTRACT: A spring stiffness testing machine was produced which differentiates a good spring from bad one using hydraulic principle and locally sourced materials were used to produce at relative low cost and high efficiency. It also categories each spring by stiffness into one of several distinct categories based on its performance under test. This is to ensure that in the final assembly process, springs with similar performance characteristics are mated to ensure a better ride, more précised handling and improved overall vehicle or equipment performance. The construction of the machine involves basically the fabrication process which includes such operation as cutting, benching, welding, grinding, drilling, machining, casting and screw fastening. Taken into consideration under test, were types of compression springs with varying spring loading and their different displacement recorded at different pressures to compare their stiffness.

Keywords - spring, stiffness, coil, extension, compression.

I. INTRODUCTION

For automotive springs, the most relevant performance characteristic is stiffness or “springiness” under load. On the coil line, assembly operators conduct performance testing on each spring at the end of the manufacturing process. These springs move through stages from raw steel into their final shape, with experienced assembler/operators monitoring all phrases of production and at the end of the line, every string undergoes a performance test on mechanical testing machine (Hydraulic system). For coil spring, a typical performance test include applying a series of variable loads to each spring, literally bouncing it up and down for a specified period of time at a high rate of speed to determine its stiffness quality. The results are collected via a gauge and compared to an established performance design standard. Due to a spring coil design, it generates side loads and moments in addition to axial loads. The most important part of maintaining an accurate load tester is the calibration and verification of the spring. When springs are used in a moving mechanism, their dynamic behavior has to be analyzed. However, the machine might not be able to test the stiffness for all forms of spring available on the automobile or equipment but to test only compressive spring.

A spring is basically an elastic body whose purpose is to detect or distort under loading conditions and consequently store energy and release it slowly or rapidly depending on the particular application. In 1932, Lucien Lacoste invented the zero-length spring. A zero length spring has a physical length equal to its stretched length. Its force is proportional to its entire length, not just the stretched length and is therefore constant over the range of flexures in which the spring is elastic [1]. Springs are usually made from alloys of steel [2]. Hooke’s law of elasticity is an approximation which state that the amount by which a material body is deformed (strain) is linearly related to the force causing the deformation (stress). The materials for which Hooke’s law is a useful approximation are known as linear- elastic or “Hookean” materials [3]. For systems that obey Hooke’s law, the extension, x produced is proportional to the load, F . When this holds, we say that the spring is a “Linear spring”. There are three basic principles in spring design: The heavier the wire, the stronger the spring, the smaller the coil, the stronger the spring and the more active the coils, the less load you will have to apply in order to get it to move a certain distance [4].

Extension and compression springs are literally on opposite sides of the spring spectrum. Extension springs are used primarily to hold two components together, while compression springs are best for keeping components from meeting one another. Both employ a coil design for elasticity and strength, but they work under two different principles of elastic potential energy. Torsion spring provide torque around the axis of the helix, rather than a force in line with the axis of the helix, as in compression and extension springs. The ends of the torsion spring are attached to other components that rotate around the middle of the spring. Springs are used to absorb and reduce shock, support moving masses or isolated vibration and apply definite force or torque. Few

examples of application of springs are in control valve, safety valve, torque converter, clutch manual transmission, brake system, damper, stamping machine etc.

1.1. Spring Testing Machine

There are many types of spring testing machine manufactured by foreign companies. This includes: SF1240 series spring testers is commonly used to test stiffness of all types of coil springs, disc springs and wire springs and spring-types components. This series features a robust dual column design with 40mm lead screw and two 50mm precision guide column for maximum stiffness.

Spring testing machine by FSA Canada conduct compression, shear, bending and hardness tests. It comes in two models, STM for helical coil springs and FST for leaf springs. The leaf spring testing machine model FST is used to test wide range of leaf/laminated springs for load rate as per IS 1.155 -1984 while the helical compression spring testing machine model STM is used to test wide range of helical compressions spring and disc springs.

Other types of testers are : Asphalt tensile designed to measure the strain at failure for asphalt binders at very low temperature and Creep and stress rupture tester for testing application of metallic materials.

1.1. Hydraulic

Hydraulic drive and controls have become more and more important, due to automation and mechanization [5]. Hydraulic refers to pressurized fluid, which can be oil, water or other liquids. It employs these to transmit energy from an energy generating source to areas where it is needed. In general, any application that requires a large force to be applied smoothly by small linear or rotary displacement unit (actuator) needs hydraulic and powered fluid technology. Pump converts mechanical energy into hydraulic energy [6].

Table1 Properties of spring materials

Material	Common size (mm)
Music wire	0.08 – 6
Oil tempered wire (OT)	0.25 -16
Chrome silicon, chrome vanadium	0.12 – 13
Stainless steel	0.125 – 13
Inconel, Monel, Beryllium, copper, Phosphor Bronze	0.25 – 3
Titanium	0.8 – 13

II. DESIGN OF COMPONENTS.

The design procedure entails all the construction and design to specification of the feature and system used and also the standard parts.

1.2. The Spring Design

The basic equation for spring design are:

1.2.1. Spring Load

$$P = \frac{F}{K} = \frac{\pi d^2 S}{8KD} \quad (1)$$

When P = maximum allowable load, F = nominal spring load, S = allowable fiber stress, D = mean coil diameter

d = wire size, K = Wahl stress factor

$$K = \frac{4c-1}{4c-4} + \frac{0.615}{c} = \text{Wahl factor} \quad (2)$$

Where $C = D/d$

$$f = \frac{8pD^2}{Gd^4} \quad (3)$$

Where G = Modulus of elasticity, F = deflection per coil

$$Su = \frac{(LF)Q}{(Dw)^x} \quad (4)$$

Where Q = expected ultimate strength of inch bar, x = factor, LF = loading factor

Loading factor (LF) for:

- 0.405 – light Service
- 0.324 – Average Service
- 0.263 – Severe Service [7]

1.2.2. Torsional Shear Stress

$$S_s = \frac{TC}{J} = \frac{16T}{\pi D W^2} = \frac{8FDm}{\pi D W^3} \quad (5)$$

Where A = wire cross sectional area, C = radius of wire cross section, J = Polar moment of inertia

D = diameter of wire

$$J = \frac{\pi D^4}{32}$$

$$T = \frac{FDm}{2}$$

Where F = Transverse Shear Force

1.2.3. Deflection of springs:

$$\delta = \frac{8FD^2mNa}{GDW^4} = \frac{8FC^2Na}{GDW} \quad (6)$$

Where G = Shear modulus of wire material

Na = Number of active coils

At a time t , the crank makes an angle $\theta = \omega t$ with the line of traverse of the plunger whose

$$\text{Displacement } x = R(1 - \cos\omega t) \quad (7)$$

$$\text{Velocity } v = \omega R \sin\omega t \quad (8)$$

$$\text{Acceleration } f = \omega^2 R \cos\omega t \quad (9)$$

The instantaneous volume flow rate of the oil due to V is $A\omega R\sin\omega t$ where A is the cross sectional area of the cylinder. The corresponding velocity of the oil in the pipe is;

$$V_s = \frac{A}{a} \omega R \sin \omega t \quad (10)$$

And acceleration

$$f_s = \frac{A}{a} \omega^2 R \sin \omega t \quad (11)$$

Where a = area of cross section of the suction pipe

V_s = velocity at the suction

f_s = acceleration at the suction

1.2.4. Inertia force.

The mass of oil in the suction pipe is

$$m = \rho a L_s \quad (12)$$

Where ρ = density of oil

L_s = Suction length

And the inertia force due to acceleration f_{is} [8]

$$f_{is} = m f_s = \rho a L_s \omega^2 R \cos \omega t \quad (13)$$

Or Head

$$H_{is} = \frac{1}{g} \times \frac{A}{a} L_s \omega^2 R \cos \omega t \quad (14)$$

Similarly, an inertia head in the discharge pipe can be expressed as

$$H_{id} = \frac{1}{g} \times \frac{A}{a} L_d \omega^2 R \cos \omega t \quad (15)$$

1.3. The Reservoir Design

Area = $L \times B$

Volume = $L \times B \times h$ (16)

Where L = Length of the tank, B = breath of the tank, h = height of the tank.

III. OPERATING PRINCIPLE OF THE MACHINE

The lever connected to the pump which is situated in the reservoir is raised and lowered; this movement causes the plunger to move with a motion which can be considered as simple harmonic. The plunger displacement causes a partial vacuum inside the cylinder the cylinder, leading to opening of the suction valve and lifting of the oil through the discharge pipe to the ram cylinder. The oil flows through the one way Non-return valve which is locked with the aid of the locker at the top of reservoir to the hose that connects the hydraulic circuit. The force generated forces the ram down for compression to take place and the corresponding pressure reading is taken. When the control knob (locker) on reservoir (top) is released, the pressure in the line is released and ram gradually coned back to its normal position. The escaped oil that could not be held back by seal passes through the opening at the bottom of cylinder back to the reservoir so that there is no loss of oil.

IV. RESULT AND DISCUSSION

From the results obtained, it can be deduced that Sample 1 spring stiffness in TABLE 2 is within tolerance limit of ± 0.3 when subjected to various loading. At 2, 4, 6, 8 and 10 bars, the spring stiffness is within the limit. This suggests that the spring will give the optimal performance if used together with other springs of the same stiffness and properties. TABLE 3 shows that the Sample 2 spring stiffness is within tolerance limit when subjected to 2, 6 and 10 bars, but deviated from the limit at 4 bars and 8 bars. If this spring is used, the performance at certain loading will not be accurate and might cause damage to engine valve, piston and the connecting rod. This sample failed the test. Sample 3 spring stiffness as shown in TABLE 3 is within tolerance limit when subjected to only 4

Table 2 Reading of Pressure and Displacement of spring stiffness for Volkswagen Passat, Sample 1

Pressure (Load) bar	Displacement (Deflection) (mm)	Standard spring Displacement (deflection) (mm)	Difference (mm)	Tolerance Limit (mm)
2	5.0	4.7	0.3	±0.3
4	8.0	7.8	0.2	±0.3
6	9.5	9.4	0.1	±0.3
8	11.0	10.8	0.2	±0.3
10	11.8	11.6	0.2	±0.3

Table 3 Reading of Pressure and Displacement of spring stiffness for Volkswagen Passat, Sample 2

Pressure (Load) bar	Displacement (Deflection) (mm)	Standard spring Displacement (deflection) (mm)	Difference (mm)	Tolerance Limit (mm)
2	4.9	4.7	0.2	±0.3
4	8.2	7.8	0.4	±0.3
6	9.7	9.4	0.3	±0.3
8	11.2	10.8	0.4	±0.3
10	11.9	11.6	0.3	±0.3

Table 4 Reading of Pressure and Displacement of spring stiffness for Volkswagen Passat, Sample 3

Pressure (Load) bar	Displacement (mm)	Standard spring (deflection) (mm)	Difference (mm)	Tolerance Limit (mm)
2	5.2	4.7	0.5	±0.3
4	8.1	7.8	0.3	±0.3
6	10.0	9.4	0.6	±0.3
8	11.2	10.8	0.4	±0.3
10	12.1	11.6	0.5	±0.3

bars. At 2, 6, 8 and 10 bars loading, the spring stiffness deviated from the limit and thus are not suitable for use in an engine, if used, it will cause damage to the engine. It was discovered during test that same springs of the same material produced under the same condition vary in stiffness as a result of one being distorted or previously used and when used together in the valve of gasoline engine does not return valve on time and could damage the piston.

V. CONCLUSION

For automotive springs, the most relevant performance characteristic is stiffness or “springiness” under load. For a coil spring, a typical performance test include applying a series of variable loads to each spring, literally bouncing it up and down for a specified period of time at a high rate of speed to determine its stiffness quality. The results are collected via a gauge and compared to an established performance design standard or master part for that specific spring type, each part is either accepted or rejected based on this precise data analysis. This work has been able to evaluate, design and construct a spring stiffness testing machine as a step towards making testing of spring stiffness easier and affordable by our automobile industries, hydro plants, local mechanics and also some manufacturing industries that use heavy equipment that has spring as an important integral of their part. However the machine might not be able to test the stiffness for all forms/types of spring available on the automobile/equipment.

REFERENCES

- [1] A. Eugene, T.B. Avallon, *Marks' Standard Handbook for Mechanical Engineers* (10th Edition McGraw-Hill International.2001).
- [2] A.O. Jimoh, *Properties of Engineering Materials* (Kwara State Polytechnic, Ilorin, Nigeria.1992).
- [3] M. Mike, Measurement of the spring constant of a Helical Compression Spring (University of California, Davis.2004).
- [4] M. Askland, R. Donald, P. Pradeep and G. Phule, *The science and Engineering of Materials* (Fifth Edition, Thomson Engineering.2005).
- [5] J. Thomas, *Hydraulic Handbook* (5th Edition Trade & Technical Press Ltd. England, 1971).
- [6] J.M. Duke, *Essentials of Engineering Hydraulics*, (Macmillan Press Ltd 1980).
- [7] M.M. John, *Properties and Selection of Irons and Steel Metals Handbook* (Ninth Edition. ASM, Metal Park, Ohio.1988).
- [8] V.M. Faires, *Design of machine Element* (Macmillan Company, New York 1965).

Influence of Pva, Pvp on Crystal and Optical Properties of Europium Doped Strontium Aluminate Nanoparticles.

¹, Abutu.A. Nathan, ², AuduD. Onoja, ³, AlexanderN. Amah

(Department of Physics, Federal University of Agriculture, Makurdi, Benue State, Nigeria)

ABSTRACT: The Photoluminescence properties of Polymer passivized Europium doped Strontium Aluminate powder with Polyvinyl Alcohol, Polyvinylpyrrolidone, as dispersing agent by direct chemical-combustion process was reported in this research work. XRD results confirmed the formation of SrAl₂O₄ Orthorhombic phase, yielding crystal sizes of 39.00nm –42.00nm, for the samples. The calculated band gap and the Optical linear absorption coefficient were in the ranges of, 4.69eV –4.97eV, and 5.81m⁻¹- 6.10m⁻¹ respectively. Photoluminescence analysis excited at 365nm wavelength, gave concise Eu³⁺ transition between ⁵D₂ →⁷F₁ to ⁵D₀→⁷F₄ of the colour wavelengths. Higher broadband was observed majorly within the Bluish -Green colour wavelengths with Polyvinylpyrrolidone sample having the highest photoluminescence intensity and unpassivized sample having the lowest photoluminescence intensity. The results from this research suggest that significant Photoluminescence enhancement could be achieved for SrAl₂O₄:Eu³⁺ using polymer passivation without significant changes in the crystal size of the powder; hence can possibly be applied as the newly developed blue-green efficient phosphor in the field of lighting and display.

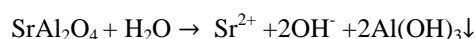
Keywords: Photoluminescence, PVA, PVP, Strontium Aluminate, XRD.

I. INTRODUCTION

Nanostructured functional material in recent time has drawn much research interest due to their distinguished size, shape, and surface morphology which play important role in controlling the physical, chemical, optical and electronic properties of these nanoscale materials [1, 2]. Strontium aluminate when activated with a suitable dopant like europium acts as a photoluminescent phosphor with long persistence of phosphorescence [3]. The excitation wavelengths range from 200 to 450nm. The wavelength for its green formulation is 520nm, its blue-green version emits at 505nm, and the blue one emits at 490nm.

In the present work, we aimed to study the influence of polyvinyl alcohol (PVA) and Polyvinylpyrrolidone(PVP) on SrAl₂O₄:Eu³⁺ preparation by chemical-combustion method at higher temperature. Polyvinyl alcohol (PVA) [C₂H₄O] and Polyvinylpyrrolidone(PVP) [C₆H₉NO] has a relatively simple chemical structure with a pendant hydroxyl group. The hydrolysis reaction does not go to completion resulting in polymer with certain degree of hydrolysis reaction that depends on the extent of reaction. The degree of hydrolysis or the content of acetate groups in the polymer has overall effect on its chemical properties, solubility and the crystallites.

The degree of hydrolysis and polymerization affect the solubility of PVA or PVP in water [4-5]. These polymers, (high physical-chemical stability, high degree of transparency, high melting and transition temperatures, lack of toxicity) grades with high degrees of hydrolysis have low solubility in water, that is, the higher the solubility (%), the lower the degree of hydrolysis (%). As good dispersing agents on the host materials. Weak water resistance is still a well-known drawback for this type of phosphors. Hydrolysis occurs if they are into water as indicated by the equation below [6]:



Invariably, the pH value of the suspension will increase spontaneously. This will deteriorate badly the luminescence of the phosphor. Guo *et al* 2007 analysed the rate of hydrolysis that is observed in $\text{SrAl}_2\text{O}_4:\text{Eu}^{2+}, \text{Dy}^{3+}$ intensively as quoted by Zhu *et al* [7]. Recently, the polymer was used as template to prepare a number of oxide nanoparticles where polymer skeleton eventually limits the growth in a specific shape of the lattice [8-11]. A metal ion-polymer complex forms via a kind of ligand reaction with active OH groups of surfaced PVA molecules.

Metal oxide semiconductor nanoparticles (SNPs) have strong absorption as well as emission behaviour than that of organic dyes and phosphors. Various chemical and physical techniques are employed overtime to investigate the optical properties of nanocrystal SrAl_2O_4 [12]. This has to do with organic layers and inorganic layer. Organic layers cover phosphors by precipitation, which entails elaborate equipment. It's worth noting that neither the organic nor inorganic layer phosphors are water repellent. Inorganic layers are inclined to crack, while organic layer are subject to water infiltration. Aluminate phosphor capped with organic or inorganic layer undergoes luminescence degradation [13-14].

II. MATERIALS AND METHODS

2.1 Materials

The following materials were used in the synthesis, characterization of $\text{SrAl}_2\text{O}_4:\text{Eu}^{3+}$ passivized with PVA and PVP at 1000°C for 2 hours. Strontium Nitrate [$\text{Sr}(\text{NO}_3)_2$], Europium (III) Chloride [$\text{EuCl}_3 \cdot 6\text{H}_2\text{O}$], Aluminium Nitrate [$\text{Al}(\text{NO}_3)_3 \cdot 9\text{H}_2\text{O}$], Boric Acid [H_3BO_3], ThioUrea [$\text{CH}_4\text{N}_2\text{S}$] (all the chemicals used are of analytical grade, no further purification was carried out) and Deionized water.

2.2 Method of Preparation of the Nanoparticles

For the synthesis of $\text{SrAl}_2\text{O}_4:\text{Eu}^{3+}$, 0.98g of $\text{Sr}(\text{NO}_3)_2$, 0.02g of $\text{EuCl}_3 \cdot 6\text{H}_2\text{O}$, 2g of $\text{Al}(\text{NO}_3)_3 \cdot 9\text{H}_2\text{O}$, 3.90g of $\text{CH}_4\text{N}_2\text{S}$ as the starting material was dissolved in 10ml of deionised water and stirred well for 20 minutes at a temperature of 80°C on a magnetic stirrer until a clear solution was formed. The precursor was introduced into a vacuum oven for drying at 80°C for 20hrs. Initially, the solution boiled and gave room for dehydration and decomposition with evolution of large gases such as oxides of carbon, ammonia, and nitrogen. Spontaneous ignition occurred at which smouldering combustion with swelling of the sample with white foamy and voluminous SrAl_2O_4 . The dried sample was further annealed at 300°C for 30 minutes to remove remaining moisture content. The white powder obtained was crushed and 0.30g of Boric acid was added as a reflux [15]. These were subsequently annealed at 1000°C for 2hrs in a muffle furnace, producing $\text{SrAl}_2\text{O}_4:\text{Eu}^{3+}$ phosphor nanoparticles labelled SAE.

The above procedure was repeated with addition of 0.326g of PVA or 0.326g of PVP into the solution as a passivation agent respectively to the starting material before drying in an oven for 20hrs; forming PVP-SAE and PVA-SAE phosphor nanoparticles.

The samples were characterized using the following: An X-Ray Diffractometer (X'pert Pro, PANalytical) made in Netherland with Cu K α radiation at 40kv, 40mA and a scan rate of $0.02^\circ/\text{s}$ in the 2 θ range from 10° to 70° for the verification of the crystal structure and the average size of the particles at Sheda Science and Technology Complex Abuja-Nigeria. The morphology of the powders were obtained using SEM model PhenomproX desktop. The elemental chemical composition was obtained using XRF model OXFORD Instrument Benchtop XRF Analyser-X-Supreme 8000 (+carousel). Jenway 6405 UV/vis spectrophotometer analyser was used to obtain the various absorption values of the nanomaterial at Chemical Engineering and Multi-purpose Research Centre, A.B.U Zaria-Nigeria; Photoluminescence Spectrometer, Perkin-Elmer LS-55 Fluorescence spectrometer at CSIR Pretoria South Africa.

III. RESULTS AND DISCUSSION

3.1 Structural Analysis

Fig. 1(a,b,c) illustrates the XRD patterns of $\text{SrAl}_2\text{O}_4:\text{Eu}^{3+}$ (SAE), PVP-SAE, and PVA-SAE nanoparticles respectively. Four strong characteristics XRD peaks of spinel strontium aluminate at (27.135° , 30.150° , 32.830° & 44.354°), (27.068° , 30.016° , 32.763° & 44.287°) and (27.001° , 30.016° , 32.696° & 44.072°) 2θ were considered respectively from the curves. These were indexed to spinel (021), (211), (121), (311) for SAE, PVP-SAE and PVA-SAE crystal planes. Both samples showed orthorhombic structure which is in agreement with the standard ICDDs card values of 089-0954.

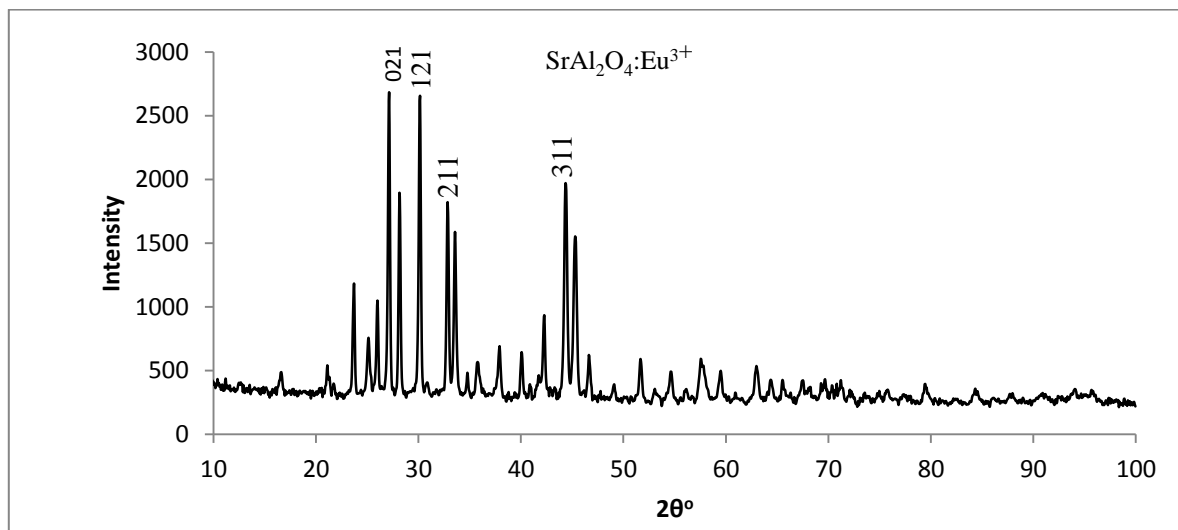


Fig.1a XRD patterns of sae

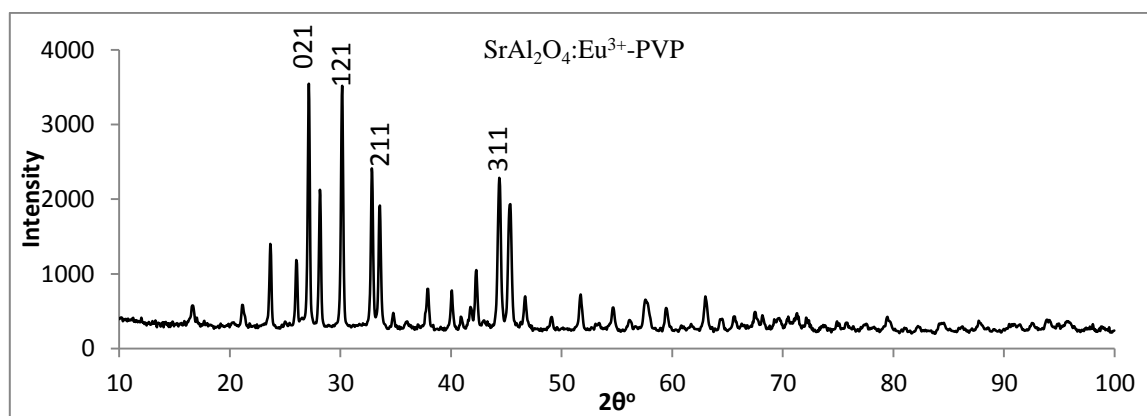


Fig.1b XRD patterns of SAE-PVP

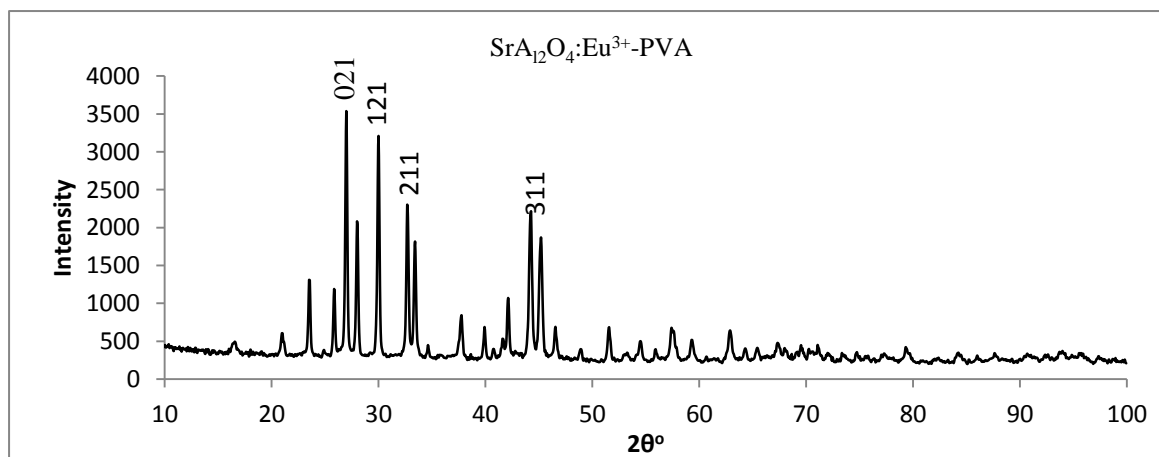


Fig.1c XRD patterns of SAE-PVA

The obtained diffraction patterns was found to be consistent with data reported in ICDD [16], indicating that a pure SrAl_2O_4 phase was successfully prepared at a temperature of 1000°C . In the conventional solid-state process, the required temperature for synthesizing SrAl_2O_4 is around 1400°C - 1600°C [17]. It clearly indicates that chemical-combustion process can significantly lower the heating temperature for preparing SrAl_2O_4 phase. As can be seen, pure monoclinic phase diffraction peaks of SrAl_2O_4 are predominant in the XRD patterns, which is similar with that obtained by Peng [18].

The broadening of the diffraction peaks indicates nanocrystalline nature of the samples. Debye-Scherrer's formula $D = \frac{k\lambda}{\beta \cos\theta}$ was used to estimate the average particle size, where D is the particle size, k is the geometric factor 0.89, λ is the X-Ray wavelength 1.54056\AA , β is the FWHM of diffraction peak, and θ is the diffraction angle.

The crystal size of the unpassivized SAE; PVA-SAE and PVP-SAE particle calculated from the highest peaks are 39.35nm, 40.81nm, and 41.54nm respectively as the inter-planar distance. These sizes of nanocrystals of the powder are in strong charge conferment regime.

3.2 Optical Analysis

In determining the true value of the optical band gap, the fundamental absorption which corresponds to electron excitation from the valence band to conduction band helps. The band gap was evaluated from the absorbance A versus wavelength λ_{nm} curve. The band gap is therefore, obtained from the relation (Song *et al.*, 2010) $E_n = \frac{hc}{\lambda_c}$; where E_n is the band gap, h Planck's constant, c speed of electromagnetic wave and λ_c wavelength of the absorption edge. The calculated band gap energies are 4.69eV, 4.78eV and 4.94eV respectively.

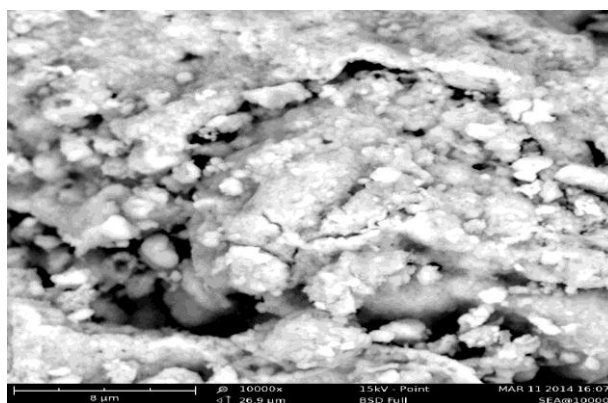
3.3 Optical Linear Absorption Coefficient

This is obtained using Beer Lamber's relation $\alpha = \frac{2.303A}{l}$

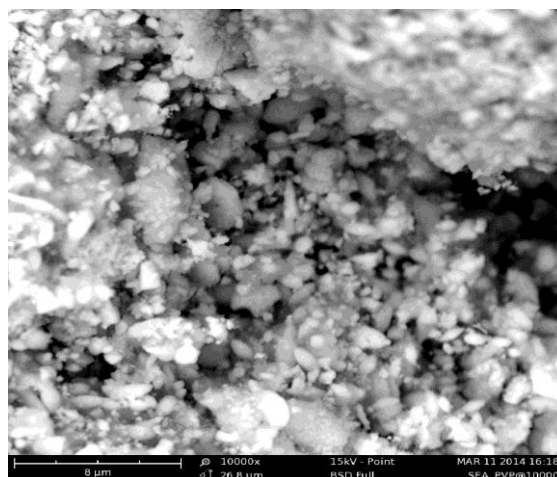
where A is the absorbance wavelength from the UV results above and l is the optical path length (1cm). The various optical linear absorption coefficients for SAE, SAE-PVA and SAE-PVP are 5.81m^{-1} , 5.98m^{-1} and 6.10m^{-1} respectively.

3.4 Surface Morphology Analysis

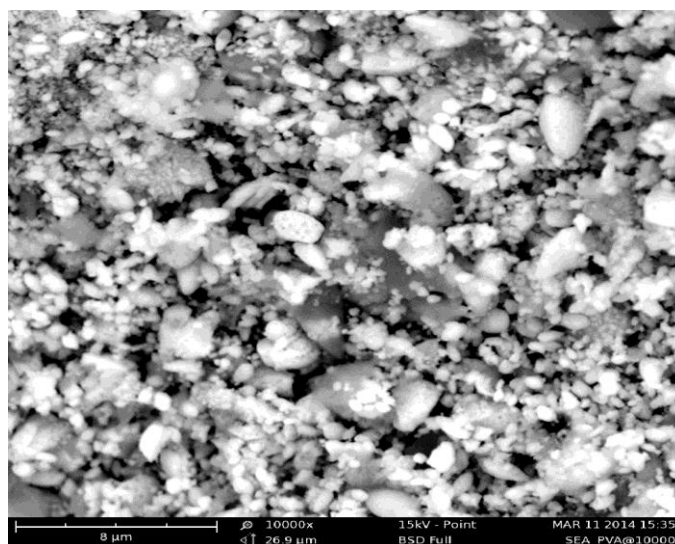
Fig.3 shows the SEM images of (a) SAE (b) PVP-SAE and (c) PVA-SAE nanoparticles. Sr and Al elements are the main chemical element compositions of the samples as indicated by the EDX analysis.



(a)



(b)



(c)

Fig.2 The SEM micrograph analysis results of sample (a) unpassivized sae (b) PVP-SAE (c) PVA-SAE nanoparticles.

3.4 Chemical Analysis

The XRF chemical analysis of sample of SAE unpassivized, PVP-passivized SAE and PVA-passivized SAE searched in the current research is present in Table 1. H_3BO_3 and Europium levels of the phosphors could not be determined by XRF [21].

Table 1. The XRF chemical analysis results of sample SAE, SAE-PVP and SAE-PVA

Element	SAE-Weight %	SAE-PVP Weight %	SAE-PVA Weight %
Al_2O_3	16.886	20.940	21.885
SiO_2	23.102	22.223	26.533
SO_3	16.512	17.819	19.974
SrO	43.136	37.497	29.987
P_2O_5	0.329	0.470	0.506
Mn_2O_3	0.035	0.489	0.338
Na_2O	-	0.562	0.777

3.5 Photoluminescence analysis

Fig.3. shows the PL emission spectrum of the samples as indicated. In comparing PL properties of these samples, the PVP passivized $\text{SrAl}_2\text{O}_4:\text{Eu}^{3+}$ is having more PL intensity followed by PVA due to controlled and homogeneous growth of the nanoparticles in the solution prepared.

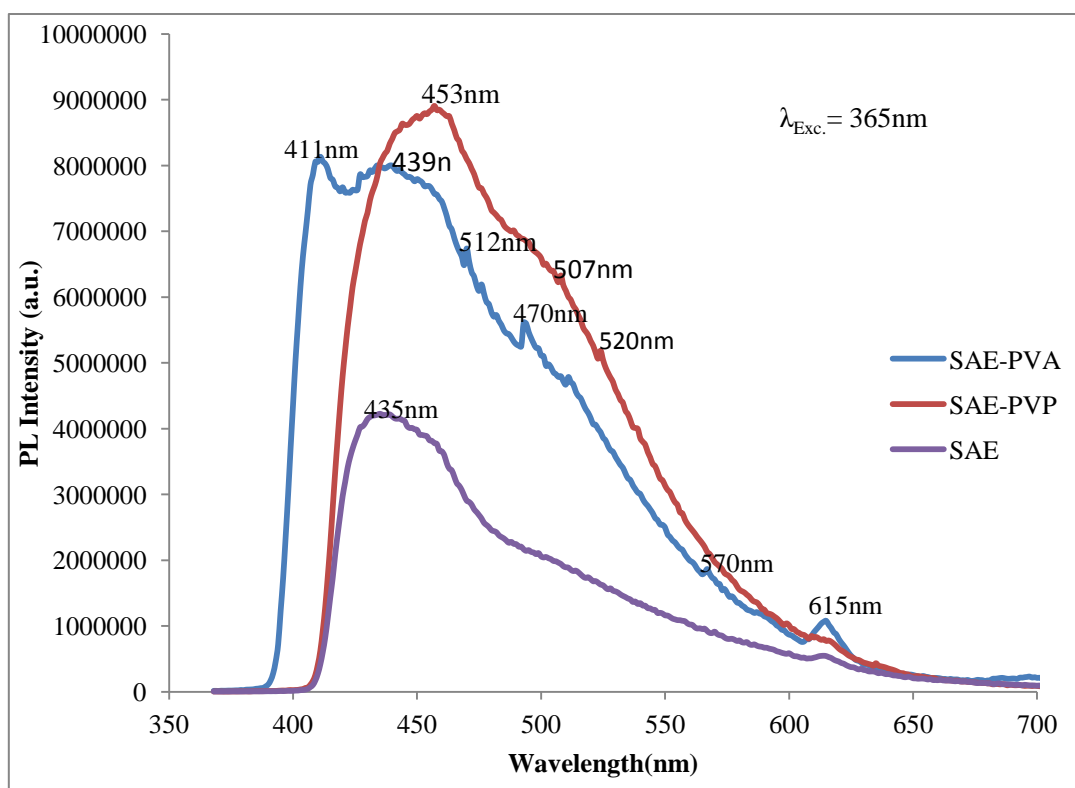


Fig. 3: photoluminescence emission spectral of the samples

Inhibition of diffusion is the limiting procedure for the crystal growth in this research, since coiled structures of the polymer chains will alter the diffusion-driven mechanism within the network. There's possibility that polymer chains may be blocked by connecting to the same nanoparticles and so many of such bridged chains crystals could lead to particle clustering [19]. At temperature below 400°C , higher ionic content in PVA, PVP has effected a more efficient clustering of the ionic groups into domains of small size [2]. Crystalline nature of PVA or PVP results from the strong intermolecular interaction between PVA, PVP chains through the intermolecular hydrogen bonding. This may be the reason that the interaction between their chain and $\text{SrAl}_2\text{O}_4:\text{Eu}^{3+}$ particles led to increase of intermolecular interaction, resulting in increasing the crystalline degree of PVP, PVA and enhanced PL intensity for both emission above the host nanoparticles when annealed at higher temperature.

Table 2: Summary of work results table

Samples	XRD Intensity (a.u.)	Crystal size (nm)	Band Gap energy (eV)	Optical Linear Coefficient (m^{-1})	PL Intensity (a.u)
PVP-SAE	3543.7	41.54	4.69	6.10	8797200
PVA-SAE	3539.1	40.81	4.78	5.98	8135300
SAE	2685.5	39.35	4.94	5.81	4228100

IV. Conclusion

Passivation $\text{SrAl}_2\text{O}_4:\text{Eu}^{3+}$ nanoparticles via chemical precipitation and combustion method with different polymers as capping agents were successfully carried out. The passivated samples and the unpassivated Strontium Aluminate nanoparticles were researched in with respect to the effect of passivation on the structural, morphological, optical and PL intensity properties of SrAl_2O_4 nanoparticles.

Observed increase in crystal sizes from XRD analysis depicts the influence of passivation materials on the SrAl₂O₄ nanoparticles was not in line to those obtained for PVA, polymers capped ZnO and ZnS nanoparticle at room temperature [20,2], indicating that high temperature give rise to higher crystal size. The analytical result has shown that the nanomaterials phosphor have pure orthorhombic SrAl₂O₄ phase at 1000°C with the increase crystal size in the range of 39nm-42nm. Optical properties of SrAl₂O₄ nanoparticles decrease revealed in the band gap energy with decrease in absorption edge are green shifted due to decrease in particle sizes emanating from passivation agent due to confinement effects.

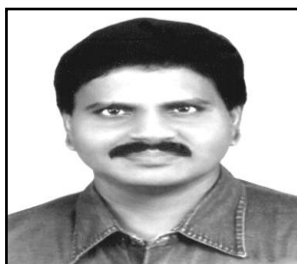
From SEM micrographs, it is observed that passivation on SrAl₂O₄ nanoparticles enhances the optical properties of the nano-materials. The SEM with EDX analysis carried out shows the passivation effects on the particle surface by passivizing agent with micrographs of smooth surface of pure SrAl₂O₄ nanoparticles.

At the photoluminescence excitation of 365nm, SrAl₂O₄:Eu³⁺ with the three samples phosphor emits in the bluish-green between 411-650 nm which agrees with the emission characteristics of Eu³⁺. The maximum emission intensity was obtained for sample with PVP-SAE (⁵D₂ → ⁷F₁). The emission bands can be attributed to the Eu³⁺ transition of ⁵D₂ → ⁷F₁ state to the ⁵D₀ → ⁷F₄ as shown in Fig.3 above.

In all ramifications, the result shows that the higher the crystal size of the nanomaterial, the better its PL, XRD intensity spectra and its UV-optical linear absorption coefficient; but it inversely proportional to the energy band gap depicted in Table 2. The results from this research suggest that significant Photoluminescence enhancement could be achieved for SrAl₂O₄:Eu³⁺ using polymer passivation without significant changes in the crystal size of the powder; hence can possibly be applied as the newly developed blue-green efficient phosphor in the field of lighting and display.

REFERENCES

- [1]. C. Burda, X. Chen, R. Narayanan, M.A. El-Sayad: "Chemistry and Properties of Nanocrystals of Different Shapes." *Chem. Rev.* **105**(2005)1025
- [2]. G. Murugadoss, B. Rajamannan, V. Ramasamy: "Synthesis and Photoluminescence study of PVA-Capped ZnS:Mn²⁺ Nanoparticles." *Dig. Jour. Nanomaterial and Biostructures.* **5**(2),2010, 339-345.
- [3]. M.L. Stanciu, M.G. Ciresan, N.M. Avram: *ACTA PHYSICA POLONICA* **116**(2009)223-235
- [4]. C.A. Finch (1973): *Poly(Vinyl alcohol): properties and applications*. Wiley, New York
- [5]. C.M. Hassan, N.A. Peppas. (1999): *Polymer science and Engineering Lab. Sch. Chem. Eng. Purdue Uni. West Lafayette. IN 4790, 1283*
- [6]. X.D. Lü: "Surface modification of oxide phosphors using nano-powders". *Mater. Chem. Phys.* **93**(2005)526
- [7]. Y. Zhu, M. Zheng, J. Zeng, Y. Xiao, Y. Liu: "Luminescence enhancing encapsulation for strontium aluminate phosphors with phosphate." *Materials Chemistry and Physics* **113** (2009) 721–726
- [8]. S. Biswas and S. Ram: "Morphology and stability in a half-metallic ferromagnetic CrO₂ compound of nanoparticles synthesized via a polymer precursor." *Chem. Phys.* **306**(2004)163-169.
- [9]. S. Ram: "Synthesis and structural and optical properties of metastable ZrO₂ nanoparticles with intergranular Cr³⁺/Cr⁴⁺ doping and grain surface modification." *J. Mater. Sci.* **35**(2003)643-655.
- [10]. S. Ram and T.K. Kundu: "Synthesis and unusual electron paramagnetic resonance spectrum of ZnO semiconductor in a metastable structure of nanoclusters." *J. Nanosci Nanotechnol.* **4**(2004) 1076-1080.
- [11]. A. Jana, T.K. Kundu: "Microstructure and dielectric characteristics of Ni ion doped BaTiO₃ nanoparticles." *Mater. Lett.* **61** (2007) 1544–1548.
- [12]. A. Lopez, M.G. da Silva, E. Baggio-Saitoritch, A.R. Camara, R.N. Silveira Jr, R.J. Mauricio da Fonseca. *Jour. Mat. Sci.* **43** (2008) 464
- [13]. Y. Ge, Y. Zhang, S. He, F. Nie, G. Teng, N. Gu: *Nanoscale Res. Lett.* **4**(2009)287-295
- [14]. Y. Zhu, M. Zheng, J. Zeng, Y. Xiao, Y. Liu: "Luminescence enhancing encapsulation for strontium aluminate phosphor with phosphate." *Mat. Chem and Phys.* **113**(2009)721-726
- [15]. D. Haranath, V. Shanker, H. Chander, P. Sharma: "Tuning of emission colours in strontium aluminate long persisting phosphor." *J. Phys. D: Appl. Phys.* **36**(2003) 2244–2248
- [16]. X-Ray Powder Data File, International Centres of Diffraction Data Card No 74-0794 (1997)
- [17]. T. Matsuzawa, Y. Aoki, N. Takeuchi, Y. Murayama, "A New Long Phosphorescent Phosphor with High Brightness SrAl₂O₄:Eu²⁺, Dy³⁺" *J. Electrochem. Soc.* **143** (1996) 2670
- [18]. T. Peng, H. Yang, X. Pu, B. Hu, Z. Jiang, C. Yan: "Combustion, synthesis and photoluminescence of SrAl₂O₄:Eu, Dy phosphor nanoparticle." *Material Letters* **58** (2004) 352-356
- [19]. H. Du, G. Q. Xu, W. S. Chin, L. Huang, W. Ji, "Synthesis, Characterization, and Nonlinear Optical Properties of Hybrid CdS-Polystyrene Nanocomposites." *Chem. Mater.* **14**, 4473 (2002).
- [20]. G. Bhoopathi, K. Vidya, V.P. Devarajan, S. Subanya: "Structural and optical characterization of pure and starch-capped ZnO quantum dots and their photocatalytic activity." *Applied Nanoscience.* **5**(2015)235-243
- [21]. H.N. Luitel "Preparation and properties of Long Persistent Sr₂Al₁₄O₂₅ Phosphors activated by Rare Earth Metal Ions", A Dissertation Presented in Partial Fulfillment of the Requirements for the Degree of Philosophy in Applied Chemistry; Department of Energy and Material Science, Saga University Japan, 2010.

TAMIL NEW YEAR COOL DRINK?...**(“PANAKARAM”)**

M. Arulmani, B.E.
(Engineer)



V.R. Hema Latha, M.A., M.Sc.,
M.Phil.
(Biologist)

This scientific research focus that “**PANAKARAM**” (Panai + Akaram) shall be considered as “**Ancient Medicinal drink**” which was considered in practice since Ancient Period say 3,00,000 years ago. Panakaram drink considered regulating “**Blood PH value**” for energetic and Healthy life and sustainability to the Particular climatic environmental system. Panakaram drink shall be called by author as “**DARK WINE**” (Panai Neer) considered derived naturally from “**DARK PALM TREE**”. Natural dark palm water shall mean “**ACIDIC**” (or) “**INORGANIC**”.

This research further focus that the origin of **Dark Palm Tree** shall be considered descended from **WHITE PALM TREE** (also called as wild coconut Palm). In proto Indo Europe root word Dark Palm Tree shall be called as “**PANAI**” and White Palm tree shall be called as “**THENNAI**”. The White Palm tree shall be considered as “**NATURAL PALM**” derived from **MARS PLANET** (or) “**EZHEM**” during Dark Age. The Natural water derived from **THENNAI** shall be called as “**EZHEM NEER**” (or) **THENKA NEER**. The Natural white palm water shall be called by author as “**WHITE WINE**” (Ezhem Neer). **EZHEM NEER** shall also mean “**ORGANIC**” (or) “**NON-ACIDIC**”. The Thenka-Neer, Panai-Neer shall be considered having genetically varied chemical property, characteristics used as medicinal dring in different occasion for maintaining the Human blood System under **Balanced PH Value**. It is further focused that the source of **Tenka Neer** shall be considered as derived from **SUPER FLUID** (or) **UNIVERSAL SOLVENT** called in Indo Europe root word as **PANI** or **PANI NEER** (Natural dew).

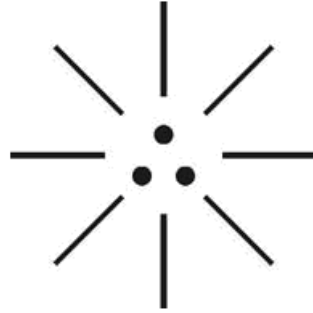
The philosophy of **PANI**, **THENKA NEER**, **PANAKARAM** (Panai Neer) shall be narrated as below.

(i)



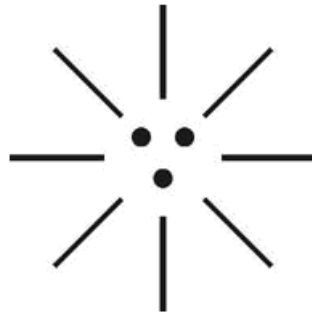
புனி
(Super Fluid)

(ii)



ஈழம் நீர்
(Organic)

(iii)



பானக்காரம்
(Inorganic)

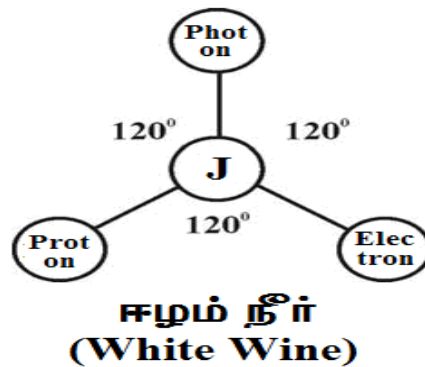
This research further focus that white palm tree shall be considered as Natural Plant originated due to impact of "J-RADIATION" (Zero hour radiation) considered exist under **Endothermic environment** and the Natural liquid Produced by white palm shall be considered as **Highly Organic (Non-alcoholic)** composed of only fundamental particles **Photon, Electron, Proton** and free from atomic elements like **Hydrogen, Carbon, Nitrogen, Ozone**.

"MARS PLANET HAS PURE WATER (KUDI NEER)?..." NO... NO... NO... It is hypothesized that the Mars planet environment shall be considered as ACIDIC and the HUMAN ANCESTORS (Deva Angel Race) shall be considered as having blood of PH value around 3.0 to 4.0. The natural white palm tree shall be considered as converting acidic water into natural water. The human ancestors might have taken white palm water for regulation of PH value of blood system. Further the OZONE WATER (pronounced as OCEAN) considered having acidic value and during the dark age the acidic water might have been descended to EARTH PLANET and become organic water. The earth ocean water shall be considered as highly pure water in ancient time around 3,00,000 years ago and the earth ocean water might gradually becoming acidic in three nuclear ages in expanding Universe. The PH value of ocean water shall be considered as consistently undergoing change in micro level and the PH value of ocean water may become highly acidic around 3000AD.

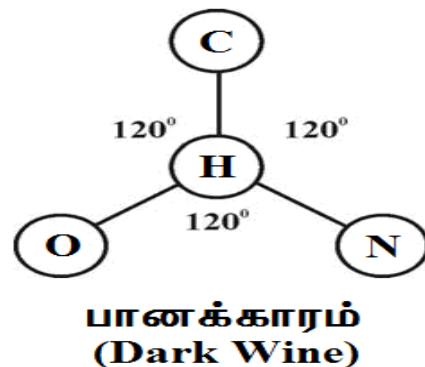
- M. Arulmani.
Tamil Based Indian.

During the expanding Universe the seed of white palm Tree considered descended to Earth planet and become DARK PALM TREE consider exist under low Exothermic environment. The Natural Dark Palm tree further considered exist under influence of "HYDROGEN RADIATION" (3,00,000 Years ago) during dark age of Universe. Further the Natural liquid derived from Dark Palm tree shall be considered as INORGANIC (Alcoholic) composed of primitive atomic elements Hydrogen, Carbon, Nitrogen, Ozone. The philosophy of Natural organic, Natural inorganic Fluid shall be described as below:

(i)



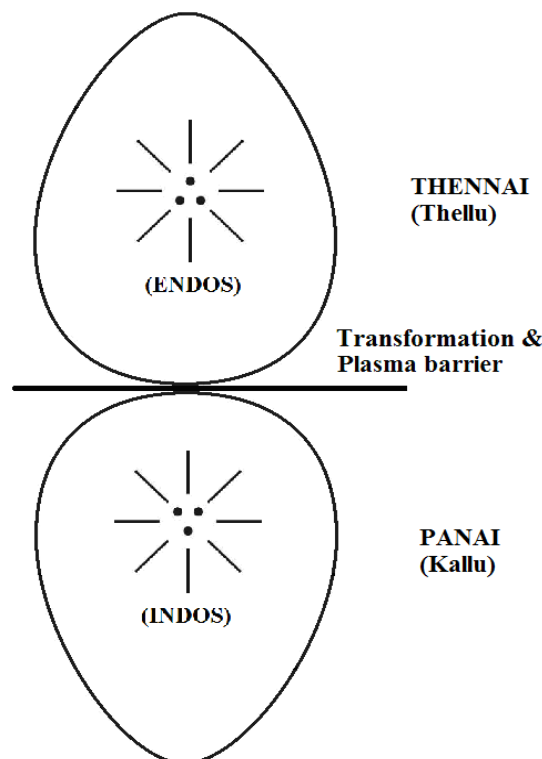
(ii)



The fundamental domain elements of white wine, Dark wine shall be considered regulating DNA, HORMONE, RNA of blood system under different environmental condition of **Endo, Exothermic state** in the expanding universe. The Philosophy of **PANAKAM** drink composed of dark jaggary, dark tamarind served in earthen pot might be derived from the philosophy of **"PANAKARAM"**. Further the etymology of word wine might be derived from proto Indo Europe root word OONU. Oonu shall mean **divine food**.

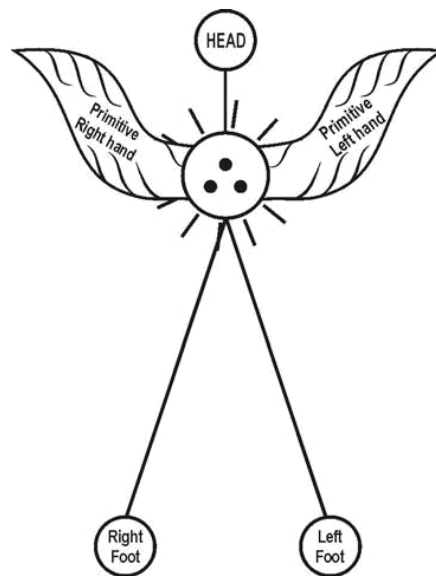


This research further focus that the natural white palm tree shall be considered having only **three chromosome (Trisomy Aceae family)** derived from **THREE-IN-ONE** fundamental particles. The Dark Palm tree originated from white palm tree considered as **'SPECIES'** having genetically varied chromosome level. Say **4.0 (or) 6.0**. The philosophy of white palm tree, dark palm tree shall be hypothetically narrated as below. The male gene of dark palm tree might be derived from the gene of white palm tree.



This research further focus that the Ancient Dark palm tree considered as very tall **say 100 - 200 mts**. Our human ancestors lived in ancient time shall be considered having distinguished genetic structure and capable of **'FLYING'** for easily fetching the **palm products** from the tall trees without any difficulty. The human ancestors probably arrived to earth planet from mars planet during **April 14** (Chittirai month).

(i)



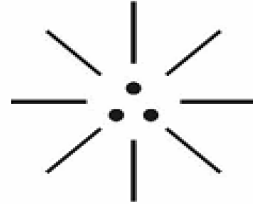
ST. RAMA
(Father of Kachcha Theevu)
(April 14)

(ii)



ST. SITA
(Mother of Kachcha Theevu)
(April 14)

The human ancestors shall be considered as ‘**Dark population**’ lived in ‘**Kachcha Theevu**’ in ancient time (3,00,000 years ago) even before origin of first sun rays on the earth planet. The ancient population shall also be called as “**AETHIANS**” (Proto Indos).



அமுதம்
(EZHEM NEER)

தமிழுக்கு மறு பெயர் அமுதம்!...
ஆம்!... ஆம்!!... இல்லை!!!...
தமிழுக்கு ஆதி பெயர் ஈழத்தமிழ்...
ஈழத்தமிழ் என்றால் வேதம்... வேதாதமிழ்...

ஈழம் என்றால் வெந்நாடு, வேநாடு (MARS PLANET)...
ஈசல்... ஈசன்... என்றால் தேவதை... தேவன்...
ஈசன் என்றால் ஈசல் போல் பறப்பவன்...
ஈழம் நீ (இளநீ) ஈசனின் குடிநீ... குளிப்பானம்...

தேவதை தேவதூதர்கள் குடிப்பார்களோ?...
இல்லை... இல்லை... ஆம்...
தேவதைகள் குடிக்கும் பாணம் குடிநீ... மதுரமல்ல...
குடிநீ, ஈழம் நீ தேவபானம் Devas Drink

ஈழம்நீ, குதத்தோலைபானம் என்றால் வேதா மகுந்து...
ஈழம்நீ என்றால் ஈசனின் குடிநீ (Palm white wine)
ஈழம் நீ என்றால் அமுதம் (White blood)
அமுதம் எனும் சொல்லுக்கு நோய்கொல்லி என்றும் பொருள்.

திரிசூலத்தில் முமிக்கு வந்த மக்கள் முதல்வர் சித்தர் எனலாம்...
சித்தருக்கு மறுபெயர் கச்சா தமிழன் என்று கூறலாம்...
கச்சா தமிழன் என்றால் ஐதியல்ல ஐனம்...
கச்சா தமிழன் என்றால் இரத்தத்தோடு கலந்தவன்...

ஈழம் நீ என்றால் இரத்தத்தை சுத்திகரிக்கும் பாணம்...
ஈழம் நீ என்றால் இதயத்தாடிப்பை சீர் செய்யும் பாணம்...
ஈழம் நீ என்றால் இயற்கை குடிநீ...
ஈழம் நீ என்றால் உயிர் நீ (Life Tonic)

ஈழம் நீ தந்த கொடைதான் பூநீ... பனைஓலை நீ...
பூநீ எனும் சொல்லுக்கு மறுபெயர் பாணைகரம் (Dark wine)
பாணைகரம் என்றால் சித்தர் மகுந்து எனலாம்...
பாணைகரம் என்றால் மதுரம், மதுபானம் (Acidic)

அமுதம் எனும் சொல்லுக்கு தெள்ளுதமிழ் எனலாம்...
தெள்ளுதமிழ் என்றால் வேதா மகுந்து (Organic white wine)
பாணைகரம் எனும் சொல்லுக்கு கள்ளுதமிழ் எனலாம்...
கள்ளுதமிழ் என்றால் சித்தர் மகுந்து (Inorganic Dark wine)

... ஆசிரியர்

The Philosophy of state of white wine, dark wine, colourful wine shall be further narrated as below for universal understanding.

(i)



**SUPER SOLVENT
(Pani Neer)**

(ii)



**DEVAS RACE
(White Wine)
(Thellu)**

(iii)



**RAMA
(Dark Wine)
(Panakaram)**

(iv)

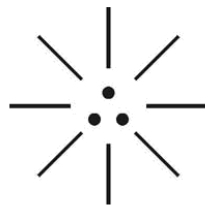


**PATTAI APPA
(Yellow Wine)
(Kallu)**

GANJA (Marijuana) has medicinal property?... Case study shows that scientists believe marijuana is used as psycho active drug and as medicine, herbal therapy. Scholars also believe that ancient Hindus of India and Nepal treat ancient drug SOMA mentioned in Vedas was cannabis. If so what is the origin of marijuana?...

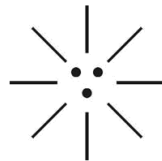
It is hypothesized that marijuana plant shall be considered as descended from Mars planet. It is focused that **VETRI ELAI** shall be considered as the natural plant originated due to impact of **J-RADIATION**. The vetri elai plant shall be considered as having only three chromosomes (trisomy aceae family) derived from **THREE-IN-ONE** fundamental particles **PHOTON**, **ELECTRON**, **PROTON**. The vetri elai shall also be called as **WHITE BETEL LEAF**. During the course of expanding Universe the seed of white betel leaf might be transferred to Earth planet during dark age and become **MARIJUANA** plant. It is focused that the medicinal marijuana shall be considered as having medicinal property for relief from **ASTHMA**. It is suggested by the author that Government of India, Government of Tamilnadu may review the possibility of cultivation of marijuana with suitable act for promoting rural employment and fetching revenue for development. The Philosophy of vetri elai, marijuana shall be described as below.

(i)



VETRI ELAI
(White Betel Leaf)

(ii)



MARIJUANA
(Dark Betel Leaf)

தமிழன்னை உதித்த நாள்
April 14

தமிழன் என்றால் தமிழன்னையின் பிள்ளைகள்...
தமிழன் என்றால் உலகிற்கு வழிகாட்டுபவன்...
தமிழனின் தாய் உதித்த நாள்தான் “சித்திரை”...
தமிழ்தாய்க்கு “அன்னை” “அமுதம்” என்றும் பொருள்...

தமிழ்த்தாய் தந்த தமிழ் மருந்து “அமுதம்”...
அமுதம் எனும் சொல்லுக்கு ஆங்கிலத்தில் “White Blood”...
“மட்டையா” (THAILAND) எனும் சொல்லுக்கு பாட்டி, பாட்டன் எனலாம்...
பாட்டன் பாட்டி என்றால் “மக்கள் ஆச்சி” (Ancestor)

கொம்பன் என்றால் தெம்பு உடையவன்...
கொம்பன் என்றால் ஈழத்தமிழன் (ஈசன்)
கொம்பன் என்றால் ஜாதியில்வா தமிழன் (சித்தன்)
கொம்பனுக்கு மறுபெயர் “தந்தை பெரியார்” (Mars Father)...



Tamil Annai, Madurai
(Mother of Mars Planet)

- ஆசிரியர்

This scientific research focus and recommends to Government of India, Government of Tamilnadu and international organizations that bottled EZHEM NEER (White wine), bottled PANAKARAM (Dark wine) shall also be sold at approved wine shops as these natural drinks have medicinal effect in regulating PH value of human blood system under varied environmental conditions.



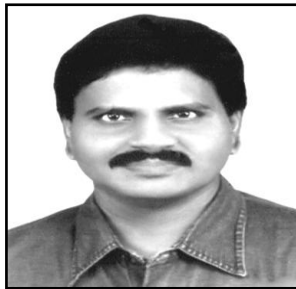
**Headmistress of Government School (Solapuram)
inaugurating Panakaram drink on 30.03.2015
for the public (Virudhunagar District)**

Previous Publications:

1. YUGADI WISHES (IARA, March 2015)
2. TAMIL PUTHANDU!... (AJER, April 2015)
3. THEN MADURAI?... (IJERD, April 2015)

ARENKA NAYAKI IS MOTHER OF RAMA?...

(“SRIRANGAM”)



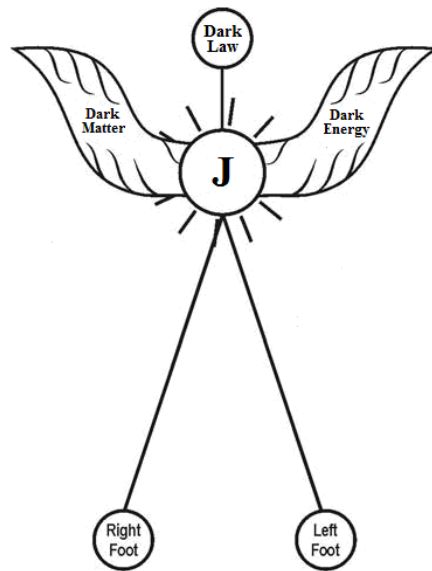
M.Arulmani, B.E.
(Engineer)



V.R.Hema Latha, M.A., M.Sc.,
M.Phil.
(Biologist)

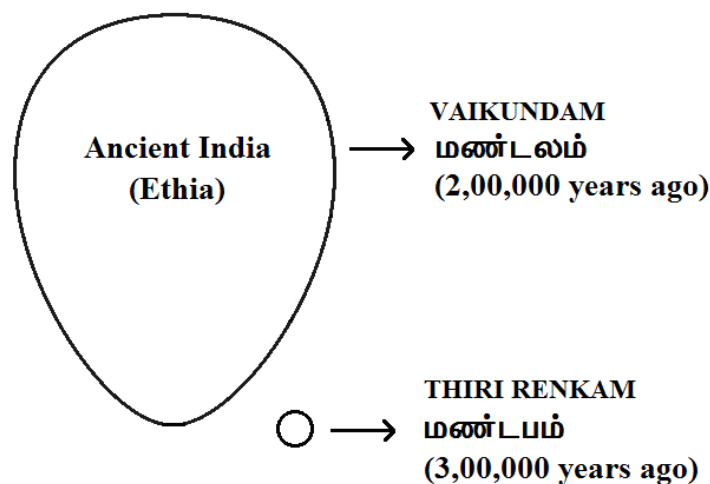
Mother of “Sri Rama” is Kausalya?... NO... NO... NO... This Scientific research focus that mother of “RAMA” shall be considered as “ARENKA NAYAKI” having “Head quarters” at “THIRI RENKAM” in ancient time.

This scientific research further focus that “ARENKA NATHAN” “ARENKA NAYAKI” shall be considered as “Devas Populations” (Angel race) Lived in “MARS PLANET” (5,00,000 years ago). In proto Indo Europe root word the Mars Planet shall be called as “EZHEM” (or) “THEN THIRIPATHI”. The Deva population shall be considered created by supreme artist RAMANUJAM. Ramanujam shall be considered as Atheist as he is the supreme god and NO MORE GOD.



RAMANUJAM
(Father of Then Thiripathi)
(Atheist)

During the Darkage of universe the Devas Populations shall be considered as “Transformed” to “EARTH PLANET” and started living at “Ancient Virgin Island” called by Author as “THIRI RENKAM”. Thiri Renkam shall mean Holy landmass transformed from “THEN THIRIPATHI”. Further Thiri Renkam shall be considered as “SOUL” of origin of Ancient Single Continental mass on the earth planet called by Author as “VAIKUNDAM” (or) “VAIYAKAM”. During expanding universe (Triassic period) the single continental mass considered SPLIT into three major land mass and thereafter thousands of Various islands, Nations shall be considered evolved from “VAIKUNDAM”. The philosophy of origin of THIRI RENKAM, VAIKUNDAM shall be described as below.



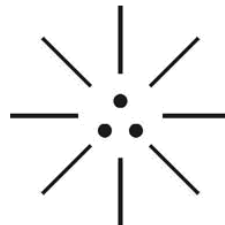
It is further focused that the first human ancestors lived in Earth Planet shall be considered as RENKA NATHAN, RENKA NAYAKI who shall be considered genetically varied from Devas Populations (3,00,000 years ago) having distinguished Principle of life. The distinguished Principle of life shall be described as below.

(i)



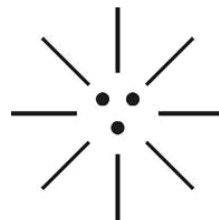
RAMANUJAM
(Universal Vedhas)

(ii)



ARENKAM
(Law of Ethics)

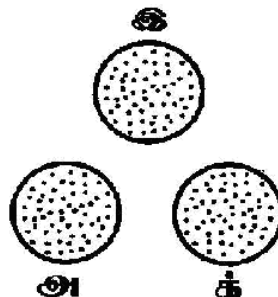
(iii)



RENKAM
(Law of Humanism)

- (i) Center dot is like "BRAHMA" (wisdom)
- (ii) Left dot is like "KARMA" (Intelligence)
- (iii) Right dot is like "DHARMA" (Common sense)

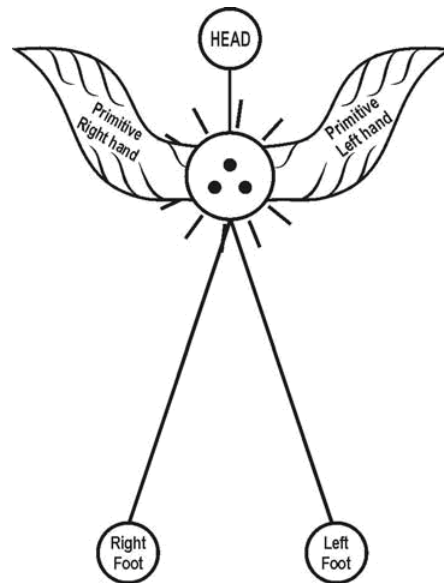
It is further focused that "SIVAM" shall be considered as 3rd generation Principle of life (say 1,00,000 years ago). Billions of Varied Principle of life vedhas shall be considered derived from **Three-in-One** vedhas.



SIVAM
(3G Vedhas)

This research further focus that **ST.RAMA** (Renkanathan) **ST.SITA** (Renkanayaki) shall be considered as descended from the Devas origin of **ARENKA NATHAN**, **ARENKA NAYAKI** (Angel race) Probably during APRIL 14 (Chittirai month).

(i)



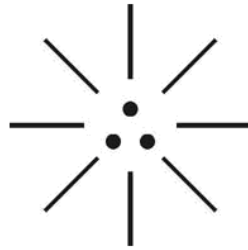
RENKA NATHAN
(Father of Thiri Renkam)
(April 14)

(ii)



RENKA NAYAKI
(Mother of Thiri Renkam)
(April 14)

This research focus that in ancient time the human ancestors lived in **VAIKUNDAM** (Single continent) considered having single Principle of life "**ARENKAM**" (also called as **VAINAVM**) and undergone three divisions in the Principle say "**ACHARYAN GROUP**", "**DASAN GROUP**", "**NATHAN GROUP**" (around 1,50,000 years). The Principle of "**SIVAM**" shall be considered evolved probably by populations of "**POST INDOS**" around 1,00,000 years ago. This research further focus that the Principle of life adopted by **ST.RAMA**, **ST.SITA** shall be considered as "**RENKAM**" rather than "**SIVAM**".



RENKAM SPLIT

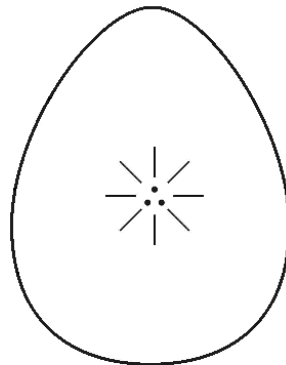
- (a) Right dot - ACHARYAN Group (Dharma)
- (ii) Left dot - DASAN Group (Karma)
- (iii) Center dot - NATHAN Group (Brahma)

It is focused that the **Renkan Split** probably considered took place in ancient time around 1,50,000 years ago in **THIRIKOSHTIYUR (Thirukoshtiyur)** of present Sivaganga district of Tamilnadu.

Case study shows that SRIRANGAM in Trichy District of Tamilnadu is considered as foremost of eight self manifested shrines of "LORD VISHNU" Srirangam is also considered as most important of 108 main temples (Divyadesams) of 'Sri vaishnavitas'.

Case study further shows that the "ANGKOR WAT" temple is considered as bigger than Srirangam presently non-functional. Hindu mythology focus that the place where 'LORD RAMA' performed Pooja to "Vishnu Idol" is Rameswaram of South Tamilnadu.

*It is hypothesized that 'ANGKOR WAT' shall be considered as integral part of THIRI RENKAM, VAIKUNDAM (Ancient single continent) about 3,00,000 years ago. The **Philosophy of Then Thiripathi** where Devas populations (Arenka Nathan, Arenka Nayaki) lived shall be indicated as below.*



THEN THIIRIPATHI
(Mars Planet)

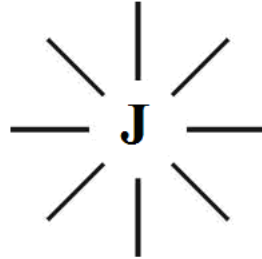
...Author

Facing South direction is auspicious?...

Case study shows that experts of 'Vastu Shastra' stipulates that most of the gods are facing in the direction of "East" except **Dakshnamurthy, Hanuman.**

Further International Scientist focus that the 'SOLAR PANELS' responsible for converting solar energy into **electric energy** are placed in such a way that the panels are facing the direction of 'SOUTH DIRECTION'?... Why it so?...

It is hypothesized that "ARENKA NAYAKI" shall be considered as the source of **Universal energy** radiating energy from "SOUTH DIRECTION" from THEN THIRIPATHI.



ARENKA NAYAKI
(Mother of Then Thiripathi)

Previous Publications:

1. YUGADI WISHES (IARA, March 2015)
2. TAMIL PUTHANDU!... (AJER, April 2015)
3. THEN MADURAI?... (IJERD, April 2015)
4. TAMIL NEW YEAR COOL DRINK?... (AJER, April 2015)
5. SCIENTIFIC RAMANUJAM?... (IJERD, April 2015)

Weight Reduction of 12"-150 Class Plug valve Casting Body by Finite Element Analysis and Experimental Method

¹, Prof. Laukik B. Raut, ², Pradnyawant .K.Parase
(SVERI's COE Pandharpur, Mechanical Department,)

ABSTRACT: Now-a-days cost of the materials is very high, so there is need to minimize the cost. For this purpose, it is necessary to optimum use of man, machine and material. So that's why it is essential to reduce the weight of the plug valve body. The stress analysis means determining the stress value of the valve body when internal pressure is applied. Ultimate aim of the current experiment is to reduce the casting weight of the body. The finite element method (FEM), sometimes referred to as finite element analysis (FEA), is a computational technique used to obtain approximate solutions of boundary value problems in engineering. Simply stated, a boundary value problem is a mathematical problem in which one or more dependent variables must satisfy a differential equation everywhere within a known domain of independent variables and satisfy specific conditions on the boundary of the domain. Boundary value problems are also sometimes called field problems. The field is the domain of interest and most often represents a physical structure. In the field of competition, all companies should supply their goods and services with high quality, in shortest period with lower prices than its competitors in order to keep their capacity and power to compete. Plug valves are machine elements which are commonly used for regulation of fluid, semi-liquid and granular medium flow on variety of tanks and pipeline systems. This experiment discusses FEA analysis of Plug-valve body followed by Experimental stress analysis using strain gauge method for weight reduction. New reduced weight models were prepared on the basis of validation of the results obtained from stress analysis procedure. The weight reduction is done by changing the wall and rib thickness. The results clearly shows the maximum weight reduction is 9.95 kg (7.11 % of original weight) while keeping maximum stress level up to 125.187 N/mm² which is safe for the applied pressure as per standard.

Key words: Plug valve, Strain Gauge, rosettes, standard.

I. INTRODUCTION

Plug Valves :

A plug valve is a rotational motion valve used to stop or start fluid flow. The name is derived from the shape of the disk, which resembles a plug. A plug valve is shown in Figure 1.10. The simplest form of a plug valve is the petcock. The body of a plug valve is machined to receive the tapered or cylindrical plug. The disk is a solid plug with a bored passage at a right angle to the longitudinal axis of the plug. In the open position, the passage in the plug lines up with the inlet and outlet ports of the valve body. When the plug is turned 90° from the open position, the solid part of the plug blocks the ports and stops fluid flow. Plug valves are available in either a lubricated or non lubricated design and with a variety of styles of port openings through the plug as well as a number of plug designs.

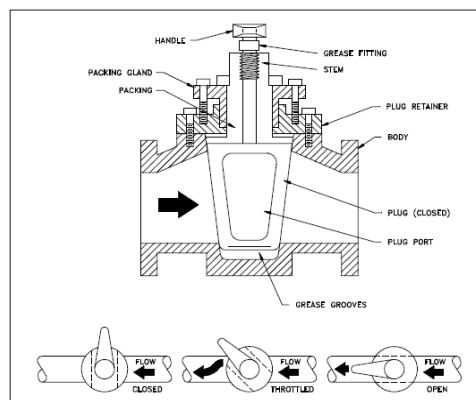


Figure1.1: Cross Section Plug Valve

Valve Operations

The Accuseal plug valve is a non-lubricated, resilient seal, plug- type valve which has a mechanical means of freeing the plug before it is rotated from the closed to the open position.

- **Opening of the valve**

For opening of plug valve, hand wheel has to turn counter clockwise. During this operation the plug is raised while the slips are retracted away from the body. When the slips are fully retracted from the body seating area, the plug is then able to rotate 90 degrees to fully open position. When the valve is in the full open position, slips and slip seals are completely protected from line flow.

- **Closing the valve**

For closing of plug valve, hand wheel has to turn clockwise. During this operation the retracted plug and slips are rotated 90 degrees without body contact. This rotation continues until the slips are positioned over the upstream and downstream port areas. Continued rotation of hand wheel mechanically forces the plug downward and forces the slips outward to seal firmly against the valve body. This produces a secondary metal to metal seal on both upstream and downstream areas providing double isolation.

Applications of plug valves

Biofuels Product isolation, Multi product manifolds, Custody transfer units, Tank farms (Oil Depots) Aviation fueling system:

II. LITERATURE REVIEW

2.1 Introduction:

Literature survey is carried out for getting the information regarding FEA and optimization techniques. This literature survey provided useful information regarding the experimental stress analysis method. The literature is collected from various international published papers, International journals and company documents. The literature review of work done by different researches in the area of weight optimization, FEA and experimental stress analysis technique is discussed below:

2.2 Present Literatures & Reviews:

[1] **Mona Golbabaee, Rouhollah Torabi, Ahmad Nourbakhsh, Karo Sedighiani:**

This article carried out work of centrifugal pumps engaged in high pressures must have smooth and safe operation without leakages. To control this phenomenon, optimal geometry and proper materials must be considered in design of all mechanical components including, significantly, the volute casing.

[2] **Deokar Vinayak Hindurao, D. S. Chavan:**

In the field of competition, all companies should supply their goods and services with high quality, in shortest period with lower prices than its competitors in order to keep their capacity and power to compete .

[3] **Xue Guan Song, Lin Wang, Seok Heum Baek, Young Chul Park:**

This paper carried out work related to a butterfly valve is a type of flow control device, typically used to regulate fluid flow. This paper proposes a new process to meet desired needs in valve design that is characterized by the complex configuration.

[4] **A. Dorogoy, D. Rittel:**

This paper analyzes the errors inherent to the determination of mixed mode stress intensity factors from data obtained by using a three strain gauge rosette. The analysis shows that the errors are mainly due the third characteristic value (3/2) and its corresponding coefficients. It is also shown that the errors do not depend on the orientation angle of the rosette, the angle between the strain gauges and the material properties.

[5] **Aleksandar Petrovic:**

The paper consists a stress analysis of a cylindrical pressure vessel loaded by axial and transverse forces on the free end of a nozzle. The nozzle is placed such that the axis of nozzle does not cross the axis of cylindrical shell. The method of finite element was applied to determine the state of stress in the cylindrical shell. [11] **B. Prabu, N. Rathinam, R. Srinivasan, K.A.S. Naarayan:**

[6] **K. H. Jatkar, Sunil S. Dhanwe:**

In this paper carried out study on the dynamic analysis of single cylinder petrol engine was conducted. Finite element analysis was performed to obtain the variation of the stress magnitude at critical locations of connecting rod and crankshaft. This load was then applied to the FE model and boundary conditions were applied according to the engine assembly. It is observed that maximum stress is developed at crank pin of crank shaft. The maximum stresses are developed at the fillet section of the big and the small end of connecting rod.

[7] Joseph F Dues:

This paper examining the mechanics of a soda can is an exciting way to get students interested in strength of materials by relating classroom concepts to everyday objects. A soda can containing a carbonated drink is a thin wall pressure vessel. The geometry of the soda can is optimized to minimize the amount of aluminum required. The wall thickness is very thin and is subject to an appreciable amount of stress and strain. By mounting a strain gage to the can, and then relieving the stress by opening the can, the change in strain from the pressurized to unpressurized condition can easily be measured.

[8] Dr. K. H. Jatkar, Sunil S. Dhanwe:

This paper carried out FEA work on gate valves are used when a straight-line flow of fluid and minimum restriction is desired. Gate valves are so named because the part that either stops or allows flow of fluid through the valve acts somewhat like the opening or closing of a gate and is called, appropriately, the gate. The objective of this paper to perform a stress analysis of the critical component of Gate Valve..

III. FINITE ELEMENT ANALYSIS

Simple mathematical model can be solved analytically, but more complex model requires use of numerical methods.

4.1 3D modeling of Valve Body

In ANSYS it's very difficult to model the part with parametric modeling as compared with the available modeling software such as CATIA and Pro-E. To create a 3D model of valve body with all intricate geometric details, CATIA software is used. The created 3D model of valve body is as shown in fig 4.1.

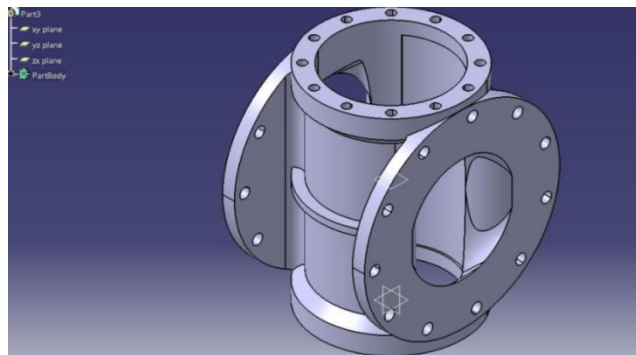


Figure 4.2 – 3D model of valve body

While creating 3D model care has been taken to model it with parametric expression, so as the dimensions changes it will reduce the repetitive time required for modeling. Small steps and chamfers are eliminated while modeling. The created 3D model is saved in part.igs file format, as this file format is suitable during importing this model for meshing in Hypermesh software.

4.2 Meshing of the 3D valve body model

In simple term meshing means connecting elements with each other. Elements are the building blocks of the finite element analysis. Meshing is carried out by using Hypermesh software. Model is meshed by using SOLID 45 element and with 7 element size. Total **175364** elements and **13293** nodes were created after meshing.

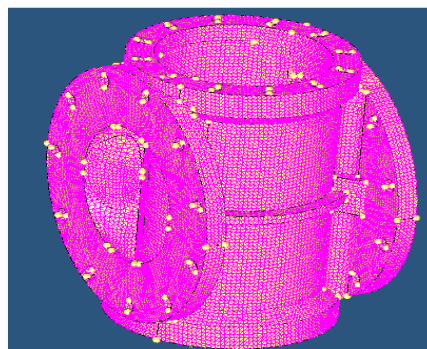


Figure 4.3 - Meshed model

Material properties assigned

After completion of meshing material properties are assigned to meshed model. These properties are listed below.

Material used-	ASTM A216 Grade WBC
Young's Modulus-	2.1E5 N/mm ²
Poissons Ratio -	0.28

The maximum principal stress 87.709 N/mm² and 131.512 N/mm² founds in the rib at 2 MPa and 2.99 MPa internal pressures respectively. While minimum principal stress (2nd principal stress) 34.431 N/mm² and 51.626 N/mm² found at flange corner for 2 MPa and 2.99 MPa internal pressures respectively. As the internal pressure acts on the internal effective pressurizing area of valve body, results to expand the valve body .Ribs tries to hold the valve body in original position so ribs subjects to heavy tensile stress. As the internal pressure increases stresses in the valve body increases linearly.

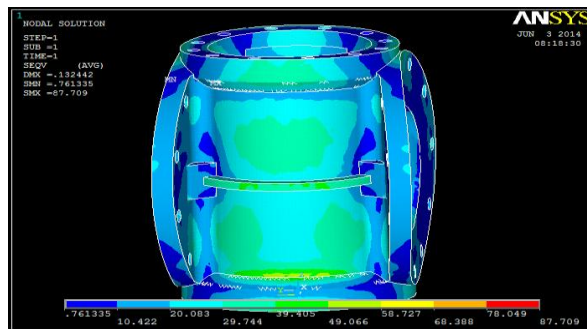


Figure 4.5 - Von-mises stresses for 2 MPa internal pressure applied

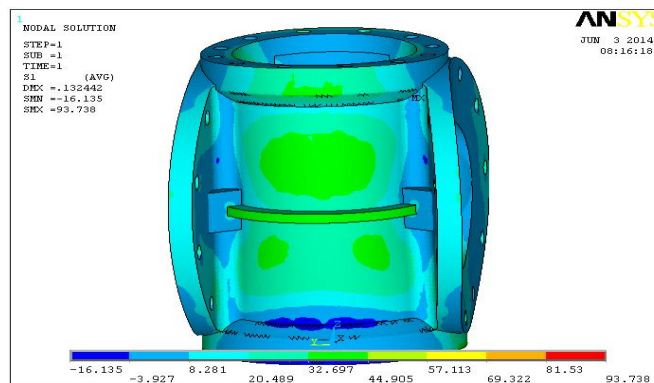


Figure 4.6 - 1st principal stress for 2 MPa internal pressure applied

4.3 FEA results for 2.99 MPa internal pressure applied.

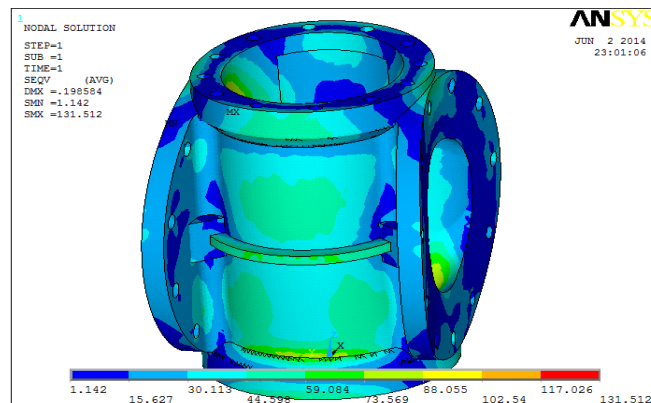


Figure 4.9 - 1st principal stress for 2.99 MPa internal pressure applied.

4.4 Selection of locations for mounting strain gauge rosettes.

Finite element results shows that vertical rib is subjected to heavy tensile stress. But it is not possible to mount strain gauge rosette exactly on this rib, because thickness of rib is less for mounting of strain gauge rosette. For the convenience strain rosette will be mounted different portions of valve body. Four different locations decided by carefully analyzing the FEA results. Figure 4.10 showing the different four locations selected for mounting of the strain gauge rosettes.

1st and 2nd principal stress results from FEA at these four locations will be compared with experimental stress results at the same point for validation of FEA results. Further to this, FEA and experimental stress analysis comparison will be useful to do reduction of the plug valve casting body.

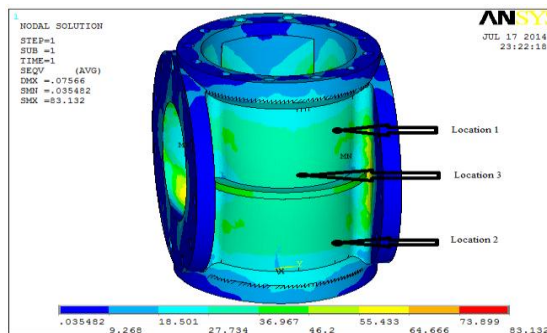


Figure 4.11 - Different locations selected for mounting strain gauge rosette

Summarized principal stress data using FEA

The principal stresses (σ_1 and σ_2) at the same points of interest selected for mounting of strain gauge rosette on valve body are found out. The stresses are found at two different cases by applying (2 MPa and 2.99 MPa) internal pressures. Following tables shows 1st and 2nd principal stress results found by FEA.

Location Number	Von Mises stress (N/mm ²)
1	18.91
2	21.01
3	31.2

Table 4.1 - FEA results at 2 MPa internal pressure applied

Location Number	1 st principal stress (N/mm ²)
1	31.18
2	33.93
3	43.2

Table 4.2- FEA results at 2.99 MPa internal pressure applied

IV. EXPERIMENTAL STRESS ANALYSIS

4.1 Experimental setup

In this experimental work stain gauge technique is used to calculate stress at a point of interest. One opening made for fitting of relief valve kept open for the purpose of filling coolant in a valve body. Once the body totally filled with coolant that opening also make closed under slandered pressure 290 psi (2Mpa). One plug opening is provided to inlet closing plate, for connecting outlet pipe of the pressurizing unit. Testing has completed as per API 598.

After body test strain gauge rosettes (0-45-90) are mounted on four locations which were decided previously by analyzing the FEA results. Strain readings are taken in two stages at 2MPa and 2.99MPa. Strain developed in each arm of the rosette is noted from display of straingauge indicator. The experimental setup is as shown in the photograph.

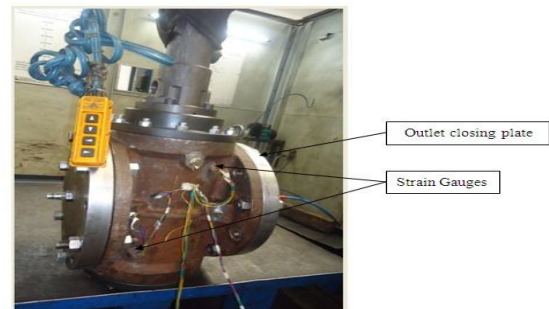
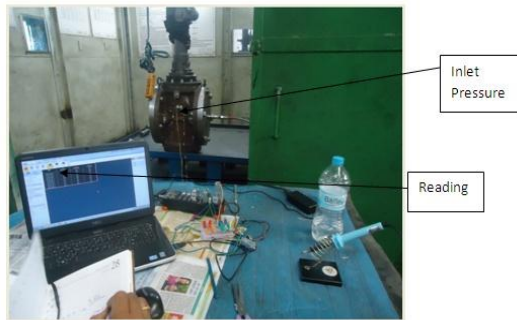


Figure 5.2 (a) Actual Experimental Setup

Figure 5.2 (b) Photograph Experimental Setup

4.8 Experimental observations

For each load case the three readings are observed. The three readings are respective to the three axis of rosette namely ϵ_a , ϵ_b , ϵ_c . For getting the three axis readings lead wires of the respective directions are to be connected in the circuit to the rear panel of 10 channel balancing and switching unit along with strain indicator. The readings shown by strain indicator are in microstrains. Two sets of the readings are taken at two different load conditions (2 MPa and 2.99 MPa). Finally, the principal strains and principal stresses of the respective points of interest where rosettes mounted are calculated by analytical method. Tables are showing the results.

Rosette Number	ϵ_a (μ strain)	ϵ_b (μ strain)	ϵ_c (μ strain)	σ_1 (N/mm ²)	σ_2 (N/mm ²)	Von Mises Stress (N/mm ²)
1	53	61	62	18.26	16.33	17.38
2	61	72	69	20.92	18.19	19.70
3	89	93	98	28.89	27.36	28.16

Table 5.1 - Experimental Results at internal pressure 2 MPa applied.

Rosette Number	ϵ_a (μ strain)	ϵ_b (μ strain)	ϵ_c (μ strain)	σ_1 (N/mm ²)	σ_2 (N/mm ²)	Von Mises Stress (N/mm ²)
1	61	72	69	30.94	26.82	29.10
2	102	115	103	32.95	28.72	31.05
3	128	135	142	41.80	39.43	40.66

Table 5.2 - Experimental Results at internal pressure 2.99 MPa applied.

V. COMPARISION BETWEEN FEA AND EXPERIMENTAL ANALYSIS

The values of deviation in 1st and 2nd principal stress, calculated based on experimental result and FEA results, for the valve body having wall thickness 19.5 mm are shown in Table no. 6.1 and 6.2 and at the same point where strain gauge rosettes was mounted. Results clearly show that the maximum deviation in these results is equals to 9.75 % which is allowed. While carrying the experimental validation the readings depends on environmental conditions like temperature difference, measuring instrument sensitivity, human errors, casting defects inbuilt while manufacturing valve body by casting these are some possible reasons for the deviation.

Strain Gauge Mounting location number	FEA results	Experimental results (N/mm ²)	% Error in (N/mm ²)
	Von Mises Stress (N/mm ²)		
1	18.91	17.38	8.09
2	21.01	19.70	6.23
3	31.2	28.16	9.75

Table 6.1 - Comparison of Von Mises Stress values at internal applied pressure 2 MPa

Strain Gauge Mounting location number	FEA results	Experimental results (N/mm ²)	% Error in N/mm ²
	Von Mises Stress (N/mm ²)		
1	31.18	29.10	6.68
2	33.93	31.05	8.48
3	43.9	40.66	7.37

Table 6.2 - Comparison of Von Mises stress values at internal applied pressure 2.99 MPa

As the FEA and Experimental results are coming close to each other, different models of valve body by varying wall and rib thickness can be made. FEA of these models will be carried out without affecting original geometry as the 3D parametric modeling is built up in the CATIA.

VI. MODIFICATION OF BODY

6.1 Introduction

The aim of design review is to reduce the cost of the valve body by reducing its weight, without compromising the casing strength. There are many ways of cost reduction

6.2 Steps for the modification of body

- Modeling of the valve body using CATIA.
- Stress analysis of above model using FEA.
- Repetition of above steps for different newly modified models.

6.3 FEA results after reducing wall thickness by 2mm and flange by 2.5 mm increase neck radius to 180 mm

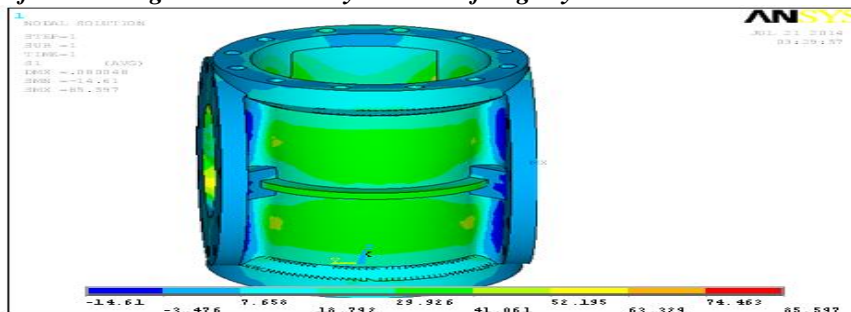


Figure 7.9 - Von Mises Stress stress for FEA results after reducing wall thickness by 2mm and flange by 2.5 mm increase neck radius to 180 mm

VII. RESULTS AND DISCUSSION

8.1 Discussion on Results

FEA results and reduction in weight after modifications are summarized in the following tables

Reducing the wall thickness by 1 mm weight is reduced by 3.34 kg (2.39%), while maximum principal stress level value is 118.485 N/mm². Whereas when the wall thickness is reduced by 2 mm, weight is reduced by 5.38 kg by keeping the maximum stress value at 120.174 N/mm². Again for another modification, if wall thickness decreased by 2 mm flange by 1 mm, 7.34 kg of weight is reduced by keeping the maximum stress level at 88.112 N/mm² which is much lower than the yield stress of the material.

By reducing the wall thickness by 2 mm and flange by 2.5 mm, the weight reduced is 10.52 kg (7.51 %) from original weight, and maximum stresses found equals to 125.187 N/mm². While if the wall thickness is reduced by 2 mm and increase neck radius up to 180 mm, 9.15 kg (7.11 %) weight is reduced.

Results by decreasing the wall thickness by 2 and increase neck radius up to 180 mm are better than only reducing the wall thickness. Because Principal stresses are decreased in rib portion as the thickness of rib is increased. And the principal stress value coming is much lower than the yield stress value; hence it is safe for working conditions. Results by decreasing the wall thickness by 2 and increase neck radius up to 180 mm are better than only reducing the wall thickness. Because Principal stresses are decreased in rib portion as the thickness of rib is increased. And the principal stress value coming is much lower than the yield stress value; hence it is safe for working conditions.

Parameter Changed	Von-Mises Stress N/mm ²	Reduction in weight (Kg)	Percentage reduction in weight (Kg)
Reduced wall thickness by 1 mm	84.318	3.34	2.39
Reduced wall thickness by 2 mm	84.318	5.38	3.84
Reduced wall thickness by 2 mm and flange by 1 mm	83.112	7.34	5.24
Reduced wall thickness by 2 mm and flange by 2.5 mm	93.126	10.52	7.51
Reduced wall thickness by 2 and increase neck radius to 180 mm	82.84	9.95	7.11

Table 8.1 - Summarized results after reducing wall thickness in 2 mm steps

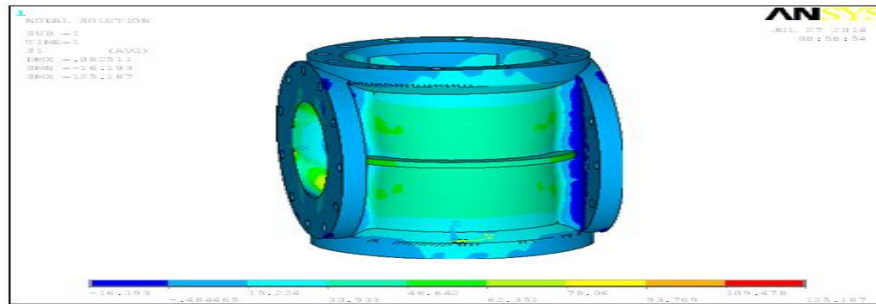


Figure 7.10 - 1st principal stress for FEA results after reducing wall thickness by 2mm and flange by 2.5 mm increase neck radius to 180 mm

From obtained stress pattern, it is concluded that the maximum 1st principal stress value is 125.187 N/mm² founded in the rib. In actual working condition, the maximum 1st principal stress found is 131.512 N/mm² at the same location i.e. in the rib portion. The stress contour results interpret that except rib section stresses are very less in other zones of the component.

The new modified valve body results are coming lower than the yield stress value; it shows that newly modified valve body is safe for same working condition. By reducing the wall thickness wall thickness by 2 and increasing neck radius to 180 mm weight is reduced by 9.95 Kg.

VIII. CONCLUSIONS AND FUTURE WORK

9.1 Conclusions

In this dissertation work an attempt has made for weight optimization of plug valve body. Various models are created by changing the design parameters and analyzed these models for better results. Experimental structural strains and stresses measured by actual pressurizing the valve body, and compared it with FEA results. Strain gauge technique gives good results for the measurement of strain and stress at the point of interest.

1. Results of finite element method for the structural analysis of the plug valve body are well in agreement with experimental results, as the deviation is maximum deviation is up to 9.75 % and minimum deviation is up to 6.23 % which is allowable.
2. Eight new different optimized models created by changing the design parameters and analyzed .As there is restriction to change the flange dimensions, wall body thickness and neck dimensions are considered for optimization.
3. Results of decreasing the wall thickness and increasing the neck size are better than only reducing the wall thickness.
4. The best modified model is that, in which wall thickness is reduced wall thickness by 2 mm and increase neck radius to 180 mm reduces 9.95 kg (7.11 %) weight, because maximum stress level is much lower than the yield stress value of the material. FEA results for this optimized model shows that stresses in ribs also decreased because of increased rib thickness.

9.2 Scope for future work

A lot scope is there for the work related to stress analysis. In connection with present dissertation work the following points are to be considered for future work.

1. The same model may analysed by another experimental method i.e. by photo elasticity method & in this method the exact model of plug valve body will be prepared, with the help of photo elastic material which is used for analysis by photo elasticity method. The loading conditions are applied on the same model and one can see the actual point to point stress values on the volute casing. As well as the deflections are visible by naked eyes. Also optimization is easier and immediate results of stress pattern for the optimized component can be seen.
2. Experimental stress analysis of ,newly modified best optimized model ,and comparing experimental stress analysis results with obtained FEA results.
3. In this analysis the effect of fluid temperature is not considered, the effect of fluid temperature could be investigated in future. Temperature distribution and thermal stresses can be found out by using FEA

REFERENCES

- [1] **Mona Golbabaeci, RouhollahTorabi, Ahmad Nourbakhsh, KaroSedighiani**, "Failure Detection and Optimization of a Centrifugal-pump Volute Casing", Proceedings of the SEM Annual Conference June 1-4, 2009, Albuquerque New Mexico USA, Society for Experimental Mechanics Inc.
- [2] **DeokarVinayakHindurao, D. S. Chavan**, "Optimization of 16" Plug Valve Body Using FEA And Experimental Stress Analysis Method", International Journal of Mechanical Engineering, Vol. No. 1, pp. 79-86.
- [3] **Xue Guan Song, Lin Wang, SeokHeumBaek, Young Chul Park**, "Multidisciplinary optimization of a butterfly valve", ISA Transactions, 2009, pp. 370-377.
- [4] **A. Dorogoy, D. Rittel**, "Optimum location of a three strain gauge rosette for measuring mixed mode stress intensity factors", Engineering Fracture Mechanics, 2008, pp. 4127-4139.
- [5] **AleksandarPetrovic**, "Stress Analysis of Cylindrical Pressure Vessels with Loads Applied to the Free End of Nozzle", International Journal of Pressure Vessels and Piping, 2001, pp. 485-493.
- [6] **B. Prabu, N. Rathinam, R. Srinivasan, K.A.S. Naarayan**, "Finite Element Analysis of Buckling of Thin Cylindrical Shell Subjected to Uniform External Pressure", Journal of Solid Mechanics Vol. 1, No. 2, 2009, pp. 148-158.
- [7] **K. H. Jatkar, Sunil S. Dhanwe**, "Dynamic Analysis of Single Cylinder Petrol Engine", International Journal of Engineering Research and Applications, Vol. 3, No. 3, May-Jun 2013, pp. 1177-1183.

A Visual Attention Based Improved Seam Carving For Content Aware Image Rescaling

¹Aparna P, ²Prabu.T

¹ PG Scholar, ² Assistant professor. Department of electronics and Communication engineering, Nehru Institutions of Engineering and Technology, Nehru Gardens.

ABSTRACT: Content-aware image resizing is a kind of new and effective approach for image resizing, which preserves image content well and does not cause obvious distortion when changing the aspect ratio of images. Saliency detection plays important roles in many image processing applications, such as regions of interest extraction and image resizing. Effective resizing of images should not only use geometric constraints, but consider the image content as well. The basic idea beyond these algorithms is the removal of vertical and/or horizontal paths of pixels (i.e., seams) containing low salient information. In The proposed system, present a method which exploits the gradient vector flow (GVF) of the image to establish the paths to be considered during the resizing. The relevance of each GVF path is straightforward derived from an energy map related to the magnitude of the GVF associated to the image to be resized. To make more relevant, the visual content of the images during the content-aware resizing, also propose to select the generated GVF paths based on their visual saliency properties and a blending method in order to obtain better visual results in joining adjacent image regions after seams removal. The depth of the scene will be considered to make more visually consistent the resized images. In this way, visually important image regions are better preserved in the final resized image. The proposed technique has been tested, both qualitatively and quantitatively, by considering a representative data set of images labeled with corresponding salient objects (i.e., ground-truth maps). Experimental results demonstrate that our method preserves crucial salient regions better than other state-of-the-art algorithms.

INDEX TERMS- Content aware image resizing, image retargeting, visual saliency, gradient vector flow.

I. INTRODUCTION

The extensive use of display devices with different resolution (e.g., on pc, tablet, Smartphone, etc.) increases the demand of image resizing techniques which consider the visual content during the scaling process. Standard resizing techniques considering only geometric constraints, such as scaling, can be used only to change the image size (width and height) of a fixed percentage with respect to the original one. Scaling does not take into account the visual importance of pixels during image resizing (i.e., a resizing with respect to only one dimension introduces artifacts and distortions). Other standard operations in which outer parts of an image are removed (e.g., cropping), could produce images with loss of salient information (e.g., removal of objects or part of them). In the last years, several techniques for content-aware image resizing (or content-based visual retargeting) have been proposed. The main aim of a content-aware image resizing is the preservation of relevant visual information into the resized image. Intuitively, the goal is to remove unnoticeable paths of pixels that blend well with their surroundings, and retain the salient pixels which are important to generate the needed visual stimuli useful to correctly perceive the visual content. The algorithm should avoid distortion and changes of perspective of the image. Moreover, they should preserve edges, important textured areas belonging to the objects, size of the objects, and relevant details of the scene. The Seam Carving, proposed by Avidan et al. in, is probably the most popular content-aware resizing approach. Such a technique reduces the image by removing connected path of pixels (called seams) having low-energy in the map related to the image to be resized. The authors of compared different strategies to compute the energy map to be considered during the resizing process (e.g., the entropy energy computed for each pixel into a fixed window, the magnitude of the gradient computed on each pixel, a saliency measure of each pixel computed as in, etc.).

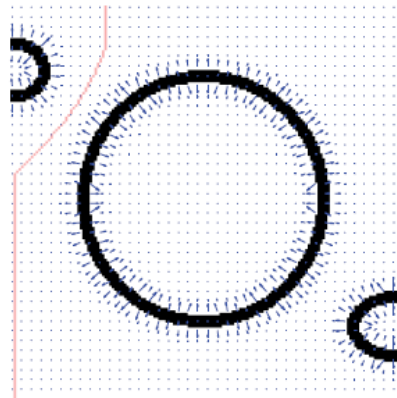


Fig 1 Input image with ITS corresponding GVF field over imposed. GVF values are higher in correspondence of the edge information. The seam derived by the proposed resizing approach is shown in red. The gradient vector field forces the seams fall from main contours of the object.

An interesting and powerful extension of standard resizing operators (i.e., scaling, cropping, etc.) and content-aware based algorithms (i.e., seam carving) can be obtained by their combination, as proposed by Rubinstein et al. in. They propose a technique able to search for the optimal sequence of operators to be applied at each step of the resizing to get better results in terms of visual quality of the final reduced image. On the other hand, the computational complexity increases due to the use of different operators. Among others, patch-based methods have been also proposed for image retargeting or summarization. In particular, Cho et al. suggested an algorithm to find an arrangement of patches of the original image that well fit in the resized image, whereas Pritch et al. introduced a method to find the best Shift-Map which defines the pixel displacement useful to produce the output image. Wu et al. propose a resizing method exploiting also high level semantic features such as symmetry. Specifically, their approach resizes symmetry regions by summarization and the remaining ones by warping. In this case the resizing method considers non-homogeneous warps to concentrate the resizing distortions in regions with low saliency information. To this aim, the resizing problem is formulated as a quadratic minimization problem and different metrics are considered to measure the image distortion. Gallea et al. proposed a fast method for image retargeting based on the solution of a linear system. This model aims to find shift values for each line (row/column) preserving the distance among the relevant ones. The linearity of the considered model allows them to elaborate even large images in reasonable computational time.

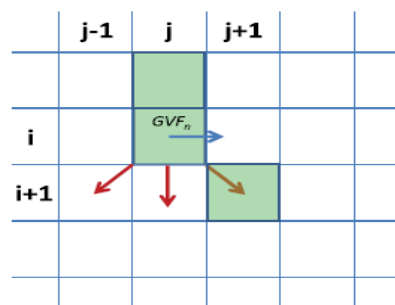


Fig 2 An example of seam generation among the three possible directions (in red) the one with angle closest to the GVF orientations (in blue) is chosen.

This paper introduces a novel algorithm for content aware image resizing. The technique exploits the properties of Gradient Vector Flow (GVF) to properly detect the seams to be removed, without introducing artifacts in the resized image. Specifically, GVF generates a vector field useful to preserve objects by enhancing edges information during the generation of the possible paths to be removed. The vector field produced by GVF is also coupled with a visual saliency map in order to refine the final selection of the paths to be removed. The proposed approach has been tested and compared, both qualitatively and quantitatively, with respect to state-of-the-art approaches on a representative dataset. Experimental results confirm the effectiveness of the proposed approach in terms of preservation of salient regions.

II. PROPOSED METHOD

One of the main issues of the content aware image resizing is the preservation of the salient information contained in the image under analysis. To this aim, our algorithm makes use of the properties of the Gradient Vector Flow (GVF). GVF is a dense force field useful to solve the classical problems that affect snakes: sensitivity to initialization and poor convergence to boundary concavity. Starting from the gradient of an image, this field is computed through diffusion equations. Formally, GVF is the field \mathbf{F} of vectors $\mathbf{v} = [u, v]$ that minimizes the energy function

$$E = \iint \mu(u_x^2 + u_y^2 + v_x^2 + v_y^2) + |\nabla f|^2 |v - \nabla f|^2 dx dy \quad (1)$$

Where the subscripts represent partial derivatives along x and y axes respectively, μ is a regularization parameter, and $|\nabla f|$ is the gradient computed from the intensity of the input image. Due to the above formulation, GVF field values are close to $|\nabla f|$ values in those areas where this quantity is large (energy E , to be minimized, is dominated by $|\nabla f|^2 |v - \nabla f|^2$), and are slow-varying in homogeneous regions (the energy E is dominated by the sum of the squares of the partial derivatives of GVF field). Hence, GVF is stronger close to the edges of Objects within the image. An example of GVF field is shown in Fig. GVF values are higher in correspondence of the edges information. The seam derived by the proposed resizing approach is shown in red. The gradient vector field forces the seams far from main contours of the objects. Its exploits this vector field to effectively build the set of pixel paths (i.e., the seams) to be considered as candidate in the removal process. The relevance of each GVF path can be straight forward derived from the energy map obtained by the GVF magnitude associated to the image under consideration.

Let I be an image with H rows and W columns to be resized with respect to the width, and $0 < N < W$ the number of seams to be removed. First the GVF and its normalized version $GVFn$ (i.e., each vector with norm one) are computed from the input image I considering the luminance channel (i.e., Compute GVF). Several seams $\{s_1, s_2, \dots, s_K\}$ are then built starting from the top of the image making use of the directions of the already computed $GVFn$ (i.e., Seams Computation). The algorithm devoted to the generation of the seam has been designed to exploit the properties of the GVF field. Specifically, this field preserves the strong edges and propagates the information related to their presence also in the neighboring pixels. Starting then from the top of the image and following the GVF field direction a seam avoiding as much as possible main edges is built. It is worth noting that the directions suggested by $GVFn$ cannot be always followed. Specifically, considering a generic pixel p of coordinates (i, j) belonging to a seam s_k , the next element of s_k has to be chosen among $(i + 1, j - 1)$, $(i + 1, j)$, $(i + 1, j + 1)$. These pixels can be related to the following unit vectors $(-\sqrt{2}/2, -\sqrt{2}/2)$, $(0, 1)$, $(\sqrt{2}/2, -\sqrt{2}/2)$. Among the aforementioned unit vectors associated to a specific direction, the one making the smallest angle with $GVFn(i, j)$ is hence considered during the seam generation. To this aim, a simple dot product between $GVFn(i, j)$ and the three considered unit vectors is employed. To sum up a generic seam s_k is built repeating $H - 1$ times the aforementioned direction selection algorithm starting from a pixel p with coordinates $(1, w)$ at the top of the image ($w = 1, \dots, W$ at the first iteration of the resizing).

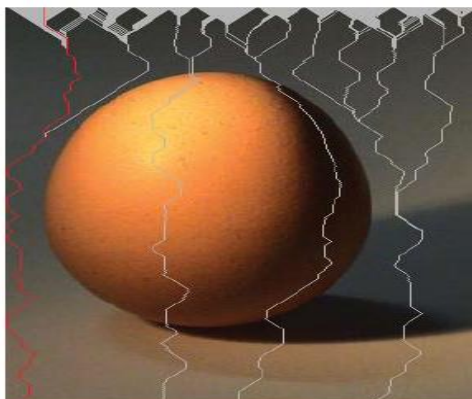


Fig 3 The seams to be removed selected considering the related path is shown in red.

The proposed algorithm works similarly for the resizing with respect to the height. After computing the set of candidate seams $\{s_1, s_2, \dots, s_k\}$, a cost is associated to each seam by considering the sum of the GVF magnitude $|GVF|$ of the pixels belonging to the seam. Specifically the cost c_k of a seam s_k is computed as follows

$$C_k = \sum_{(i,j) \in s_k} |GVF(i,j)| \quad (2)$$

The seam with the lower cost c_k is hence removed from the image at each iteration (i.e., Remove Seam). The GVF map is then updated and a new iteration of the seam removal algorithm is performed for each seam to be removed. It is worth noting that the core of the proposed resizing approach is related to the method adopted to select the seams (i.e., Seams Computation). Indeed, the seam selection method has been designed to exploit the properties of the GVF in order to maintain the strong edges of the images and propagates their contributions also in their neighboring creating then a repulsive field. On the contrary, classic Seam Carving approaches do not propagate the information of a strong edge into the close pixels. Moreover, GVF combines the contribution of several edges in a smooth way. Differently than Seam Carving], the proposed approach, due to the repulsive field that propagates the information about the presence of an edge also in its Neighboring, can perform a simple seam selection guided by the GVF field without considering all the possible paths. All the possible paths generated at iteration t are shown in gray and the best one in red. As can be easily seen, only a limited number of paths are actually considered and, usually, they do not cross the salient region.

III. SALIENCY BASED SELECTION OF GVF PATHS

The visual saliency (or visual saliency) refers to the properties of the visual stimuli which are exploited by the human visual system in the tasks of visual attention and rapid scene analysis. The automatic detection of salient regions in images can be used in a broad scope of computer vision applications such as image segmentation, content-based image retrieval, object detection and recognition.

Several saliency estimation methods have been proposed in literature. Some of them, such as the algorithm proposed by Itti et al., originate from the biologically plausible visual architecture proposed by Koch and Ullman. Others methods, such as the one presented by Achanta et al. in and by Hou et al. in, are purely computational and do not make any assumption on biological architecture. Finally, techniques based on combining both paradigms, biological and computational, have also been published, as in the work of Harel et al. All previously mentioned approaches estimate the visual importance of image pixels starting from information extracted in the uncompressed domain. Since most images (e.g., over internet) are stored in the compressed domain of joint photographic expert group (JPEG), Fang et al. Have proposed a method to extract saliency directly in the JPEG domain by exploiting information of intensity, color, and texture encoded by the discrete cosine transform (DCT) coefficients on each 8x8 block.

Visual saliency estimation algorithms have straightforward application in content based visual retargeting. Indeed, all the state-of-the-art retargeting algorithms detect the paths to be removed (i.e., the seams) taking into account of an energy map which encodes the importance of each pixel in terms of content. A successful seam carving algorithm should ensure that the most important image regions pointed out by the energy map should not be removed. The algorithm we presented in Section II makes use of the magnitude of the GVF as energy map to drive the selection of the seams to be removed. Despite this information is useful to take care of the saliency of the edges, it does not consider other saliency information. In Achanta et al. A visual saliency map able to uniformly highlight salient regions with well-defined boundaries has been used for content aware image resizing purpose; the classic seam carving algorithm proposed by Avidan et al. Has been employed by replacing the energy map computed using the L1-norm of the image intensity gradient, with the saliency map computed. Results presented emphasized the fact that by using the visual saliency better performances, with respect to the state-of-the-art methods, are achieved. This strongly motivated us to couple the proposed GVF based approach with saliency information for retargeting purpose.

In this paper propose to use visual saliency only for the selection of seams to be removed after that these paths are generated by exploiting the gradient vector flow as detailed in previous section. In this way we are able to combine different kinds of saliency information; the one related to the edges given by the GVF and the one related to the saliency objects within the image encoded by the saliency map. In our experiments we used the saliency map estimator proposed by Achanta et al. To include visual saliency information, first generate the seams exploiting the GVF, and then perform the selection based on saliency. The cost function is given by,

$$C_k = \sum_{(i,j) \in s_k} \text{Saliency}(i,j) \quad (3)$$

Where $\text{Saliency}(i, j)$ is the value of visual saliency of the pixel (i, j) computed.

IV. EXPERIMENTAL RESULTS

The performance of a content-aware image resizing algorithm strongly depends on the adopted energy map which captures the salient regions of an image. As described in previous sections, we propose to use GVF to build the seams during the resizing. The selection of the seams to be removed is then driven by GVF magnitude or by the saliency map. In order to evaluate the results of our basic approach and do not consider saliency information, we have compared it with respect to the classic Seam Carving algorithm proposed by Avidan et al, and the approach recently proposed by Gallea et al. The approach has been re-implemented, whereas the original code of the method has been provided by the authors.

While proposes a local-based approach which exploits the gradient of the image to select the seams to be removed, the approach is a global-based approach in which an objective function is considered to solve an optimization problem. In the product of the gradient of the image and the saliency map proposed by Itti et al. is taken into account as energy map during the resizing. Moreover, to underline the contribution of coupling GVF path extraction with saliency based selection compared the proposed saliency based selection approach with respect to the other systems.

In order to objectively assess the performances of the aforementioned methods compared the different approaches on the dataset used for saliency detection. For each image I of the dataset, the ground-truth map denotes which pixels of the image are important in term of saliency. In Fig. 5.1 are shown respectively an image considered in the experiments and its corresponding ground-truth map. Since the aim of content-aware image resizing is to preserve salient regions, we used the following cost function in order to objectively evaluate the performances

The cost can be used to fairly compare the performances of the different algorithms at varying of the scale factor. A lower cost value indicates better performances.

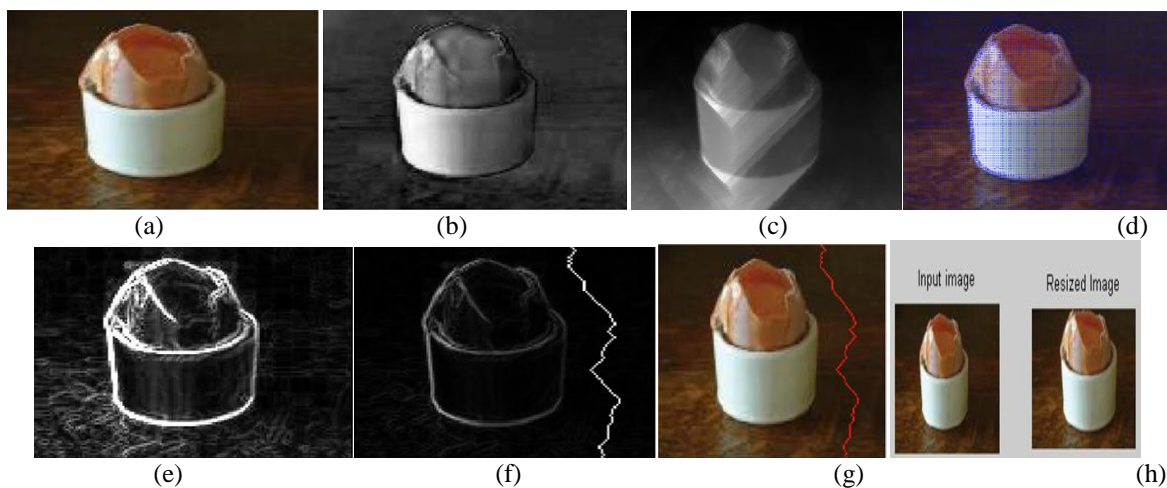


Fig 4. (a) Original image, (b) Image in lab color space, (c) Saliency map, (d) Gradient vector flow map, (e) Ground truth mask, (f) Seam generation, (g) The maps of the removed seam showed in red, (h) Resized image.

$$Cost(I, A, \lambda, d) = \sum_{p \in \Psi_{A, \lambda}(I)} G_I(p) \quad (4)$$

Where $\Psi_{A, \lambda}(I)$ is the final set of pixels removed by employing the algorithm A during the resizing of the image I of a scale factor $\lambda \in \{95\%, 90\%, 85\%, 80\%, 75\%, 70\%\}$ with respect to the maximum dimension of the image (as defined by equation (4)), and $G_I(p)$ indicates the importance of there moved pixel p in the image I .

$$d = \arg \max_{\hat{d} \in \{width, height\}} Size(I, \hat{d}) \quad (5)$$

This cost can be used to fairly compare the performances of the different algorithms at varying of the scale factor. A lower cost value indicates better performances (i.e., more salient pixels are preserved in the resizing). We have measured the performances of the different algorithms on the aforementioned dataset at varying of the scale factor.

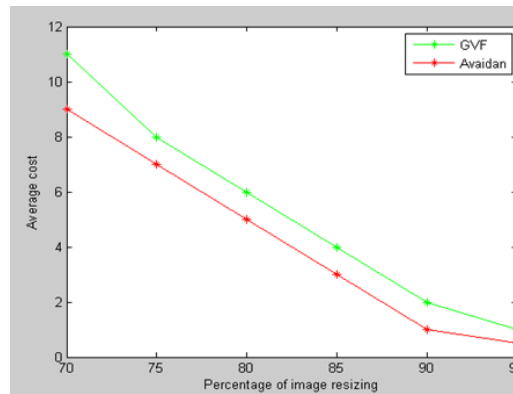


Fig 5 cost performance

The final results are obtained by averaging the results of all the executions for a specific scale factor λ .

In Fig. 5 are reported the results obtained by the three different algorithms which exploit the magnitude of the image gradient to select seams to be removed during the resizing: our Algorithm, the one proposed by Gallea et al. and the original Seam Carving algorithm proposed by Avidan et al. The results are shown at varying of the percentage of the resizing. To visually assess the results obtained with the five compared algorithms, some visual results obtained by resizing images with a scale factor of 70% with respect to their original dimension (width or height) A visual comparison reveals that the proposed approach with saliency based selection of GVF path better preserves the main salient regions (i.e., the areas with objects). The experimental results demonstrate the effectiveness of the proposal which reduces the computational cost during the resizing by maintaining almost the same performances in terms of saliency preservation.

V. CONCLUSION

The proposed novel content-aware image resizing algorithm which exploits information extracted through Gradient Vector Flow to establish the paths to be considered during the resizing of an image. The proposed GVF based approach is enriched with saliency information to achieve better results. The proposed solution has been compared with respect to state-of-the-art algorithms on a representative dataset achieving at least comparable visual results, and outperforming with good margins existent strategies in terms of preservation of salient regions. Some visual result obtained by resizing images with a scale factor of 70% with respect to their original dimension (width and height). the proposed method based just on GVF information achieves the best results demonstrating that the process of building seams by exploiting GVF more effectively preserves salient areas and hence removes less crucial pixels. A visual comparison reveals that the proposed approach with saliency based selection of GVF paths better preserve the main salient regions (areas with object). Future works can be devoted to include a blending method in order to obtain better visual results in joining adjacent image regions after seam removal.

REFERENCES

- [1]. Sebastiano battiato, and Giovanni maria ferinella, Giovanni Puglisi deniele rav, "saliency-based selection of gradient vector flow paths for content aware image resizing" IEEE transactions on image processing ,vol .23 No.5.may 2014
- [2]. S. Avidan and A. Shamir, "Seam carving for content-aware image resizing," *ACM Trans. Graph.*, vol. 26, no. 3, pp. 1–10, 2007.
- [3]. M. Rubinstein, A. Shamir, and S. Avidan, "Multi-operator media retargeting," *ACM Trans. Graph.*, vol. 28, no. 3, pp. 23:1–23:11, 2009.
- [4]. T. Cho, M. Butman, S. Avidan, and W. Freeman, "The patch transform and its applications to image editing," in *Proc. IEEE Int. Conf. CVPR*, Jun. 2008, pp. 1–8.
- [5]. R. Achanta and S. Ssstrunk, "Saliency detection for content-aware image resizing," in *Proc. 16th IEEE ICIP*, Nov. 2009, pp. 1001–1004.
- [6]. Y. Pritch, E. Kav-Venaki, and S. Peleg, "Shift—Map image editing," in *Proc. ICCV*, 2009, pp. 151–158.
- [7]. R. Gallea, E. Ardizzone, and R. Pirrone, "Real-time content-aware resizing using reduced linear model," in *Proc. 17th IEEE ICIP*, Sep. 2010, pp. 2813–2816.
- [8]. S. Battiato, G. M. Farinella, N. Grippaldi, and G. Puglisi, "Content based image resizing on mobile devices," in *Proc. Int. Conf. Comput. Vis. Theory Appl.*, 2012, pp. 87–90.
- [9]. S. Battiato, G. Farinella, G. Puglisi, and D. Ravi, "Content-aware image resizing with seam selection based on gradient vector flow," in *Proc. 19th IEEE ICIP*, Oct. 2012, pp. 2117–2120.
- [10]. H. Wu, Y.-S. Wang, K.-C. Feng, T.-T. Wong, T.-Y. Lee, and P.-A. Heng, "Resizing by symmetry-summarization," *ACM Trans. Graph.*, vol. 29, no. 6, pp. 159:1–159:9, 2010
- [11]. Y. Niu, F. Liu, X. Li, and M. Gleicher, "Image resizing via nonhomogeneous warping," *Multimedia Tools Appl.*, vol. 56, no.3 pp. 485–508, 2012.
- [12]. L. Itti and C. Koch, "A comparison of feature combination strategies for saliency-based visual attention," *Proc. SPIE*, vol. 3644, pp. 473–482, May 1999.

- [13]. C. Xu and L. Prince, "Snakes, shapes, and gradient vector flow," *IEEE Trans. Image Process.*, vol. 7, no. 3, pp. 359–369, Mar. 1998.
- [14]. R. Achanta, S. Hemami, F. Estrada, and S. Süsstrunk, "Frequency-tuned salient region detection," in *Proc. IEEE Int. Conf. CVPR*, Jun. 2009, pp. 1597–1604.
- [15]. Y. Fang, Z. Chen, W. Lin, and C.-W. Lin, "Saliency detection in the compressed domain for adaptive image retargeting," *IEEE Trans. Image Process.*, vol. 21, no. 9, pp. 3888–3901, Sep. 2012.
- [16]. J. K. Tsotsos, S. M. Culhane, W. Y. K. Wai, Y. Lai, N. Davis, and F. Nuflo, "Modeling visual attention via selective tuning," *Artif. Intell.*, vol. 78, nos. 1–2, pp. 507–545, 1995.
- [17]. L. Itti, C. Koch, and E. Niebur, "A model of saliency-based visual attention for rapid scene analysis," *IEEE Trans. Pattern Anal. Mach. Intell.*, vol. 20, no. 11, pp. 1254–1259, Nov. 1998.
- [18]. J. Han, K. N. Ngan, M. Li, and H.-J. Zhang, "Unsupervised extraction of visual attention objects in color images," *IEEE Trans. Circuits Syst. Video Technol.*, vol. 16, no. 1, pp. 141–145, Jan. 2006.
- [19]. O. Marques, L. M. Mayron, G. B. Borba, and H. R. Gamba, "On the potential of incorporating knowledge of human visual attention into CBIR systems," in *Proc. IEEE Int. Conf. Multimedia Expo*, Jul. 2006, pp. 773–776.
- [20]. K.-Y. Chang, T.-L. Liu, H.-T. Chen, and S.-H. Lai, "Fusing generic objectness and visual saliency for salient object detection," in *Proc. IEEE ICCV*, Nov. 2011, pp. 914–921.
- [21]. D. Walther, U. Rutishauser, C. Koch, and P. Perona, "On the usefulness of attention for object recognition," in *Proc. ECCV Workshop Attention Perform. Comput. Vis.*, 2004, pp. 96–103.
- [22]. C. Koch and S. Ullman, "Shifts in selective visual attention: Towards the underlying neural circuitry," *Human Neurobiol.*, vol. 4, no. 4, pp. 219–227, 1985.
- [23]. X. Hou and L. Zhang, "Saliency detection: A spectral residual approach," in *Proc. IEEE Conf. CVPR*, Jun. 2007, pp. 1–8.
- [24]. J. Harel, C. Koch, and P. Perona, "Graph-based visual saliency," in *Advances in Neural Information Processing Systems*, B. Schölkopf, J. Platt, and T. Hoffman, Eds. Cambridge, MA, USA: MIT Press, 2007.
- [25]. M. Rubinstein, A. Shamir, and S. Avidan, "Improved seam carving for video retargeting," *ACM Trans. Graph.*, vol. 27, no. 3, p. 16, 2008.
- [26]. T. Basha, Y. Moses, and S. Avidan, "Geometrically consistent stereo seam carving," in *Proc. IEEE ICCV*, Nov. 2011, pp. 1816–1823.
- [27]. S. Battiato, S. Curti, M. La Cascia, M. Tortora, and E. Scordato, "Depth map generation by image classification," *Proc. SPIE*, vol. 5302, pp. 95–104, Apr. 2004.

Evaluation of 3D segmentation methods based on a criterion of homogeneity

El Mostafa Rajaallah¹, Basma Sirbal¹, Mohcine Bouksim¹, El Hassan Essoufi¹,
Taoufiq Gadi¹

¹(Faculty of Science and Technology - Settat / University Hassan 1st, Morocco)

ABSTRACT: The majority of evaluation tools are based on a human criterion for evaluating the quality of 3D segmentation methods. An algorithm is considered efficient if it provides a better semantic segmentation as would a human being intuitively do. This evaluation is difficult to carry out because it remains dependent on the point of view of subjectivity that establishes the truth-ground and the fact that an individual may establish several semantic levels depending on the desired detail for segmentation. The metric proposed in this work evaluates the homogeneity of the faces components in the segments generated by segmentation methods, this metric is insensitive to human subjectivity and is interested in the final result of the segmentation, helps to analyze the segmentation algorithms and may also improve outcomes.

Keywords – Object 3D, Segmentation, Evaluation, homogeneity, Inertia

I. INTRODUCTION

3D segmentation is part of the classification methods (clustering), which is a mathematical tool of data analysis, in order to bring together several clusters so that the elements of a cluster are as much similar as possible and that the clusters are as much dissimilar as possible.

The evaluation of segmentation methods is very important in order to select the algorithm that works best on a specific type of data. It can also be used to analyze the results of segmentation algorithms so that they can be possibly improved.

The evaluation tools of segmentation methods can be classified into five groups (Zhang et al. 2008) [1], (Vandeborre 2012) [2]:

- a. Analytical methods have the disadvantage of focusing on the algorithm only (Principale, complexity ... etc.) And not the final result.
- b. Subjective methods, as their name tells, are dependent on human observers in each stage of the evaluation and can't be integrated into an automated system.
- c. Methods related to the user system segmentations that relies heavily on the latter and aren't generalizable.
- d. The unsupervised methods are those that depend on a defined criterion, and don't allow assessing quantitatively the segmentations.
- e. Finally, supervised methods, even if they are also dependent on human operators, they are the most represented (Martin et al., 2001) [3], (Unnikrishnan et al. 2007) [4], (Benhabiles et al., 2009) [5] because they are automated and they also provide a quantitative evaluation with a metric of comparison (calculation of the difference between truth-ground's segmentations and the segmentations obtained).

We can also include the methods based on a partial match (Moumoun et al. 2011) [6], that have a set of constraints and choices that must be made:

- ✓ Selection of a human segmentation for reference.
- ✓ The level of segmentation to use for each model.
- ✓ The choice of the shape descriptor.
- ✓ The matching algorithm.

Benhabiles and al. exposed in (Benhabiles and al. 2010) [7], a comparison study between the metric named 3DNPRI (3D Normalized Probabilistic Rand Index) and the different 3D mesh segmentation evaluation metrics. In this study, the authors stated that the 3DNPRI is better than the others in terms of features and discriminating power. The 3DNPRI belongs to the interval [-1,1], the better segmentation must have values neighboring to 1, whereas a value below zero indicates that the automatic segmentation is less expressive.

The approach proposed in our work is an automatic evaluation approach, which is a part of the empirical methods with quality. It's based on the level of homogeneity of the segments; this latter is based on the intra-classes inertia between segments (abbreviated Inertia Intra-segments).

This paper is organized as follows, first, we present the theoretical notion of Inertia intra-class, and then we will introduce our evaluation metric methods for 3D objects segmentation, the next part will be devoted to an experimental evaluation showing the performance of our metric over the 3DNPRI. Finally, a conclusion that discusses the potentials benefits and prospects of our work.

II. INTRA-CLASS INERTIA:

Definition 1:

We call inertia of a cloud $\Omega = \{\Omega_i, i = 1, \dots, n\}$ the weighted sum of the distances of the points to the center of gravity of the cloud. Therefore, if G is the center of gravity of Ω , the inertia of Ω is:

$$I = \sum_{i=1}^n w_i * d(\Omega_i, G)^2 \tag{1}$$

With w_i as $i = 1, \dots, n$ are the weights of Ω_i and G is the center of gravity of Ω .

For more theoretical details on this section, the reader can refer to the work of (Bisson 2001) [8].

Theorem 1:

For a partition of k classes with W_i weights.
 I_1, I_2, \dots, I_k are the associated inertia.
 The intra-class inertia of the partition is :

$$I = \sum_{i=1}^n W_i * I_i \tag{2}$$

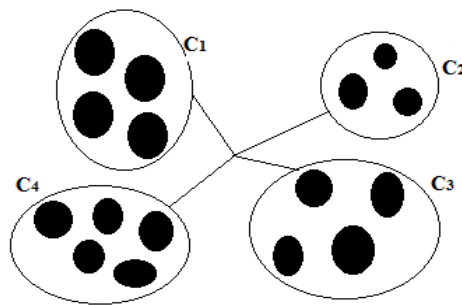


Fig. 1 : Example of clustering

Property 1:

The inertia of a cluster measures the concentration of the points of the cluster around the center of gravity. The more this inertia is low, the more the dispersion of the points around the center of gravity is lower.

Property 2:

A class is homogeneous if and only if its Intra-class inertia is low.

Property 3:

Comparing two partitions of k classes, the best is the one with the lowest inertia.

In the following we will outline our approach exploiting the properties of the intra-class inertia to evaluate the quality (homogeneity) of 3D object segmentation.

III. OUR EVALUATION APPROACH

In this section we detail our evaluation approach of segmentation based on the homogeneity measured by inertia intra-segments, the segmentation that has the lowest score is considered as homogeneous.

3.1. Construction of the point cloud

In our approach we consider that each segment is represented by a point cloud reflecting the coordinates of its faces. The coordinates of a face are its two principal curvatures k_1 and k_2 (Koenderink et al. 1992) [9], refer to Fig. 2.

The choice of the principal curvatures as coordinates for the faces is motivated by the fact that the homogeneity we seek reflects the shape of the faces that are parts of the segments.

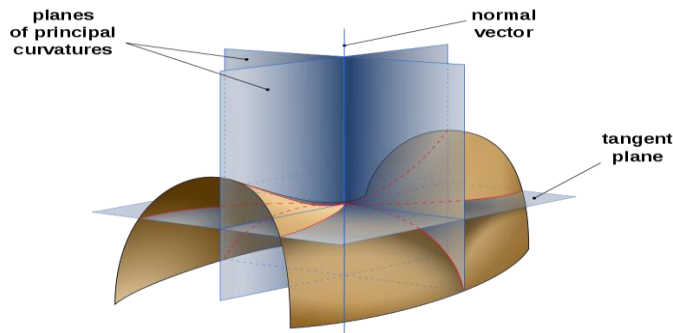


Fig. 2: principal curvatures on a surface

3.2. Estimated curvatures of a triangular mesh

The Approximation of the curvature of the faces of a triangular mesh is based on the vertices and adjacent faces. Chen and Schmitt (1992) [10], Taubin (1995) [11] & Dong and Wang (2005) [12] presented simple methods to estimate the principal curvatures of a face of a triangular mesh. We used circular arcs to approximate the curvature of a vertex by building a ring around it (Fig. 3), and then we estimate the curvature of the triangle based on the curvature of the three points that compose it.

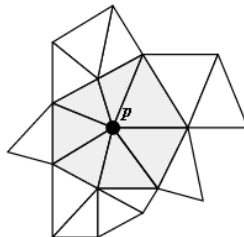


Fig. 3 : A point p and its neighborhood (a ring), composed of triangles of dark color

3.3. The face's weights

3.3.1. Categorization of faces

Based only on a local force of a face in a segment to define its weight has the disadvantage of ignoring the discriminatory power of this face, assume that the face belongs to a category of faces (refer to Table 1) which is not present in the other segments, so that this face should have a high weight in his segment.

Table 1: Categorization (Koenderink et al., 1992) of a 3D surface in function of the value of the shape index

Type of surface	Interval of shape index
Convex ellipsoid	$[0, 3/16]$
Convex cylinder	$]3/16, 5/16]$
Hyperboloid	$]5/16, 11/16]$
Concave cylinder	$]11/16, 13/16]$
Concave	$]13/16, 1]$

The shape index defined by:

$$SI = \frac{1}{2} - \frac{1}{\pi} \arctg\left(\frac{k_1 + k_2}{k_1 - k_2}\right) \quad (3)$$

With k_1 and k_2 being the principal curvatures of the surface.

Note: It is well known that the shape index is not defined for flat surfaces, where we have the equality $k_1 = k_2 = 0$.

3.3.2. Weighting function concept

In the information retrieval field a weighting function assigns each term "t" in a document "d" with a value "W". The weight of "t" is calculated on the basis of two criteria: The local force "LF" and its global force "GF" in a corpus.

$$W = F(LF(t, d), GF(t, CO)) \quad (4)$$

The local force of a term in a document $LF(t, d)$ measures the importance of the term in the document, while the global force $GF(t, CO)$ measures its importance in a corpus. A high value of LF must participate in the maximization of W , while a high value of GF must participate in the minimization of W .

To consider the discriminatory power of a term (Salton and McGill 1983) [13] propose to report the frequency of the term to the frequency of the documents containing that term. They used the relative frequency of term-document (term-document frequency TDF), calculated as follows:

$$W(i, j) = TDF[i, j] = \frac{\log(TF + 1)}{\log(DF + 1)} \quad (5)$$

With TF = Number of occurrences of the term "t_i" / number of terms of the document j.

DF = Number of documents containing the term 't' / total number of documents. (George GARDARI 1999) [14] presents more examples of the benefits of the proposition of (Salton and McGill 1983).

3.3.3. Weights of faces.

In our context we have faces and segments of a 3D mesh "M". The local force of a face "f" will be measured according to the local force of its belonging category. The local force of a category is calculated on the basis of the relative area of the faces in that category in its segment "Seg".

if " S_c " is the cumulated area of all surfaces of the faces of a category "C" that belongs to a segment "Seg" of an area S_{seg} , then the relative weight of a face "f" in "C" is the ratio: S_f / S_c , with S_f being the area of the face "f". The relative weight of the category "C" in "Seg" is: S_c / S_{seg} .

The relative weight of the face "f" in the segment "Seg" is:

$$FP = S_c / S_{seg} * S_f / S_c = S_f / S_{seg} \quad (6)$$

The local force of the face "f" in the segment "Seg" is:

$$LF = \log(FP + 1) \quad (7)$$

The global force of the face « f » is:

$$GF = \log(CP + 1) \quad (8)$$

With CP = The cumulated area of all segments containing the faces of the same category "C" of the face "f" / the total area of the mesh "M".

Therefore the weighting coefficient of the face "f" in the segment "Seg" is:

$$W(f, Seg) = \log(FP + 1) / \log(CP + 1) \quad (9)$$

3.4. Intra-segments inertia

3.4.1. Intra-segments inertia formulation

In our evaluation approach for segmentation methods, the segmentation that has the lowest score of the intra-segments inertia is considered the most homogeneous. Inertia intra-segments (our metric) of segmentation is defined by:

$$I = \sum_s W_s * I_s \quad (10)$$

With I_s being the inertia of segments "s" and W_s being weights of the segment defined by the relative areas of those segments according to the surface area of the object.

The inertia of the segment is defined by:

$$I_s = \sum_f W(f,s) * d(f,G_s)^2 \quad (11)$$

With G_s being the gravity center of the point cloud representing the segment.

3.4.2. The Tchebychev distance

The distance we have adopted in our approach is the Tchebychev distance, this measurement of the distance is appropriate, when we consider two objects as being "different" from the moment they are different in one dimension. Tchebychev distance is calculated as:

For two vectors $X = (x_1, x_1, \dots, x_n)$ and $Y = (y_1, y_2, \dots, y_n)$ of a vector space, the distance is defined by :

$$d(X,Y) = \max_{1 \leq i \leq n} |x_i - y_i| \quad (12)$$

IV. EXPERIMENTAL RESULTS Test database

The Benchmark "3D Segmentation Benchmark" proposed by [7], was created as part of the project "3D Models and Dynamic models Representation And Segmentation". The aim of this benchmark is to provide an automatic tool for the evaluation, analysis and comparison of automatic 3D mesh segmentation algorithms. In this work, we used this database to show the performance of our evaluation tool for 3D segmentation methods.

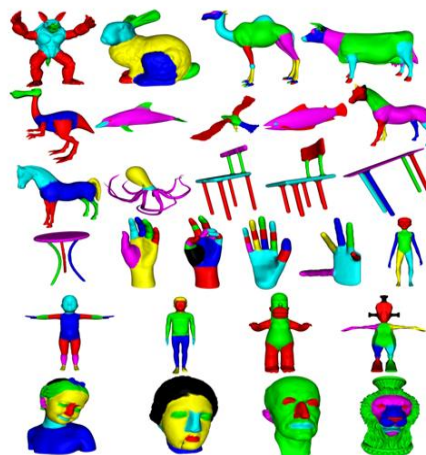


Fig. 4 : Models from the Benchmark

4.2. Performance obtained

To compare two segmentations, we must have the same number of segments, the most homogeneous is the one with the lowest inertia intra-segments I_w .

In our case, we have adopted the same number of segments recommended by the online evaluation tool of the metric 3DNPRI, the table below presents the objects of the Benchmark, which we used for our tests, with the adopted number of segments.

Table 2: number of segments for each object in the base

object	Number of segments	object	Number of segments
Alien	8	Fish	10
Armadillo	9	Hand1	7
Baby	14	Hand2	12
Bimba	13	Hand3	15
Boy	10	Hand4	6
Bunny	5	Homer	8
Camel	6	Horse1	9
Chair1	8	Horse2	7
Chair2	8	Maxplanck	7
Cow	7	Octopus	9
Dinopet	7	Robot	11
Dolphin	8	Table1	5
Eagle	7	Table2	4
Egea	9	Vaselion	7

Table 3 shows the performance of the inertia intra-segments by classes of objects (**Homogeneity is inversely proportional to the intra-segments inertia**), of two variants of the segmentation method based on spectral clustering technique (Rajaallah et al. 2014) [15], the first alternative is without surface information in the adjacency matrix for faces and the second variant is with surface information for details you can refer to the pages from 22 to 25 of [15].

Table 3 : Inertia Intra-segments for the classes of the test base

Method	Class	Animal	Bust	Furniture	Hand	Human
Spectral clustering 1		47,86	31,06	9,91	6,01	43,63
Spectral clustering 2		45,50	31,21 ₂	9,90	5,90	44,75

We can observe, in comparison with the results obtained by the 3DNPRI (refer to Table 4); there are three categories of results:

- For the classes "Animal" and "Bust" our metric has kept the same ranking given by the metric 3DNPRI for both of the tested methods: Regarding the class "Animal" the second method is ranked first, for the class "Bust" the first method is ranked first.
- For the class "Furniture", our metric recorded nearly equality between the two methods contrariwise the metric 3DNPRI that considered that the spectral Clustering 1 is the first.
- For the class "Hand", 3DNPRI recorded equality between the two methods, our metric archived nearly equality.
- Regarding the class "Human", our metric has ranked the first method in the first position contrariwise the metric 3DNPRI that considered that the second method is the first.

The table below shows the performance obtained by the 3DNPRI:

Table 4: Performance obtained by the 3DNPRI

Method	Class	Animal	Bust	Furniture	Hand	Human
Spectral clustering 1		0,50	0,15	0,78	0,57	0,51
Spectral clustering 2		0,53	0,14	0,70	0,57	0,58

Considering that our metric is interested in the quality of the segmentation, so our metric is able to detect the segmentations with semantic similarity, achieved nearly the same score of intra-segments inertia for the object "hand4" because both methods have been segmented almost in the same way (refer to Fig. 5).

Note: For the figures below, the Spectral Clustering 1 in the left.



Fig. 5: Intra-segments inertia of the object « hand4 »

Our metric recorded the same score (equal 10,2) of intra-segments inertia for the object "table2" from the class "Furniture" (refer to Fig. 6).

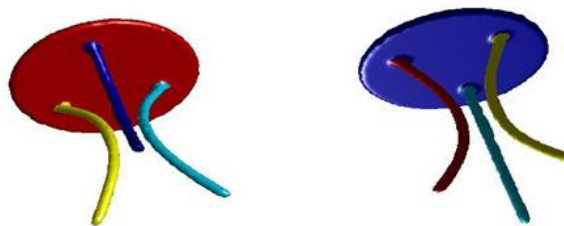


Fig. 6: Segmentation of the object « table2 »

To show the efficiency of our approach, the figure below shows three segmentations of the object "chair1" from the class "Furniture" with their inertia intra-segments scores. The segmentation above is the truth-ground plus two variants of spectral clustering segmentation down below.



Fig. 7: Inertia intra-segments for three variants of segmentations

The scores of our metric, show its efficiency and its high sensitivity to the homogeneity of the segments that compose a 3D object; we can see that the two segmentations below have very similar scores reflecting very neighboring segmentation logic. Concerning the truth-ground of the object "chair1" the score obtained distinguishes the quality of this segmentation with an excellent uniformity of the segmentation.

For the class "Human", our metric gave the first position to "Spectral Clustering 1", Table 5 present the scores obtained for the objects of this class.

Table 5: Intra-segments Inertia for objects of the class « Human »

Object	Method	Spectral clustering 1	Spectral clustering 2
alien		181,0000	187,0000
baby		0,1720	0,1670
boy		9,6900	9,3200
homer		19,3000	19,0000
robot		8,0100	8,2500

The score for the subject "alien" is very large compared to the scores of other objects of the class "Human" , with a difference of "6" between the two methods, this is due to the quality of homogeneity of segments in the segmentation of the object (refer to Fig. 8), where we can find that the chest, arms, forearms and most of the head in the same segment, also for the "Spectral Clustering 2" method we have the hand in the same segment, the last method separated one ear of the "alien" from head.



Fig. 8: Segmentation of the object « alien »

The "Spectral Clustering 1" method separated the left hand of "alien" from the forearm, which participated in the score obtained by this method, because the hand contains much more undulations than the ear, we can conclude that the metric proposed in this work is capable of indicating the heterogeneity of segmentation.

V. CONCLUSION

It is important to evaluate the segmentation methods for several reasons: first we can classify the segmentation methods, distinguish the method that gives the best results, and then analyze the results of the methods to possibly improve it.

The evaluation metric proposed in this work is one of the empirical tools with quality, that judge the quality of segmentations obtained according to a predefined criterion and is interested in the final result of the segmentation. It guarantees an independent quantitative assessment of the individuality of human segmentations that may change from one person to another. The proposed metric is able to recognize and indicate the best segmentation among other segmentations of the same object.

As prospects of this work, we will work on improving the proposed metric so that it can compare segmentations that don't have the same number of segments.

REFERENCES

- [1] H. Zhang, J. E. Fritts, and A. Sally. Goldman, Image segmentation evaluation: A survey of unsupervised methods, *Computer Vision and Image Understanding*, 2008, 110 :260–280.
- [2] J-P Vandeborre, Contributions to the research and analysis of 3D models, *Computer Vision and Pattern Recognition*. University of Science and Technology of Lille - Lille I, France, 2012. <tel-00834372>.
- [3] D. Martin, C. Fowlkes, D. Tal and J. Malik, A database of human segmented natural images and its application to evaluating algorithms and measuring ecological statistics, *International Conference in Computer Vision 2*, 2001, 416–423.
- [4] R. Unnikrishnan, C. Pantofaru, et M. Hebert, Toward objective evaluation of image segmentation algorithms, *IEEE Transaction on pattern analysis and machine intelligence*, 29(6), 2007, 929–944.
- [5] H. Benhabiles, G. Lavoué and J.P. Vandeborre, A new similarity metric for 3D mesh segmentation evaluation using a corpus of truth-ground, *AFIG 22*, Arles (France), 2009.
- [6] L. Moumoun, M. Chahhou, M. El Far, T. Gadi and R. Benslimane, Indexing of 3D objects based on partial analogy of segments, *Review of Mediterranean Telecommunications (RMT)*, vol. 2, July 2011, 93-98.
- [7] H. Benhabiles, J. P. Vandeborre, G. Lavoué and M. Daoudi, A comparative study of existing metrics for 3D-mesh segmentation evaluation, *Visual Computer International Journal of Computer Graphics, Springer Editions*, vol. 26(12), December 2010, 1451-1466.
- [8] G. Bisson, Catégorisation et textes, *Atelier Applications, Apprentissage et Acquisition de Connaissances à partir de Textes électroniques (A3CTE)*, University Paris1. 28 June 2001.
- [9] J. Koenderink et J. V. D. Andrea. Surface shape and curvature scales. *Image and Vision Computing*, vol. 10, no. 8, October 1992, 557-564.
- [10] X. Chen and F. Schmitt, Intrinsic surface properties from surface triangulation, *ENT*, Paris (France), (1992).
- [11] G. Taubin., Surface from a Polyhedral Approximation, *the Fifth International Conference on Computer Vision*, 199, 902-907.
- [12] D. Chen-shi and W. Guo-zhao, Curvature estimation on triangular mesh. *Journal of Zhejiang University SCIENCE*, 2005, 6A(Suppl. D):128-136.
- [13] G. Salton and M. McGill, Introduction to Modern Information Retrieval, *New-York, Mcgraw-Hill*, 1983.
- [14] G. GARDARIN, Internet / intranet et bases de données, *Edition Eyrolles*, 1999, 89-90, ISBN 2-212-09069-2.
- [15] E. Rajaallah, O. Herouane, L. Moumoun and T. Gadi, 3D Segmentation by spectral clustering using shape index, *Journal of Computer Science and Information Technology (American Research Institute for Policy Development)*, Vol. 02, NO. 3 & 4, December 2014, 15-33.

Problem of calculating time delay between pulse arrivals

Olugboji Oluwafemi Ayodeji.¹, Jiya Jonathan Yisa.²
Ajani Clement Kehinde³

Mechanical Engineering Department, Federal University of Technology, P.M. B. 65, Minna, Niger State.
NIGERIA.

ABSTRACT: This work compares the performance of four different methods of estimating the time delay between pulse arrivals at the sensors subjected to different levels of attenuation, distortion and noise. The accuracy of the calculated time between the pulse arrivals at the sensors is determined and analysed for each of the methods based on the ideal attenuation (no change in shape), ideal attenuation with added noise to the pulse signal and ideal attenuation but with distortion. Based on the analysis carried out, it is clear the cross correlation method gives the best estimate of the delay in pulse arrival times irrespective of the signal to noise ratio and so is the preferred technique used in the remainder of this research.

KEYWORDS: attenuation, pulse, signal, distortion, correlation

I. INTRODUCTION

When calculating the location of an event, the ability to accurately determine the time delay ($t_2 - t_1$) between the arrivals of a pulse at the sensors is very important. During the propagation of the pulse due to an event as shown in Figure 1, the shapes and amplitudes of the pulse signals at the sensors are different due to distortion, frequency dependent attenuation and noise. If sensor 1 is closer to the event, the pulse travelling to it suffers less propagation loss than does that travelling to sensor 2, and therefore has a larger amplitude and higher signal to noise ratio, and is also less distorted. This effect of distortion, frequency dependent attenuation and noise on the pulse shape introduces uncertainty in the measurement of the time of arrivals and hence in the estimation of the time delay between arrivals, thus resulting in uncertainty in the location of the event site.

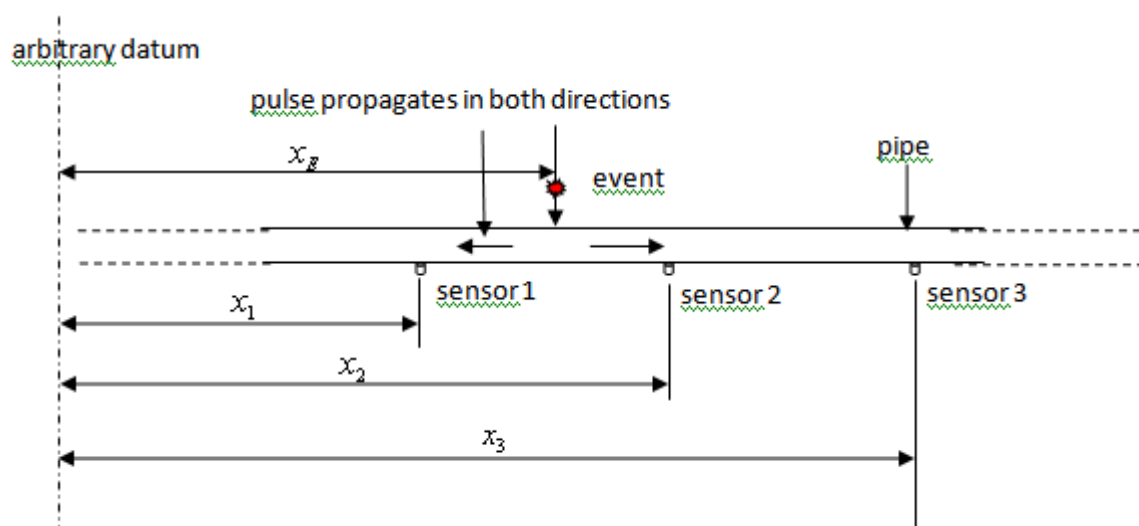


Figure 1 Schematic representation of sensors on a pipeline

Attenuation

As the pulse propagates along the pipeline, its intensity diminishes with distance. The amplitude of the pulse is reduced by the spreading of the pulse. Further weakening of the pulse results from scattering, which is the reflection of the pulse in directions other than the direction of propagation. Attenuation is the decay rate of the pulse as it propagates along the pipeline and is normally exponential. The amplitude change of the decaying pulse can be expressed as;

$$A = A_0 e^{-\beta x} \quad (1)$$

In this expression A_0 is the unattenuated amplitude of the propagated pulse at some location. The amplitude A is the reduced amplitude after the pulse has travelled a distance x from that initial location. The quantity β is the attenuation coefficient of the pulse travelling in the x -direction. This value of the attenuation is generally proportional to the square of frequency [1] and it can be obtained experimentally.

1.1 Dispersion

Dispersion is a phenomenon caused by the frequency dependence of velocity of the pulse. As the pulse propagates, the phase relation between the spectral components of the pulse varies with distance and hence the pulse shape becomes progressively distorted, generally widening as the propagation distance increases.

A pulse normally comprises a range of different frequencies. The pulse as a whole propagates at the “group velocity”, whereas each frequency component propagates within the pulse at its own “phase velocity”. This, coupled with the frequency dependent attenuation, can cause the pulse shape to change considerably with long distances.

II. METHODS OF CALCULATING TIME DELAY BETWEEN PULSE ARRIVALS

The four methods of estimating the time delay in arrivals between the pulse as considered by this research are:

- (i) peak detection
- (ii) threshold crossing
- (iii) cross correlation
- (iv) pulse centroid

2.1 Peak Detection

This process involves locating the position of the highest peak of the pulse signals at the sensors. Consider the pulse propagating along the pipeline as illustrated in Figure 1; the generated pulse propagates in both directions of the pipeline arriving first at sensor 1 then later after some time at sensor 2. Figure 2 shows the arrival of an idealised pulse at sensors 1 and 2. The true arrival times are the points where the signals first leave the zero level and the measured arrival times are the points of highest magnitude. If the pulses are the same shape, i.e. there is no distortion during the propagation, then the delay (d_1 and d_2) between the measured and true time of arrivals of the pulse signals at the sensors are the same and the calculated time delay is correct but the distortion of the pulse will introduce error in the calculation.

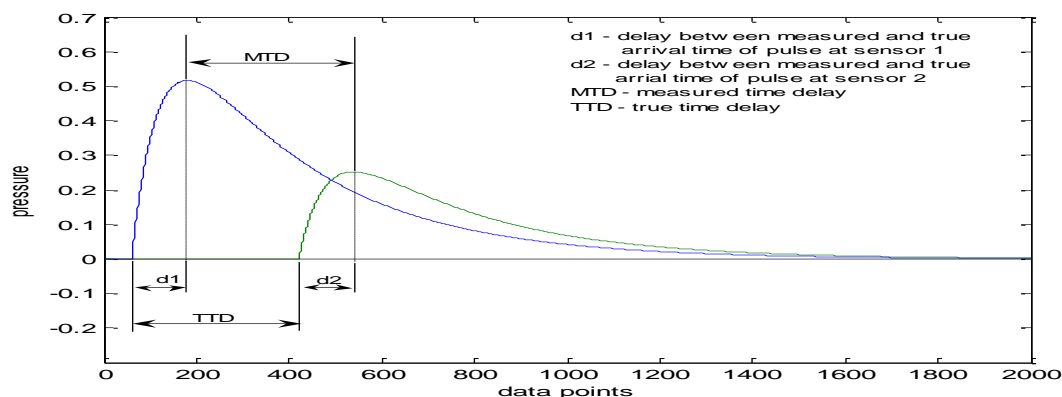


Figure 2 Pulse arrival time measurements by peak detection

Figure 3 shows the effect of noise on the estimate of the time delay by peak detection. The addition of noise to the otherwise undistorted pulse signals at the sensors results in the blurring of the peaks which makes it uncertain where the highest instantaneous peak value will occur. The horizontal lines within the envelope bounding the noisy signals give the range of possible measured peaks since the highest measured data points must lie on or above these lines. These are shown expanded in Figures 4a and 4b. If the noise level is the same at both sensors as shown, then the amount of uncertainty at sensor 2 is greater because the smaller signal has a lower signal to noise ratio. This uncertainty in the measured arrival times of the pulse signals results in uncertainty in the estimate of the time delay and hence in the estimate of the location of the event site.

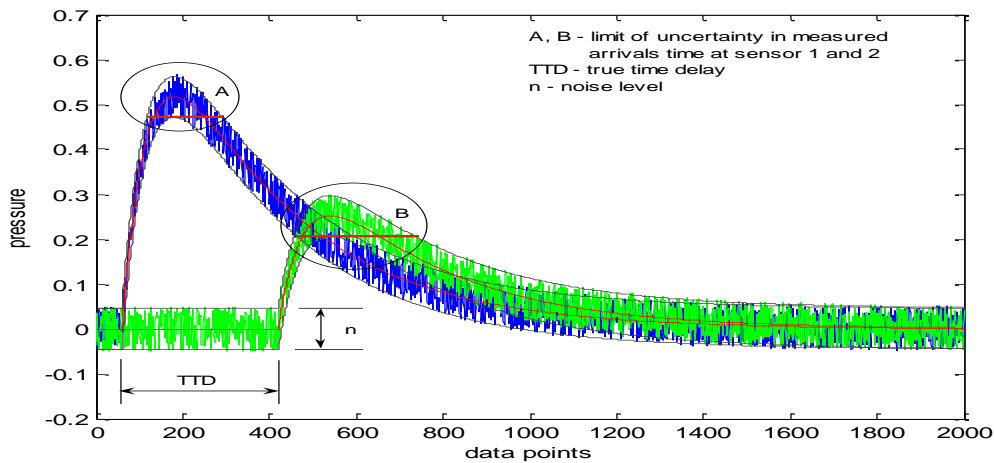


Figure 3 Effect of noise on pulse arrival time by peak detection

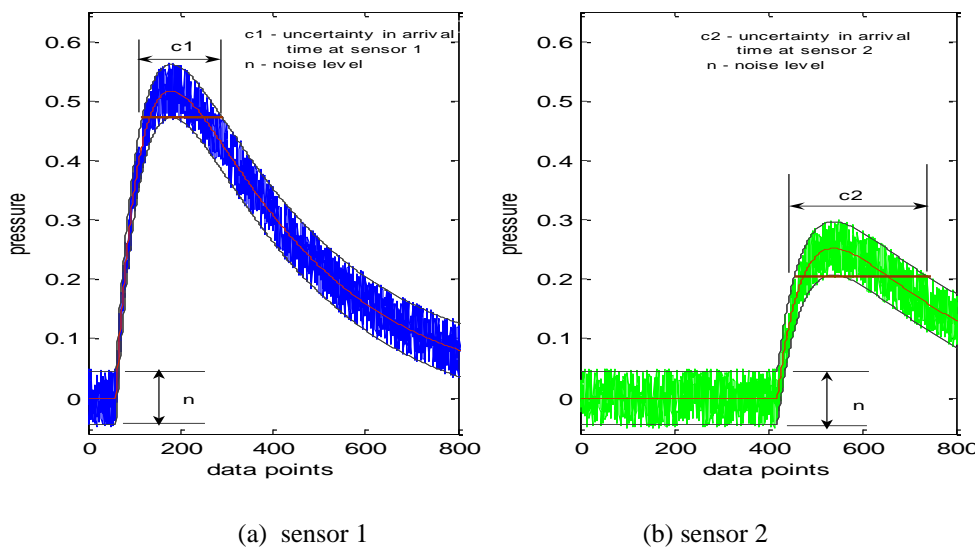


Figure 4 Showing detailed section of limit of uncertainty (c1 and c2) in arrivals time by peak detection at the sensors with the same level of noise (n)

Figure 5 shows the effect of distortion on the estimate in time delay in arrivals between the pulse signals by peak detection. The shape of the pulse signal at sensor 2 indicates that the high frequency components of the pulse responsible for the sharp pulse rise have attenuated in the course of pulse propagation, resulting in the peak of the pulse arriving late. With the pulse signal at sensor 2 distorted, the delay (d2) between the measured and true arrival times at this sensor is greater than the delay (d1) at sensor 1. The difference in estimate of the time delay of the measured and true arrivals between the pulse signals is large in this case, but it could be small if the distortion happened to leave the maximum point in the same place. This suggests that the error obtained in the estimate of the time delay in arrivals will depend on the form and amount of distortion encountered by the pulse during propagation.

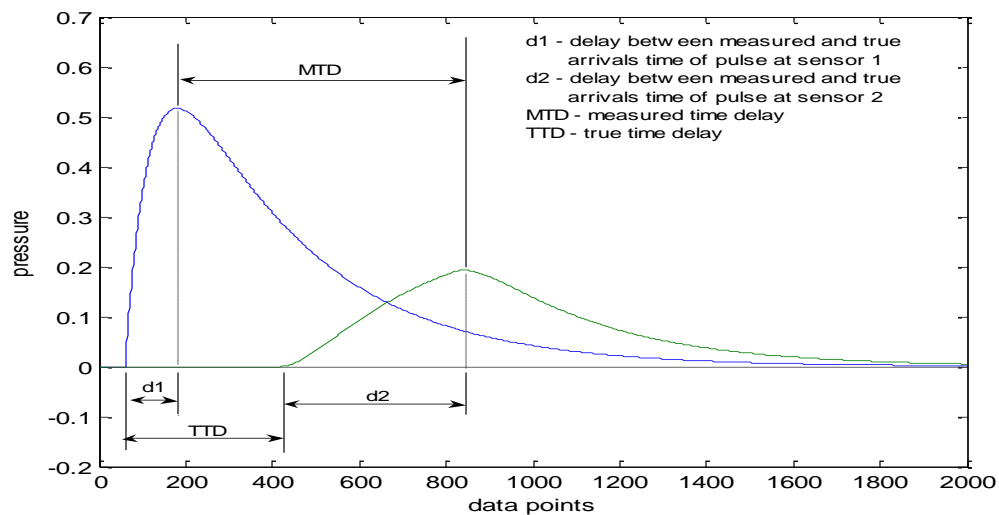


Figure 5 Effect of distortion on pulse arrival time by peak detection

2.2 Threshold Crossing

The threshold crossing method is another simple technique for calculating the time delay in arrivals using estimates of the arrival times [2]. The time of arrival is taken as the time when the pulse first crosses a predetermined threshold level as shown in Figure 6. For this case where the pulse is attenuated but undistorted, the delay (d_1 and d_2) between the measured and true arrival times of the pulse signals are quite different and the estimate of the time delay is overestimated.

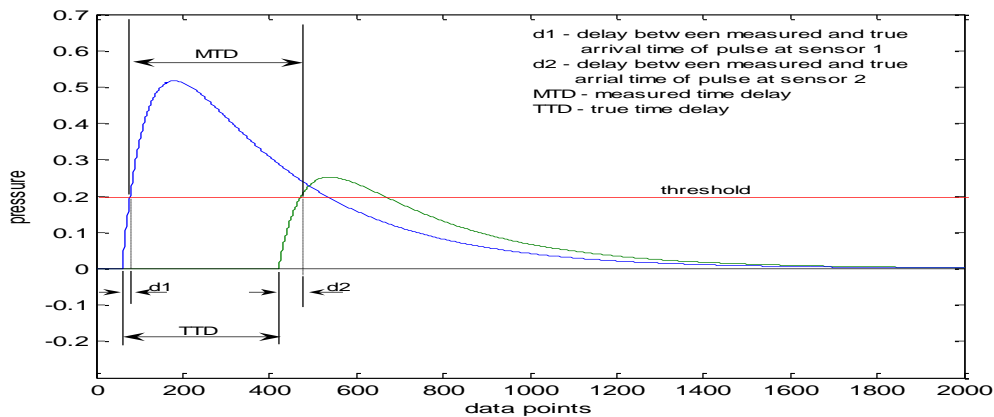


Figure 6 Pulse arrival time measurements by threshold crossing

A practical limitation in the use of the threshold crossing method is shown in Figure 6 where setting of the threshold level too high (above 0.27, the highest peak of the pulse at sensor 2) would result in non-detection of the pulse at sensor 2, making it impossible for the estimate in the time delay to be determined. This requires some advance knowledge of pulse height and limits the smallest pulse that can be detected in the presence of noise. To ensure large signals, sensors therefore need to be spaced relatively closely along the pipeline thus making this process of damage detection expensive.

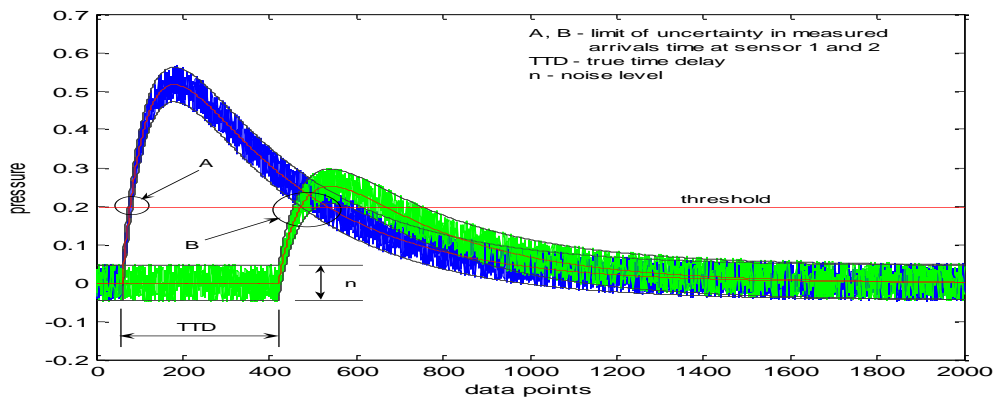


Figure 7 Effect of noise on pulse arrival time by threshold crossing

Figure 7 shows the effect of noise on the estimation of the time delay in arrivals between the pulse signals based on the threshold crossing. The region of the threshold crossings are shown expanded in Figure 8.

Figures 8a and 8b shows how the uncertainty in the arrivals time measurements of the pulse signals at the sensors are determined. The slope θ of the true pulse signals at the threshold crossing level is taken as the underlying slope of the noisy pulse signals. The noise level n is measured near to the pulse and is assumed to be approximately constant over the short period of the pulse. The uncertainty of the arrival time, obtained from the first threshold crossing of the pulse signal at sensor 2 is thus given by equation 2;

$$c_2 = \frac{n}{\tan \theta_2} \tag{2}$$

Similarly, the uncertainty in the arrival time at sensor 1 is given by equation 3;

$$c_1 = \frac{n}{\tan \theta_1} \tag{3}$$

The values of c_1 and c_2 give the uncertainty in arrival times at sensors 1 and 2, respectively.

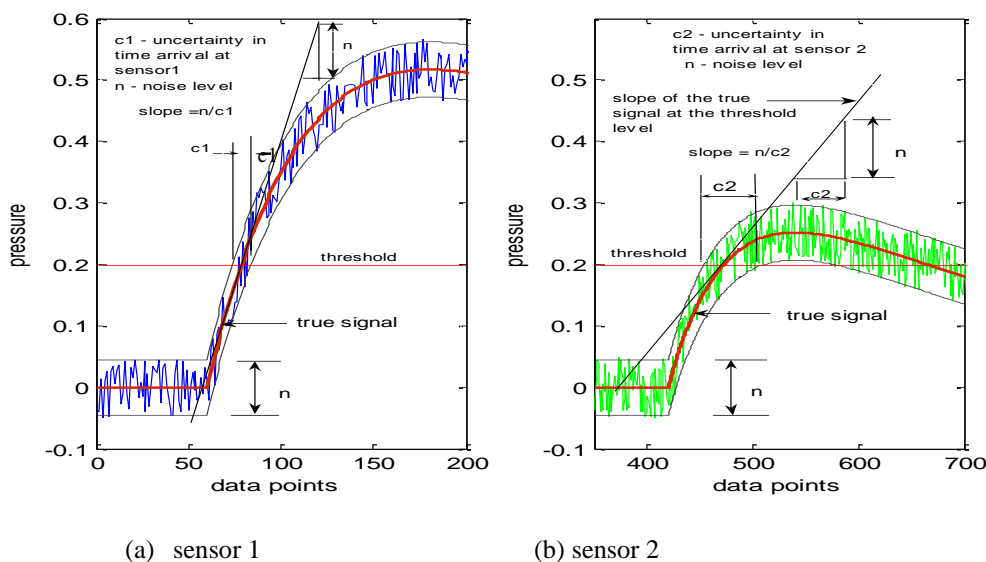


Figure 8 Showing detailed limit of uncertainty in the measured arrivals time by the threshold crossing.

The calculated uncertainty of the pulse at sensor 1 which has a steep slope is smaller than that of the pulse at sensor 2 having a less steep slope at the threshold crossing. This clearly shows that as the pulse propagates farther away from the event site, the uncertainty in measurements of arrival times of the pulse increases. Thus, the estimate of the time delay between the measured and true arrivals will be significantly large using the threshold crossing when the signal to noise ratio is small.

Setting of the threshold level is also an important task in the use of this method with the presence of noise. Although, setting the threshold level reduces uncertainty in the time of arrival measurement, it presents the inconvenience of a high probability of false alarm. It causes the background noise to cross the threshold, resulting in a great deal of unwanted data being recorded. On the other hand, a high threshold level result in greater uncertainty but reduced probability of false alarms due to noise.

Figure 9 shows the effect of distortion due to frequency dependent attenuation on time delay estimate by the threshold crossing method. In this case, there is a large difference in the delay (d1 and d2) between the true and measured arrival times; hence there will be a large error in the calculated time between arrivals. This also suggests that the magnitude and form of the distortion determines the size of the error in the calculated time delay using this method.

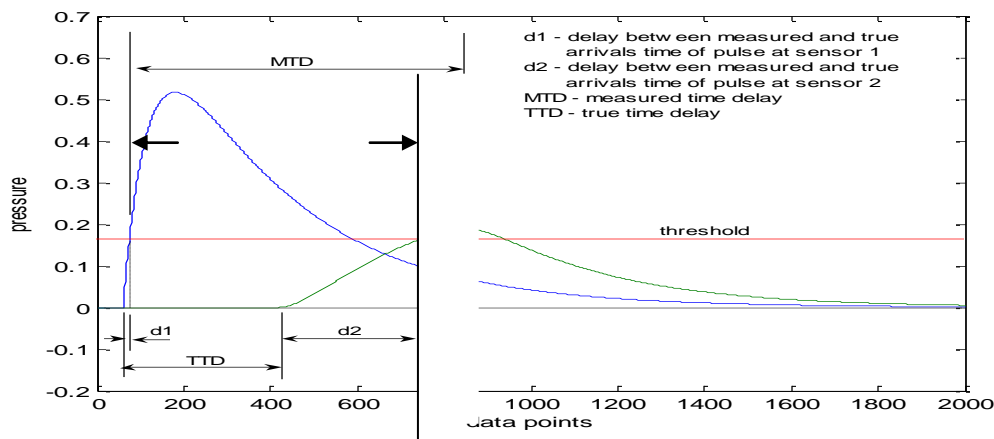


Figure 9 Effect of distortion on pulse arrival time by threshold crossing

2.3 Cross Correlation

Cross-correlation is a method used to determine the similarities between two signals as a function of a time lag applied to one of the signals [3]. The cross correlation $CC_{x_1x_2}(\tau)$ of two signals, $x_1(t)$ and $x_2(t)$ is given by equation 3;

$$CC_{x_1x_2}(\tau) = \int_{-\infty}^{\infty} x_1(t)x_2(t + \tau)dt \tag{4}$$

Similarly, for discrete-time signals, this equation is written as in equation 5;

$$CC_{x_1x_2}(m) = \frac{1}{N} \sum_{i=0}^{N-1} x_1(i)x_2(i - m) \tag{5}$$

The process of cross correlation of the pulse signals involves movement of the propagating pulse signal at sensor 2 along the time axis by a small time increment and looking at the similarities it has with the pulse signal at sensor 1. By calculating the cross correlation function of the sensor signals a measure of the time delay is obtained from the position of the maximum peak of the cross correlation function as illustrated in Figures 10a and 10b. Figure 10b shows the cross correlation function with a clear peak indicating the location of the maximum best fit between the two pulses in Figure 10a. An advantage of using this method is that it does not require measurements of the time of arrivals of the pulse signals at the sensors in order to calculate the time delay, but rather gives the delay directly.

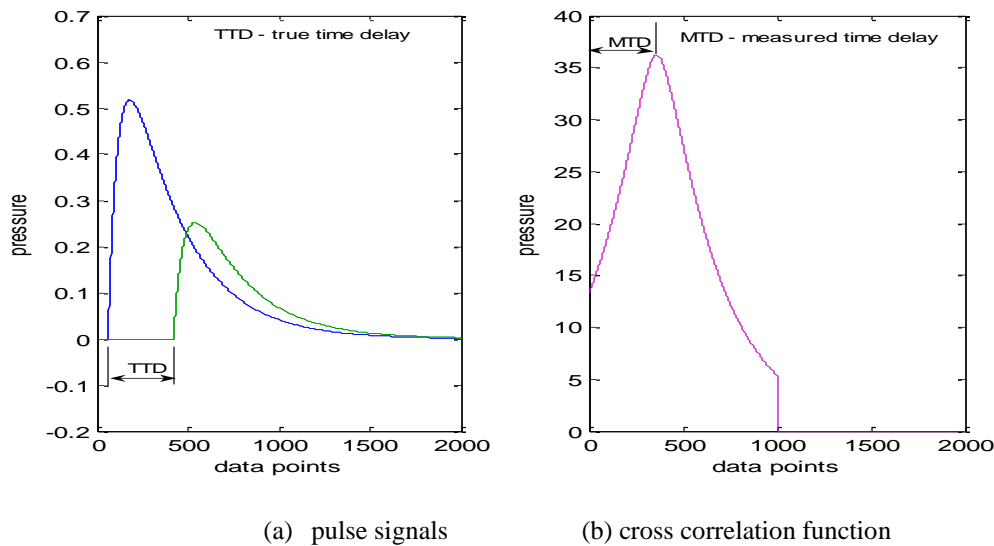


Figure 10 Pulse time delay estimation by cross correlation

Figure 11 shows the cross correlation of the pulse signals with the addition of noise. It can be seen that even with the addition of noise to the pulse, performing a correlation between the pulse signals still gives a good estimate of the measured time delay in arrivals of the pulse signals. This is attributable to the cross correlation method acting as an integrator (equation 5) which averages the random noise present in the pulse signals.

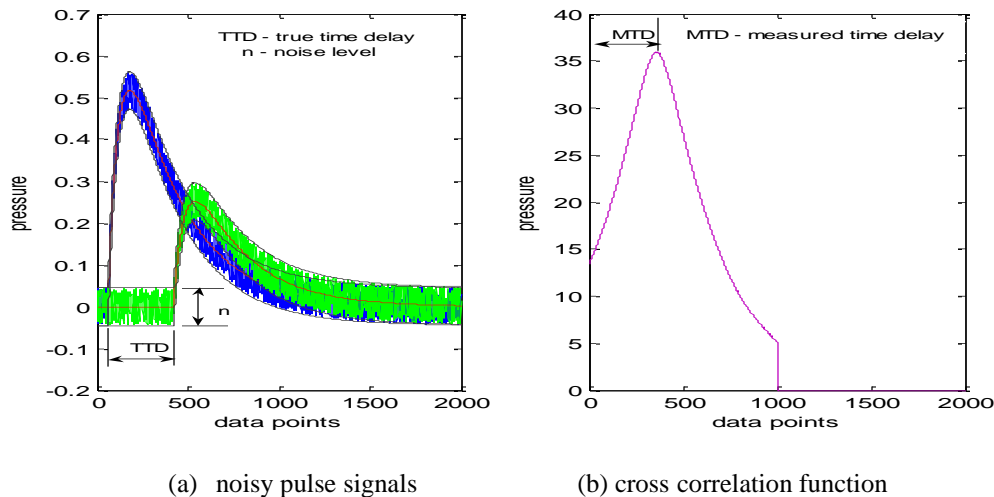
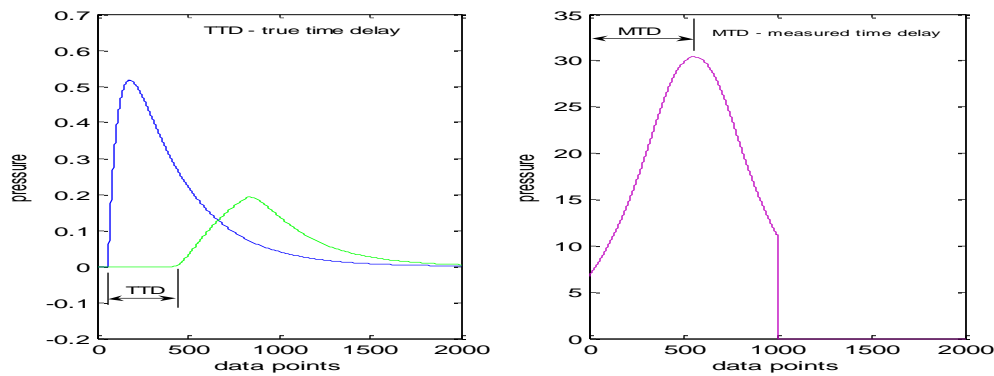


Figure 11 Effect of noise on pulse time delay estimation by cross correlation

Figure 12 shows the effect of distortion on the time delay measurement by cross correlation. There is some error using this method, though not as much as the uncertainty in the peak detection and threshold crossing methods. The magnitude of the cross correlated peak is lower due to the poorer fit and the size of the error will depend the size and form of the distortion in each application.



(a) distorted and undistorted signals

(b) cross correlation function

Figure 12 Effect of distortion on pulse time delay estimation by cross correlation

Figure 12 shows the unfiltered and filter pulse signals at the sensors and Figure 12 shows their cross correlation.

2.4 Pulse Centroid

Another way to measure between pulse arrivals is by the use of a centroid timing technique. The centroid of a pulse is its geometrical centre. For complicated shapes such as experimentally measured pulses the centroid can be found by numerical integration.

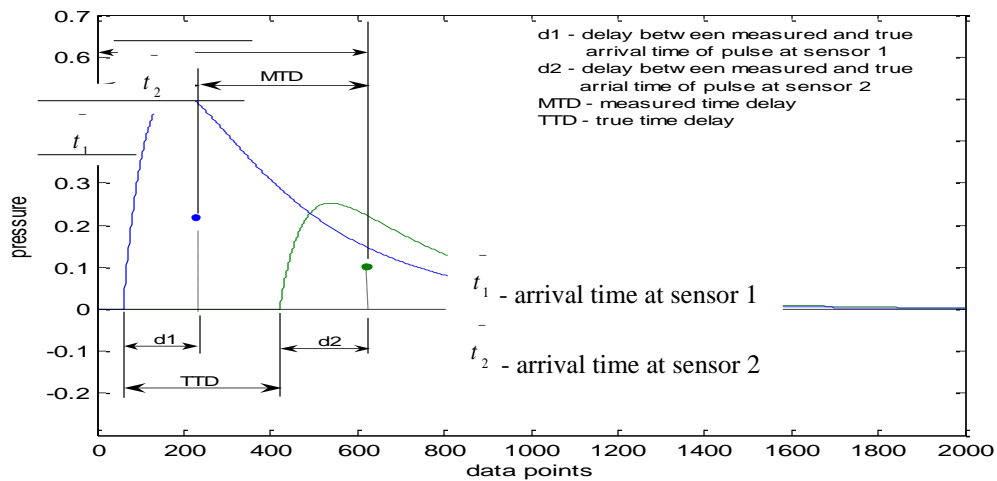


Figure 13 Pulse arrival time by use of centroid

Figure 13 shows how the centroid of the pulse signals is used in estimating the time delay between the pulse signals. The centroid of each pulse signal is determined by equation 6 using numerical integration;

$$t = \frac{\int_0^L t_i q(t_i) dt}{\int_0^L q(t_i) dt} \tag{6}$$

where L is the length of the pulse, t_i and t are both measured from the same datum.

The delay is difference between the calculated values of t .

Considering Figure 13, the two pulse signals shown only differ in magnitude with no noise or distortion on them. The positions of the centroids from the start of the pulses (d_1 and d_2) are the same and so there is no error in the calculated delay.

Figure 14 shows the pulses with added noise on which the method of centroids was tried. The noise on the pulse signals makes it impossible to determine the exact limits of integration to be taken and this affects computation of the centroid. Hence, it is not possible to determine the delay by the centroid method.

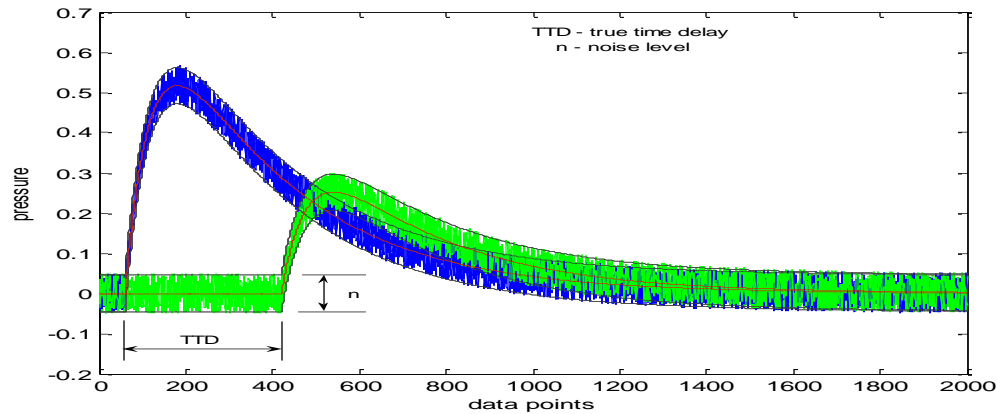


Figure 14 Effect of noise on pulse arrival time by centroid

Figure 15 shows the effect of distortion on the estimate of the time delay in arrivals by the use of centroid. It can be seen that the difference in delay (d_1 and d_2) between the measured and true arrivals time are different. This indicates that when pulse signals are distorted there will be errors in the estimate of the time delay.

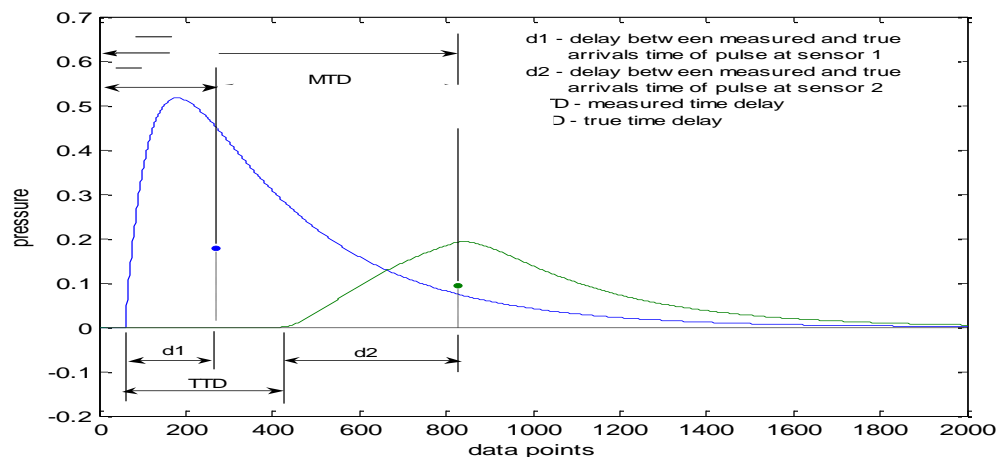


Figure 15 Effect of distortion on pulse arrival time by centroid

III. RESULTS

Test for Effectiveness of the Methods using Experimental Pressure Pulse Signals

To test for the effectiveness of these methods in estimating the time delay between arrivals of the pulse signals, sensor signals from a true pressure pulse obtained in an experimental work were used. These signals, shown in Figure 16, were analysed using a program written in Matlab programming language to measure the time delay using the peak detection, threshold crossing and cross correlation methods. The centroid is not used for the reasons given above.

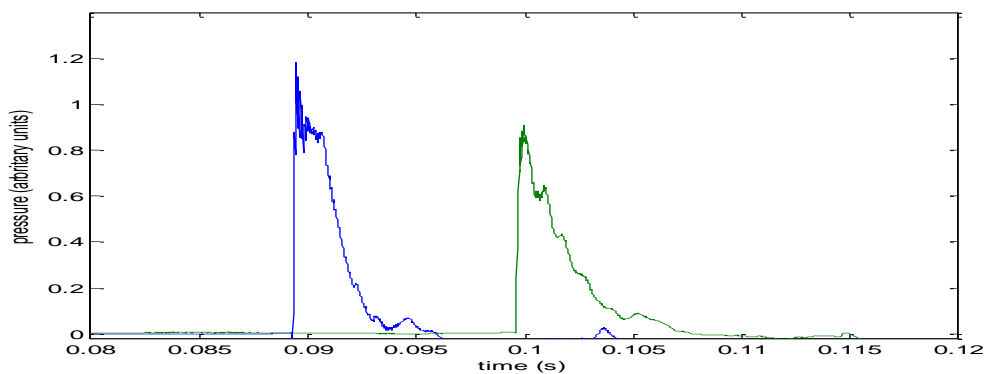


Figure 16 True pressure pulse signal from experiment

Considering Figure 16, the true time delay between the starting points of the two pulses is 0.0104s. The delay calculated using the peak detection method was 0.0105 s; both the cross correlation and threshold crossing methods gave 0.0103s.

The effect of noise was investigated by adding a random number to each data point of the experimental signals. Ten repetitions at various noise levels were carried out for each of the three methods and the spread of values of the calculated delay determined and plotted against noise level in Figure 17. The noise level is measured in the same arbitrary units as the pulse pressure, so that the maximum noise level (0.3 units) is approximately one third of the magnitude of the smaller pulse.

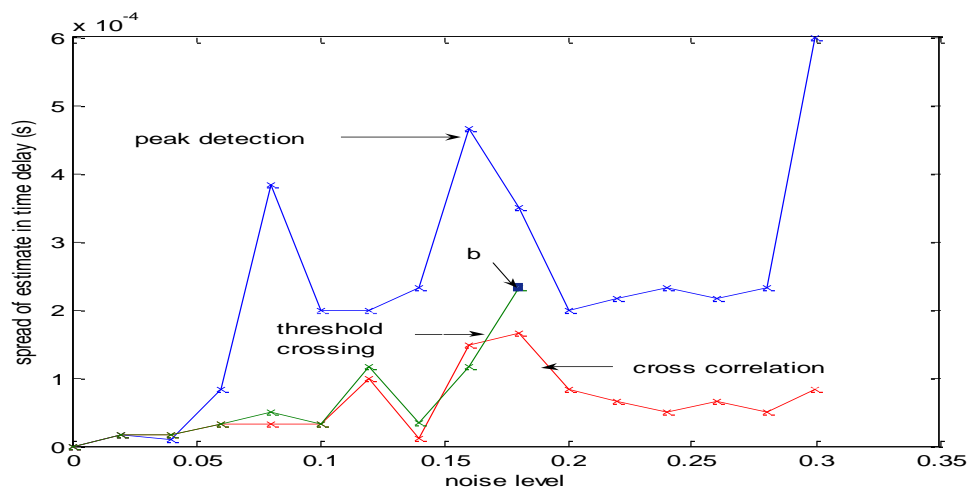


Figure 17 Graph of spread in time delay against increasing noise level

At low noise levels below 0.05 units (5% of the magnitude of the smaller pulse) the three techniques give very similar results with very small spread (<0.02 ms). At higher noise levels the peak detection method became progressively less reliable than the threshold crossing and cross correlation methods, though it should be noted that even at the highest noise level investigated the spread of results was only 0.6ms, or $<6\%$ of the true value. Up to a noise level of 0.18 the threshold crossing and cross correlation methods gave similar results, with spread of results below 0.16ms (1.5% of the true value). Above a noise level of 0.18 (position "b" in Figure 17) the threshold crossing method could not be used reliably, but the cross correlation method continued to give similarly reliable results up to the maximum noise level investigated.

IV. DISCUSSION OF RESULTS

Four methods have been presented to measure the time delay in arrivals between pulse signals.

The peak detection method uses the measured time between pulse arrivals, defined as the time of the highest peak values. When noise and distortion are not present, this method works well and is accurate. Noise causes blurring of the peaks of the pulse and therefore introduces uncertainty.

The threshold crossing method uses arrival times in the same way, but in this case defined as the time where the signal first crosses a threshold level. This method, though simple, resulted in overestimation of the time delay. The threshold method is effective at high signal to noise ratios but becomes unreliable in higher noise and becomes unusable when the noise level approaches the size of the smaller pulse.

The cross correlation method estimated the time delay directly without the need for measuring the arrival times. The method is effective even in the presence of high noise. The only disadvantage is that it requires much more computation time than the other methods, but this is not significant with today's modern computers.

The use of the pulse centroid estimated the time delay effectively for pulse signals of similarly shapes but results in errors when the pulse signals are distorted and could not be used in the presence of significant noise because of the difficulty of determining the limits of the pulses.

V. CONCLUSION

Based on the foregoing analysis, it is clear the cross correlation method gives the best estimate of the delay in pulse arrival times irrespective of the signal to noise ratio and so is the preferred technique used in the remainder of this research.

REFERENCES

- [1] Cao, C.F., Baik, S., Choi, J.B. and Kim, Y.J., "Protection of Underground Gas Pipelines from Third Party Damage by On-Line Monitoring Using Piezoelectric Accelerometers," Proc. of the Institution of Mechanical Engineers, Part E, J. Process Mechanical Engineering, 221, pp. 61 – 67.
- [2] Walker, J. F., 1971, "Performance Data for a Double-Threshold Detection Radar", IEEE Transactions on Aerospace and Electronic System, 7(1), pp. 142 - 146.
- [3] Sung, P. J., Chan, Y.C., Jin, H.N., Si-Hyung, L., Donghoon, S. and Tae-Yong, C., 2010, "Numerical Study of Leakage Detection and Location in a Simple Gas pipeline branch using an Array of Pressure Sensors," J. Mechanical Sci. and Tech., 24(24), pp. 983 – 990.
- [4] Steven, W. S., 1997, "The Scientific and Engineer's Guide to Digital Signal Processing," California Technical Publishing.

Non-Auditory Health Hazard Vulnerability to Noise Pollution: Assessing Public Awareness Gap

Tanjir Ahmed¹, Taimur Rahman²

¹ Department of Civil Engineering, Ahsanullah University of Science and Technology, Bangladesh

² Department of Civil Engineering, Ahsanullah University of Science and Technology, Bangladesh

ABSTRACT: *In Dhaka, one of the top ten megacities in Asia and the capital of Bangladesh, the problem of noise related pollution is prevalent. In almost every part of Dhaka city, the levels of noise which are established by W.H.O. are regularly exceeded, thus prompting adverse health effects on its inhabitants. This sort of pollution is more acute in central portion of Dhaka than its periphery. Therefore, if the greater Dhaka is taken as a study area, the central's problem may be underestimated. This study is prepared to find out the actual condition of auditory and non-auditory health effect of noise among roadside people and provide recommendation to ameliorate the same and consequently reduce noise level in Dhaka city as an effort to make Dhaka a better place to live in. The result shows that both auditory and non-auditory effects of noise are at alarming condition in all zones of the city.*

KEYWORDS: *Dhaka, Decibel, Health hazard, Noise, Pollution*

1. INTRODUCTION

Noise, an important element of environment and also undoubtedly a source of atmospheric pollution. Noise is a part of daily life although when surpassed the acceptable limit, becomes pollution. Dhaka, the capital of Bangladesh, is one of the most atmospheric polluted cities in the world. In spite of epic adverse health effect of such pollution, there is less work done for Dhaka city in this regard. Almost all the previous studies focused on health of elderly, children or pregnant women due to excess noise but overlooked those who are exposed to such environment for at least eight hours. Hence, this paper concentrated to the people who work under high decibel of noise in the street namely street hawker and roadside vendors.

II. OBJECTIVE AND SCOPE OF THE STUDY

The goal of the study is to evaluate the present state of adverse health effect due to noise pollution on the people who are more exposed to noise than others (like roadside shopkeepers, traffic police, rickshaw puller and street hawker), identification the causes and to develop appropriate remedial measures according to the define causes.

III. METHODOLOGY

3.1. Study Area

Study areas of this project were central Dhaka city which are further divided into five categories namely residential, silent, commercial, industrial and mixed area. Finally ten location were selected, two under each area. Motijheel and Newmarket, Farmgate and Mouchak, Shahbag and Agargaon, Mohakhali and Mirpur-10, Moghbazar and Gulshan were selected as a representative of commercial, mixed, silent, industrial and residential area respectively. Further the selected locations were divided into two sections.

- Main Roads: Specially the intersections and major roads which connected Dhaka city roadway network.
- Outside Buildings: Especially those buildings which are located 100 meters or less from the selected intersections.

3.2. Procedure

- At the onset of the study, intersections of the selected zones were taken under supervision as a study area.
- People who are most exposed to noise were further divided into two categories. They are: Roadside Shopkeeper and Street Hawker.
- Effects of noise were categorized as auditory and non-auditory, and then three non-auditory effects were selected arbitrary.
- A survey questionnaire was prepared.
- Collection of data through this survey among the selected categories of people in all selected intersections having any age group.
- After collecting all necessary data, an analysis is conducted.
- A recommendation is drawn from the analysis.

IV. REVIEW OF LITERATURE

4.1. Background

Dhaka is known to be one of the busiest, noisiest and over-crowded modern cities in the world. The range of noise pollution has been causing different types of public health hazards. Millions of people regardless of age-groups are being affected every year due to continued exposure to the deafeningly loud noise leading to deafness to even heart ailments.[daily sun]. This is mainly an urban phenomenon and affects mostly who works outdoors, for example the rickshaw-puller, street vendors, traffic police, small shopkeepers etc. ^[1]

4.2. Noise Measuring Unit

The intensity of sound pressure is measured by decibel. The decibel is a logarithmic unit used to express the ratio between two values of a physical quantity, often power or intensity. ^[2] This unit is expressed as dB.

4.3. Noise Level Standards in Bangladesh

According to the Department of Environment, Bangladesh, the level of noise in Bangladesh should be as follows

Table I: Noise quality standards, by zones and time of day ^[3]

Serial No.	Category of Areas	Limits in dB	
		Day time (6 am- 9 pm)	Night time (9 pm- 6 am)
1	Silent Area	45	35
2	Residential Area	50	40
3	Mixed Area	60	50
4	Commercial Area	70	60
5	Industrial Area	75	70

4.4. Scenario of Dhaka

Noise of any busy street in Dhaka city has been estimated at 60 to 80 dB , with the sound of vehicles being 95 dB , loud speakers 90 to 100 dB ,mills and factories 80 to 90 dB , restaurants and cinema halls 75 to 90 dB , scooter or motorbike 87 to 92 dB , trucks and buses 92 to 94 dB . But the desired sound measure is 25 dB in

the bedroom, 40 dB in the dining or drawing room, 35-40 dB in the office, 30-40 dB in the classroom, 35-40 dB in the library, 20-35 dB in hospital, 40-60 dB in a restaurant and 45 dB in the city at night. However, according to World Health Organization (W.H.O.), generally 60 dB sounds can make a man deaf temporarily and 100 dB sounds can cause complete deafness. [4]

4.5. Sources of Noise Pollution

The sources of noise pollution fall into two categories: the indoor and the outdoor sources. The indoor sources include watching TV in high volume; listening to music in radio, cassette recorder, i-pod, CD or DVD players, mobile-phone ring-tones or alarm-tones, playing computer games with intense sound effects. It may even be playing a guitar or drums or other musical instruments with the help of an amplifier or other electrical appliances or power tools like drill machine or a lawnmower. [5]

But the outdoor sources play a fatal role in disturbing the environment and public-health. Bus, truck, baby-taxi and other three wheeler-vehicles, automobiles, motorbikes, trains, airplanes, jetfighters – all create excessive noise. Besides, the hydraulic horns used by buses and trucks, loud-speakers, generators, brick-breaking machines, whistle of trains, sirens of emergency vehicles, lightning, high sound of welding factories, building construction activities and the machines used in any construction works create high level of sound pollution. [5] Furthermore, sometimes religious institute play role as a source of noise pollution.



Photo 1: Outdoor source of noise pollution

4.6. Effects on Health

The health-hazards of noise pollution can be categorized into physiological and psychological or mental hazards. The former includes hearing-loss, high blood-pressure, nervous-disorder, headache, lung problems and breathing complications, indigestion, peptic ulcer, backbone curving etc. It also causes heart-attack, stroke and sleep-disorder. The latter includes 9 types of mental diseases. According to the psychiatrists, loud sounds increase emission of adrenal hormone in blood that increases mental impatience and excitement. As a result, various mental disorders including anger, annoyance, aggression, stress, anxiety, frustration, tension and depression occur. It also turns the students apathetic or indifferent towards their studies. [5]

V. ANALYSIS

5.1. Street Hawker

Table II: Health effect on Street Hawker

Area	No. of Person	Hearing Impairment	Blood Pressure	Agitation	Task Performance
Commercial	30	22	8	18	17
Residential	30	20	25	27	16
Industrial	30	21	27	17	17
Silent	30	20	18	20	22
Mixed	30	20	14	18	14

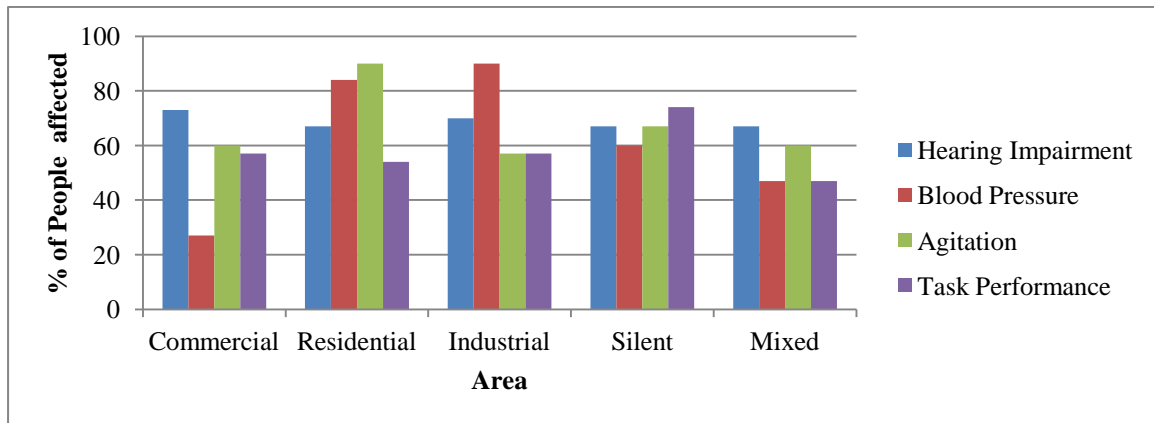


Figure 1: % of street hawkers affected in different selected zones

For street hawkers, noise induced hearing impairment is almost same in all the areas. But when it comes to non-auditory effects like blood pressure, the percentage fluctuated largely. Although only 27% of surveyed hawkers blamed noise for their blood pressure in commercial zones, the rate is exact 90 in term of industrial areas. Another non-auditory effect namely agitation is severe in residential areas, yet other areas have quite similar result. Task performance is greatly hampered for the hawkers in silent zones. The most significant feature of this graph is, at least 60% of surveyed hawkers is suffering from noise induced hazards in silent zones.

5.2. Roadside Shopkeeper

Table III: Health effect on Roadside Shopkeepers

Area	No. of Person	Hearing Impairment	Blood Pressure	Agitation	Task Performance
Commercial	30	23	20	22	24
Residential	30	23	12	15	21
Industrial	30	17	21	17	18
Silent	30	18	16	23	20
Mixed	30	14	17	16	15

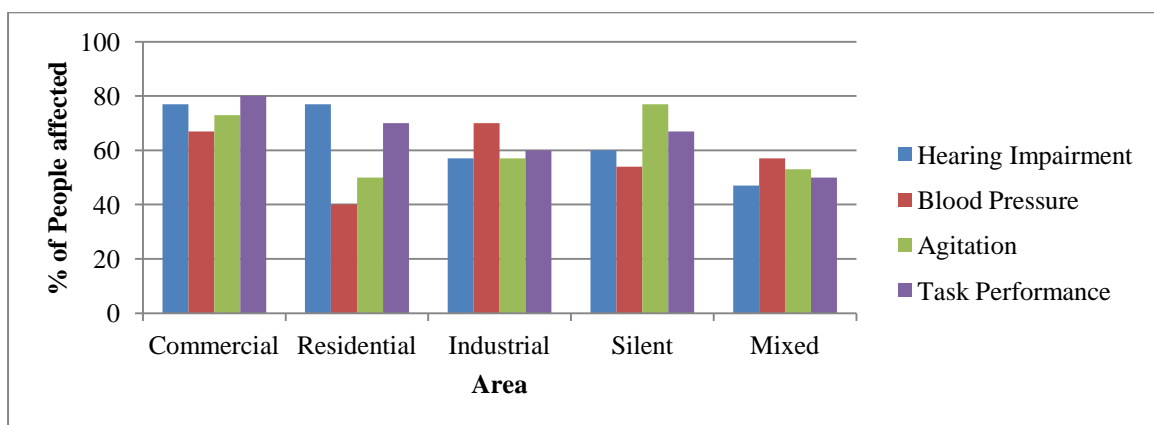


Figure 2: % of roadside shopkeepers affected in different selected zones

For roadside shopkeepers, selected sorts of health hazard is severe in commercial zones. Lackluster performance is the most accused problem among roadside vendors regarding all zones. Auditory effects are at peak in commercial and residential areas. Although blaming blood pressure as a health hazard of noise is at nadir in residential areas, 70% of surveyed vendors from industrial area pointed out this phenomenon as a major hazard to them due to continuous exposure in high noise. Agitation is high at silent zones while in mixed zones, every single health effect is noticeably in quite similar range.

VI. PROPOSAL

6.1. Traffic Control

As vehicle is considered as the main source of noise pollution, not only the commercial or industrial areas but also silent and residential areas. Therefore amount of traffic must be controlled to reduce noise related pollution.

6.2. Relocation of Industry

Industries inside the city not only producing noise pollution but also air pollution and traffic congestion. Hence industry must be relocated at the periphery or outside of the city.

6.3. Prohibit Deteriorating Business Policy

To attract customers, playing CD or DVD at a very high volume or shouting by the name of selling price is a common scenario in streets of commercial places in Dhaka city. Such activities by vendors create pollution thus must be stopped.

6.4. Ban Hydraulic Horn

Although the use of hydraulic horn is restricted inside the city for a certain period of time, especially 6 am to 9 pm. But to reduce noise level further it should be banned for 24 hours.

6.5. Stop Unnecessary Honking

Honking when not necessary is a common practice mostly in commercial and industrial zones. Hence create excess noise. Unnecessary honking must be stopped to mitigate noise pollution.

6.6. Tree Plantation

Planting tree can play a great role by creating natural barrier to noise. Besides, it will keep the air clean. Therefore planting tree on road island should initiate at a large extent.

6.7. Law Enforcement

Certainly existing law to control noise pollution is not adequate, yet their application must be ensured to mitigate the situation in some extent. Government should come forward to reduce noise related hazards by levying various laws and carry them out accordingly.

6.8. Public Awareness

Overall public awareness is the key to reduce noise level and related health hazards in Dhaka city.

VII. CONCLUSION

This paper is dedicated to explore the actual scenario of noise induced health hazards among roadside population in Dhaka, Bangladesh. From analysis it is found that, auditory effect namely hearing impairment is affecting these people mostly. In case of non-auditory effect, people gets muddled up and the fluctuation of graph depicts their lack of knowledge regarding non-auditory effects of noise pollution. Besides, lack of implementing governmental rules also worsening the present condition. Moreover, current noise control rule, 2006 is largely inadequate to mitigate the noise level and its consequent hazards. Further failure of government or responsible authority will proliferate the deteriorating effects of noise. This study provides a strong ground for all responsible to consider non-auditory effects are as important as auditory effect. Therefore the legal legislator should levy rules to protect the health of workers working under such environment and implement the rules strictly alongside enhancing public awareness, in future.

REFERENCES

- [1] <http://omnibangla.blogspot.com/2012/06/noise-pollution-in-bangladesh.html> (accessed December 12, 2014).
- [2] <http://en.wikipedia.org/wiki/Decibel> (accessed December 12, 2014).
- [3] Noise Pollution (Control) Rules 2006. Dhaka: Department of Environment, September 7, 2006.
- [4] Tuhin, Farhad. "Sound pollution - a severe health hazard." The Daily Star, November 15, 2008.
- [5] Ahmed, Kazi Arif. "Noise Pollution and Dhaka City." The Daily Sun, 2010.

An Internet Based Anonymous Electronic Cash System

Israt Jahan¹, Mohammad Zahidur Rahman², K M Akkas Ali³, Israt Jerin⁴

^{1,2}Department of Computer Science and Engineering, Jahangirnagar University, Dhaka, Bangladesh

³Institute of Information Technology, Jahangirnagar University, Dhaka, Bangladesh

⁴Britannia University, Paduar Bazar, Bissaw Road, Comilla, Bangladesh

ABSTRACT: There is an increase activity in research to improve the current electronic payment system which is parallel with the progress of internet. Electronic cash system is a cryptographic payment system which offers anonymity during withdrawal and purchase. Electronic cash displays serial numbers which can be recorded to allow further tracing. Contrary to their physical counterparts, e-cash have an inherent limitation; they are easy to copy and reuse (double-spending). An observer is a tamper-resistant device, issued by the Internet bank, which is incorporated with the Internet user's computer that prevents double-spending physically, i.e., the user has no access to her e-cash and therefore he cannot copy them. In this paper, we shall present an anonymous electronic cash scheme on the internet which incorporates tamper-resistant device with user-module.

KEYWORDS- E-cash, Double-spending, Tamper-resistant device, Blind signature, Internet banking.

I. INTRODUCTION

Electronic commerce is one of the most important applications for the internet. The prerequisite for establishing an electronic marketplace is a secure payment. Several electronic protocols have been proposed to implement different kinds of payment: credit card payments, micropayments, and digital e-cash. Cryptographically, the most challenging task is the design of digital e-cash for every payment system mentioned above we have the requirement that the payment token has to be unforgeable. In 1982, D. Chaum [7] presented the notion of blind signatures that offer the possibility to design electronic e-cash. The bank signs a set of data chosen by the user which guarantees both the unforgeability of the e-cash and their anonymity, since the bank does not get any information about data it signed. But blind signatures solve only half of the problem: since digital data can be copied, a user can spend a valid e-cash several times (double-spending) if the deposit of e-cash is not done on-line [3]. To validate each e-cash on-line means that the vendor has to contact the bank in every purchase. From the efficiency's point of view this is undesirable. Therefore, we restrict our attention to off-line systems, i.e., the vendor has to check the validity of e-cash without contacting the bank. An e-cash is constructed in a way that allows its owner to spend it anonymously once, but reveals his identification if he spent it twice [5]. From a theoretic point of view this solution is quite elegant. But in practice it is unsatisfactory. A way to prevent the user physically from copying her coins is to store essential parts of a coin in a tamper-resistant device called the observer [7].

II. AN E-CASH MODEL WITH TAMPER-RESISTANT DEVICE

An internet based anonymous off-line electronic e-cash scheme [1, 8 and 9] with tamper-resistant device consists of three collections of probabilistic, polynomially-bounded parties [2], a bank B, users U_i , and shops S_j , and four main procedures: withdrawal, blind signature issuing, payment and deposit (Figure 1). Users and shops maintain separate account with the Internet Bank [10].

- When user (U_i) needs e-cash, then Bank issues e-cash from user's account in his (user's) tamper-resistant device T_i over an authenticated channel.
- When user (U_i) wants to spend this e-cash, it is validated by bank (B) by blind signature issuing protocol.
- U_i spends an e-cash by participating in a payment protocol with a shop S_j over an anonymous channel, and
- S_j performs a deposit protocol with the bank B, to deposit the user's e-cash into his account.

- (1) Withdrawal protocol
- (2) Blind signature issuing protocol
- (3) Payment protocol
- (4) Deposit protocol

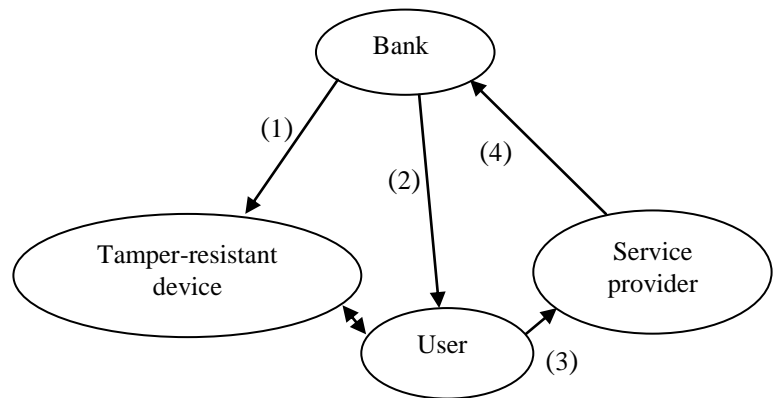


Figure 1: Model of e-cash with tamper-resistant device

III. AN INTERNET BASED ANONYMOUS E-CASH SYSTEM

We shall now represent an anonymous off-line e-cash transaction system on the Internet.

3.1 The Bank’s setup protocol

- All arithmetic is performed in a group G_q of prime order q chosen by bank (B). The bank generates independently at random four numbers $g_0, g_1, g_2, h \in G_q$ and a number $x \in Z_q$. The bank also determines a collision-free hash function $H(\cdot)$ such as to make the Schnorr signature scheme secure [4]. A public key that is issued by the bank to the user is a pair $(h'_i, a'_i) \in G_q * G_q$.
- The number x is the secret key of the bank, and the corresponding public key is the tuple $(g_0, g_1, g_2, h, G_q, H(\cdot))$. A certificate of the bank on the public key (h'_i, a'_i) of the user is a triple (z'_i, c', r) such that $c' = H(h'_i, a'_i, z'_i, g_0^{r'} h^{-c'})$.
- The secret key that corresponds to the public key (h'_i, a'_i) of the user is a pair $((\beta_1, \alpha_1), (\beta_2, \alpha_2))$, such that $h'_i = g_1^{\beta_1} g_2^{\alpha_1}$ and $a'_i = g_1^{\beta_2} g_2^{\alpha_2}$.

3.2 The actions

The Internet bank will be denoted by B, the user by U_i , and the service provider by S_j . The computer of U_i is denoted by C_i , and his tamper-resistant device by T_i .

3.2.1 Account establishment protocol

U_i installs on his computer, a software program for performing the protocols. When U_i opens an account with B, the following procedure takes place.

- C_i generates independently at random a secret key $x_{i2} \in Z_q$, and stores it. C_i sends $h_{i2} = g_1^{x_{i2}}$, to B, together with an appropriate verifiable description of the identity of U_i . It then generates independently at random a secret key $x_{i1} \in Z_q$ for U_i . B lists this number (h_{i2}) in its so-called account database, together with at least a balance variable that keeps track of the amount of money that U_i has in its account with B, and the description of U_i 's identity.
- B then issues to U_i a tamper-resistant device T_i which has stored in non-volatile memory at least the following items: the numbers x_{i1} and g_1 , and a description of G_q ; code to perform its role in the protocols; and a counter variable, from now on denoted by *balce*, that keeps track of the amount of money that is held by U_i .
- B makes $h_{i1} = g_1^{x_{i1}}$, known to U_i ; this is the public key of T_i . B then computes $h_i = h_{i1} h_{i2}$ (the joint public key of T_i and U_i and stores h_i in his account database along with its other information on U_i). The bank B does not know the joint secret key, $(x_{i1} + x_{i2}) \bmod q$, of T_i and U_i .
- Finally, B computes $(h_i g_2)^x$, which will henceforth be denoted by z_i known to U_i .

3.2.2 Withdrawal protocol

The withdrawal of electronic cash appears as follows:

T_i is assumed to have in common with B a secret key k . This secret key, and a sequence number, seq , (which has been set to some initial value, such as zero), have been stored by B before issuing T_i to U_i . In addition, the description of a one-way function $f_1(\cdot)$ has been stored by B in T_i . B decreases the balance, $balce'$, of U_i by amount. It then increases seq by one, and transfers $v \leftarrow f_1(k, seq, amount)$ to T_i by sending it to C_i . T_i receives v from C_i . It then computes $f_1(k, seq, amount)$, and compares it for equality with v . If equality holds, it increases seq by one, and balance by amount.

The withdrawal protocol appears as follows:

Tamper-resistant Device (T_i)		Bank (B)
		$balce' \leftarrow balce' - amount$
Verify	$\leftarrow (v)-----$	$v \leftarrow f_1(k, seq, amount)$
$v = f_1(k, seq, amount)$		$seq \leftarrow seq + 1$
then, $seq \leftarrow seq + 1$		
$balce \leftarrow balce + amount$		

Table 1: The withdrawal protocol

3.2.3 The Pre-processing of blind signature issuing protocol

Payment of an amount requires U_i to provide the service provider with a signature on the amount (and additional data). To prepare for the withdrawal of a blind signature on e-cash, T_i and C_i perform the following off-line processing.

- T_i generates independently at random a number $w_i \in_R Z_q$, and sends $a_i g_1^{w_i}$ to C_i . T_i stores w_i for later use in the payment protocol.
- C_i generates independently at random a vector $(\alpha_1, \alpha_2, \alpha_3, \alpha_4, \alpha_5) \in Z_q^5$, such that $\alpha_i \neq 0 \pmod q$. It then computes $h_i' \leftarrow (h_i g_2)^{\alpha_1}$, $a_i' = a_i^{\alpha_1} g_1^{\alpha_2} g_2^{\alpha_3}$, $z_i' \leftarrow z_i^{\alpha_1}$, $temp_1 = h_i^{\alpha_4} g_0^{\alpha_5}$, $temp_2 \leftarrow (z_i')^{\alpha_4} (h_i g_2)^{\alpha_1 \alpha_5}$.
- C_i stores (h_i', a_i') and $(\alpha_1, \alpha_2, \alpha_3)$ and $temp_1, temp_2, \alpha_4$ and α_5 for the later use in the payment protocol.

3.2.4 The blind signature issuing protocol

The issuing of blind signature [6] is done by means of the following on-line certificate issuing protocol between C_i and B. The blind signature issuing appears as follows:

Computer(C_i)		Bank(B)
		$w \in Z_q$
		$a \leftarrow g_0^w$
		$b \leftarrow (h_i g_2)^w$
	$\leftarrow (a,b)-----$	
$c' \leftarrow H(h_i', a_i', a temp_1, b^{\alpha_1} temp_2)$		
$c \leftarrow c' + \alpha_4 \pmod q$	$----- (c) \rightarrow$	
	$\leftarrow (r)-----$	$r \leftarrow cx + w \pmod q$

Table 2: The blind signature issuing protocol

3.2.5 The pre-processing of payment protocol

To pay to S_j an amount, T_i and C_i perform the following pre-processing.

- C_i determines the specification, denoted by $spec$, of the payment. This number is a concatenation, in a standardized format, of that is to be transferred, the time and date of transaction, and an identification number that is uniquely associated with S_j . Additional data fields may be included in variable $spec$. C_i then sends (h_i', a_i') and $spec$ to T_i .
- T_i verifies that w_i is still in memory, and that balance exceeds amount (T_i can read this value from $spec$). If this is the case, it computes $d = H(h_i', a_i', spec)$ and $r_1 = dx_{i1} + w_i \pmod q$. It then decreases balance by amount, erases w_i from memory, and sends r_1 to C_i .
- C_i computes $d = H(h_i', a_i', spec)$, and verifies that $g_1^{r_1} h_{i1}^{-d} = a_i$. If this is the case, C_i computes $r_1' = \alpha_1(r_1 + dx_{i2}) + \alpha_2 \pmod q$, $r_2 \leftarrow d\alpha_1 + \alpha_3 \pmod q$. The pre-processing of payment protocol appears as follows:

<p>User computer(C_i)</p> <p>----- (h_i' , a_i') →</p> <p>←(r₁)-----</p> <p>d=H(h_i' , a_i' ,spec)</p> <p>verify</p> <p>$g_1^{r_1} h_{i1}^{-d} = a_i$</p> <p>$r_1' \leftarrow \alpha_1(r_1 + dx_{i2}) + \alpha_2 \text{ mod } q$</p> <p>$r_2 \leftarrow d\alpha_1 + \alpha_3 \text{ mod } q$</p>	<p>Tamper-resistant device(T_i)</p> <p>d=H(h_i' , a_i' ,spec)</p> <p>balce → balce - amount</p> <p>$r_1 = dx_{i1} + w_i$</p> <p>erases w_i</p>
---	--

Table 3: The preprocessing of payment protocol

3.2.6 The payment protocol

The actual payment is done by means of the following on-line payment protocol between C_i and S_j.

- C_i sends (h_i' , a_i'),(z_i' ,c' ,r'),(r₁' ,r₂')to S_j.
- S_j computers d in the same way as did C_i and T_i and accepts the transferred information if and only if $h_i' \neq 1$, $c' = H(h_i' , a_i' , z_i' , g_o^r h^{-c'} , (h_i')^{r'} (z_i')^{-c'})$ and $g_1^{r_1'} g_2^{r_2'} (h_i')^{-d} = a_i'$
- The payment protocol appears as follows:

<p>Computer(C_i)</p> <p>-- (h_i' , a_i'),(z_i' ,c' ,r'),(r₁' ,r₂') →</p>	<p>Service Provider(S_j)</p> <p>Check</p> <p>d=H(h_i' , a_i' ,spec)</p> <p>$c' = H(h_i' , a_i' , z_i' , g_o^r h^{-c'} , (h_i')^{r'} (z_i')^{-c'})$</p> <p>$g_1^{r_1'} g_2^{r_2'} (h_i')^{-d} = a_i'$</p>
--	---

Table 4: The payment protocol

3.2.7 The deposit Protocol

At a suitable time, preferably when network traffic is low, S_j sends the payment transcript, consisting of (h_i' ,a_i'), (z_i' , c' , r'), (r₁' ,r₂') and spec, to B.

B verifies that spec has been formed correctly by S_j. If this is the case, it searches its so-called deposit database to find out if it has stored (h_i' ,a_i') before.

There are two possible situations:

1. (h_i' ,a_i') is not in the deposit database. B then computes $d = H(h_i' , a_i' , spec)$, and verifies the payment transcript by verifying that $h_i' \neq 1$, $c' = H(h_i' , a_i' , z_i' , g_o^r h^{-c'} , (h_i')^{r'} (z_i')^{-c'})$ and $g_1^{r_1'} g_2^{r_2'} (h_i')^{-d} = a_i'$. If these verifications hold, B stores (h_i' , a_i'),(z_i' ,c' ,r') and (r₁' ,r₂') in the deposit database, and credits the account of S_j by amount.
2. (h_i' ,a_i') is already in the deposit database. In that case a fraud has occurred. If spec of the already stored information is identical to that of the new payment transcript, then S_j is trying to deposit the same transcript twice.

Otherwise, B verifies the transcript as described insituation 1. If the verification holds (the payment transcript is valid), then the certified public key (h_i' ,a_i') must have been double-spent with overwhelming probability. Since, B now has at its disposal a pair (r₁' ,r₂') from the new transcript and a pair, say (r₁'',r₂''), from the already deposited information, it can compute $(r_1' - r_1'') / (r_2' - r_2'') \text{ mod } q$. B then searches its account database for joint public key $g_1^{(r_1' - r_1'') / (r_2' - r_2'')}$. Since, the identity of the corresponding account holder is known to B, appropriate legal actions can be taken. The number $(r_1' - r_1'') / (r_2' - r_2'') \text{ mod } q$ serves as the proof of B that the traced user has compromised his tamper-resistant device and has double-spent the certified public key (h_i' ,a_i') .

IV. DISCUSSIONS

In the e-cash scheme with tamper-resistant device, the user's secret is shared between the user and his observer. The combined secret is a modular sum of the two shares, so one share of the secret reveals no information about the combined secret. Co-operation of the user and the tamper-resistant device is necessary in order to create a valid response to a challenge during a payment transaction. It prevents the tamper resistant device from leaking any information about the user.

V. CONCLUSIONS

We presented electronic cash system which provides a physical defense against double-spending detection. To guarantee the prevention of double-spending, the bank has to be sure that the tamper-resistant device cannot be tampered with by the users. The use of a tamper-resistant device is a kind of first line of defense. If the user cannot manipulate the device, the tamper-resistant device can prevent double-spending. If the user succeeds in tampering the observer, the double-spending detection identifies the user afterwards.

REFERENCES

- [1] Ogiela, M.R., & Sulkowski, P. Improved Cryptographic protocol for digital coin exchange. *15th International Symposium on Soft Computing and Intelligent Systems (SCIS)*, 2014, 1148-1151.
- [2] Miers, I., Garman, C., Green, M., & Rubin, A.D. Zerocoin: Anonymous Distributed E-Cash from Bitcoin. *IEEE Symposium on Security and Privacy (SP)*, 2013, 397-411.
- [3] Jiangxiao Zhang., Zhoujun Li., Hua Guo., & Chang Xu. Efficient Divisible E-Cash in the Standard Model. *IEEE International Conference on Green Computing and Communications (GreenCom)*, 2013, 2123-2128.
- [4] Yun-kyung Lee., Seung-Wan Han., Sok-joon Lee., Byung-ho Chung., & Deok Gyu Lee. Anonymous Authentication System Using Group Signature. *International Conference on Complex, Intelligent and Software Intensive Systems*, 2009, 1235-1239.
- [5] Israt Jahan., Mohammad Zahidur Rahman., & Md. Golam Moazzem. Review of Anonymous Electronic Payment System. *Journal of Electronics and Computer Science*, 2003, 25-39.
- [6] Tsiounis, Y.S. Efficient Electronic Cash: New Notions and Techniques. *Northern University, Massachusetts*. PhD Thesis, 1997.
- [7] Chaum, D., & Pedersen, T. Wallet Databases with Observers. *In proceedings of CRYPTO*, 1993, 89-105.
- [8] Brands, S. Untraceable Off-line Cash in Wallets With Observers. *In proceedings of CRYPTO*, 1993, 303-318.
- [9] Schnorr, C.P. Efficient Signature Generation by Smart Cards. *Journal of Cryptology*, 1991, 4(3), 161-174.
- [10] Chaum, D. Blind Signatures for Untraceable Payments. *Advances in cryptology-Proceedings of Crypto '82, Lecture Notes in Computer Science*. Springer-Verlag, 1982, 199-203.

Mammogram Image Segmentation Quality Enhancement Using Clustering Techniques

¹Mrs. Sandhya G, ²Dr. D Vasumathi, ³Dr. G T Raju,

¹Assoc. Prof, Dept. of CS&E ICEAS, Bangalore, Karnataka

²Prof, Department of CS&E JNTU-H, Kukatpally, Hyderabad

³Professor, Department of CS&E, RNSIT, Bangalore, Karnataka

Abstract: Breast cancer is the most commonly observed cancer in women both in the developing and the developed countries of the world. Cancer refers to the uncontrolled multiplication of a group of cells in a particular location of the body. A group of rapidly growing or dividing cells may form lump or mass of extra tissue. These masses are referred to as tumors. Cancer cells are termed as malignant tumors. Any form of malignant tumor developed from breast cells is nothing but breast cancer. Breast cancer detection is the standard diagnosis and prognosis. Mammogram Image segmentation is best method used for detection breast cancer by using various clustering techniques such as K-Means modified K-Means (KM), Fuzzy C-Means. The 14 Haralick features are extracted from mammogram image using Gray Level Co-occurrence Matrix (GLCM) for different angles.

Keywords: Mammogram, Breast cancer detection, K-Means, K-Medoids, Fuzzy c-means

I. INTRODUCTION

The mammography is the most effective procedure to diagnosis the breast cancer at an early stage. This paper proposes mammogram image segmentation quality enhancement using various clustering techniques such as K-Means, modified K-Means (KM), Fuzzy C-Means. The 14 Haralick features are extracted from mammogram image using Gray Level Co-occurrence Matrix (GLCM) for different angles. The features are clustered by K-Means, Fuzzy C-Means (FCM) and modified K-Means algorithms to segment the region of interests (ROIs) for classification. The results of these clustering techniques compared and analyzed using Mean Square Error (MSE) and Root Mean Square Error (RMSE). It is observed that the modified K-Means method gives better results compared to all the other methods clustering is defined as the optimal partitioning of a given set of n data points into specified number of subgroups, such data points belonging to the same group are as similar to each other [5]. The data points from two different groups share the different group. Image segmentation is considered as a clustering problem where each pixel corresponds to a pattern, and each image pattern region corresponds to a cluster. Some of hard clustering approaches do not consider overlapping of classes which occur in many practical image segmentation problems.

The main objective in cluster analysis is to group objects that are similar each other and separate other objects that are dissimilar by assigning them to different clusters. One of the most popular clustering methods is K-Means clustering algorithm. It classifies object to a pre-defined number of clusters, which is given by the user (assume K clusters). The idea is to choose random cluster centers, one for each cluster. These centers are preferred to be as far as possible from each other. In this algorithm mostly Euclidean distance is used to find distance between data points and centroids [7]. The Euclidean distance between two multidimensional data points are

$$X = (x_1, x_2, x_3, \dots, x_m) \text{ and}$$

$Y = (y_1, y_2, y_3, \dots, y_m)$ is described as follows:

$$D(X, Y) = \sqrt{\sum_{i=1}^m (x_i - y_i)^2} \quad (1)$$

The K-Means method helps to minimize the sum of squared distances between all points and the cluster center. This procedure consists of the following steps, as described below.

K-Means Algorithm:

Require: $D = \{d_1, d_2, d_3, \dots, d_n\}$ // Set of n data points.

K - Number of desired clusters

Ensure: A set of K clusters.

Steps-1: Arbitrarily choose k data points from D as initial centroids;

Steps-2: Repeat: Assign each point d_i to the cluster which has the closest centroid;

Calculate the new mean for each cluster;

Steps-3: Until convergence criteria is met.

Though the K-Means algorithm is simple, it has some drawbacks in final clustering, since it highly depends on the arbitrary selection of the initial centroids. Data clustering is the process of dividing data elements into classes or clusters so that items in the same class are as similar to each other, and items in different classes are as dissimilar as possible. Depending on the nature of the data and the purpose for which clustering is being used, different measures of similarity may be used to place items into classes, where the similarity measure controls how the clusters are formed. Some examples of measures that can be used as in clustering include distance, connectivity, and intensity.

In hard clustering, data is divided into distinct clusters, where each data element belongs to exactly one cluster. In fuzzy clustering (also referred to as soft clustering), data elements can belong to more than one cluster, and associated with each element is a set of membership levels in cluster. These indicate the strength of the association between data element and a particular cluster. Fuzzy clustering method is a process of assigning membership levels, and then using them to assign data elements to one or more clusters.

Fuzzy C-Means Algorithm

Input: Dataset X of n objects with d features, value of K and fuzzy value $m > 1$

Output: Membership matrix U_{ij} for n objects and K clusters

Procedure:

Step-1: Declare a membership matrix U of size $n \times K$.

Step-2: Generate K cluster centroids randomly within the range of the data or select K objects randomly as initial cluster centroids. Let the centroids be c_1, c_2, \dots, c_K .

Step-3: Calculate the distance measure d_{ij} using Euclidean distance, for all cluster centroids $C_i, j = 1, 2, \dots, K$, and data objects $x_i, i = 1, 2, \dots, n$.

Step-4: Compute the Fuzzy membership matrix U_{ij}

Step-5: Compute new cluster centroids c_j

Step-6: Repeat steps 3 to 5 until convergence.

II. Modified K-Means Clustering

The modified K-Means algorithm uses three basic steps

1. A data object can be a member of one lower approximation cluster.
2. A data object that is a member of the lower approximation of a cluster is also, a member of the upper approximation of the same cluster.
3. A data object that does not belong to any lower approximation is a member of at least two upper approximations.

According to the above steps, the lower approximation is a subset of the upper approximation. The difference between upper and lower approximation is called boundary region, which contains objects in multiple clusters. The membership of each objects in lower and upper approximation is determined by three parameters W_l, W_u and ϵ the parameters W_l

and W_u correspond to the relative importance of lower and upper bounds, and W_l and $W_u = 1$.

The ϵ is a threshold parameter used to control the size of boundary region.

Input: Dataset of n objects with d features, number of clusters k and values of parameters W_{lower}, W_{upper} and ϵ .

Output: Estimate Lower as $V(K)$ and Upper as $V'(k)$ of k clusters.

Procedure:

1. Randomly assign each data object as one Lower $V(k)$ by step 2, the data object also belong to Upper $V'(k)$ of the same cluster
2. Compute cluster centroids C_j .

If $V(k) \neq \emptyset$ and $V'(k) - V(k) = \emptyset$

$$C_j = \frac{\sum_{x \in V(k)} x^j}{|V(k)|}$$

Else

$V(k) \neq \emptyset$ and $V'(k) - V(k) = \emptyset$

$$C_j = \frac{\sum_{x \in (V'(k) - V(k))} x^j}{|V'(k) - V(k)|}$$

$$C_j = W_1 X \frac{\sum_{x \in V(k)} x^j}{V(k)} + W_u X \frac{\sum_{x \in (V'(k) - V(k))} x^j}{|V'(k) - V(k)|}$$

3. Assign each object of the Lower $V(k)$ or Upper approximation $V'(k)$ of cluster i cluster respectively, for each object vector x , let $d(x, C_j)$ is the distance between itself and the centroid d of cluster C_j , Let $d(x, C_j)$ is min
 $1 \leq i, j = K,$
 Then ratio
 $d(x, C_i) / d(x, C_j)$
 $i \leq j, j \leq K$ is used to determine the member ship of x as follows.
4. Repeat the steps 2 and 3 until Convergence

III. EXPERIMENTAL RESULTS AND DISCUSSIONS

In this paper the image samples are taken from the benchmark MIAS database for analyzing the proposed method. 14 Haralick features were extracted using Gray level Co-occurrence Matrix (GLCM). The sub-matrices of size 5×5 is used for constructing GLCM at different angle with distance $d = 1$ and then feature are extracted. Further feature are clustered into five groups by modified KM algorithm, each groups is partition into one segment, the each segmented image show in Figure 1. The same features are used to cluster using K-Means and FCM algorithms with five groups each groups is partition into one segment. The quality of segmentation result are measured using MSE and RMSE if the error value becomes low means that the better results. The MSE and RMSE values for the modified KM segmentation, FCM segmentation and K-Means segmentation are tabulated in tables 1,2,3 and 4 respectively. According to the segmentation errors: means square error (MSE) and root mean square error (RMSE), the GLCM at distance 1 and angle 450 gives the best result for all tested image as shown in figures 1,2,3,4 and 5 K-means and FCM are helpful in early stage of clustering in medical diagnosis [7]. The cancerous mode can easily be separated from a fatty breast region as well as from dense region. As the number of cluster increases more and more information is obtained about the tissue which can't be identified by the pathologists

Breast Images	MDB 017	MDB 072	MDB 018	MDB 0114	MDB 213	MDB 290
Original						
Angle 0°						
Angle 45°						
Angle 90°						
Angle 135°						

Figure.1 Results of Segmentation using modified K-MeansAlgorithm

Table.1 MSE values for modified K-Means Segmentation

Sample Image	Mdb 17	Mdb 72	Mdb 18	Mdb 114	Mdb 213	mdb290
Angle 0°	9.75E+03	7.65E+03	6.27E+03	8.23E+03	5.63E+03	7.38E+03
Angle 45°	8.05E+03	9.17E+03	6.34E+03	8.26E+03	5.77E+03	7.31E+03
Angle 90°	9.82E+03	8.09E+03	6.02E+03	8.06E+03	5.79E+03	8.06E+03
Angle 135°	9.11E+03	7.15E+03	5.74E+03	1.10E+04	6.18E+03	6.91E+03

Table.2 RMSE values for modified K-Means Segmentation

Sample Image	mdb17	mdb72	mdb18	mdb114	mdb213	mdb290
Angle 0°	98.76	87.51	79.19	90.73	75.04	85.91
Angle 45°	89.17	95.77	79.63	90.91	75.97	85.54
Angle 90°	99.15	89.97	77.6	92.75	76.13	89.79
Angle 135°	100.91	84.59	75.77	104.96	78.65	83.13

Table 3 MSE values for FCM segmentation

Sample Image	mdb17	mdb72	mdb18	mdb114	mdb213	mdb290
Angle 0°	1.08E+04	1.18E+04	1.41E+04	8.77E+03	8.84E+03	1.10E+04
Angle 45°	8.11E+03	1.06E+04	1.01E+04	8.41E+03	7.94E+03	9.43E+03
Angle 90°	1.11E+04	1.30E+04	1.19E+04	9.97E+03	9.86E+03	1.07E+04
Angle 135°	1.16E+04	1.29E+04	1.10E+04	1.17E+04	1.01E+04	1.09E+04

Table.4 RMSE values for K-Means segmentation

Sample Image	Mdb 17	Mdb 72	Mdb 18	Mdb 114	Mdb 213	Mdb 290
Angle 0°	111.61	127.26	119.82	114.64	107.27	108.91
Angle 45°	108.97	111.41	109.81	102.23	101.85	104.26
Angle 90°	109.34	135.16	112.85	103.77	103.29	108.93
Angle 135°	111.99	136.69	111.66	113.55	107.38	111.58

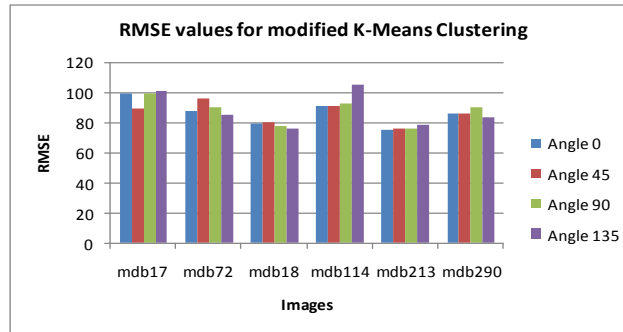


Figure.2 RMSE values for Segmentation using modified K-MeansClustering

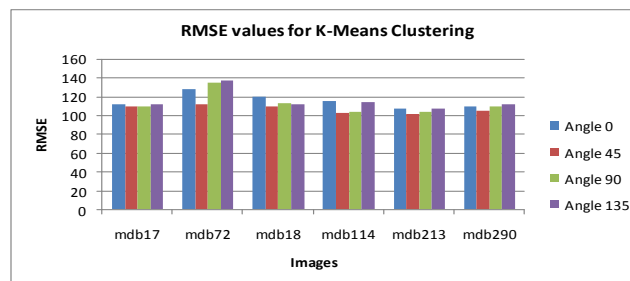


Figure.3 RMSE values for Segmentation usingK-MeansClustering

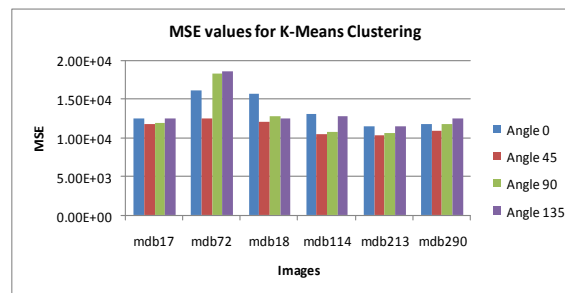


Figure.4 MSE values for Segmentation using K-MeansClustering

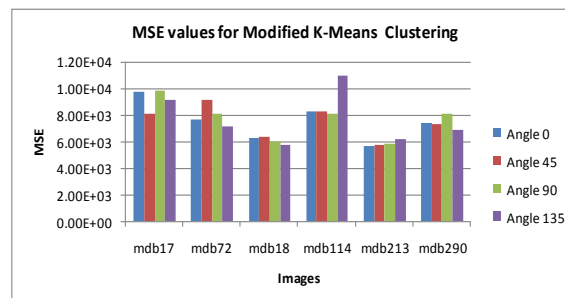


Figure 5 MSE values for Segmentation using modified K-MeansClustering

IV. CONCLUSION

In this paper, modified K-Means algorithm is proposed for mammogram image segmentation. The 14 Haralick features are extracted from mammogram image using Gray Level Co-occurrence Matrix (GLCM) for different angles. The features are clustered by K-Means, Fuzzy C-Means (FCM) and modified KM algorithms in order to segment the region of interests for further classification. The performance of the modified KM segmentation is evaluated using MSE and RMSE measures. The proposed segmentation algorithm is compared with K-Means algorithm and FCM algorithm. It was observed that modified KM segmentation algorithm performs the benchmark K-Means algorithm and FCM algorithm. Further the resultant mammogram can be used for the detection of abnormalities in human breast like calcification, circumscribed lesions etc. This is the direction for further research.

REFERENCES

- [1] Sampat, M.P., Markey, M.K., Bovik, A.C.: Computer-Aided Detection and Diagnosis in Mammography. In: Bovik, A.C.(ed.) Handbook of Image and Video Processing. ElsevierAcademic Press, Amsterdam (2005)
- [2] Cheng, H.D., Shi, X.J., Min, R., Hu, L.M., Cai, X.P., Du,H.N.: Approaches for Automated Detection and Classification of Masses in Mammograms. Pattern Recognition 39(4), 646–668 (2006)
- [3] Brzakovic, D., Luo, X.M., Brzakovic, P.: An approach to automated detection of tumors in mammograms. IEEE Transactions on Medical Imaging 9(3), 233–241 (1990)
- [4] Li, H.D., Kallergi, M., Clarke, L.P., Jain, V.K., Clark, R.A.: Markov Random Field for Tumor Detection in Digital Mammography. IEEE Transactions on Medical Imaging 14(3), 565–576 (1995)
- [5] Li, L.H., Qian, W., Clarke, L.P., Clark, R.A., Thomas, J.: Improving Mass Detection by Adaptive and Multi-Scale Processing in Digitized Mammograms. Proceedings of SPIE—The International Society for Optical Engineering 3661 1, 490–498 (1999)
- [6] Székely, N., Tóth, N., Pataki, B.: A Hybrid System for Detecting Masses in Mammographic Images. IEEE Transactions on Instrumentation and Measurement 55(3), 944–951 (2006)
- [7] Zheng, B., Mello-Thoms, C., Wang, X.H., Gur, D.: Improvement of Visual Similarity of Similar Breast Masses Selected by Computer-Aided Diagnosis Schemes. In: 4th IEEE International Symposium on Biomedical Imaging: From Nano to Macro, ISBI 2007, April 12-15, pp. 516–519 (2007)
- [8] Pappas, T.N.: An Adaptive Clustering Algorithm for Image Segmentation. IEEE Transactions on Signal Processing 40(4), 901–914 (1992)
- [9] Sahiner, B., Hadjiiski, L.M., Chan, H.P., Paramagul, C., Nees, A., Helvie, M., Shi, J.: Concordance of Computer-Extracted Image Features with BI-RADS Descriptors for Mammographic Mass Margin. In: Giger, M.L., Karssemeijer, N. (eds.) Proc. of SPIE Medical Imaging 2008: Computer-Aided Diagnosis, vol. 6915 (2008)
- [10] Rangayyan, R.M.: Biomedical Image Analysis. CRC Press LLC, Boca Raton (2005)
- [11] Fauci, F., Bagnasco, S., Bellotti, R., Cascio, D., Cheran, S.C., De Carlo, F., De Nunzio, G., Fantacci, M.E., Forni, G., Lauria, A., Torres, E.L., Magro, R., Masala, G.L., Oliva, P., Quarta, M., Raso, G., Retico, A., Tangaro, S.: Mammogram Segmentation by Contour Searching and Massive Lesion Classification with Neural Network. In:2004 IEEE Nuclear Science Symposium Conference Record, Rome, Italy, October 16–22, vol. 5, pp. 2695–2699 (2004)
- [12] Petrick, N., Chan, H.P., Sahiner, B., Wei, D.: An Adaptive Density Weighted Contrast Enhancement Filter for Mammographic Breast Mass Detection. IEEE Transactions on Medical Imaging 15(1), 59–67 (1996)
- [13] Zou, F., Zheng, Y., Zhou, Z., Agyepong, K.: Gradient Vector Flow Field and Mass Region Extraction in Digital Mammograms. In: 21st IEEE International Symposium on Computer-Based Medical Systems, CMBS 2008, Jyväskylä, June 17-19, pp. 41– 43 (2008)
- [14] Ferreira, A.A., Nascimento Jr., F., Tsang, I.R., Cavalcanti, G.D.C., Ludermir, T.B., de Aquino, R.R.B.: Analysis of Mammogram Using Self-Organizing Neural Networks Based on Spatial Isomorphism. In: Proceedings of International Joint Conference on Neural Networks, IJCNN 2007, Orlando, Florida, USA, August 12-17, pp. 1796–1801 (2007)
- [15] Yuan, Y., Giger, M.L., Li, H., Sennett, C.: Correlative Feature Analysis of FFDM Images. In: Giger, M.L., Karssemeijer, N. (eds.) Proc. of SPIE Medical Imaging 2008: Computer-Aided Diagnosis, vol. 6915 (2008)